UNCLASSIFIED

[redacted]

NATIONAL AERONAUTICS AND SPACE ADMINISTRATION

Space Programs Summary No. 37-40, Volume I

for the period May 1, 1966 to June 30, 1966

The Lunar Program

(Title Unclassified)

UNCLASSIFIED
JPL - Letter to Authority NASA-Langley
dtd Nov. 4, 1970, signed by W.E. Hanson
Date Jan. 4, 1971 By

JET PROPULSION LABORATORY
LIBRARY
SEP 30 1966

Copy No. 482

CALIFORNIA INSTITUTE OF TECHNOLOGY

LAB-C01933

JET PROPULSION LABORATORY
CALIFORNIA INSTITUTE OF TECHNOLOGY
PASADENA, CALIFORNIA

July 31, 1966

[redacted]

UNCLASSIFIED

149555

UNCLASSIFIED CONFIDENTIAL

Preface

The *Space Programs Summary* is a six-volume, bimonthly publication that documents the current project activities and supporting research and advanced development efforts conducted or managed by JPL for the NASA space exploration programs. The titles of all volumes of the *Space Programs Summary* are:

Vol. I. The Lunar Program (Confidential)

Vol. II. The Planetary–Interplanetary Program (Confidential)

Vol. III. The Deep Space Network (Unclassified)

Vol. IV. Supporting Research and Advanced Development (Unclassified)

Vol. V. Supporting Research and Advanced Development (Confidential)

Vol. VI. Space Exploration Programs and Space Sciences (Unclassified)

The *Space Programs Summary,* Vol. VI consists of an unclassified digest of appropriate material from Vols. I, II, and III; an original presentation of technical supporting activities, including engineering development of environmental-test facilities, and quality assurance and reliability; and a reprint of the space science instrumentation studies of Vols. I and II.

W. H. Pickering, *Director*
Jet Propulsion Laboratory

Space Programs Summary No. 37-40, Volume I

Copyright © 1966, Jet Propulsion Laboratory, California Institute of Technology

Prepared under Contract No. NAS 7-100, National Aeronautics & Space Administration

This document contains information affecting the national defense of the United States, within the meaning of the Espionage Laws, Title 18, U.S.C., Sections 793 and 794, the transmission or revelation of which in any manner to an unauthorized person is prohibited by law.

UNCLASSIFIED CONFIDENTIAL

UNCLASSIFIED
CONFIDENTIAL

Contents

I. *Surveyor* Project 1
A. Introduction 1
B. System Engineering 2
C. System Analysis 22
D. Launch Vehicle Integration 41
E. Systems Testing 47
F. Launch Operations 51
G. Spaceflight Operations 54
H. Aerospace Ground Equipment 56
I. Flight Control 59
J. Electronics 65
K. Electrical Power Source 70
L. Propulsion 74
M. Spacecraft Vehicle and Basic Bus Mechanisms 89
N. Payload and Scientific Mechanisms 95
O. Thermal Control 102
P. Engineering Mechanics 104

References 113

UNCLASSIFIED
CONFIDENTIAL

UNCLASSIFIED
CONFIDENTIAL

I. *Surveyor* Project

A. Introduction

Surveyor I, first of a series of spacecraft designed to span the gap between *Ranger* flights and Project *Apollo*, completed a three-day flight June 1 with a soft landing on the Moon. On June 16, when lunar sunset occurred, *Surveyor I* had received approximately 100,000 commands and transmitted 10,338 pictures of itself and its immediate environment.

Six additional *Surveyor* Series A-21 launches will be attempted at preselected sites to extend knowledge of lunar conditions, and determine suitability of sites for proposed *Apollo* landings.

Hughes Aircraft Company's (HAC) Space Systems Division is under contract to fabricate the next six *Surveyors*, each of which is scheduled to be launched by a combination *Atlas/Centaur* vehicle provided by General Dynamics/Convair. JPL's Deep Space Network and Missions Operations System will be used to control, command, and track the spacecraft.

It is presently anticipated that the second *Surveyor* launching will take place during the third quarter of 1966.

A major portion of the following information in this publication was derived from material prepared by HAC. Remaining material, prepared by JPL technical sections, is identified by footnotes to the article titles.

Principal *Surveyor* model designations and vehicles discussed herein are described in Table 1.

Table 1. Model and vehicle designations

Designation	Description
SC-1—7	Flight spacecraft with engineering payload
A-21	Model designation for spacecraft with engineering payload (SC-1—7)
A-24	Model designation for spacecraft with scientific payload
T-21	Model A-21 prototype system test spacecraft
T-2N-1, -2	Test vehicles for T-2N descent dynamics test program
S-2	Test spaceframe for vibration, shock, and static structural tests
S-6, -7	Test spaceframe for vernier propulsion system tests
S-9	Structural test model
S-10	Temperature control model

UNCLASSIFIED
CONFIDENTIAL

UNCLASSIFIED
CONFIDENTIAL

B. System Engineering

1. Surveyor 1 *Mission*

Surveyor I (SC-1) was launched on *Atlas/Centaur-10* (AC-10) from pad 36A at Cape Kennedy May 30, 1966. The launch trajectory was nearly perfect. A midcourse trajectory correction was performed successfully. The spacecraft soft-landed on the Moon June 1, 63 hr and 36 min after launch, 23:17 Pacific Daylight Time (PDT). The landing location was 2.36 deg south latitude and 43.36 deg west longitude, within 9 mi of the aim point. Telemetry was received continuously from the spacecraft during touchdown. The television camera was placed in operation a few minutes after the landing; thousands of excellent quality pictures have since been received. The

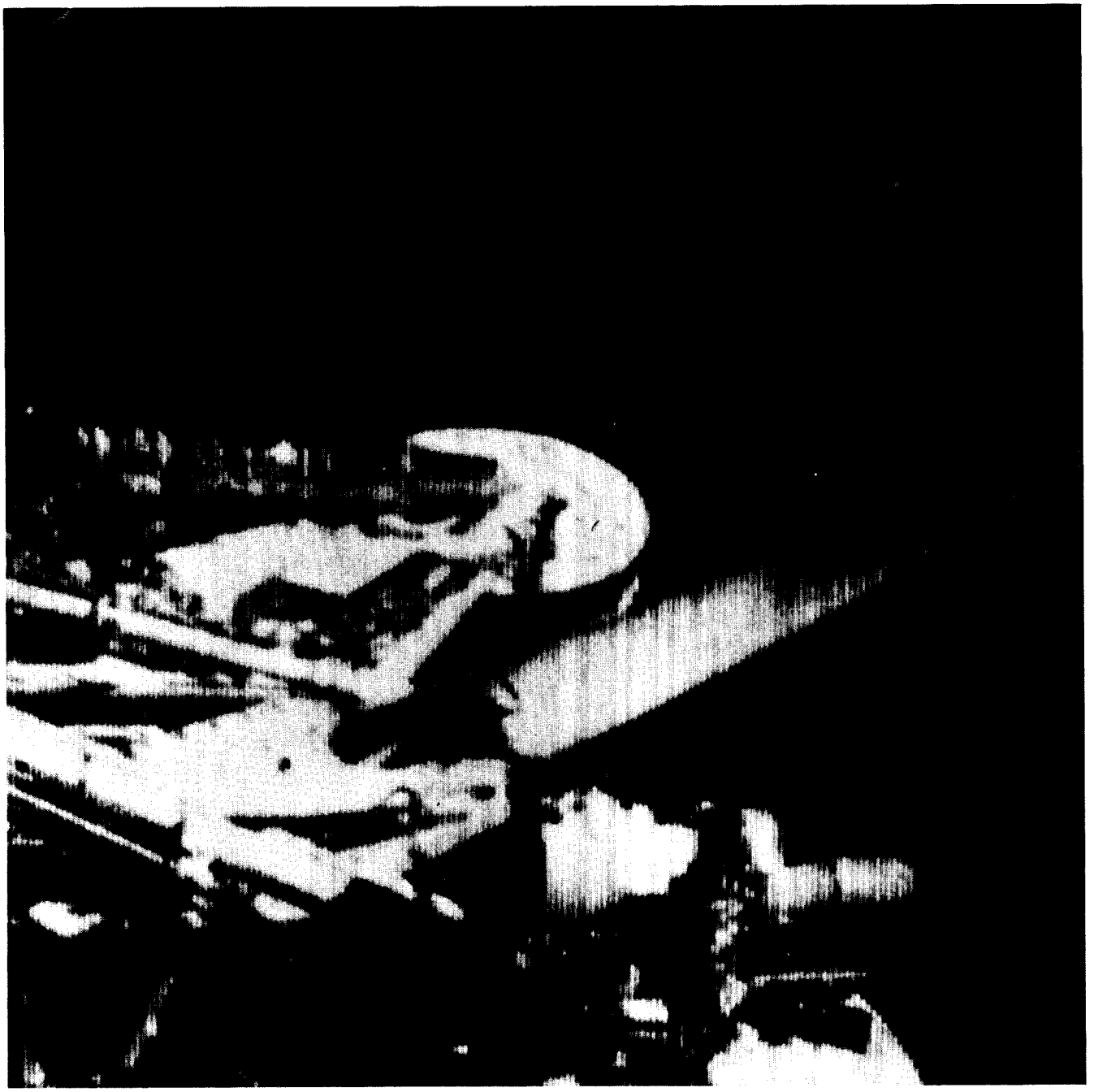

Fig. 1. First photograph transmitted from *Surveyor 1* 35 min after lunar touchdown (200 line scan)

UNCLASSIFIED
CONFIDENTIAL

UNCLASSIFIED
CONFIDENTIAL

spacecraft performed as designed throughout the 12 Earth days remaining after landing, until lunar nightfall. At the close of the report period, SC-1 is into the second Earth day of the lunar night.

Pictures returned from the spacecraft are shown in Figs. 1 through 4.

A listing of the major mission events is given in Table 2, and a complete event history including all 288 commands sent to the spacecraft during transit is given in Table 3. Each mission phase is briefly described below.

a. Launch injection and separation. The boost phase was normal and resulted in SC-1 being injected on a

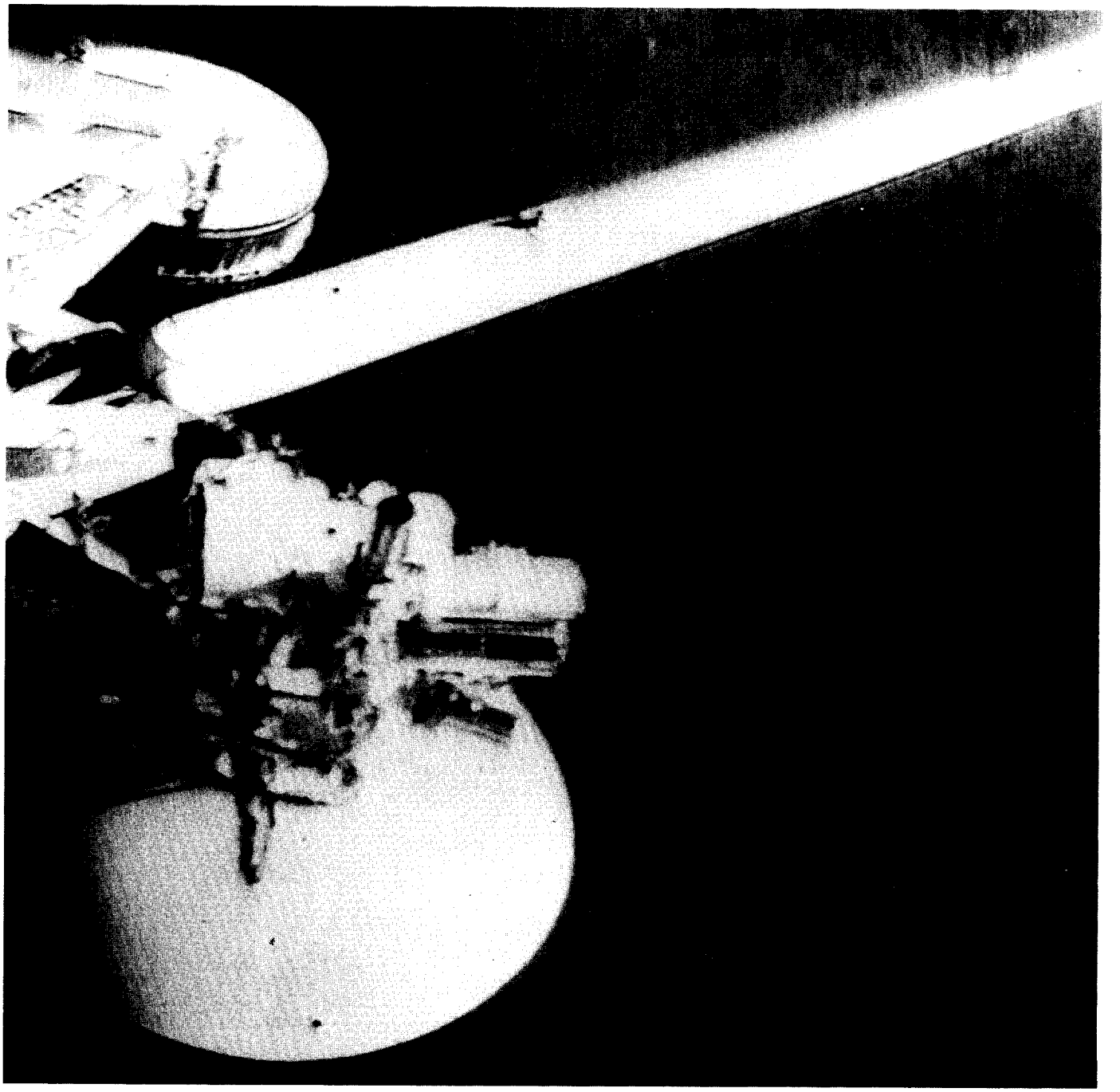

Fig. 2. *Surveyor 1* footpad and imprint created by impact (600 line scan)

UNCLASSIFIED
CONFIDENTIAL

UNCLASSIFIED CONFIDENTIAL

Fig. 3. Composite photograph showing 6 x 18 in. lunar rock approximately 12 ft from the spacecraft

UNCLASSIFIED CONFIDENTIAL

UNCLASSIFIED
CONFIDENTIAL

trajectory that insured a landing in the near vicinity of the target area. Just prior to its separation from the spacecraft, *Centaur* issued the preprogrammed commands for accomplishing spacecraft operations required for the postseparation phase, namely, extend landing gears at launch + 11 min 55.5 sec (L+11M55.5S), extend omni-antennas at L+12M5.7S, and transmitter high power on at L+12M25.4S. Normal response to the first and third commands was verified from telemetry received by the down-range ships, but only omnidirectional antenna B extension in response to the second command was confirmed (i.e., telemetry indicated that omnidirectional

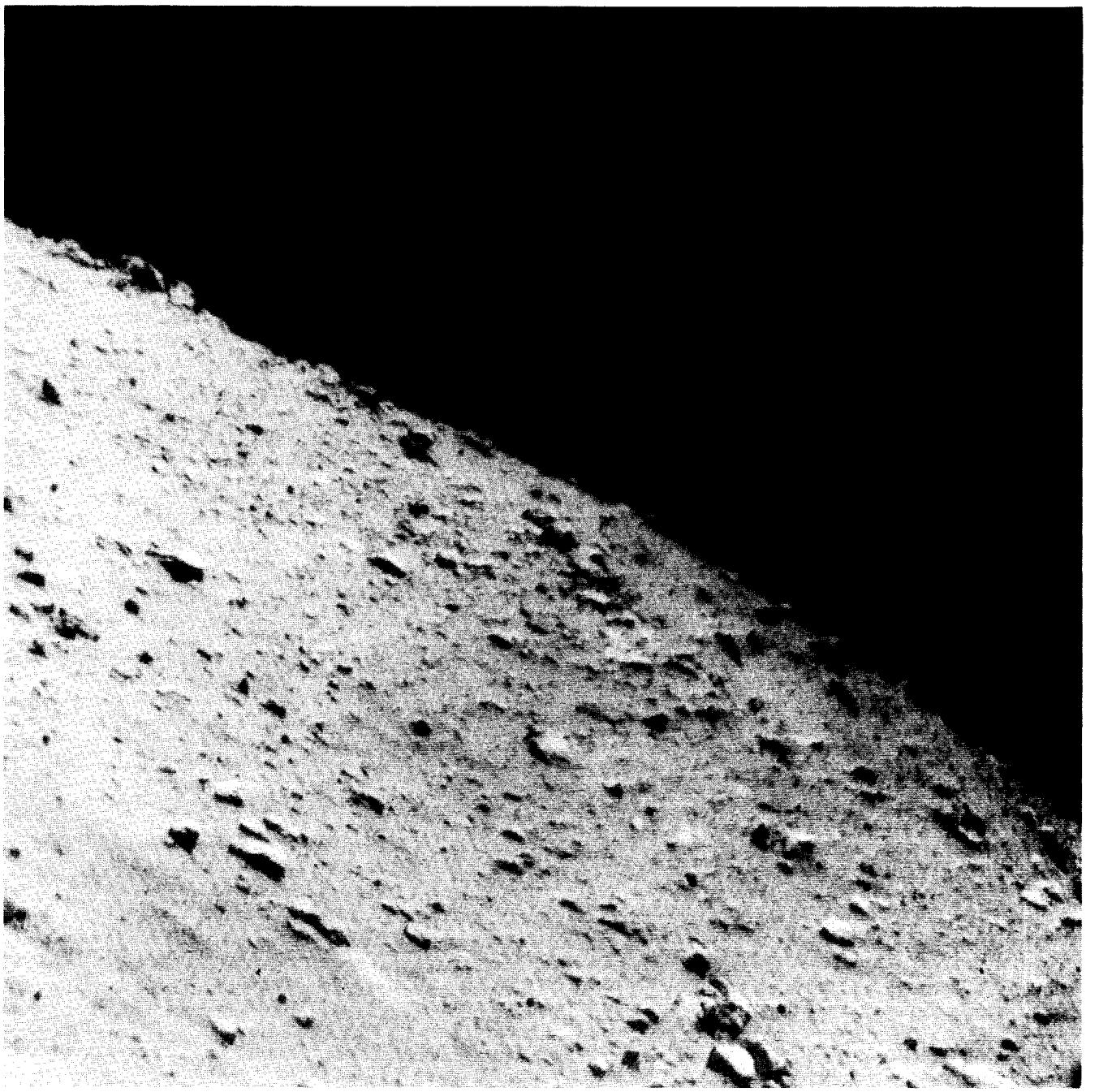

Fig. 4. Boulder strewn lunar surface looking slightly south of east (distance from camera to horizon is estimated at several hundred yards)

UNCLASSIFIED
CONFIDENTIAL

UNCLASSIFIED

Table 2. SC-1 mission milestones

Event	Date	PDT
Launch	May 30, 1966	7:41:01
Injection		7:52:30
Separation		7:53:38
Automatic Sun acquisition completed		8:00:34
Automatic solar panel deployment completed		8:03:20
Spacecraft visibility at Johannesburg began		8:04:31
Initial Deep Space Instrumentation Facility (DSIF) acquisition (two-way lock) completed		8:08:41
First ground command sequence initiated		8:20:42
Canopus verification started		11:53:39
Canopus acquisition completed		12:13:20
First premidcourse attitude maneuver initiated		23:30:13
Midcourse thrust executed		23:45:03
Sun reacquired		23:54:51
Canopus reacquired	May 31, 1966	00:00:55
First terminal descent attitude maneuver initiated	June 1, 1966	22:36:46
Retrorocket thrust direction properly positioned		22:43:47
Altitude marking radar (AMR) mark generated		23:14:41
Vernier engine ignition		23:14:48
Retrorocket engine ignition		23:14:49
Retrorocket separation		23:15:40
Radar control initiated		23:15:42
Touchdown		23:17:36

antenna A had not extended). Separation was initiated by *Centaur* at L+12M32.3S and was accomplished satisfactorily at L+12M37S.

Following separation, the spacecraft executed the automatic sequences as designed. By using its cold-gas jets, which were then enabled, the flight control subsystem nulled out the rotational rates imparted by the separation springs and initiated a roll-yaw sequence to acquire the Sun. At L+19M33S, after a minus roll of approximately 100.5 deg and a plus yaw of 86 deg, acquisition and lockon to the Sun by the spacecraft Sun sensors were complete. Concurrently with the Sun acquisition sequence, the antenna/solar panel positioner (A/SPP) initiated its solar panel axis and roll axis deployment, and at L+22M the solar panel was in its proper transit position. All these operations were confirmed in real time by telemetry received by the downrange ships.

b. Deep Space Instrumentation Facility acquisition. At approximately L+24M, the spacecraft became visible to DSS 51 (Johannesburg), and the initial DSIF acquisition procedure for establishing the communication and tracking link between the spacecraft and the ground station was initiated. In less than 4 min (L+27M40S), acquisition was completed when two-way lock was established.

The first ground controlled sequence (initial spacecraft operations) was initiated at approximately L+40M. It consisted of commands for turning off equipment required only for the launch-to-DSIF acquisition phase (transmitter high power off, accelerometer amplifiers off, etc.), seating the solar panel and roll axis locking pins securely (i.e., commands for rocking the axis back and forth), increasing the telemetry bit rate to 1100 bits/sec and initially interrogating all telemetry commutator modes so that the spacecraft overall condition could be assessed. All spacecraft responses to commands were normal. However, the telemetry still indicated that omnidirectional antenna A was not extended. An attempt was made to command the extension of omnidirectional antenna A at L+1H40M, but the spacecraft did not respond. Since the spacecraft was using omnidirectional antenna B, and the spacecraft-to-DSS vector was located on the best part of this antenna pattern, there was no need to use omnidirectional antenna A.

c. Coast Phase I (including Canopus acquisition). The spacecraft continued to coast normally with its pitch-yaw attitude controlled to track the Sun and with its roll axis held inertially fixed. Tracking and telemetry data were being obtained by use of transponder B and transmitter B operating in low power.

At L+4H9M a roll sequence was initiated for making a star map and for acquiring Canopus in order to fix the roll attitude to a precise position from which the midcourse maneuvers could be iniated. During the first revolution of the maneuver, star intensity signals from seven stars (Merak, Regulus, Alpha Hydrae, Naos, Tau Puppis, Markab, and Alderamin), in addition to Canopus, were identified, with Canopus being observed and identified after 220 deg of roll. It was also noticed that a Canopus lockon signal was not obtained as the star sensor swept past Canopus, since the Canopus intensity signal was above the upper threshold of the lockon range. As the vehicle continued to roll, the time for sending the proper command to achieve manual lockon to Canopus (when the vehicle rolled around to the proper position) was computed. This command was sent at the computed time, and manual lockon was achieved at L+4H32M.

UNCLASSIFIED

UNCLASSIFIED
CONFIDENTIAL

Table 3. Summary of transit phase events

Mission phase: launch to separation				
Time		Command sequence		Event
Mission (time after launch)	Greenwich mean time (GMT)[a]	Major	Minor	
	14:41:01 (5/30/66)			Launch
11M56S	14:52:57			Extend landing gears commanded by *Centaur*
12M06S	14:53:07			Extend omniantennas commanded by *Centaur*
12M25S	14:53:26			Transmitter high voltage on commanded by *Centaur*
12M32S	14:53:33			Spacecraft/*Centaur* electrical disconnect
12M37S	14:53:38			Separation
16M49S	14:57:50			Sun acquisition cell illuminated after 100.5-deg roll
18M19S	14:59:20			Solar panel locked in transit position
19M33S	15:00:34			Sun lockon achieved (primary Sun sensor cell illuminated after 82-deg yaw)
22M19S	15:03:20			Roll axis locked in transit position
27M59S	15:09:00			Initial DSIF acquisition completed (two-way lock)
Mission phase: DSIF acquisition through star acquisition				
		0040		Initial spacecraft operations
39M58S	15:20:59		0552	(1) Turn off transmitter high power
			0050	(2) Turn off basic bus accelerometer amplifiers and solar panel deployment logic
			0454	(3) Rock solar panel back and forth to seat locking pin
46M56S	15:27:55		0455	(4) Rock roll axis back and forth to seat locking pin
53M14S to 1H46M56S	15:34:15 to 15:56:04		0051, 0052, 0055, 0251, 0056, 0550	(5) Perform interrogation of all engineering signal processor data modes at 1100 bps
1H40M20S to 1H45M07S	16:21:21 to 16:26:08	Nonstandard sequence for attempting to extend omnidirectional antenna A	0601 sent 6 times	Attempt to extend omnidirectional antenna A by ground command
				Star verification/acquisition
3H50M53S	18:31:54	0247	0250, 0251, 0252	(1) 1100 bits/sec engineering interrogation of modes 4, 2, and 1
4H01M20S	18:42:21	0247	0652, 0653	(2) Transmitter high power turnon prior to star verification (high voltage on at 18:44:24 GMT)
4H08M33S	18:49:34	Unscheduled sequence for selecting coast mode commutator for use in star verification to obtain additional telecommunication telemetry data for possible confirmation of omnidirectional antenna A failure to extend	0550	(3) Selection of coast mode commutator

UNCLASSIFIED
CONFIDENTIAL

UNCLASSIFIED

Table 3. Summary of transit phase events (Cont'd)

Time		Command sequence		Event
Mission (time after launch)	Greenwich mean time (GMT)[a]	Major	Minor	
Mission phase: DSIF acquisition through star acquisition				
4H09M43S	18:50:44	0642	0654	(4) Execution of positive roll (roll began at 18:53:39 GMT)
4H32M19S	19:13:20	Unscheduled sequence	Commands 0704, 0716	(5) Manual star lock achieved
4H40M03S	19:21:04	0044		(6) Return to low-power operation
Mission phase: coast phase I				
6H13M01S to 9H10M09S	20:54:02 to 23:51:10	0342	0354, 0054	Gyro drift check
10H57M18S	01:38:19 (5/31/66)	0141	0151	Bit rate reduction from 1100 bits/sec to 550 bits/sec
11H59M00S to 12H06M08S	02:40:01 to 02:47:09	0447	0250, 0251, 0550	Low-power engineering interrogation of modes 4 and 2
13H33M04S to 13H37M02S	04:14:05 to 04:20:03	0247	0250, 0251, 0252	Engineering interrogation at 1100 bits/sec made with low power
13H45M03S to 13H49M16S	04:26:04 to 04:30:17	0341	0350, 0351, 0215	Gyro speed check and return to 550 bits/sec telemetry data
13H52M36S to 13H52M43S	04:33:37 to 04:33:44	0546	0550	Return to coast mode commutator data
14H14M35S	04:55:36	Nonstandard command to manually lock on star	0716	Achieve manual lockon to Canopus to null out star error signal prior to midcourse execution
Mission phase: midcourse correction				
15H20M14S to 15H25M45S	06:01:15 to 06:06:46	0247	0250, 0251, 0252	Midcourse correction sequence (1) Engineering interrogation of modes 4, 2, and 1 at 1100 bits/sec conducted with transmitter low power
15H25M45S	06:06:46	0247	0652, 0653	(2) Turnon of high power transmitter (high voltage on at 06:08:25 GMT)
15H29M22S	06:10:23	0440	0253	(3) Increase telemetry rate from 550 to 4400 bits/sec
15H38M07S	06:19:08	0740	0750	(4) Pressure vernier system (helium)
15H39M22S	06:20:23	1140	1150	(5) Command desired roll maneuver magnitude and direction (minus roll of 86.5 deg)
15H49M12S	06:30:13	1140	1251	(6) Execute roll
15H53M13S	06:34:14	1141	1151	(7) Command desired yaw maneuver magnitude and direction (minus yaw of 57.99 deg)
15H53M47S	06:34:48	1141	1253	(8) Execute yaw
15H57M03S	06:38:05	0741	0751	(9) Propulsion strain gauge powered
15H58M06S	06:39:07	0741	0157	(10) Unlock engine 1 to permit roll control
16H02M04S	06:43:05	0741	0752	(11) Thrust phase power on

UNCLASSIFIED

UNCLASSIFIED
CONFIDENTIAL

Table 3. Summary of transit phase events (Cont'd)

Time		Command sequence		Event
Mission (time after launch)	Greenwich mean time (GMT)[a]	Major	Minor	
Mission phase: midcourse correction				
16H02M41S	06:43:42	0741	0753	(12) Command desired thrust duration (20.8 sec)
16H04M02S	06:45:03	0742	0754	(13) Execute midcourse thrust
16H04M25S	06:45:26		0737	(14) Turn off thrust phase power
16H05M21S	06:46:22		0754	(15) Turn off propulsion strain gauge power
16H08M01S to 16H09M36S	06:49:02 to 06:50:37	Unscheduled sequence to obtain coast phase commutator data at 550 bits/sec during reverse maneuvers	0503, 0204, 0220, 0215, 0232, 0506	(16) Operations to obtain coast mode data at 550 bits/sec (for obtaining receiver A antenna gain control data in an attempt to verify condition of omnidirectional antenna A)
16H10M45S	06:51:46	1240	1252	(17) Command reverse yaw maneuver magnitude and direction (plus 57.99 deg)
16H11M54S	06:52:55	1240	1253	(18) Execute yaw (Sun reacquired at 06:54:51 GMT)
16H16M03S	06:57:04	1244	1250	(19) Command reverse roll maneuver magnitude and direction (plus 85.5 deg)
16H47M01S	06:58:02	1244	1251	(20) Execute roll (Canopus reacquired at approximately 07:00:55 GMT)
16H23M29S to 16H30M52S	07:04:30 to 07:11:53	1245	0051	(21) Postmidcourse engineering interrogation of modes 1, 2, and 4
16H31M42S	07:12:43	0547	0552	(22) Return to transmitter low-power operation
16H45M38S	07:26:39	Unscheduled sequence to insure turn off auxiliary accelerometer amplifier and touchdown strain gauge power	0512, 0516	(23) Sequence to turn off auxiliary accelerometer amplifier and touchdown strain gauge power (if they were inadvertently turned on when propulsion strain gauge power on was commanded)
Mission phase: coast phase II				
17H51M01S	08:32:02	0447	0250, 0251, 0550	Low-power interrogation of modes 4 and 2 to obtain thermal data
18H49M13S to 21H49M15S	09:30:14 to 12:30:16	0342, 0343	0354, 0054	Gyro drift check
22H55M16S	13:36:17	Unscheduled sequence	0702	Start drift check of roll axis only
25H32M27S to 25H46M20S	16:13:28 to 16:27:41	0447	0250, 0251, 0550	Low-power interrogation of modes 4 and 2 to obtain thermal data
29H51M41S to 30H02M43S	20:32:42 to 20:43:44	0447	0250, 0251, 0550	Low-power interrogation of modes 4 and 2 to obtain thermal data
32H56M37S	23:37:38	Unscheduled sequence	0716, 0702	Terminate roll drift check and null out accumulated error produced by drift
37H24M54S to 37H30M53S	04:05:55 to 04:11:54 (6/1/66)	0447	0250, 0251, 0550	Low-power interrogation

UNCLASSIFIED
CONFIDENTIAL

UNCLASSIFIED
CONFIDENTIAL

Table 3. Summary of transit phase events (Cont'd)

Time		Command sequence		Event
Mission (time after launch)	Greenwich mean time (GMT)[a]	Major	Minor	
Mission phase: coast phase II				
37H37M38S to 39H34M56S	04:18:39 to 06:25:57	0342	0354	Gyro drift check for pitch and yaw gyros; roll gyro drift check allowed to continue
39H50M16S	06:31:17	Unscheduled sequence	Command 0601	Attempt to extend omnidirectional antenna A
Mission phase: coast mode II				
40H53M14S to 43H11M58S	07:34:15 to 09:52:59	0342	0354 plus commands 0702, 0716	Gyro drift check (roll gyro drift check also terminated)
43H14M41S	09:55:42	Unscheduled sequence	0354	New gyro drift check initiated
43H17M44S to 43H26M22S	09:58:45 to 10:07:23	0447	0250, 0251, 0550	Low-power interrogation of modes 4 and 2
45H05M33S to 45H36M56S	11:46:34 to 12:17:57	1741	2053	Start power mode cycling remaining in auxiliary battery mode to check rate of temperature rise of auxiliary battery
45H36M56S	12:17:57	1741	2053	High current mode on—both batteries directly on line
45H56M57S	12:37:58	1341	1350	Vernier tanks' thermal control on
46H24M02S	13:05:03	Unscheduled sequence	Command 0702	Terminate yaw and pitch gyro drift check, but allow roll check to continue
49H06M13S	15:47:14	Unscheduled sequence	Command 0317	Return to auxiliary battery mode to increase rate of temperature rise of auxiliary battery
49H07M19S to 49H21M36S	15:48:20 to 16:02:37	0447	0250, 0251, 0550	Low-power interrogation of modes 4 and 2
49H48M44S to 49H53M17S	16:29:45 to 16:34:18	1742	2054	Power mode cycling, with return to auxiliary battery (to insure proper auxiliary battery temperature rise)
52H03M15S to 52H20M19S	18:44:16 to 19:01:20	0447	0254, 0251, 0550	Low-power interrogation of modes 4 and 2
52H34M13S	19:15:14	Unscheduled sequence	Command 0716	Terminate roll gyro drift check and null accumulated error
52H39M42S	19:20:43	Unscheduled sequence (0342)	Command 0700	Begin new gyro drift check
55H00M50S	21:41:51	Unscheduled sequence	Command 0702	Terminate yaw and pitch drift check and null out accumulated error
56H38M52S to 56H54M06S	23:19:53 to 23:35:07	0447	0250, 0251, 0550	Low-power interrogation of modes 4 and 2
57H29M40S to 57H43M03S	00:10:41 to 00:24:04 (6/2/66)	1742	2054	Power mode cycling, with return to auxiliary battery mode (to insure proper auxiliary battery temperature rise)

CONFIDENTIAL
UNCLASSIFIED

UNCLASSIFIED
CONFIDENTIAL

Table 3. Summary of transit phase events (Cont'd)

Mission phase: coast mode II				
Time		Command sequence		Event
Mission (time after launch)	Greenwich mean time (GMT)[a]	Major	Minor	
58H35M41S	01:16:42	1740	1750	Turn on survey TV electronic thermal control power
58H41M59S	01:23:00	Unscheduled sequence	0320	Restore main battery, placing both batteries on line in preparation for terminal descent
59H10M22S	01:51:23	Unscheduled sequence	Command 0716	Terminate roll gyro drift check and null accumulated error
59H14M23S to 59H19M22S	01:55:24 to 02:00:23	0446	0250	Low-power interrogation of mode 4 only
60H26M59S to 60H35M53S	03:08:00 to 03:16:54	0446	0250	Low-power interrogation of mode 4 only
61H14M23S to 61H20M06S	03:55:24 to 04:01:07	0247	0250, 0251	Engineering interrogation of modes 4, 2, and 1 (accomplished with low power at 550 bits/sec
61H24M41S to 61H28M14S	04:05:42 to 04:09:15	0344	0550, 1050, 1053	VCXO check
	No time confirmation (communication line out)	Special sequence	Command 1133	Vidicon temperature control on survey camera
Mission phase: terminal descent				
				Terminal descent
62H37M06S to 62H44M36S	05:18:07 to 05:25:37	1646	0250, 0652, 0653, 0255, 2057, 0056, 0252	(1) Interrogation of modes 4, 2, and 1 and turn on of high-power transmitter (at 05:20:18 GMT) and adjustment of telemetry rate to 1100 bits/sec (at 05:21:27); summing amplifiers off (to turn off presumming amplifier) and turn on of phase summing amplifier
62H44M36S	05:25:37	1345	1755	(2) Propulsion strain gauge power turned on
62H45M13S	05:26:14	1345	1756	(3) Touchdown strain gauge power and subcarrier oscillators turned on
62H48M46S to 62H51M08S	05:29:47 to 05:32:09	1040	1050	(4) Transponder power turned off and one-way lock achieved
62H51M08S	05:32:09	1144	1154	(5) Roll maneuver magnitude and direction commanded (plus 89.3 deg)
62H55M45S	05:36:46	1144	1251	(6) Execute roll
62H59M43S	05:40:44	1145	1155	(7) Yaw magnitude and direction commanded (plus 59.9 deg)
63H00M46S	05:41:47	1145	1253	(8) Execute yaw (retro rocket thrust direction aligned properly at approximately 05:43:47 GMT)
63H03M28S	05:44:29	1147	1157	(9) Roll maneuver magnitude and direction commanded (plus 94.1 deg)
63H04M16S	05:45:17	1147	1257	(10) Roll executed

UNCLASSIFIED
CONFIDENTIAL

Table 3. Summary of transit phase events (Cont'd)

Mission phase: terminal descent				
Time		Command sequence		Event
Mission (time after launch)	Greenwich mean time (GMT)[a]	Major	Minor	
63H09M22S	05:50:23	1640	1751, 1656	(11) Vernier thrust level (200 lb) for retro rocket phase and delay between AMR mark and vernier ignition (7.825 sec) commanded
63H19M33S	06:00:34	1644	0251	(12) Command on mode 2 data
63H25M26S	06:06:27	1644	1657	(13) Retrorocket sequence mode on commanded
63H25M51S	06:06:52	1644	1752	(14) Vernier lines and tanks thermal control commanded off
63H28M56S	06:09:57	1644	1753	(15) AMR on
63H29M56S	06:10:57	1644	1754	(16) Thrust phase power on
63H31M56S	06:12:57	1644	2051	(17) AMR enabled
63H33M37S	06:14:38	1644	2052	(18) Backup AMR mark commanded
63H33M39.7S	06:14:40.7[b]			(19) AMR mark
63H33M47.6S	06:14:48.6[b]			(20) Vernier ignition
63H33M48.65S	06:14:49.65[b]			(21) Retro rocket ignition
63H33M49.2S	06:14:50.2[b]			(22) Radar altimeter and doppler velocity sensor (RADVS) on
63H34M19S	06:15:20[b]			(23) Reliable operate doppler velocity sensor (RODVS)
63H34M28S	06:15:29[b]			(24) Reliable operate radar altimeter (RORA)
63H34M27.85S	06:15:28.85[b]			(25) Retro rocket burnout
63H34M40S	06:15:41[b]			(26) Retro rocket eject
63H34M41S	06:15:42[b]			(27) Retro rocket separation
63H34M43S	06:15:44[b]			(28) Enable doppler control
63H34M43S	06:15:44[b]			(29) Beam 3 loses lock
63H34M45S	06:15:46[b]			(30) Beam 3 regains lock
63H35M00S	06:16:01	1644	0056	(31) Mode 3 commanded
63H35M01S	06:16:02	1644	1252	(32) Presumming amplifier on commanded (to get touch-down strain gauge data)
63H36M15S	06:17:16[b]			(33) 1000-ft mark
63H36M28S	06:17:29[b]			(34) 10-ft/sec mark
63H36M34S	06:17:35[b]			(35) 14-ft mark
63H36M36S	06:17:37[b]			(36) Touchdown indicated by retro rocket accelerometer (Note: could be off by 0.5 sec owing to commutation delay)

[a]Subtract 7 hr from GMT values to obtain PDT.
[b]Time telemetry data were received in performance analysis area at Space Flight Operations Facility (SFOF) (i.e., includes transit time from spacecraft to ground, SFOF processing delay, and commutation delay).

The vehicle continued to coast as before, but with its roll attitude controlled so that the star sensor remained locked on Canopus. During this coasting phase, which continued until the execution of the midcourse correction sequence, continuous telemetry was received from the spacecraft at 1100 bits/sec until approximately L+11H, and at 550 bits/sec subsequently. Three engineering interrogations (including the two interrogations scheduled for transmitter high power), plus a 3-hr check of the drift of the three gyros, were performed during this period of low-power transmitter operation. All subsystem performances were satisfactory.

UNCLASSIFIED

d. Midcourse correction. All midcourse operations were performed normally. With the spacecraft visible to and controlled by DSS 11 (Goldstone), the maneuver sequence for applying the midcourse thrust in the proper direction was initiated with the first maneuver, a minus roll of 86.5 deg, starting at L+15H49M. The second maneuver, a minus yaw of 57.9 deg, was executed at L+15H54M. With the vehicle thrusting direction now positioned properly, the midcourse thrust was applied by igniting the vernier engines and controlling their thrust to achieve a constant spacecraft acceleration of 0.1*g* for 20.8 sec. Analog recorder data verified that the thrust duration was correct (i.e., time actually measured was 20.75 sec, which is well within the accuracy of the recorder).

Following the midcourse thrusting, the reverse maneuvers were performed successfully, with the Sun and Canopus sensors being illuminated properly, which confirmed that the gyros had retained their inertial reference during the vernier engine shutdown, and the need for performing a postmidcourse star verification was eliminated.

Spacecraft injection accuracy, midcourse correction, and resulting landing point accuracy are summarized in the following table, which shows: (1) lunar latitude and longitude for initial aim point; (2) unbraked impact point, if no midcourse correction were made; (3) revised aim point for which the midcourse correction was computed; and (4) actual landing point, as determined from postmidcourse orbit determination.

	Latitude, deg S	*Longitude, deg W*
Initial aim point	3.25	43.83
Uncorrected impact point	11.43	54.25
Final aim point	2.33	43.83
Actual landing point	2.36	43.36

In terms of miss, the spacecraft injection errors would have resulted in only a 264-mi miss on the Moon. After midcourse correction, the miss was less than 9 mi.

e. Coast Phase II. The postmidcourse coasting phase (coast phase II) continued until terminal descent maneuvers were initiated. Throughout this period, a telemetry rate of 550 bits/sec was obtained, and during this interval, five additional gyro drift measurements and ten engineering interrogations were made. The results of the gyro drift measurements were consistent and indicated that the drift of all gyros was below their specified upper limit. Interrogations confirmed that the temperature data channels not being sampled continuously were indicating normal performance.

Also during coast phase II, power mode cycling checks were made to help predict the percentage of the electrical load that would be supplied by each of the spacecraft batteries (main and auxiliary) during the terminal descent when both batteries are connected directly to the bus. To insure that the auxiliary batteries would be at the desired temperature of $>60°F$ at the time of terminal descent, a slight change, which called for placing both batteries directly on the line following these checks, was made in the procedure. The auxiliary battery was used to supply most of the load (auxiliary battery mode) so that its rate of temperature rise would be increased from 1 to 2 deg/hr to 3 deg/hr.

f. Terminal descent. The terminal descent sequence was initiated at L+62H37M with the turnon of the high-power transmitter and the performance of the last engineering interrogation. Three attitude maneuvers were then performed, the first two for orienting the retrorocket engine thrust direction properly and the last maneuver for insuring optimum telecommunication performance during the retrorocket and vernier descent sequences. The first maneuver (+ roll of 89.3 deg) was executed at L+62H56M, and the second maneuver (+ roll of 94.1 deg) was executed at L+63H4M.

The AMR was turned on at L+63H29M and was enabled at L+63H32M. Except for two commands: turn on of touchdown strain gauge data and establish optimum sampling rate for the flight control telemetry data, the remaining operations were automatically performed by the spacecraft.

The automatic descent sequence was initiated by the AMR; generation of the mark was confirmed on the ground at L+63H33M40S. The automatic sequence of events (including vernier ignition, retrorocket ignition, radar altimeter and doppler velocity sensor (RADVS) on, retrorocket burnout and separation, enable doppler control, 1000-ft mark, 10 ft/sec mark, and 14-ft mark) occurred normally as indicated in Table 3. Quick-look analysis of the telemetry indicates that touchdown occurred between 1 and 2 sec following the occurrence of the 14-ft mark at approximately L+63H36M36S. Confirmation of the soft landing was provided by the DSIF receiver retaining its lockon to the spacecraft transmitter signal and by the low magnitude of the force telemetered by the shock absorber strain gauges (<1600 lb indicating touchdown velocities on the order of 10 ft/sec).

UNCLASSIFIED

g. Summary of anomalies. The only significant spacecraft anomaly in the transit phase of the mission was the failure of the omnidirectional antenna A mechanism. Either the omnidirectional antenna boom had not deployed at *Centaur* separation as it should have, or it had deployed and the lock and indicator mechanism had not functioned. Preliminary analysis of antenna pattern data during the mission indicates that the boom most likely did not deploy. In either event, sometime during the landing phase, probably either at retrorocket ignition or at touchdown, the boom extended and the lock indication came on. The time of this event cannot be determined as the lock indication telemetry is not on the commutator modes used during terminal descent. This failure gave very little trouble throughout the mission as all objectives were met using omnidirectional antenna B. The center of gravity effects of having omnidirectional antenna A in the wrong position were significant, but small enough to be acceptable.

Just prior to the initiation of the premidcourse maneuver, there was a short duration transient on the Canopus error signal. This occurred (75 sec) after the vernier system pressurization squib was blown. The timing is such that this transient was very likely caused by a particle released by the squib and passed through the Canopus field of view. It had no effect on the mission.

A third anomaly occurred during lunar operations. On June 12 a loss of television mirror deviation position telemetry occurred at one elevation position. On subsequent stepping, the mirror did respond, and the telemetry was once again obtained, thus indicating that the failure was a bad spot on the elevation position readout potentiometer. This anomaly did not impede the taking of television pictures in any way.

h. Spacecraft performance parameters. Based on real time analysis and preliminary postmission analysis, a summary of some significant spacecraft performance parameters is given in Table 4. These parameters are not complete and are quite preliminary and, therefore, subject to change.

Table 4. Summary of significant spacecraft performance parameters

Parameter	Value	Comments
Launch to injection phase		
Launch time	Day 150—1441 GMT	Window opened at 1440 GMT
Launch azimuth	(May 30 at 0741 PDT) 102.285 deg	for 102-deg launch azimuth
Maximum spacecraft static acceleration during boost	To be determined	
Maximum spacecraft dynamic acceleration during boost	0.1 to 0.4 *g* rms with a >10-*g* spike of insulation panel jettison and *Atlas/Centaur* separation	
Spacecraft angular rates at separation	Data not currently available	
Time required to null separation rates		
Angular motion during rate stabilization		
Roll		
Pitch		
Yaw		
Acquisition phase		
Solar panel deployment time	10 min 16 sec	Expected nominal—9 min 40 sec
Sun acquisition time	6 min 10 sec from separation	Maximum expected of 15 min
Required maneuvers to acquire Sun		
Roll	≈−100 deg	
Yaw	≈+86 deg	
Time from first predicted visibility to DSS 11		
One-way tracking	−11 sec	
Two-way tracking	4 min 10 sec	
Transmission of first command	16 min 28 sec	
Time of initiation of Canopus acquisition	150—18-53-39 GMT (L+4H 12M)	
Canopus telemetry intensity indication	To be determined	Nominal should be 1.5 by Canopus owing to the Sun channel filter change

UNCLASSIFIED

UNCLASSIFIED

Table 4. Summary of significant spacecraft performance parameters (Cont'd)

Parameter	Value	Comments
Coast phases		
Attitude orientation accuracy		
Maximum error from Sun line	To be determined	
Maximum error from Canopus (when tracking)	To be determined	
Gas jet limit cycle parameter		
Average amplitude—roll	0.44-deg peak to peak	
Average amplitude—pitch	0.31-deg peak to peak	
Average amplitude—yaw	0.37-deg peak to peak	
Average period—roll	340 sec	
Average period—pitch	250 sec	
Average period—yaw	220 sec	
Gyro drift measurements (range)		
Roll	+0.08 to +0.30 deg/hr	
Pitch	+0.07 to −0.02 deg/hr	
Yaw	+0.64 to +0.9 deg/hr	
Midcourse correction phase		
Midcourse maneuver angles		
Roll	−86.5 deg	−86.5 deg commanded
Yaw	−57.9 deg	−57.9 deg commanded
Midcourse engine burn time	20.8 sec	20.8 sec commanded
Acceleration during burning	3.21 ft/sec^2	0.10 g (3.21 ft/sec^2) designed
Vernier propellant used	16.8 lb	
Time of vernier engine ignition	L+16H 45M 3S	
Peak attitude transients at ignition		
Roll	−0.1 deg	
Pitch	−0.15 deg	
Yaw	−0.15 deg	
Mean attitude error during burning		
Roll	0.2 deg	
Pitch	+0.15 deg	
Yaw	0.06 deg	
Peak attitude transients at shut down		
Roll	+0.7 deg	
Pitch	−0.6 deg	
Yaw	−1.9 deg	
Roll actuator position		
Peak at ignition	+0.7 deg	0.6 deg predicted based on bracket bending
Mean during burning	0.4 deg	
Terminal descent phase		
Terminal descent maneuvers		
Roll	+89.3 deg	+89.3 deg commanded
Yaw	+59.9 deg	+59.9 deg commanded
Roll	+94.1 deg	+94.1 deg commanded
Time of initiation of first maneuver	38 min before AMR mark time	
Gyro drift compensation incorporated in terminal maneuvers		
Roll	+0.2 deg/hr	
Pitch	0	
Yaw	+0.75 deg/hr	
Spacecraft roll orientation at touchdown	+X axis 88 deg clockwise from east	
Approach angle (velocity vector to lunar vertical)	5.95 deg	
AMR marking altitudes	95.45 km (59.6 mi)	
Main retrorocket burning time (from ignition to 3.5 g switch)	38–39 sec	38.5 predicted

UNCLASSIFIED

UNCLASSIFIED CONFIDENTIAL

Table 4. Summary of significant spacecraft performance parameters (Cont'd)

Parameter	Value	Comments
Main retrorocket thrust level	≈9500 lb	
Peak attitude transient at retrorocket ignition		
Roll	+0.2 deg	
Pitch	+0.3 deg	
Yaw	−1.0 deg	
Mean attitude error during burning		
Roll	<0.5 deg	
Pitch	0 deg	
Yaw	0.1 deg	
Roll actuator position		
Peak at retrorocket ignition	−0.67 deg	
Mean during burning	−0.4 to −1.13 deg	
Retrorocket burnout conditions		
Altitude	≈28,000 ft	28,600 ft
Velocity	428 ft/sec	392 ft/sec
Flight path angle (angle between Z axis and velocity vector)	To be determined	
RADVS initial lockon conditions		
Velocity sensor—altitude	56,000 ft	
Velocity sensor—velocity	To be determined	
Altimeter—altitude	To be determined	
Altimeter—velocity	To be determined	
Lunar reflectivity	To be determined	
At X band (9.3 kM Hz)—AMR	≈4–6 db below nominal lunar	
At K_A band (13 kM Hz)—RADVS	model at 25 deg aspect angle	
Descent segment intercept conditions		
Altitude	17,840 ft	
Velocity	440 ft/sec	
GMT	153-06H16M06 sec	
Vernier engine shutoff conditions		
Altitude (from footpads)	≈12 ft	
Velocity	≈4 ft/sec	
Angle to local vertical	To be determined	
Time before touchdown	1.5 sec	
Touchdown conditions (based on telemetry data)		
Vertical velocity	≈12 ft/sec	
Lateral velocity	≈0	
Angle to local vertical	To be determined	
Time of touchdown (time telemetry indication was received)	153-06H17M36 sec GMT	
Touchdown conditions (based on interpretation of touchdown strain gauge data)		
Vertical velocity	≈10 ft/sec	
Lateral velocity	≈2 ft/sec	
Angle to local vertical	≈1 deg	
Vernier propellant remaining at touchdown	≈40 lb (total)	
Postlanding phases		
Time required to position solar panel and planar array to Sun and Earth	75 min	
TV video signal-to-noise ratio (SNR)—200 line mode (omnidirectional antenna)	13 db	7.5 db above threshold
TV video SNR—600 line mode (planar array)	14 db	2.6 db above threshold
Maximum temperatures near lunar noon	78°F	
Compartment A top	86°F	
Compartment A bottom	118°F	
Compartment B top	123°F	
Compartment B bottom		

CONFIDENTIAL UNCLASSIFIED

UNCLASSIFIED

Table 4. Summary of significant spacecraft performance parameters (Cont'd)

Parameter	Value	Comments
Spacecraft landed attitude	+X axis within 1 deg of south Overall slope <1 deg North/South slope −0.85 deg south	From Earth and Sun direction data via antenna/solar panel positioner positions
Overall elect power parameters		
Battery energy at touchdown—total	74 ± 15 amp-hr	Nominal predicted—70.5 amp-hr
Battery energy at touchdown—main	54.7 ± 14 amp-hr	
Battery energy at touchdown—auxiliary	19.3 ± 5 amp-hr	
Solar panel output power at maximum output power point	≈90 w	
Average optimum charge regulator output power	69.5 w	
Average boost regulator efficiency for coast phase loads	78.5%	
Overall thermal control parameters		
Temperature range during transit		
Main battery	89 to 103°F	
Auxiliary battery	35 to 70°F	
Compartment A top	66 to 100°F	
Compartment A bottom	88 to 99°F	
Compartment B top	92 to 100°F	
Compartment B bottom	95 to 103°F	
RF data link parameters		
Telemetry bit error rate in low power, omnidirectional antenna operation at lunar distance	16 per 1000 at 550 bits/sec (intentionally operated below threshold for last hour to get 550 bits/sec)	Established worst case was 3 per 1000 at 17 bits/sec
Minimum spacecraft received signal strength during coast phases	−100 dbm	14 to 18 db above threshold
Spacecraft transmitter high power output—transmitter A	To be determined	
Spacecraft transmitter high power output—transmitter B	40.65 dbm	
Flight control parameters		
Nitrogen gas remaining at touchdown	3.96 lb	4.7 lb at launch. Established nominal gas usage was 1.6 lb

2. *Spacecraft Weight Data*

The weight and center of gravity of SC-1 was determined at AFETR and is listed in Table 5.

Table 5. Actual launch weight of SC-1

Item	Weight, lb	Vertical center of gravity Z[a]	Lateral center of gravity	
			X	Y
Separated weight (after *Centaur* separation)	2192.71	11.731	−0.116	−0.090
Maximum touchdown weight	659.48	16.899	−0.084	−0.150
Minimum touchdown weight	623.66	17.487	−0.081	−0.091

[a] Inches above landing gear hinge line (spacecraft station 47.48).

3. *Reliability*

a. System and subsystem a priori reliability. The *a priori* reliability of the A-21 *Surveyor* spacecraft is 0.805 for the flight and landing mission. Table 6 shows the *a priori*

Table 6. A-21 subsystem *a priori* reliability, flight and landing mission

Subsystem	Reliability
Telecommunications	0.971
Vehicle mechanisms	0.983
Propulsion	0.920
Electrical power	0.960
Flight controls	0.955
System	0.805

CONFIDENTIAL
UNCLASSIFIED

UNCLASSIFIED
CONFIDENTIAL

reliability estimates by subsystem. These estimates are based on "The Reliability Math Model, A-21 *Surveyor* Spacecraft," Hughes Aircraft Company (HAC), SSD 64002R, preliminary revision A.

b. Reliability estimates for SC-2 based on test data. The current data-based reliability estimate for SC-2 is 0.49 for the flight and landing mission. This estimate is based on all applicable systems test data. Data from SC-1 systems testing is included where there are no significant design differences between the units. Flight acceptance test (FAT) data or *a priori* estimates are utilized only when system testing does not provide data on a unit. Table 7 shows the reliability estimates by subsystem.

Table 7. SC-2 subsystem reliability estimates based on test data, flight and landing mission

Subsystem	Reliability
Telecommunications	0.921
Vehicle mechanisms	0.902
Propulsion	0.991
Electrical power	0.792
Flight controls	0.938
Spacecraft	0.611
(System interaction reliability factor)	(0.802)
Spacecraft reliability = (0.611) (0.802) = 0.49	

c. Mechanisms reliability. Table 8 lists reliability data based on SC-1 units test.

Table 8. Reliability achievement based on results of SC-1 units test

Antenna/solar panel positioner	0.8914
Omnidirectional antenna mechanism (each)	1.0
Separation sensing and arming device (each)	1.0
Thermal switch (each)	1.0

Summary of problems affecting reliability. During lunar day (260°F) flight acceptance test (FAT) operation of A/SPP 287580, serial number 2 (S/N-2), the elevation axis exhibited high frictional torque because of an excess of dry lubricant in the elevation housing bearing. This condition was traced to the addition of dry lubricant during earlier rework of the sector gear. Corrective action on S/N-2 and -3 units has been accomplished by burnishing the bearing surfaces to compact the lubricant.

A/SPP 287580, S/N-2, polar and solar drives failed in the second flight acceptance low-temperature test. Investigation revealed that the return coil spring mechanism was binding, and a corrective modification was made. However, a continuation of low-temperature testing indicated that the coil spring was not the only cause of the drive failure. An engineering investigation of the drive failures is being performed.

The elevation drive of A/SPP 287580, S/N-2, was found to have a short to ground during thermal vacuum FAT. The insulation sleeving covering the solder joint of the external motor lead had sheared around the edge of the joint, allowing it to contact the edge of the raised diameter at the rear of the motor. Although the sleeving has been tested and found to be satisfactory throughout the temperature range, a fiberglass sleeve has been added over the original sleeve as a precautionary measure. Also, a 750-v ac hi-pot test has been added to the FAT procedure.

The S/N-2 unit indicated a recurrence of polar potentiometer resistance shift during "Y" axis FAT vibration at between 8 and 12 cps. The potentiometer end play was increased to prevent axial loading. Also, a third hold down lug was added at the potentiometer housing, and the pot bracket was pinned to the structure attachment.

During optical dock alignment test of A/SPP, S/N-1, the lower roll axis manual pin puller struck the back of the solar panel at approximately 80-deg roll position causing damage to the panel. The interference resulted from rotation of the roll axis beyond its range of operation. A procedure has been prepared outlining the constraints of A/SPP operation for avoiding interference situations. Drawings and graphs illustrating the constraints of operation are nearing completion, and two interference study plastic models have been updated to include roll pin pullers, TV mirror, mast supports, and finer antenna details. They will be used at spacecraft performance analysis and command to follow SC-1 during the mission. Appropriate constraints are being added to pertinent specifications and procedures.

During Air Force Eastern Test Range (AFETR) test of SC-1 mechanism A, part number (P/N) 287300, S/N-2, the retaining clip did not engage the stop when in the locked position (boom extended). Analysis of the trouble revealed that the retaining clip material had fatigued. Both the clip and lock plate were redesigned.

CONFIDENTIAL
UNCLASSIFIED

UNCLASSIFIED
CONFIDENTIAL

Alignment checkout of SC-2 at the optical dock showed that A mechanism, S/N-6, and B mechanism, S/N-3, were out of tolerance limits. Reinspection of available assembled and nonassembled fiberglass tubes revealed that hole patterns were not within drawing tolerances.

Three corrective action studies have been started: (1) an adjustable fitting for the small ends of the booms, (2) a geometry/tooling layout for mechanism A, and (3) a geometry/tooling layout for mechanism B. Revised detailed drawings are currently in work to eliminate the tolerance accumulation on the tube and tube assemblies of both mechanisms.

Several Trouble and Failure Reports (TFR) have stated that a high contact voltage drop was measured on separation sensing and arming device switches. However, the trouble could not be duplicated during subsequent verification tests, except in one case which occurred on device P/N 293400, S/N-2. The switch was removed and is now being subjected to a comprehensive failure analysis.

Further study of trouble reports that could not be verified revealed that a significant portion of the voltage drop was caused by the test equipment and cabling. Consideration is being given to increasing the current at which the contact voltage drop is measured in order to minimize test equipment and cable ambiguities.

Investigation of the sticking contact problem is continuing. Possible solutions being pursued are: (1) curing RTV-11 contact coatings at 300°F, (2) using teflon for contact coating material, and (3) applying an appropriate film to the surface of the RTV-11.

A thermal study showed that thermal painting of the pin pullers was not necessary, and the surface finish has been changed to polished aluminum.

d. Digital units — alloy transistor characteristic variance test. An experimental investigation into the life characteristic effects of transient pulses considerably exceeding maximum rated voltage as specified for the 988809-1 and -2 PNP chopper transistors used in the control signal processor, engineering signal processor, and auxiliary engineering signal processor was completed. Data reduction for this experiment was performed on the IBM 7094 computer and on a General Electric Co. computer time sharing terminal. These data are delineated in five main areas as follows:

(1) Alloy transistor life characteristics variance test

(2) Computer analysis

(3) Evaluation of the effects of time and stress on alloy transistor parameters

Offset voltage (v_1)

High-temperature leakage:

I_{cbo} at 50°C (v_2)

I_{ebo} at 50°C (v_3)

I_{eco} at 50°C (v_4)

(4) Parameter data

(5) Conclusions and recommendations

These tests showed that the 988809-2 alloy transistors exhibit extremely low leakage characteristics. The main contributing factor for this may be the structure of the device. However, this structure does not allow very high-power dissipation levels, with v_{ceo} being the primary mode of failure. Previous tests indicate that 45 v is the absolute maximum that can be tolerated by the population as a whole. Increases above this level caused puncturing of the device from collector to emitter. In the circuit used, 50 v appeared to be a very critical pulse level and definitely caused failure of a good proportion of the population. Based upon these results, the 988809-1 and -2 transistors are being replaced by the epitaxial types 988809-3 and -4, respectively.

e. Task 5 electronics.

Boost regulator design review. A reliability analysis was performed as part of the design review for the redesigned boost regulator. Results of this analysis indicated an *a priori* failure rate for the unit (λ_T) of $\lambda_T = 15.18 \times 10^{-5}$ failures/hr. The review also included a stress analysis that indicated the existence of 17 overstressed components which are now being evaluated to determine their effect on the reliability of the unit.

Battery charge regulator design review. A reliability analysis was performed as part of the design review for a redesigned battery charge regulator. Results of this analysis indicated an *a priori* failure rate of $\lambda_T = 13.32 \times 10^{-5}$ failures/hr. Detailed stress analysis indicated very few components operating at stress levels above those recommended to meet reliability requirements. Those components found to be operating at stresses above their rated value are being evaluated for their effects.

UNCLASSIFIED

UNCLASSIFIED
CONFIDENTIAL

f. Components.

Resistor 988644. The test plan for qualification of the 988644 resistor has been completed, and a step-stress test was added. RCL resistors are being substituted for Genesco.

Connectors 988202. Results of special tests on six SC-2 connectors that failed to pass the retention gauge were presented. Pins and sockets, which were rejected because of inadequate force retention, proved satisfactory in electrical continuity tests. Some combinations of pins and sockets which passed the test had high resistivity. Thus, the results of the electrical continuity tests were not conclusive. Further action consisted of sectioning connectors and performing a spectrographic and metallurgical analysis of contact points. In addition, tests will be performed at the lower current values.

Connectors 988207 and 208. Correction of procedures for 988207 and 208 connectors were implemented. This action primarily consisted of the correction of dimensional variables and the development of special procedures and instructions.

Diode 988723. Revisions to the specification incorporating an acceptance criteria that diodes having cracks or striations shall not be accepted for shipment were completed.

Microdiodes 988722. Samples of microdiodes having Kovar and silver leads were received on April 1, and tests were started April 21. Sufficient testing has not been completed to report further progress.

Transistor 988872. A study is under way regarding the use of this transistor in the Motorola SCO. This transistor presently represents a possibility of serious degradation of spacecraft reliability because of beta shift.

Fairchild zener diode (Motorola SCO) 988749. The primary failure mode of this diode was the temperature coefficient. Investigation indicated that Motorola ordered 494 parts, of which 467 were defective. After screening, 66 good diodes were finally obtained. The screening operation also indicated that 302 diodes were presently available for use. These parts are being returned for retesting. Suspected failure cause was loss of serialization of parts. Thus, a mixup in the shipment to different specifications most likely occurred.

Capacitors 988501. It was discovered that certain capacitors are not being filled with wax; this condition could result in internal lead rupture during vibration. Sprague is presently being investigated for its controls in the filling process and for its criteria of minimum fill to assure no failures during vibration. JPL reported that of 12 type 118P WESCO capacitors two failed in the open mode under vibration. Dissection of these capacitors revealed broken leads. As a result of these tests and discovery of partial fills, a full case construction is being considered as a substitute. Action to qualify the use of the full case design has been initiated.

Transistors 988808. Successful reverse bias age tests were conducted on the 988808 transistor. However, other transistors were found to have excessive leakage that might be a reliability threat under high temperatures.

As a result of these findings, Hughes (HAC) is reviewing applications of this family of transistors to determine if any will be susceptible to reverse bias mode failure, screening bonded stores for any transistors having this possible failure mode, and determining the exact threshold temperature of reverse bias leakage, paying special attention to whether such will occur at 140°C.

g. Materials.

Cleaning and repairing white inorganic thermal control paint. Investigation of cleaning and repair techniques for the white inorganic thermal control coating has produced the following conclusions:

(1) The sanding of the coating, whether contaminated or not, tends to increase its susceptibility to ultraviolet degradation. This situation may be caused by a residue of organic sandpaper adhesive.

(2) The most severe contaminant, hair oil, was not satisfactorily removed by sanding.

(3) Coating contamination can exist which is not revealed by black light inspection.

(4) When painting over previously cured paint, a room temperature cure provides proper adhesion. However, the underlying paint film must be continuous.

(5) Varying the curing temperature did not affect the thermal radioactive properties of ultraviolet resistance of the paint.

Gold coatings. Liquid bright gold No. 6518 (Englehard Industries) has been evaluated as a possible substitute for vapor deposited aluminum. The material is totally

CONFIDENTIAL
UNCLASSIFIED

UNCLASSIFIED
CONFIDENTIAL

unsuitable for use on epoxy-glass fabric laminates, e.g., the RADVS antenna and AMR reflector since a 500°F plus temperature is required for curing. Metals such as aluminum and titanium could be coated and produce a typical gold coloration after being baked at temperatures exceeding 850°F. Typical thermal-physical properties were (1) solar absorptance = 0.37 to 0.39, and (2) total emittance = 0.03 to 0.14. Unfortunately, the adhesion and abrasion properties of the gold coating are inferior to those of the vapor deposited aluminum coating. No further work is planned.

Thermal control tapes. Several pressure sensitive tapes have been tested which might be employed for thermal control. Some of the results obtained are as follows:

Tape	*Solar absorptance*	*Total emittance*
3M-Y9184 gold	0.23	0.04
3M-Y9040 aluminum	0.17	0.03
3M-Y9050 aluminum	0.14	0.03
Mystik, gold on H-film	0.47	0.04

All tapes outgassed room temperature condensables when exposed to 10^{-6} torr for 72 hr at 260°F. Additional samples of tape with thermosetting adhesive backing will be tested.

Vacuum testing of silicone polymers. Two silicone rubber polymers, RTV881 and RTV732, have recently been vacuum tested using the HAC single impact technique. Both materials had previously been tested in a multiple impact chamber where it was learned that both materials evolve room temperature condensables when the sample temperature reaches approximately 160°F. The results obtained in the single impact chamber were decidedly different. In the case of RTV732, no condensation could be seen on the room temperature window even when the sample temperature reached 260°F, at which time the test was terminated. In the case of RTV881, a slight fog was seen on the window when the sample reached 233°F, it disappeared when the window was warmed to 120°F. In a second test, the window was started at 200°F. No fogging occurred when the temperature of the window was dropped stepwise to 80°F over a 6 hr period.

h. Flight controls.

Flight control electronics. A terminal descent failure of signals to vernier engine 3 during SC-2 solar thermal vacuum test was traced to a transistor stud-mounting short (Q23) on the 1A5 chassis involving the vernier valve amplifier circuitry. A production test specification, TS 284451, paragraph 6.14, is used to screen out malfunctioning of this circuit. In this instance, solar thermal vacuum test stresses apparently uncovered a marginal assembly on amplifier 284350, S/N-14 configuration. Investigation into the cause has been initiated.

Canopus sensor. The Canopus sensor installed on SC-2 flight control sensor group was found to have a deposit on its lens. This sensor, 235300, revision E, S/N-12, has been returned to Santa Barbara Research Center for rework and to Tucson for calibration.

Gas supply. Difficulties were experienced with the nitrogen tank charging valve on SC-1 at AFETR. The full open valve condition is less than one turn. Improper operation of the valve caused packing dislodgement affecting valve closure. This operation problem is being remedied by ECR action calling for caution tagging of this valve on spacecraft up to launch time and limiting valve stem rotation to a maximum of ¾-turn in affected procedures and drawings at HAC and AFETR.

Attitude jets. One instance of excessive gas leakage occurred from the body of S/N-5 attitude jet P/N 235700 (TFR 46448) after having been placed in Bonded Stores. S/N-5 has been downgraded to class III, and an investigation into the cause of leakage is underway. At present, leakage appears to come from the threaded and then silver brazed connection inlet to the valve body. X-ray of S/N-5 has not revealed the detail necessary to pinpoint the cause. X-raying of other attitude jet bodies is planned to determine whether the same condition can be noted in them.

TFR status. TFR status during the report period is shown in Table 9.

Table 9. TFR action status

Type of TFR	TFR period	
	March 20–May 20	January 20–March 20
Production	13 (7 on T-2N upgrade)[a]	3
Flight acceptance test	4	3
Systems	5 (2 at AFETR)	5 (3 at AFETR)

[a] Five of the 13, excluding the 7 on T-2N, are two types of repetitive problems on vendor items; three are HAC's responsibility and two are the vendor's.

Note: Does not include inertial reference unit components such as gyros, accelerometer, etc.

CONFIDENTIAL
UNCLASSIFIED

UNCLASSIFIED CONFIDENTIAL

C. System Analysis

1. Dispersions in Earth Shadow Time Owing to Injection Errors

Owing to the possibility of *Surveyor* launch windows opening and closing on the Earth shadow constraint (total time spent in Earth shadow), it is important to determine the dispersions in shadow time caused by injection errors. This has been done for two trajectories in the May/June launch period, and the results are summarized in Table 10. The first case corresponds to the opening of the launch window on June 2, with 3-σ flight performance reserve (FPR); this launch window closes on the shadow constraint after several minutes. The second case corresponds to the opening of the window on June 3 with the shadow constraint. The perturbations in injection conditions are 1-σ values and are obtained from General Dynamics/Convair (GD/C) covariance matrices for *Atlas/Centaur* 10 (AC-10).

The 3-σ dispersion in shadow time for the first case is 3 min and 12 sec. It is, therefore, recommended that a margin of 3½ min be applied to the Earth's shadow constraint for the determination of launch windows.

2. Effects of Earth Shadow Transit on May/June 1966 Launch Windows

Recent studies of the *Surveyor* 1 capability to withstand the temperature variations during passage through the Earth's shadow have modified previous estimates of May/June 1966 launch windows. Table 11 presents data for the nine possible launch days that comprise this direct ascent launch opportunity.

The launch windows shown in the first column of Table 11 are based upon launch vehicle capability and are taken from targeted trajectory data received from GD/C. They reflect available launch times based upon a launch azimuth sector of 80 to 115 deg and current, AC-10, payload capability with a 3-σ FPR of 175 lb of propellant. Improvements in *Atlas/Centaur* performance or use of the 3-σ FPR could result in increased windows at a rate of about 0.05 min/lb.

These launch windows will be further restricted on the last 5 days of the opportunity, as the spacecraft must pass through the shadow of the Earth for some or all of the available launch time. The actual shadow times used in this analysis are based upon the GD/C trajectories

Table 10. Dispersions in Earth shadow time

Case	Time of entrance from injection	Time of exit from injection	Total shadow time	Shadow time dispersion
Launch 6/2/66 σ_L = 85.29 deg				
Nominal	2H 34M 51S	3H 36M 57S	1H 02M 06S	
Δx = 455 m	2H 34M 43S	3H 36M 57S	1H 02M 14S	08S
Δy = 917 m	2H 35M 07S	3H 37M 03S	1H 01M 56S	−10S
Δz = 967 m	2H 35M 09S	3H 36M 42S	1H 01M 33S	−27S
$\Delta\dot{x}$ = 0.62 m/sec	2H 34M 33S	3H 36M 57S	1H 02M 24S	18S
$\Delta\dot{y}$ = 3.82 m/sec	2H 35M 15S	3H 36M 52S	1H 01M 37S	−29S
$\Delta\dot{z}$ = 3.58 m/sec	2H 34M 32S	3H 37M 23S	1H 02M 51S	45S
			Root-sum-square (RSS) (1-σ)	64
Launch 6/3/66 σ_L = 103.75 deg				
Nominal	50M 39S	2H 4M 19S	1H 13M 40S	
Δx = 403 m	50M 37S	2H 4M 18S	1H 13M 41S	01S
Δy = 1005 m	50M 40S	2H 4M 21S	1H 13M 41S	01S
Δz = 958 m	50M 39S	2H 4M 18S	1H 13M 39S	−01S
$\Delta\dot{x}$ = 1.94 m/sec	50M 33S	2H 4M 13S	1H 13M 40S	00S
$\Delta\dot{y}$ = 3.75 m/sec	50M 41S	2H 4M 17S	1H 13M 36S	−04S
$\Delta\dot{z}$ = 3.06 m/sec	50M 37S	2H 4M 24S	1H 13M 47S	07S
			RSS (1-σ)	08

CONFIDENTIAL UNCLASSIFIED

UNCLASSIFIED
CONFIDENTIAL

Table 11. May/June launch windows

Date	Launch vehicle capability (3-σ FPR), min	Spacecraft capability[b] (TCA-2, 0°F)		
		Vernier lines: −30°F, solar panel: −200°F, min	Vernier lines: 0°F, min	Vernier lines: −30°F, solar panel: −150°F, min
May 29	3	3	3	3
30	49	49	49	49
31	85	85	85	85
June 1	105	105	105	105
2	109	30	27	27
3	98	9	6	6
4	73	4	0	0
5	38	0	0	0
6	0	0	0	0
	(5)[a]	(5)[a]		

Note: Allowable shadow times reduced by 3½ min for effect of 3-σ injection errors on shadow time.

[a] Available if the 3-σ FPR is utilized.

[b] Shock absorber capability of −25°F assumed in all columns.

discussed above and are presented in Ref. 1. The capability of the three most critical spacecraft systems to withstand shadow time is presented in Figs. 5 through 7. These graphs present the allowable shadow time for the associated lower temperature limit as a function of the time of shadow entrance measured from initial Sun acquisition. This situation occurs nominally at 30 min after launch. All shadow-constrained launch windows shown in Table 11 are based upon the allowable shadow times shown in Figs. 5 through 7, reduced by 3½ min for dispersions in shadow duration owing to 3-σ injection errors. This conclusion is the result of the study discussed above.

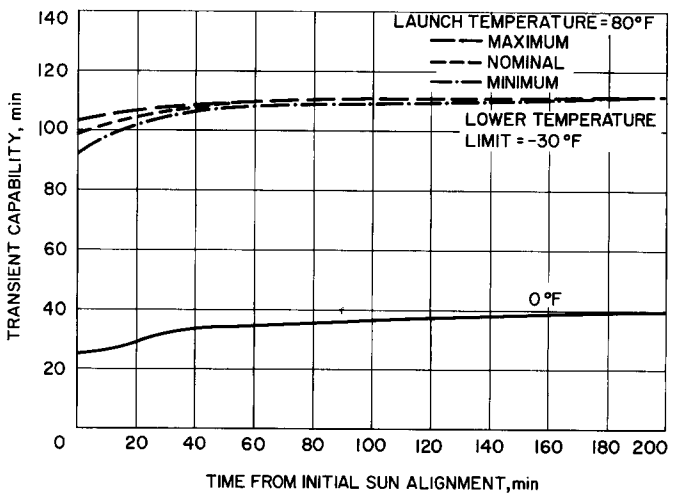

Fig. 5. Transient capability of vernier propellant lines

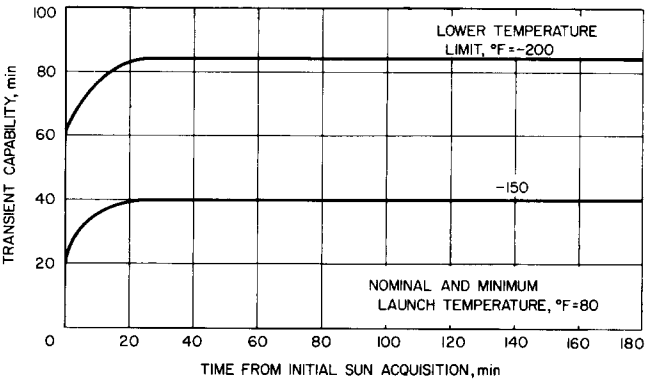

Fig. 6. Transient capability of solar panel

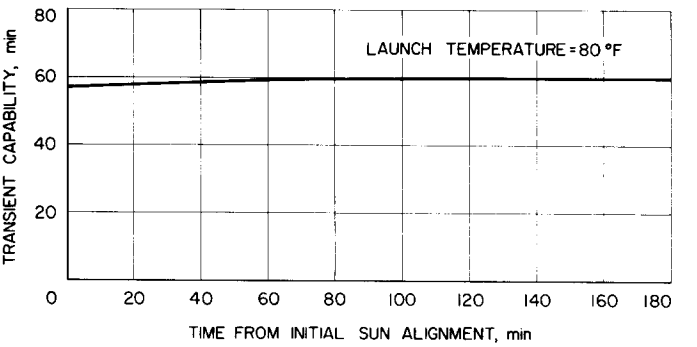

Fig. 7. Transient capability of vernier engines

Allowable shadow times for the vernier propellant lines with lower temperature limits of 0 and −30°F are shown in Fig. 5. The 0°F temperature limit is based upon not allowing any propellant to freeze; at −30°F the oxidizer in the lines will be frozen. The launch windows associated with oxidizer lines (0°F) are shown in Table 11. It is not necessary that this be a constraint as the lines thaw, without ill effect, approximately 30 min after egress from the shadow.

Fig. 8 shows the shadow time capability of the shock absorbers on the same basis as Figs. 5 through 7. It is apparent that, with a lower temperature limit of −25°F, this capability always equals or exceeds that of thrust chamber assembly 2 (TCA-2) and, hence, the shock absorbers are not constraining. However, the current shock absorber specification restricts the operational lower temperature limit to 20°F and offers no provision

UNCLASSIFIED
CONFIDENTIAL

UNCLASSIFIED

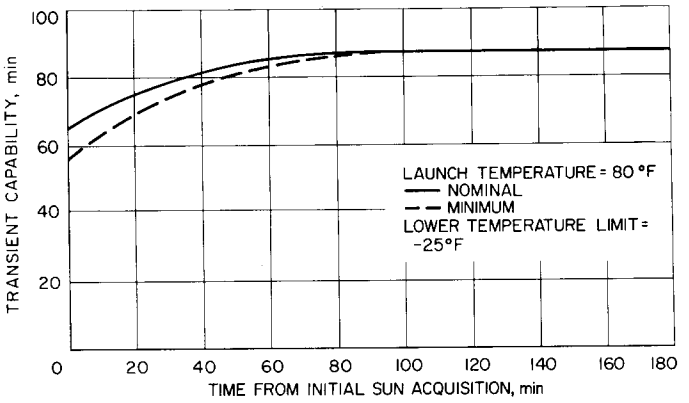

Fig. 8. Transient capability of shock absorber

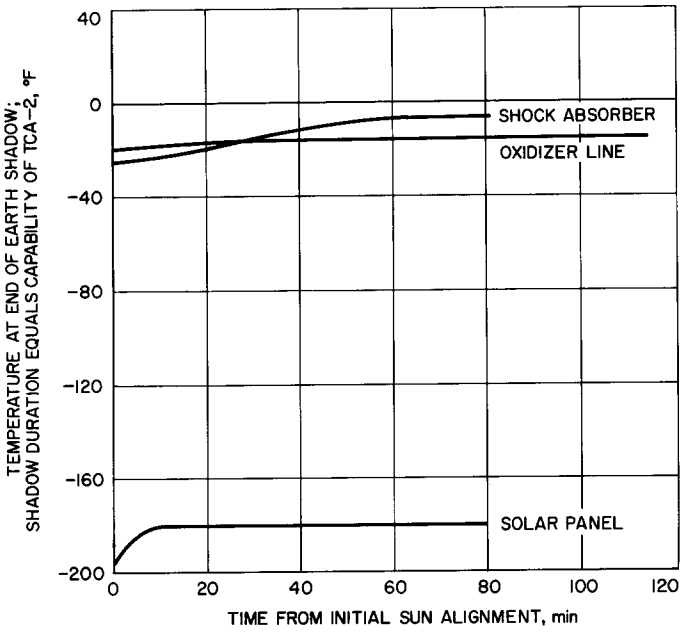

Fig. 9. SC-1 critical item temperatures

for lower temperatures in transit, where only survival is a consideration. It is felt that the −25°F temperature, which will be encountered early in transit and under the conditions involved here, is easily within the capability of the shock absorbers.

Allowable shadow times for the solar panels with lower temperature limits of −150 and −200°F are shown in Fig. 6. Launch windows for a lower temperature limit of −150°F on the panels are shown in Table 11. Using this limit on TCA-2, rather than a lower temperature limit of 0°F, results in a loss of 3 min of launch window on both June 2 and 3, and a loss of all 4 min of window which would otherwise be available on June 4.

Although the SC-1 solar panel was subjected to a lower FAT limit of only −150°F, it is recommended that a capability of at least −200°F exists, and the panel should be implemented to utilize the full thermal capability of TCA-2 (Fig. 9). When the type approval test (TAT) solar panel was subjected to a temperature of −270°F, a 4% degradation resulted. When solar panels were subjected to a temperature of −150°F, a 1% degradation resulted. Battery energy computations indicate that a nominal 89-w solar panel (during transit) will result in 1310 w-hr of capacity at touchdown (800 in the main battery and 500 in the auxiliary battery). Table Mountain tests indicate that the SC-1 solar panel will provide 94 w during transit, i.e., 5% above the nominal value used to compute the above energy capacity. Therefore, the design of the solar panel has adequate margins to withstand low temperatures during the initial stages of the flight and still yield adequate energy margin for flight and touchdown.

Accordingly, the following recommendations have been made for the SC-1 spacecraft:

(1) The vernier lines should be allowed to freeze during transit through Earth shadow as long as temperatures do not go below −30°F; in fact, the lowest temperature reached will be −20°F.

(2) The lower temperature limit on the solar panel should be considered to be −200°F.

(3) A −25°F lower limit should be used for the shock absorbers.

With the adoption of these recommendations, vernier engine thrust chamber 2 assembly becomes the critical item during Earth shadow transit. The allowable shadow time for the lower temperature limit (both operational and survival) of 0°F is shown in Fig. 7. Temperatures of the other subsystems considered, corresponding to TCA-2 as the constraining subsystem, are shown in Fig. 9. The launch windows based upon this constraint are shown in Table 11. This constraint is used in Ref. 1 which presents the trajectory data for use in the launch constraints addendum.

These shadow times will result in the vernier lines freezing during shadow transit and thawing approximately 30 min after exit. However, the vernier engines cannot be used for approximately 3½ hr after exit. This delay occurs because TCA-2 must be allowed to warm up to its steady state cruise mode temperature in order that, when the midcourse maneuver is performed (which may again cause the unit to be eclipsed), firing will occur

UNCLASSIFIED

UNCLASSIFIED

within the specified temperature range of 0 to 100°F. This delay results in an additional constraint upon an early midcourse maneuver for those trajectories passing through the Earth shadow.

During passage through the shadow, the spacecraft will normally be in an inertial hold mode so that upon exit the Sun sensor will be, except for small errors owing to gyro drift, pointed in the direction of the Sun. This assumes that Sun acquisition takes place before entrance. On both June 5 and 6, however, the spacecraft enters the Earth's shadow before the worst case Sun acquisition sequence is completed at launch plus 30 min. In this situation an additional 18 min must be allowed for the Sun acquisition sequence after shadow exit. Fig. 7 shows that the allowable shadow time at launch (plus 30 min) is 57 min. In this situation, Sun acquisition must be complete at launch plus 87 min. The spacecraft must then exit shadow at launch plus 69 min minus 3½ min for dispersions. This situation results in no launch window availability on June 5. However, the actual acquisition sequence could be completed before launch plus 23 min depending upon the particular spacecraft-Sun geometry on this day. In this case, the 57-min constraint would apply, and the full window of 38 min would be available.

3. Sun Acquisition Time Required for June 5, 1966 Launch

The position of the Sun in spacecraft coordinates at injection is shown in Fig. 10 for opening and closing trajectories on June 5 as per the coordinate system shown in Fig. 11. The coordinates are as follows:

Opening	θ =	19 deg
	ϕ =	90 deg
Closing	θ =	17.2 deg
	ϕ =	33.5 deg

The tip-off rates imparted at separation are of a random nature. For the purpose of this analysis, the assumption is made that the rate is 3 deg/sec (PD-1 specification value) and is a combination of pitch and yaw (no roll). The rate is damped out in approximately 29 sec with a total maximum angular displacement of 44 deg. At this time, the spacecraft enters a rate stabilized mode with a maximum angular rate of 0.051 deg/sec. Therefore, the maximum possible angular displacement of the Sun at the start of the acquisition sequence in spacecraft coordinates for opening and closing is 44 + 0.051 (51 − 29) = 45.1 deg, where 51 sec is the time from separation to initiation of Sun acquisition.

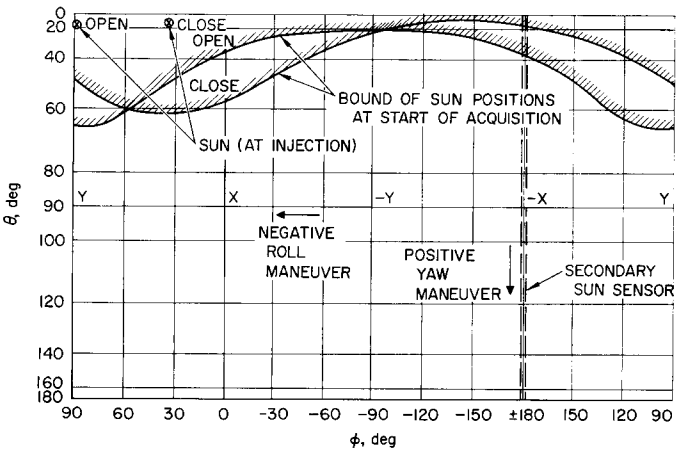

Fig. 10. Sun acquisition geometry launch June 5, 1966

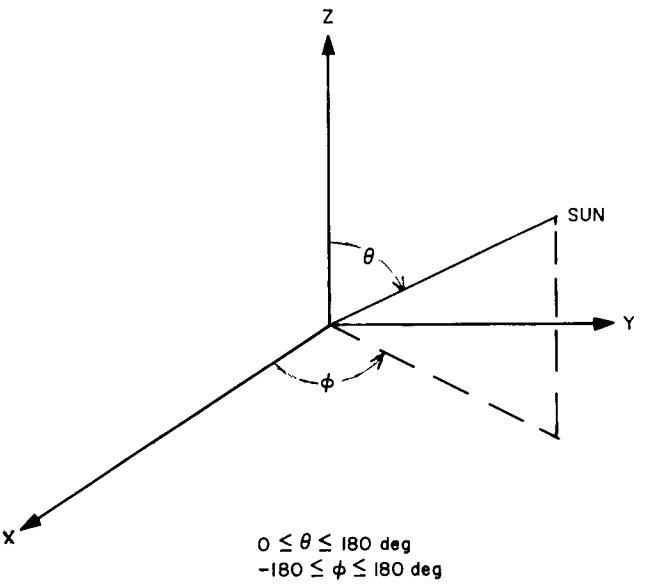

Fig. 11. Spacecraft coordinate system

Thus, the Sun at the start of acquisition is located somewhere in the shaded regions of Fig. 10, which depicts the maximum 45.1-deg displacements about the Sun positions at injection for the opening and closing trajectories on June 5.

The Sun acquisition maneuver begins at 51 sec after injection, with a 1/2 deg/sec roll in the negative direction (pitch and yaw axes still in rate stabilized mode) until the Sun is acquired by the automatic Sun sensor.

UNCLASSIFIED

UNCLASSIFIED
CONFIDENTIAL

The maneuver is then completed by a positive yaw that aligns the Sun with the negative z axis. Therefore, as shown in Fig. 10, the maximum roll maneuver is 360 deg (in the negative ϕ direction) requiring 720 sec to complete for both the opening and closing trajectories. The maximum yaw maneuver for both opening and closing launch azimuths is 180 deg, requiring 360 sec. Therefore, the time required for acquisition of the Sun could be as great as the maximum allowance of 18 min.

The above spacecraft-Sun geometry indicates that in the worst case the maximum acquisition time will be required. June 5 was, therefore, eliminated as a possible launch date for SC-1.

4. Magnitude vs SNR of Detectable Stars for Surveyor TV in Star Mode

a. Introduction. The recent modification of the survey TV camera for night landing observations of the lunar surface has considerably increased the ability to detect faint stars. The star magnitude vs SNR, developed by considering this increased capability, is plotted in Fig. 12. This information is published to assist the development of suitable star tables for the computer programs of spacecraft performance analysis and command. The results so far indicate a theoretical limit of about magnitude 8. Other factors will probably limit the sensitivity to magnitude 6 or less for typical conditions.

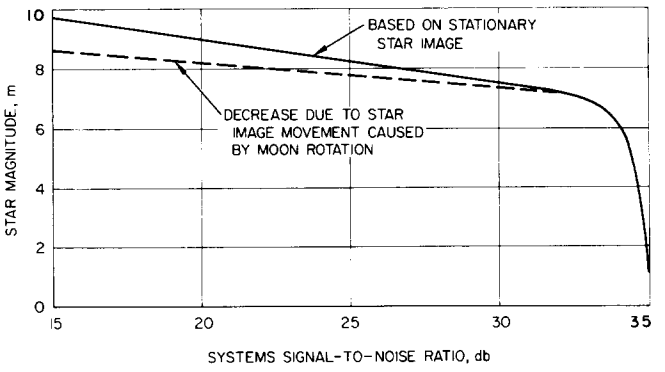
BASED ON STATIONARY STAR IMAGE
DECREASE DUE TO STAR IMAGE MOVEMENT CAUSED BY MOON ROTATION
STAR MAGNITUDE, m
SYSTEMS SIGNAL-TO-NOISE RATIO, db

Fig. 12. Star magnitude vs SNR

b. Analysis. The peak equivalent illuminance, in foot-candles, for a star of magnitude m (Fig. 13), is:

$$A = \frac{0.049}{(2.512)m} \qquad (1)$$

The star mode optimum integration time vs luminance in foot-lamberts is plotted in Fig. 14 for a typical survey camera.[1] Fig. 14 also shows results for the SC-1 survey camera recently used during the successful lunar mission A. The SC-1 camera is slightly less sensitive than the camera used for this report. The optimum integration time occurs when the slope of the log signal output-to-log luminance input is equal to 0.7. The relationship between foot-candles and foot-lamberts for the camera optical system can be obtained from the camera equation

$$S = \frac{BT_c\Delta t}{4(f/\text{No.})^2}$$

B = input luminance, foot-lamberts

T_c = camera optical transmission coefficient = 0.6

Δt = exposure time

$(f/\text{No.})$ = 4, 5.6, 8, 11, 16, or 22

S = camera sensitivity, foot-candle-seconds

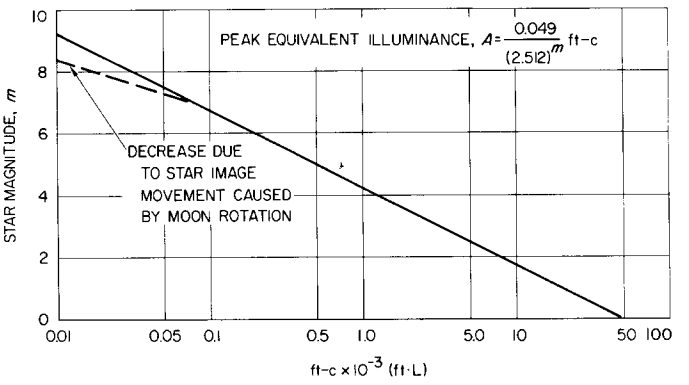
PEAK EQUIVALENT ILLUMINANCE, A = 0.049/(2.512)^m ft-c
DECREASE DUE TO STAR IMAGE MOVEMENT CAUSED BY MOON ROTATION
STAR MAGNITUDE, m
ft-c x 10^-3 (ft-L)

Fig. 13. Star magnitude vs foot-candles

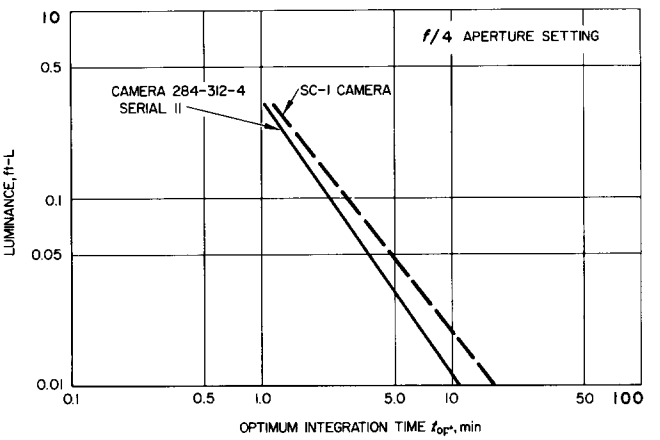

Fig. 14. Typical survey camera optimum integration time vs luminance

[1]Data were obtained from camera 284-312-4, serial 11.

CONFIDENTIAL
UNCLASSIFIED

UNCLASSIFIED

Recent unit FAT data on the camera used for this study show that the 0.7 slope point on the log-log plot mentioned above was achieved for a 0.02 ft-L scene luminance at an f/4 aperture setting, and 400-sec exposure time; thus

$$S = \frac{0.02 \times 0.6 \times 400}{4(4)^2} 0.075 \text{ ft-c/sec}$$

Now

$$\frac{S}{\Delta t} = \frac{0.075}{400} = 0.1875 \times 10^{-3} \text{ ft-c}$$

is equivalent to an input of 0.02 ft-L.

Hence

$$1 \text{ ft-L} \cong 10 \times 10^{-3} \text{ ft-c}$$

Using Fig. 14, Fig. 15 was developed to show the relationship between star magnitude m and the optimum integration time, t_{opt}. Of interest is the system SNR obtainable for a star of a given magnitude. The following expression relates SNR to V_o, the black-to-white transition voltage, for normal mode:

$$(S/N)db = 20 \log \frac{V_o}{\sigma} - 2 \text{ db}$$

where σ is the rms value of the noise.

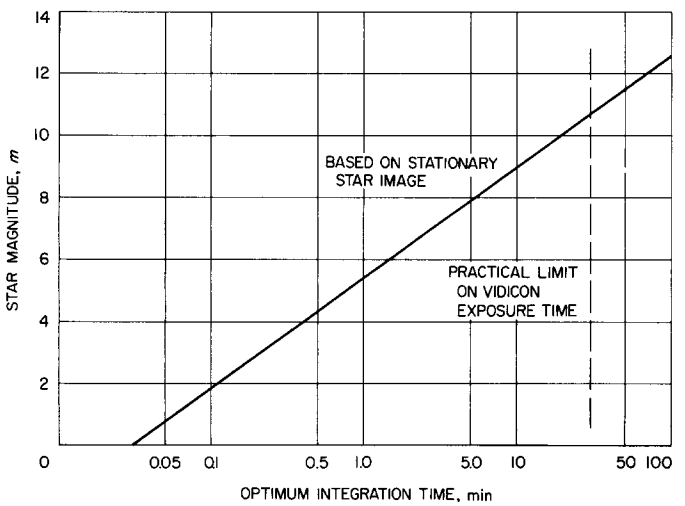

Fig. 15. Star magnitude vs integration time

For *Surveyor* TV cameras, σ is typically equal to 50 mv. Using the unit FAT data mentioned previously (Fig. 16), the σ = 50 mv, and the above equation, the curve of Fig. 17 was established. In addition, the data from Figs. 15 and 17 were replotted in Fig. 12, yielding the relationship between star magnitude and the system demodulated SNR. These data assumed a stationary star image on the vidicon faceplate. However, owing to the Moon's

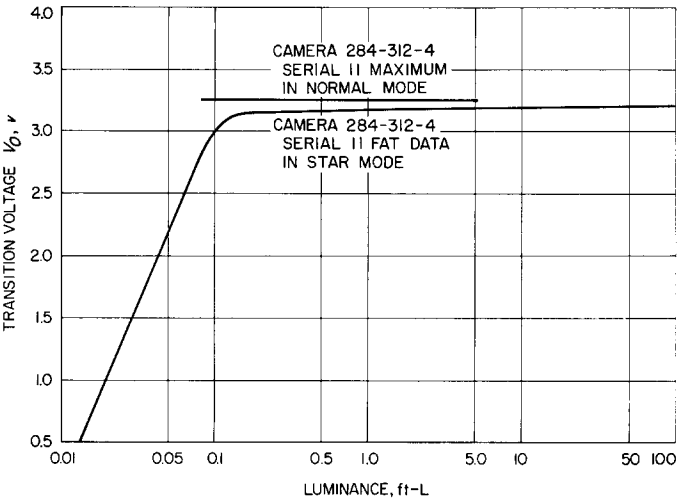

Fig. 16. Typical survey camera black-to-white transition voltage V_0

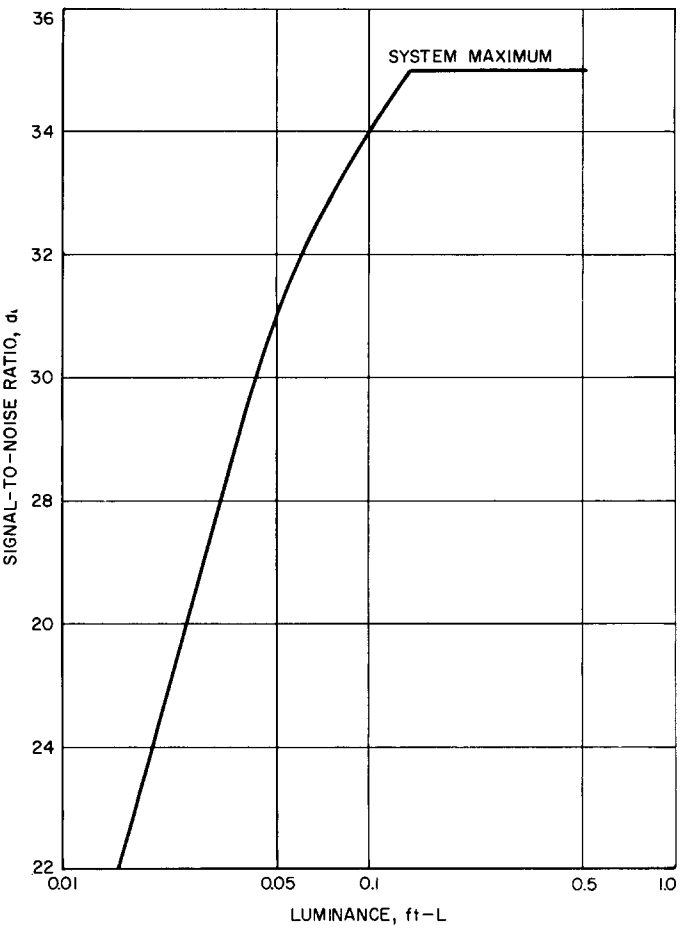

Fig. 17. System SNR vs luminance

UNCLASSIFIED

UNCLASSIFIED

rotation during long exposure times, the star image will make a trace on the vidicon rather than a point. The following analysis will present a suitable correction for a nonstationary star target.

c. Nonstationary star target. The energy distribution or illumination of a star, point image, is approximately

$$E_r = Ae^{-\left(\frac{4r}{\delta}\right)^2} \text{ lumens/unit area}$$

where r is image radius, A is the peak illumination, and δ is the characteristic aperture dimension. The point spread function is the

$$P(r) = \int_0^\infty Ae^{-\left(\frac{4r}{\delta}\right)^2} \, dr$$

Because of the Moon's rotation, the star image is moved along a line during exposure. Thus, the line spread function is of interest in developing the equivalent flux or illumination found in such an image trace. The point spread function can be found by expressing $P(r)$ in two coordinates and integrating along one coordinate, i.e.,

$$P(x, y) = \int_{-\infty}^\infty Ae^{-\left(\frac{4}{\delta}\right)^2 [x^2+y^2]} \, dx \, dy$$

and

$$L_y(x) = Ae^{-(4x/\delta)^2} \int_{-\infty}^\infty e^{-(4y/\delta)^2} \, dy$$

$$L_y(x) = \frac{A\,\delta\,(\pi)^{1/2}}{4} e^{-(4x/\delta)^2}$$

which is the desired line spread function. The flux along a star track of length L_m on the vidicon face is then

$$F = L_m \int_{-\infty}^\infty L_y(x) \, dx$$

$$F = \frac{L_m\, A\, \delta\, (\pi)^{1/2}}{4} \int_{-\infty}^\infty e^{-(4x/\delta)^2} \, dx$$

$$F = \frac{L_m\, A\, \delta^2\, \pi}{16} = \frac{A^1\, \delta^2\, \pi}{16}$$

where $A^1 = L_m\, A/L_o$, and L_o is a normalizing length equal to $\delta/2$ to adjust for the decrease in peak illumination owing to image motion. The factor $\delta/2$ was chosen as that length of the characteristic aperture for which little or no amplitude variation would be experienced owing to the integrating effect of the aperture, since the star image diameter, owing to the lens system, is much less than δ.

Eq. (1) can be modified and stated as

$$A^1 = \frac{0.049\, L_o}{L_m(2.512)^m} \text{ ft-c}$$

The Moon has an angular rate of 0.5 deg/hr, or 0.145 mrad/min. Now

$$v = \omega r$$

$$L_m = vt_m = \omega r t_m = \omega f t_m, \text{ for } \infty \text{ focus } r = f = 4 \text{ in.}$$

then

$$L_m = 0.145 \times 10^{-3} \times 4 = \frac{0.58 \times 10^{-3} \text{ in.}}{\text{min}} \cdot t_m$$

The size of the characteristic aperture δ is given as

$$\delta = 3.3 \times 10^{-3}$$

Thus far a line trace $L_m = \delta/2$ requires an exposure time of 2.85 min. Thus from Fig. 16, stars of magnitude 7 or less are essentially unaffected by image motion. However, for stars of magnitude 10, $t_{10} = 15$ min, and

$$L_{10} = 8.6 \times 10^{-3} \text{ in.} = 2.64\, \delta$$

then

$$A^1 = \frac{0.049 \times 0.5\, \delta}{2.64\, \delta\, (2.512)^{10}} = 9.3 \times 10^{-7} \text{ ft-L}$$

Figs. 12–14 show the effects of the Moon's rotation on illuminance and SNR.

d. Results. The results of this analysis tend to indicate that stars above $m = 8$ cannot be viewed by the *Surveyor* television system. In addition to the Moon's rotation, other factors, such as diffuse reflection from the camera mirror, stray light in the lens barrel, vignetting effects, shading across the format, etc., tend to reduce the above expectations to star magnitudes of 6 and below. Fig. 18

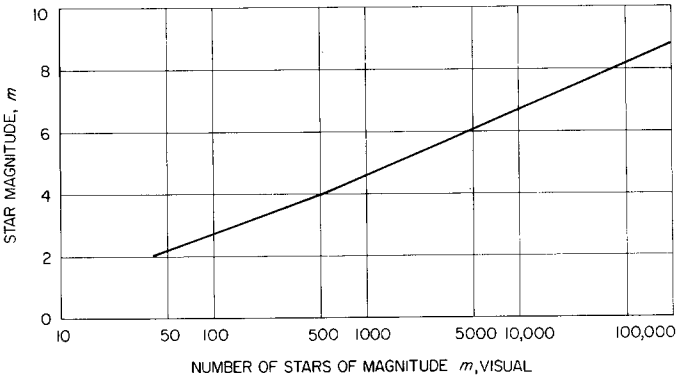

Fig. 18. Stars of visual magnitude

UNCLASSIFIED

UNCLASSIFIED
CONFIDENTIAL

shows that the available stars in this range, approximately 5000, should ensure that at any given time a suitable number would be viewable by the television camera.

5. Expected Maximum Composite Camera Shading for Approach and Survey Cameras

a. Introduction. When light passes through a dielectric medium it is, in general, attenuated. The resultant loss in brightness is often referred to as the transmission loss of the medium. If the transmission varies as a function of format position (where the light passes through the medium), then a reference point can be chosen and the change in transmission as a function of position from that point is referred to as shading. In the case of a lens, the optical center of the format at the image plane is generally chosen as the reference point and the relative brightness of the lens image is called vignetting.

In this discussion, even though there are other sources of shading, three sources of shading in the TV camera subsystem are considered: (1) the lens assembly, (2) the shutter assembly, and (3) the vidicon tube.

b. Summary. The maximum expected composite shading has been calculated for both the approach and survey cameras. The results indicate that the approach camera has less shading than the survey camera. The primary shading component in both cases is radial and is the same for all *f*/numbers except *f*/4, which has greater shading. Variations in shading, due to changes in temperature, are small—less than 1% for the survey camera and negligible for the approach camera.

The following analysis considers the three sources of shading and their combination to obtain the composite shading.

c. Analysis.

Lens assembly. Fig. 19(a) shows the vignetting curve provided by Bell & Howell for the variable focal-length lens assembly. In the test report for prototype X-8 (Ref. 2), the following comment is made: "The curves presented in the reports for lenses S/N X-5, X-6, X-7, and X-8 represent average data for these 4 lenses and S/N TA-1. A total of 60 off-axis points is plotted, 30 for each focal length and 5 for each *f*/number. If data for each individual lens are plotted, the average point will vary only 1½% between extremes, and no variations will exceed 3%. Thus, the average curves submitted closely represent each individual lens."

Fig. 19(b) is the respective calibration curve for the fixed focal-length lens assembly prototypes X-3, X-2, and TA-1.

Shutter assembly. Because the velocity of the shutter blades across the format is not constant, the exposure time (and therefore the amount of light passed through the shutter assembly) varies with format position. This gives the effect of shading that is rectilinear, not radial.

In FAT data analyzed, the exposure time was measured at three points in the format by light-sensitive diodes, arranged as shown in Fig. 20.

The percent shading with respect to the center of the format (diode 2) is given by

$$\text{Shading (at point } X) = (D2 - DX)\ 100/P \text{ percent where}$$

$D2$ = exposure time measured at diode 2

DX = exposure time measured at diodes 1 or 3

P = programmed input signal time

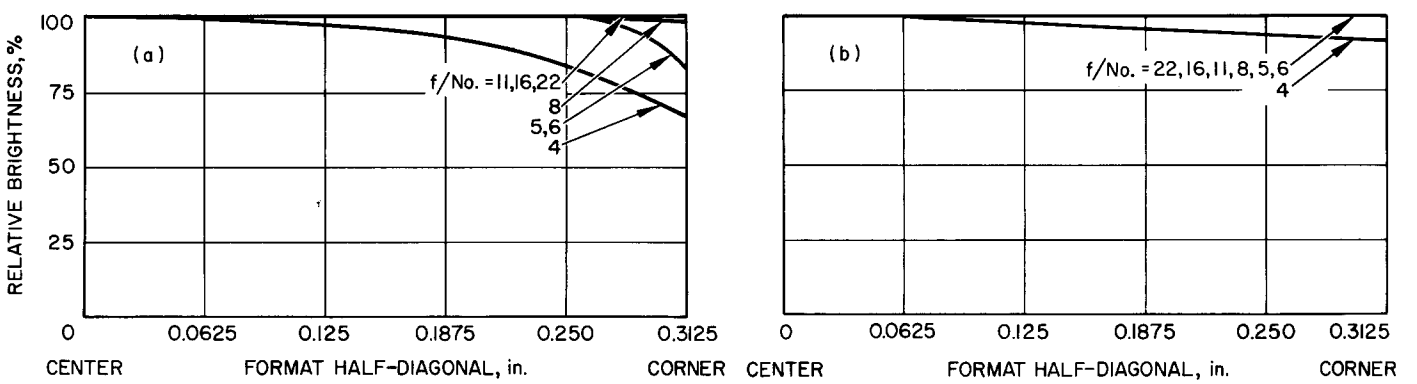

Fig. 19. Nominal lens assembly vignetting curves: (a) variable focal length lens; (b) fixed focal length lens

UNCLASSIFIED
CONFIDENTIAL

UNCLASSIFIED
CONFIDENTIAL

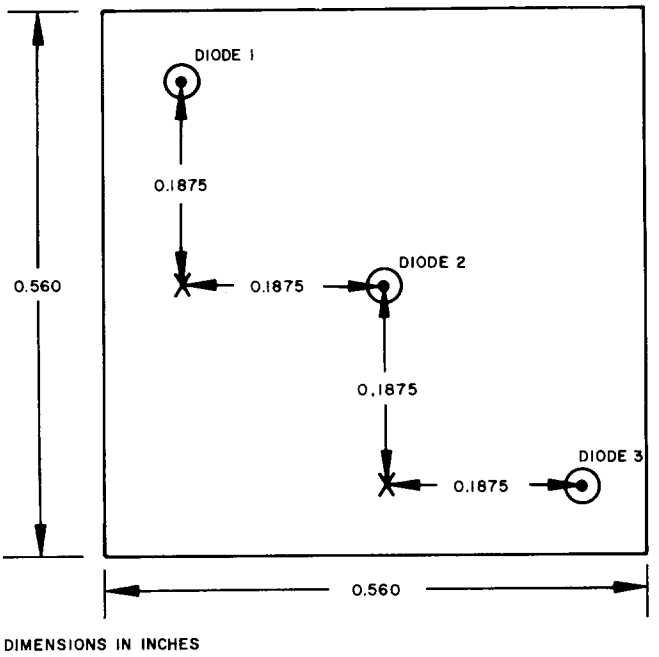

Fig. 20. Location of photodiodes in shutter format

The results of shading calculations indicated a consistent negative shading. That is, the exposure time was longer at the edges of the format than at the center. A three-dimensional picture of the typical shading experienced is shown in Fig. 21. Note that the shading is constant in the x-direction because the shutter blades move only in the y-direction.

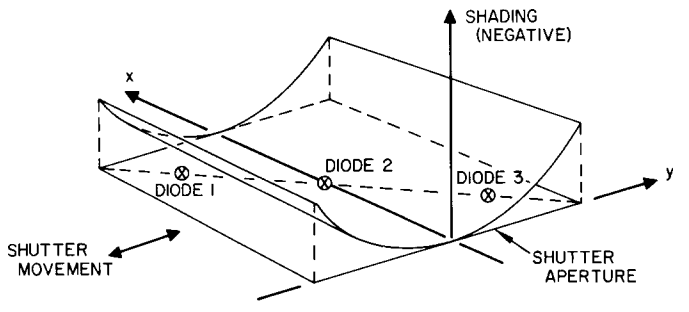

Fig. 21. Typical shading for shutter format

Fig. 22 shows how the 2-σ limits of the shading vary with temperature and the y-coordinate of Fig. 21. The points plotted for each temperature are for the applied voltage variation which gives the largest shading.

Fig. 22(a) indicates that well over 95% of all shutters would be expected to have shading values between 1.1 and -4%, at 20 msec nominal exposure, over the entire

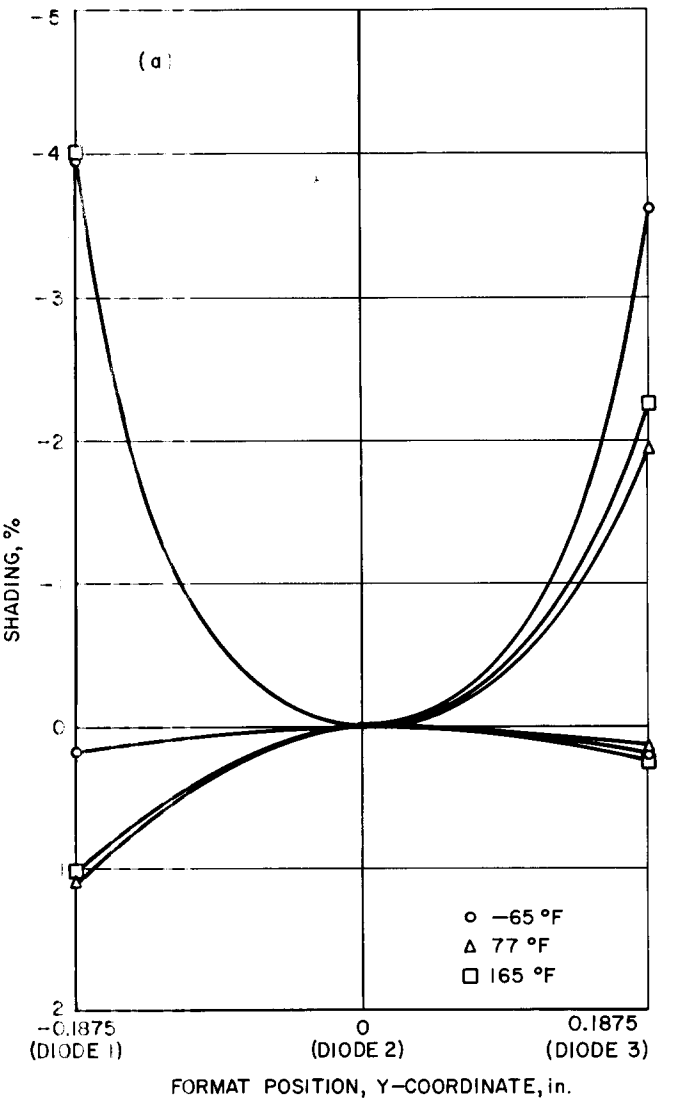

Fig. 22(a). Two-sigma limits of shading vs shutter format position: 20-msec nominal exposure

voltage-temperature range. In the 150 msec case the expected shading values should lie between 0.14 and -0.64% [Fig. 22(b)].

Vidicon tube. A major component of vidicon shading is due to the beam landing angle. Other components of vidicon shading can take complex forms. These components are not necessarily centered about the vidicon format center and can change with changes in vidicon parameters. The shading data for ten vidicons were recently analyzed to determine the type and degree of shading exhibited by *Surveyor* vidicons. It was determined that the primary shading component was radial

UNCLASSIFIED
CONFIDENTIAL

UNCLASSIFIED
CONFIDENTIAL

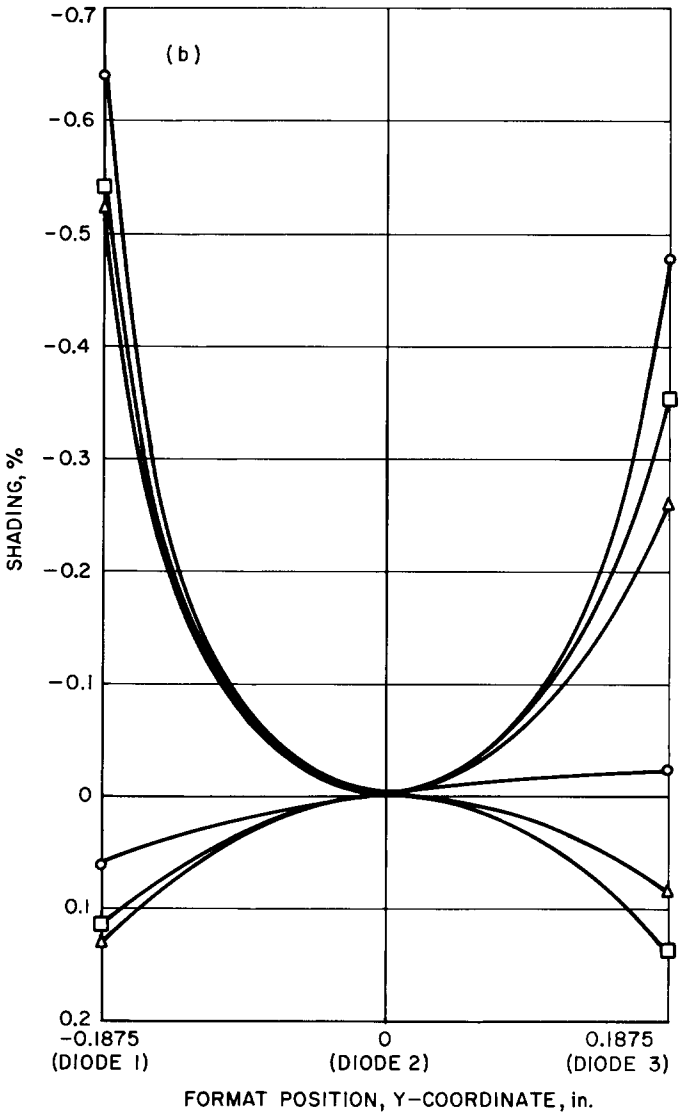

Fig. 22(b). Two-sigma limits of shading vs shutter format position: 50-msec nominal exposure

and that the maximum shading measured, at two different radii from the center of the format R_E and R_C, was

$R_E = 0.194$ in., maximum shading $= 21.8\%$

$R_C = 0.275$ in., maximum shading $= 31.1\%$

These two points are plotted, and the resultant shading curve extrapolated to zero at the center of the format, in Fig. 23.

Composite shading. The composite shading includes the total shading encountered when light passes through the lens and the shutter, and its conversion to electrical

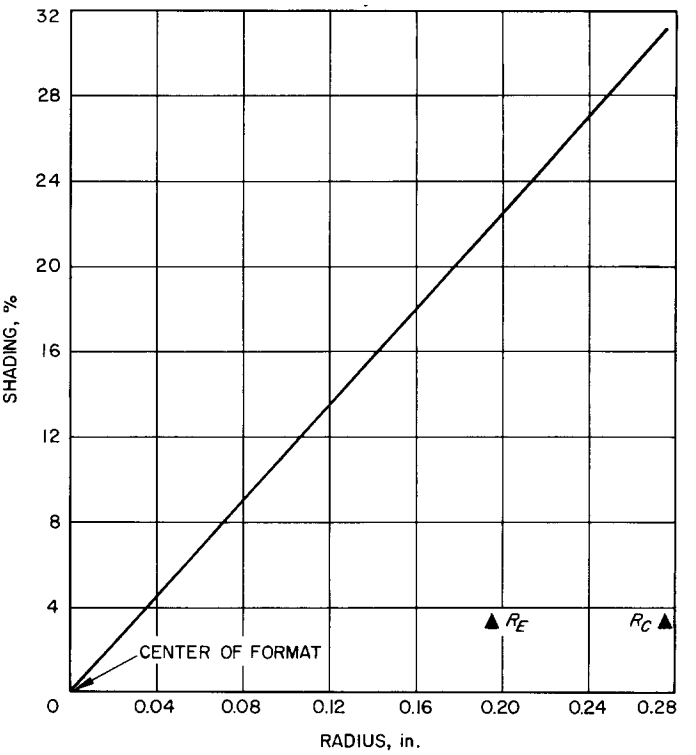

Fig. 23. Maximum vidicon shading vs radius from format center

signals by the vidicon. When the individual components are known, the composite shading is given by

$$S_C = 100-(100-S_L)(100-S_S)(100-S_V)10^{-4}\%$$

where

S_C = composite shading

S_L = shading introduced by lens

S_S = shading introduced by shutter

S_V = shading introduced by vidicon

Two sets of composite shading calculations were made, one for each of the camera types to be used on *Surveyor*. The two cameras are as follows:

(1) The approach camera consists of the following:
Fixed focal-length lens assembly
20 msec nominal exposure time shutter assembly
Vidicon tube

(2) The survey camera consists of the following:
Variable focal-length lens assembly
150 msec nominal exposure time shutter assembly
Vidicon tube

CONFIDENTIAL
UNCLASSIFIED

UNCLASSIFIED
CONFIDENTIAL

The composite shading data calculated for the approach camera were based on Figs. 19(b), 22(a), and 23. Although the shading due to the shutter assembly is not radial, it is small compared to the shading introduced by the vidicon and lens assembly and can be isolated by operating the camera in "open shutter" exposure mode. Therefore, the composite shading was assumed to be radial, and the largest positive values of shading shown in Fig. 22(a) were used at any given radius. The results are presented in Fig. 24, which shows the composite shading values computed for various temperatures and f/numbers as a function of radial distance from the format center. It appears that for the approach camera the shading is independent of f/number for f/numbers above 5.6. The maximum shading is at $f/4$, and, for all f/numbers, the temperature variations cause shading changes $\leq 1\%$.

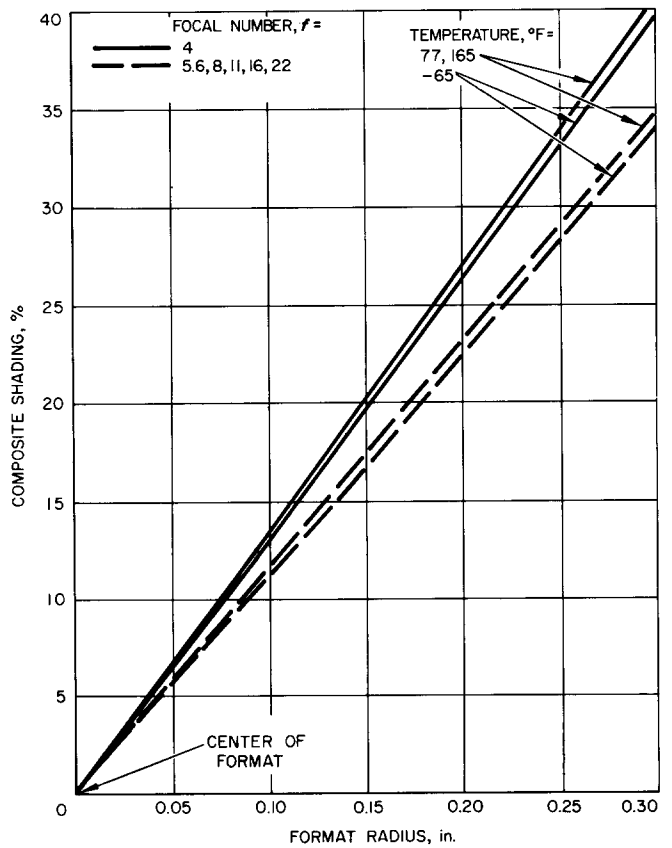

Fig. 24. Composite shading: *Surveyor* approach television camera

The composite shading results for the survey camera, based on Figs. 19(a), 22(b), and 23, are shown in Fig. 25. Fig. 25 shows the composite shading values computed for various f/numbers as a function of radial distance from the format center. Since the maximum shading introduced by the shutter was only a few tenths of a percent, this maximum shading was used, and variations with temperature were ignored. As a result, Fig. 25 shows variations with f/number only. Again, the maximum shading is at $f/4$, and, at the higher f/numbers, the shading is the same except at the extreme edge of the format.

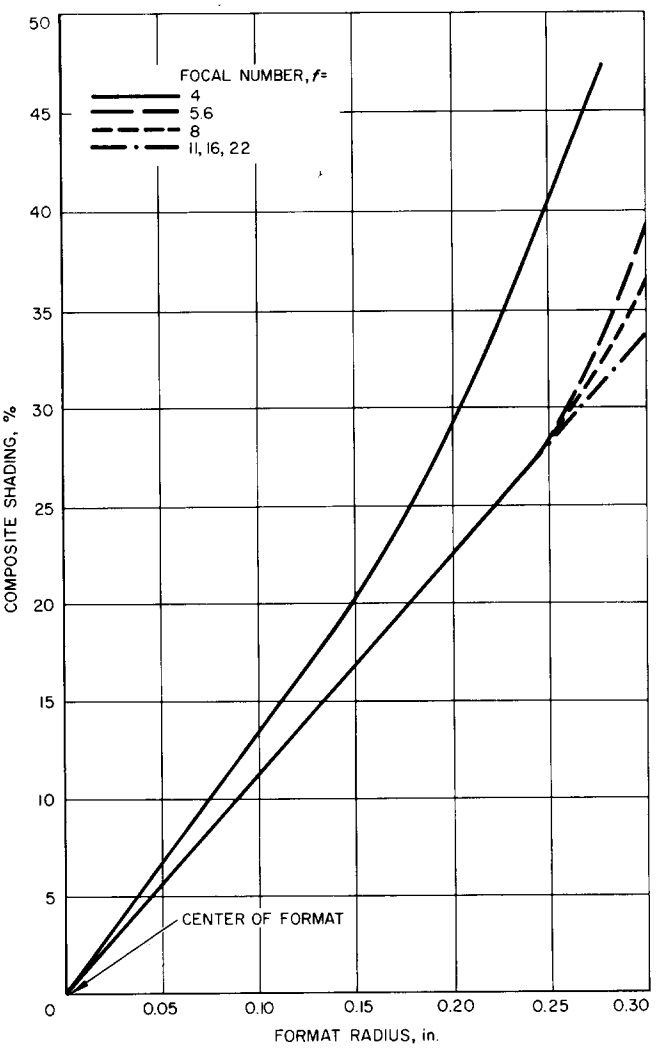

Fig. 25. Composite shading: *Surveyor* survey television camera

It should be noted that the accuracy of the data presented for the lens assemblies, shutter assemblies, and vidicon is not the same. The lens vignetting curves are average, the shutter shading curves are worst-case 2-σ limits, and the vidicon shading curve is a worst-case maximum. Similarly, the only temperature variations considered were for the shutter assemblies.

CONFIDENTIAL
UNCLASSIFIED

UNCLASSIFIED
CONFIDENTIAL

6. *An Operational Analysis for Planar Array Earth Acquisition With Unknown Sun Direction*

a. Introduction. The standard procedure for acquiring the Earth with the planar array antenna after touchdown for a lunar day landing is first to acquire the Sun by utilizing the broad field of view of the secondary Sun sensor and then to describe the possible locations of the Earth by an arc drawn about the spacecraft-Sun line at the known Earth-Moon-Sun angle. The length of this arc is determined by the assumed possible tilt of the spacecraft Z axis from lunar local vertical.

If the Sun direction cannot be determined, or Sun acquisition is to be bypassed in favor of an immediate Earth acquisition, the Earth search procedure to be initiated by the attitude analysts will be basically the same as would be performed during a lunar night acquisition. This procedure involves scanning the areas of probable Earth location which are algebraic composites of all uncertainty areas from those appreciable sources contributing to the uncertainty of the postlanding spacecraft attitude.

These attitude dispersions consist primarily of uncertainties in (1) landing site, (2) spacecraft roll orientation after touchdown, and (3) lunar slope. The landing site uncertainty is small compared to items 2 and 3. Latest studies reveal that the spacecraft roll uncertainty after touchdown will be within ±30 deg of the known postlanding orientation with a greater than 99% probability. The 3-σ figure relating to lunar slope has been defined as 15 deg.

b. Earth uncertainty areas to be scanned. The uncertainty areas of Earth location are attributed in part to a 15-deg tilt of the spacecraft Z axis from local vertical, which is a function of the nominal zero tilt Earth elevation angle in spacecraft coordinates. A computer program is available to compute these areas which vary from a circle for a nominal overhead Earth to an almost straight line when the Earth lies along the horizon. These are the dashed areas in Fig. 26.

The total uncertainty area to be searched for the Earth is then that area traced out by a ±30-deg roll of this figure. The solid areas in Fig. 26 present the composite 3-σ probability areas of Earth location for nominal Earth elevation angles of 0, 45, and 90 deg, respectively.

c. Two available search techniques. Two methods have been investigated for scanning the previously presented

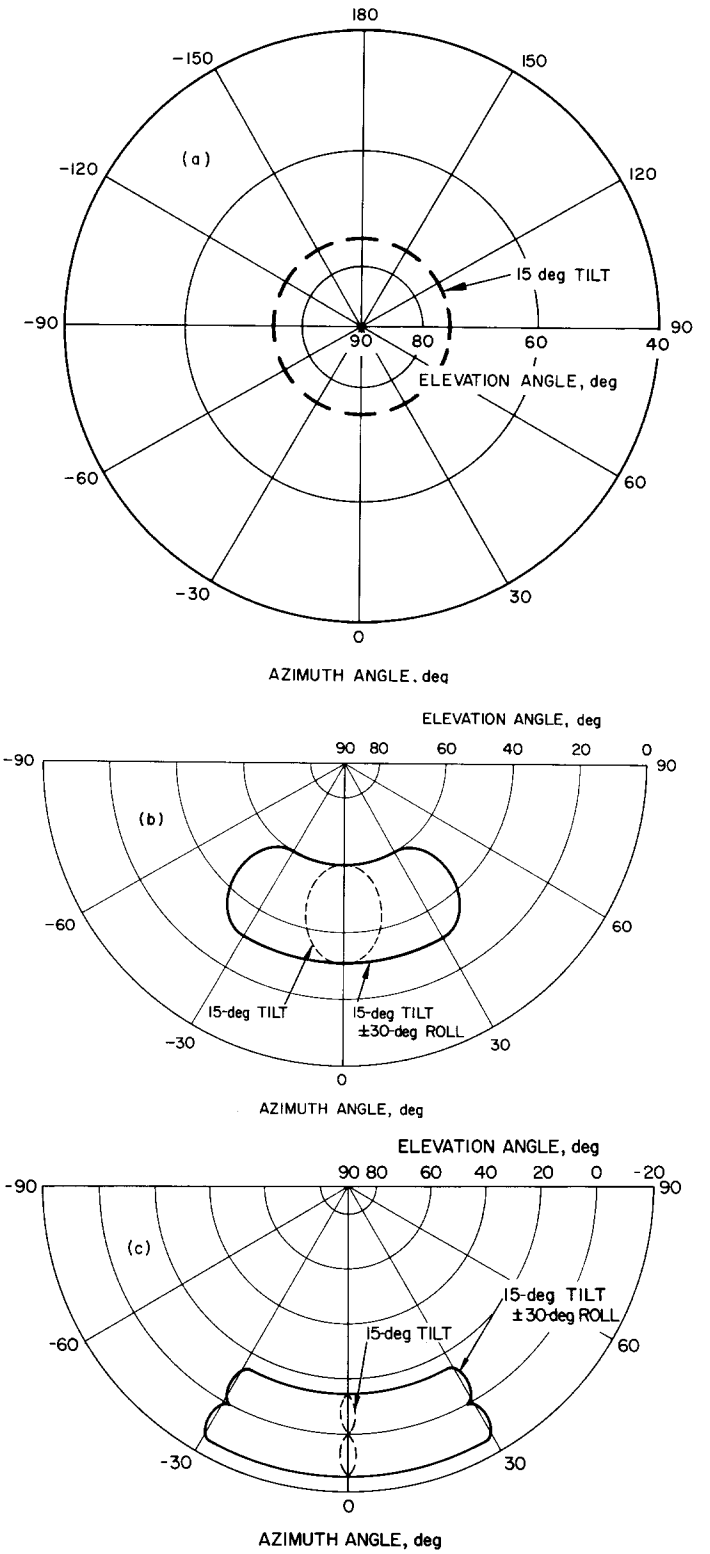

Fig. 26. Uncertainty areas: (a) nominal Earth elevation angle of 0 deg; (b) nominal Earth elevation angle of 45 deg; (c) nominal Earth elevation angle of 90 deg

CONFIDENTIAL
UNCLASSIFIED

UNCLASSIFIED
CONFIDENTIAL

areas of Earth location uncertainty. The pattern recognition method utilizes knowledge of the entire planar array antenna gain patterns. The procedure is to sweep the 3-σ area with either the broad feedline or broad branchline arms of the planar array gain patterns. When automatic gain control data are received, they are compared to the measured representative contour maps, and the data are correlated to determine subsequent positioning commands. The second search technique is to scan the area of uncertainty with the high-gain main lobe only. The gain of the main lobe is 13 db higher than that of any side lobe, consequently, as seen in Fig. 27, a 10-deg diameter of the main lobe can be used to provide a gain 6 db above the strongest side lobe peak. The total uncertainty area is systematically traversed with this section of the main lobe until the telecommunications analysts of the Space Flight Operations Facility at JPL can verify from the received data that this is indeed the main lobe.

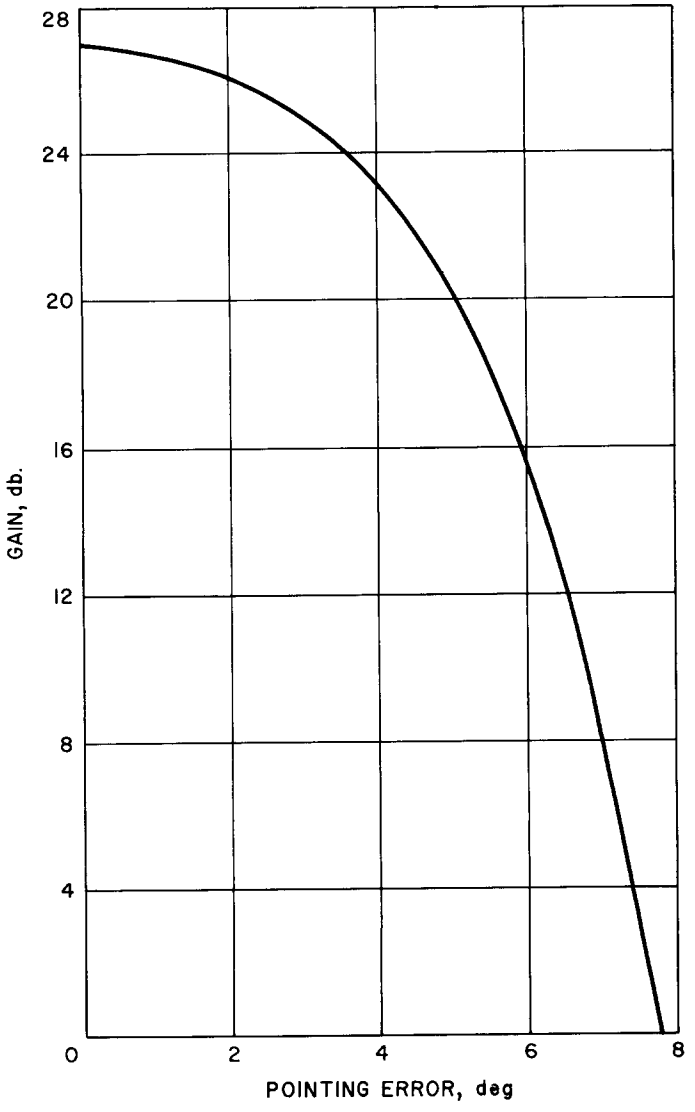

Fig. 27. Planar array main lobe gain

The desirability of each technique varies as related parameters change. For instance, owing to a recent analysis of spacecraft touchdown dynamics, the expected 3-σ spacecraft roll uncertainty has decreased from a pessimistic ± 90 deg to ± 30 deg. It appears at this time that the optimum search pattern would be a hybrid system composed of a main lobe scanning of the uncertainty area which would branch to the pattern recognition search if the data strongly warranted doing so.

d. Planar array antenna search technique using main lobe scanning. As stated above, a 10-deg diameter of the main lobe would be used because 5 deg out from its peak the main lobe is still 6 db higher than the strongest side lobe. The route to be followed would be an approximate spiral which begins at the nominal Earth position, as shown in Fig. 28. By beginning in the nominal Earth location, the area of greatest probability is explored first; moreover, since a 2-min on, 3-min off duty cycle exists for each axis, this mode of cycling, the alternate stepping of the polar gimbal angle, and the roll gimbal angle for this case conserves time.

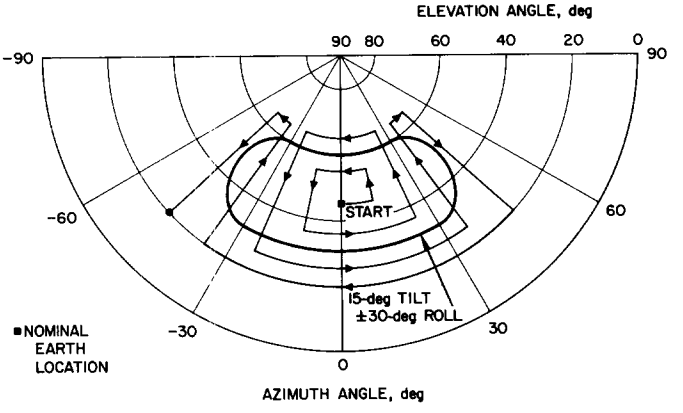

Fig. 28. Planar array antenna main lobe search route

e. Planar array antenna search technique utilizing pattern recognition. Two modes of search operation exist. The first mode is the planar array stepping procedure used prior to receiving antenna gain control (AGC) data from the Deep Space Station (DSS) receiver which can be distinguished from background noise; the second mode is the procedure initiated after the DSS receiver AGC data indicate a lobe has been detected.

CONFIDENTIAL
UNCLASSIFIED

UNCLASSIFIED

A typical set of procedures for a roll/polar, or low Earth situation is presented in the logic flow diagrams of Figs. 29 and 30. Fig. 31 is a logic diagram describing the technique used in centering any detected lobe when the location of the Earth cannot yet be predicted. Once it has been determined from the AGC data that a particular side lobe is pointed at the Earth, the steps necessary to position the main lobe toward the Earth are

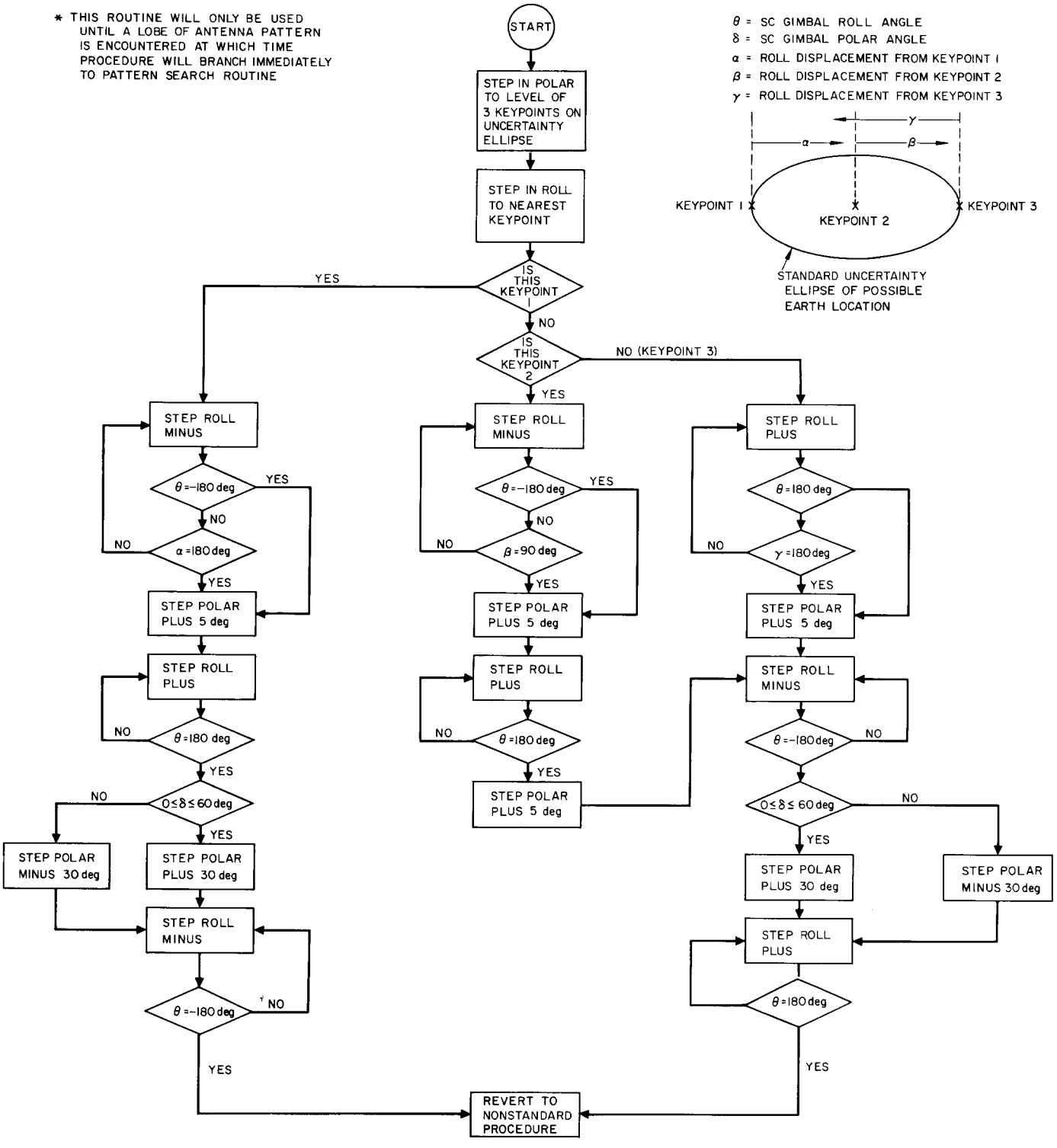
* THIS ROUTINE WILL ONLY BE USED UNTIL A LOBE OF ANTENNA PATTERN IS ENCOUNTERED AT WHICH TIME PROCEDURE WILL BRANCH IMMEDIATELY TO PATTERN SEARCH ROUTINE
START
STEP IN POLAR TO LEVEL OF 3 KEYPOINTS ON UNCERTAINTY ELLIPSE
STEP IN ROLL TO NEAREST KEYPOINT
IS THIS KEYPOINT 1
YES
NO
IS THIS KEYPOINT 2
NO (KEYPOINT 3)
YES
θ = SC GIMBAL ROLL ANGLE
δ = SC GIMBAL POLAR ANGLE
α = ROLL DISPLACEMENT FROM KEYPOINT 1
β = ROLL DISPLACEMENT FROM KEYPOINT 2
γ = ROLL DISPLACEMENT FROM KEYPOINT 3
KEYPOINT 1
KEYPOINT 2
KEYPOINT 3
STANDARD UNCERTAINTY ELLIPSE OF POSSIBLE EARTH LOCATION
STEP ROLL MINUS
θ = −180 deg
α = 180 deg
STEP POLAR PLUS 5 deg
STEP ROLL PLUS
θ = 180 deg
0 ≤ δ ≤ 60 deg
STEP POLAR MINUS 30 deg
STEP POLAR PLUS 30 deg
STEP ROLL MINUS
θ = −180 deg
STEP ROLL MINUS
θ = −180 deg
β = 90 deg
STEP POLAR PLUS 5 deg
STEP ROLL PLUS
θ = 180 deg
STEP POLAR PLUS 5 deg
STEP ROLL PLUS
θ = 180 deg
γ = 180 deg
STEP POLAR PLUS 5 deg
STEP ROLL MINUS
θ = −180 deg
0 ≤ δ ≤ 60 deg
STEP POLAR PLUS 30 deg
STEP POLAR MINUS 30 deg
STEP ROLL PLUS
θ = 180 deg
REVERT TO NONSTANDARD PROCEDURE

Fig. 29. Initial planar array Earth search routine

UNCLASSIFIED

UNCLASSIFIED
CONFIDENTIAL

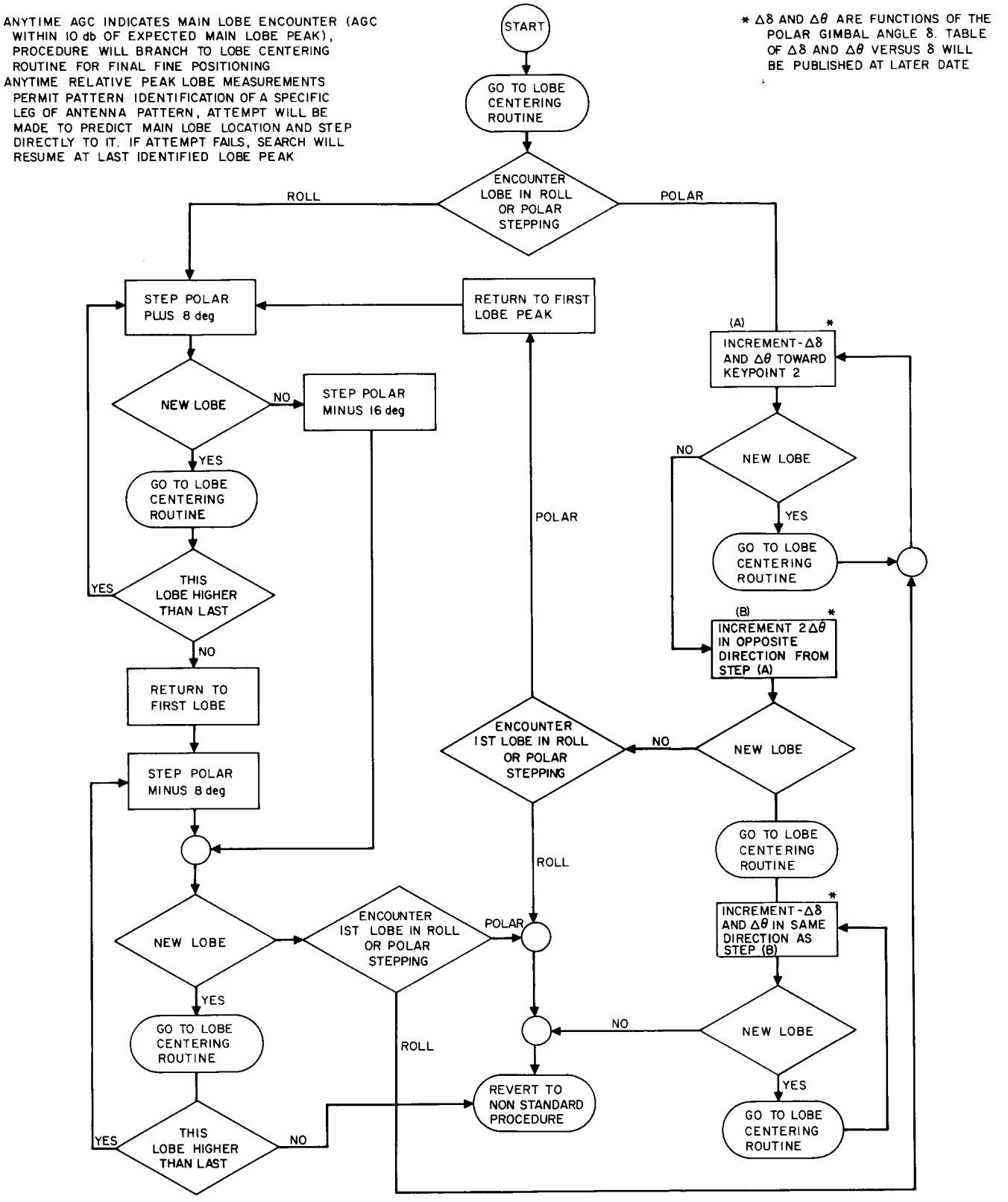
ANYTIME AGC INDICATES MAIN LOBE ENCOUNTER (AGC WITHIN 10 db OF EXPECTED MAIN LOBE PEAK), PROCEDURE WILL BRANCH TO LOBE CENTERING ROUTINE FOR FINAL FINE POSITIONING
ANYTIME RELATIVE PEAK LOBE MEASUREMENTS PERMIT PATTERN IDENTIFICATION OF A SPECIFIC LEG OF ANTENNA PATTERN, ATTEMPT WILL BE MADE TO PREDICT MAIN LOBE LOCATION AND STEP DIRECTLY TO IT. IF ATTEMPT FAILS, SEARCH WILL RESUME AT LAST IDENTIFIED LOBE PEAK
* Δδ AND Δθ ARE FUNCTIONS OF THE POLAR GIMBAL ANGLE δ. TABLE OF Δδ AND Δθ VERSUS δ WILL BE PUBLISHED AT LATER DATE
START
GO TO LOBE CENTERING ROUTINE
ENCOUNTER LOBE IN ROLL OR POLAR STEPPING
ROLL
POLAR
STEP POLAR PLUS 8 deg
RETURN TO FIRST LOBE PEAK
(A) *
INCREMENT -Δδ AND Δθ TOWARD KEYPOINT 2
NEW LOBE
NO
STEP POLAR MINUS 16 deg
YES
GO TO LOBE CENTERING ROUTINE
THIS LOBE HIGHER THAN LAST
YES
NO
RETURN TO FIRST LOBE
STEP POLAR MINUS 8 deg
POLAR
NO
NEW LOBE
YES
GO TO LOBE CENTERING ROUTINE
(B) *
INCREMENT 2Δθ IN OPPOSITE DIRECTION FROM STEP (A)
ENCOUNTER 1ST LOBE IN ROLL OR POLAR STEPPING
NO
NEW LOBE
GO TO LOBE CENTERING ROUTINE
ROLL
*
INCREMENT -Δδ AND Δθ IN SAME DIRECTION AS STEP (B)
NEW LOBE
ENCOUNTER 1ST LOBE IN ROLL OR POLAR STEPPING
POLAR
YES
GO TO LOBE CENTERING ROUTINE
ROLL
NO
NEW LOBE
YES
GO TO LOBE CENTERING ROUTINE
REVERT TO NON STANDARD PROCEDURE
YES
THIS LOBE HIGHER THAN LAST
NO

Fig. 30. Pattern search routine

UNCLASSIFIED
CONFIDENTIAL

UNCLASSIFIED
CONFIDENTIAL

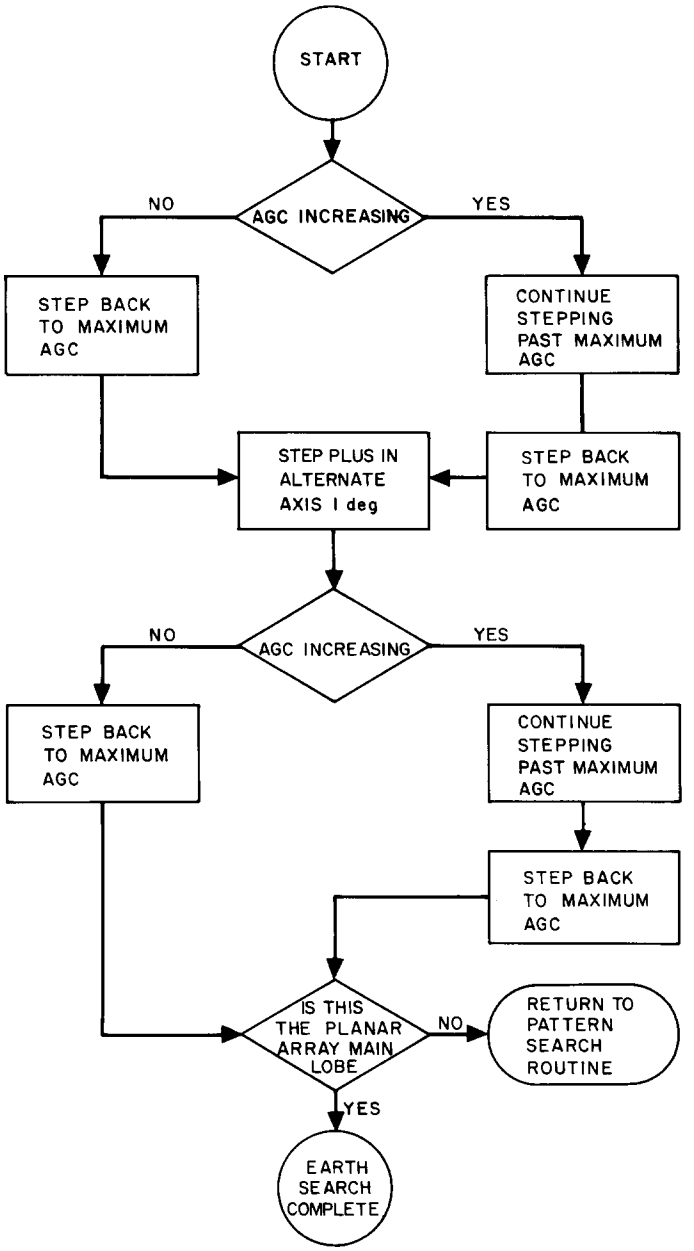

Fig. 31. Lobe centering routine

immediately commanded. In order to determine that a particular side lobe has been acquired, or in order to predict the resultant steps required for main lobe centering, a clear hemisphere is utilized in conjunction with a concentric opaque sphere in the four-axis gimbal model. A contour map of the antenna pattern is plotted on this hemisphere to the same angular scale as the sphere. The hemisphere can be moved over the sphere to simulate roll, polar, and elevation motion of the antenna in the spacecraft system; therefore, AGC data can be correlated with the antenna contour map to predict the Earth's location in the spacecraft system.

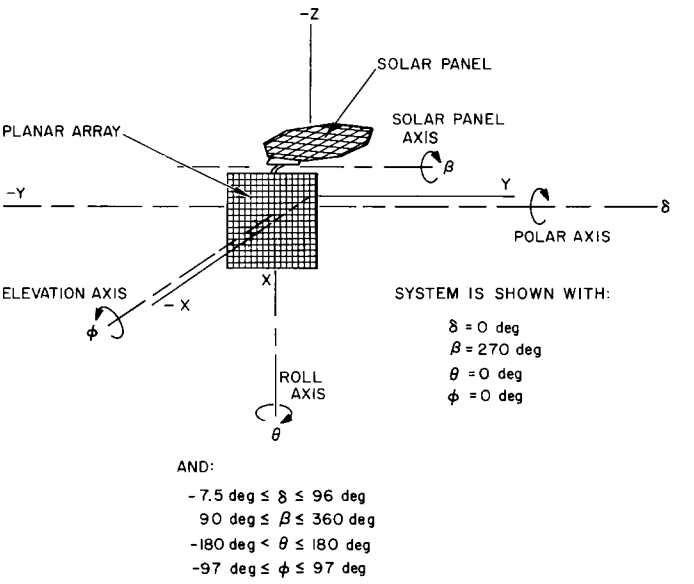

Fig. 32. Spacecraft gimbal system

The roll, polar, elevation, and solar panel gimbal angles are defined in Fig. 32. When the polar angle is 6.5 deg (equal to the main lobe depression angle), the series of antenna side lobes in the feedline (horizontal) and branchline (vertical) planes are projected as straight lines on the inner globe. When the polar angle increases, however, and the elevation angle remains zero, the vertical set of side lobes remains straight with respect to a polar line on the globe, but the horizontal set of side lobes bends downward with respect to the horizontal roll lines on the globe. This means that a roll motion alone will not move the pattern relative to a given Earth location from one horizontal side lobe to another for any polar angle other than 6.5 deg. This result is shown in Fig. 33.

f. Pre-AGC search pattern. The initial search procedure is to sweep the uncertainty area of Earth location plotted on the inner opaque globe with the broad side lobe arms of the antenna pattern. Fig. 34 shows a representative Earth location figure to be searched. The Earth search procedure for the representative area would be as follows.

If the initial roll setting of the planar array places the main lobe in area 1, the main lobe will be commanded to key point 1, and a roll maneuver to the right will be executed. If the initial roll angle places the main lobe in area 2, it will be stepped to the polar value of key point 2, and a roll maneuver in the direction of key point 2 will be performed which will sweep across that portion of the figure.

UNCLASSIFIED
CONFIDENTIAL

UNCLASSIFIED
CONFIDENTIAL

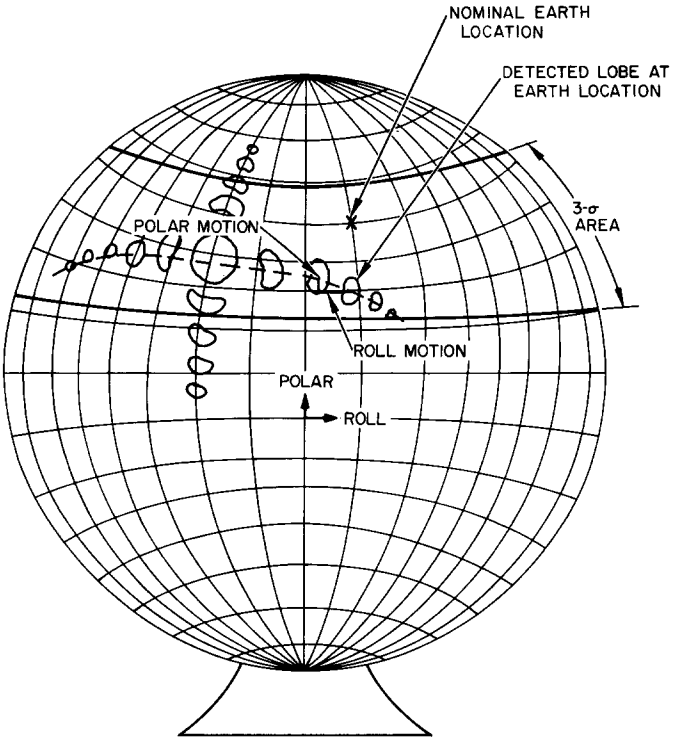

Fig. 33. Roll/polar motion

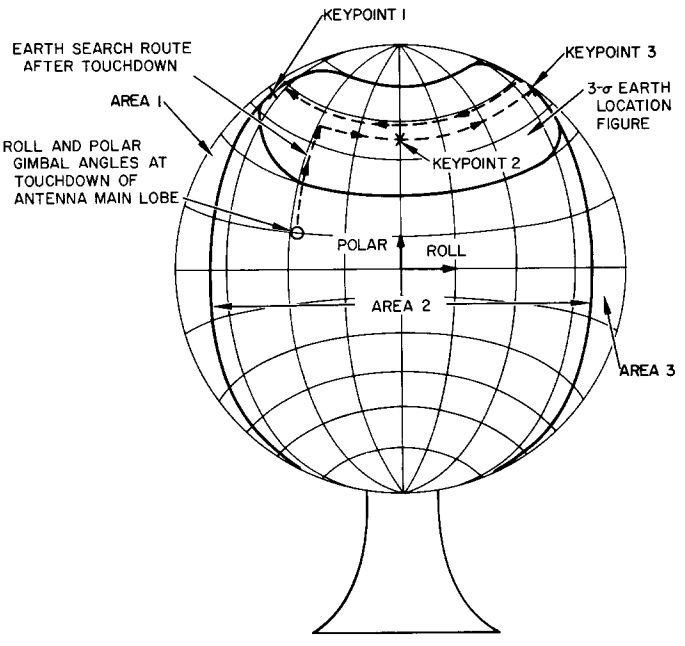

Fig. 34. Procedure for initial AGC acquisition

In any of these maneuvers, if a lobe is not detected on one sweep across the area, or a portion of the area, the polar angle is increased 5 deg, and the entire figure is traversed by being rolled in the opposite direction. Any portion of the figure that has only been traversed once will again be swept across in this manner. Five deg is chosen because the vertical side lobes, displayed in Fig. 35, are on the average 10 deg apart. It is difficult to develop a search procedure that would reflect optimum stepping based upon the Earth location probability distribution because the search is being made with the entire antenna pattern, not a single point, and the efficiency of stepping of the various gimbal angles is related to the values of the remaining gimbal angles.

g. Post-AGC search pattern. If AGC is received on the beginning polar maneuver, it is assumed that the lobe encountered, after centering it and determining that it is not the main lobe, lies on a horizontal arm of the antenna pattern shown in Fig. 33; moreover, the detected lobe is assumed to lie on the horizontal arm which is on the same side of the main lobe as the nominal Earth location. Assume that this is the right horizontal arm. A roll and polar motion would be performed, as shown in Fig. 33. If no lobe were detected, it would be assumed that the detected lobe had been on the left horizontal arm, and an appropriate roll and polar motion would be initiated to locate an adjacent lobe on this arm. If another lobe is still not detected, it is assumed that the detected lobe did instead lie on a vertical arm; thus, after recentering, a polar motion is executed. In either case, by the time the third lobe is discovered, the Earth location may well be determined because of the distinct antenna pattern characteristics. A similar technique is employed when a lobe is encountered while originally moving in roll; however, the Earth location is now assumed to be under one of the vertical arms.

The above search patterns depict a low Earth search situation. If the nominal Earth is above 45 deg in elevation, the elevation gimbal angle stepping becomes more efficient than the roll gimbal angle stepping; consequently, whenever appropriate conditions arise, the attitude analysts may elect to use this angle in the search procedure. Elevation angle stepping is not presented here because it is difficult to visualize without the aid of the four-axis gimbal model. The four gimbal angles are presented in Fig. 32. The search techniques will remain similar to those previously discussed.

7. Surveyor *Planar Array Field Pattern*

A series of planar array field pattern tests was recently conducted on two A-21 antennas with measurements made at a frequency of 2295 MHz. The disparities between the two patterns were small enough that a realistic

CONFIDENTIAL
UNCLASSIFIED

UNCLASSIFIED
CONFIDENTIAL

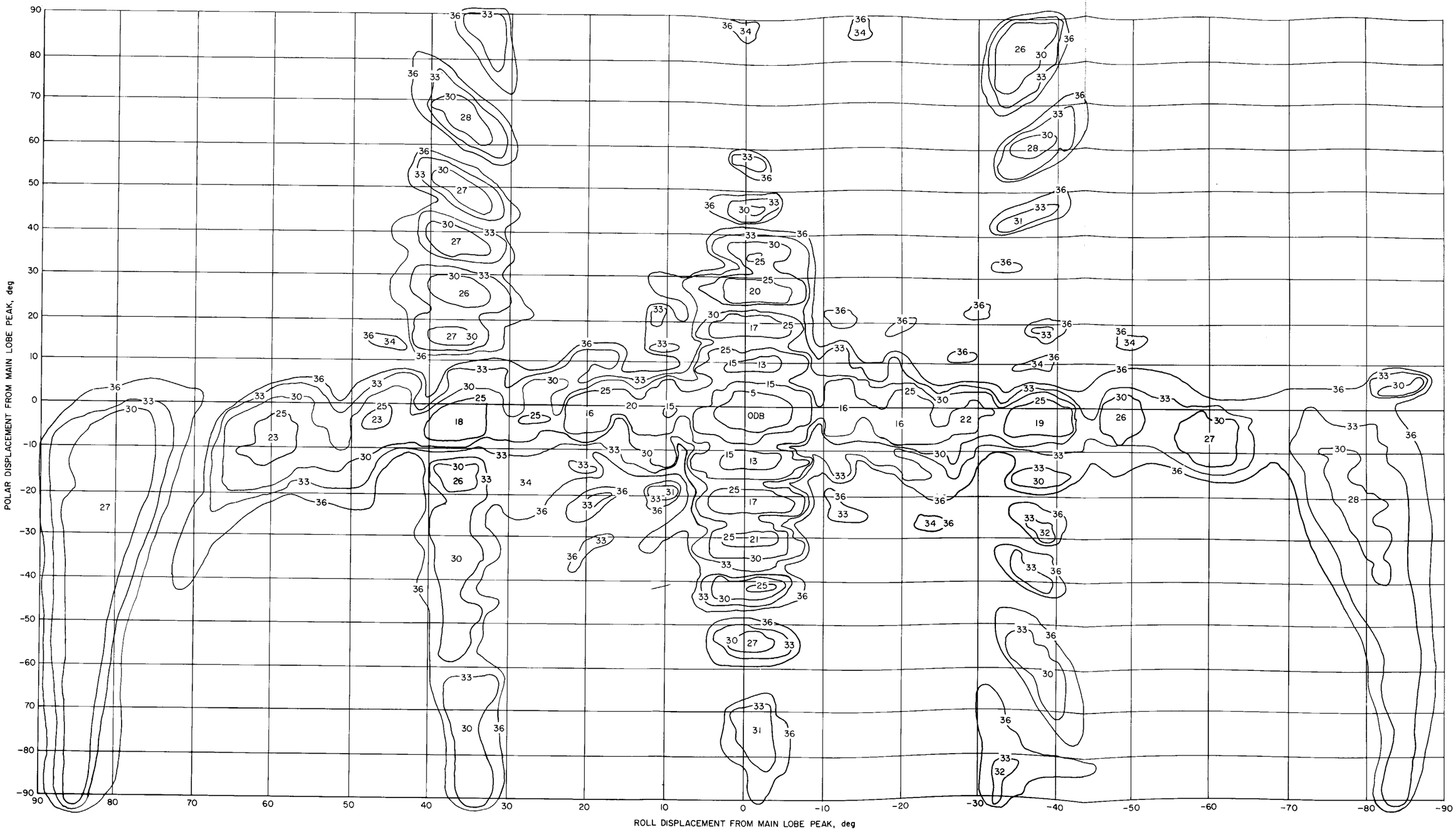

Fig. 35. Displacement from main lobe peak

UNCLASSIFIED
CONFIDENTIAL

UNCLASSIFIED

representative field pattern could be determined by averaging the patterns of the two antennas. Fig. 35 shows this average nominal contour plot. These contours are expressed in db below the peak of the main lobe, which is at a level of 27 db relative to an isotropic antenna with right-hand circular polarization. The coordinate system for the measurement is shown in Fig. 36. These antenna field patterns will be used during lunar operations to facilitate Earth acquisition.

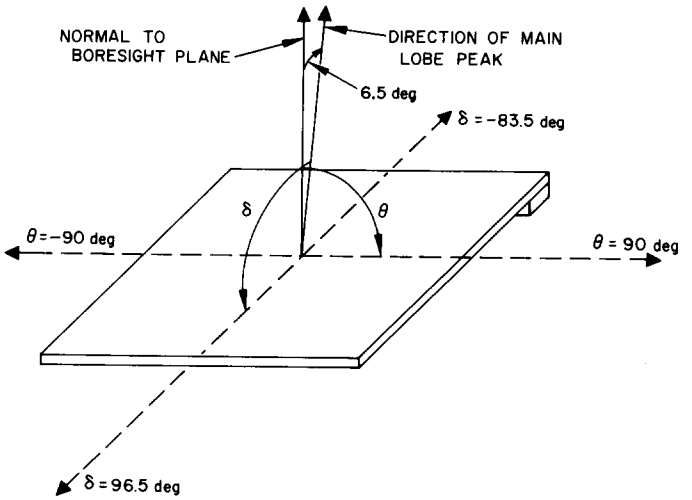

Fig. 36. Coordinate system

D. Launch Vehicle Integration[2]

1. Spacecraft/Launch Vehicle Integration Schedule

Atlas/Centaur vehicle, AC-10 with its payload, *Surveyor* spacecraft SC-1 (*Surveyor* mission A) was successfully launched from AFETR complex 36-A May 30, 1966, as scheduled. The launch vehicle composite readiness test (CRT) to revalidate and verify the proper operation of the vehicle and GSE electrical systems in launch configuration was satisfactorily completed May 25, followed by the final spacecraft/launch vehicle mate on May 26. Countdown operations proceeded without incident on May 30, resulting in lift-off on time.

The spacecraft was lofted into a lunar intercept trajectory, in a single burn direct ascent mission. The flight through boost phase, *Centaur* main engine firing, spacecraft separation and retromaneuver was normal and only a slight midcourse correction was necessary to place the spacecraft on target. Additional prelaunch activity is discussed in paragraph 2 below. Flight results through *Centaur* retromaneuver are discussed in paragraph 3.

Joint spacecraft/launch vehicle milestone planning dates for *Surveyor* mission B (spacecraft SC-2 and *Atlas/Centaur* AC-7) have been established as follows:

Ship spacecraft from HAC to AFETR	July 19,1966
First mate [for joint flight acceptance composite tests (J-FACT)]	Aug 9, 1966
Demate (after J-FACT)	Aug 17, 1966
Final mate	Sept 15, 1966
Complete AFETR operations	Sept 19, 1966

Under this schedule, time does not permit cycling the spacecraft through a combined systems test (CST) at General Dynamics/Convair, San Diego, and it will be shipped directly to the AFETR. The above schedule is extremely tight and requires HAC to utilize a seven-day work week during the entire period at the AFETR. The eight work days between first mate and demate is two days short of the ten desired for the launch vehicle. Lewis Research Center (LeRC) and the AFETR are investigating means for accommodating this reduced time period.

The launch vehicle (AC-7) for mission B has arrived at AFETR complex 36-A. The *Atlas* arrived June 18 and was erected June 22, 1966. The *Centaur* arrived June 25 and was erected June 29. Preparations are under way to be ready for spacecraft mate by August 9, 1966.

2. AC-10/SC-1 Prelaunch Activity

a. Readiness reviews. Two readiness review meetings were held prior to launch with the launch vehicle system managing agency, LeRC, and with ULO following the J-FACT April 26, 1966.

On May 6, 1966 the meeting was held at AFETR to review performance of and problems resulting from the FACT. Although there were some problems with both the launch vehicle and the spacecraft, none were serious enough to threaten the launch schedule.

On May 24, 1966 another readiness review was held at AFETR. All major systems areas reported to the mission director on their respective status to support mission A.

[2]Prepared by JPL Section 291.

CONFIDENTIAL UNCLASSIFIED

UNCLASSIFIED
CONFIDENTIAL

The launch vehicle system, reported by ULO, was ready to support the launch.

b. Launch vehicle prelaunch activity. AC-10 prelaunch activities, after quad tanking and J-FACT testing, consisted of:

(1) A number of small modifications and changes to the launch vehicle equipment such as: replacement of valves with questionable leak rates; new H_2O_2 attitude control engines, to preclude a failure as experienced on the AC-8 vehicle; replacement of the *Atlas* autopilot programmer, to resolve a minor gyro drift problem of 18 deg/hr and an anomaly experienced during J-FACT; replacement of the *Atlas* gyro back-up units (-3 gyros) with flight qualified units (-5 gyros); rework of the *Centaur* timer and A.E.U. for resequencing relative to the *Centaur* vent valves; replacement of the *Centaur* LOX fill and drain valve; deletion of the inadvertent payload separation switch circuits; shim-up of the RP-1 staging valve; rework of the T-4 aft umbilical plate and chute, to preclude hang-up and abort as experienced on AC-8; replacement of the pitch and yaw actuators on the sustainer engine; repair of the minor computer case leak; enlargement of the guidance system optical alignment aperture; addition of rubber sealant to ducting seals, to preclude contaminant release into the spacecraft cavity; modification of the *Centaur* insulation panel hinges and the addition of break wire instrumentation to monitor panel jettison; and the accomplishment of several other minor tasks.

(2) Inspecting and performing functional checks on portions of the launch vehicle systems and equipment.

X-raying servo valves.

X-raying some questionable connectors.

Checking capacitor installations in the PU system.

"Wiggle" checking some cables and connectors for shorts.

Repeat leak checking the *Atlas* engines.

Revalidating the inadvertantly water soaked RF No. 1 system on the *Atlas*.

Full scale firing of the attitude control engines.

(3) Rechecking the *Centaur* programmer and partial LOX tanking test to verify LOX valve change acceptability.

(4) Cleaning of the nose fairing, payload adapter, and associated equipment.

(5) Checking calibration on the guidance and autopilot systems.

(6) Cleaning, pyrotechnic installation, propellant loading, gas pressurization to flight levels, final weight balance and alignment, and participation in systems readiness tests of the spacecraft.

(7) Mating of payload to the adaptor.

(8) Installing *Surveyor* destruct system, pin puller squibs, in-flight disconnect squibs.

(9) Performing final encapsulation, loading of nose fairing thruster bottles to flight pressures.

(10) Mating payload to the *Centaur*.

(11) Installing launch vehicle pyrotechnics and destruct packages.

(12) Final guidance auto pilot (GAP) testing on the vehicle.

(13) Participating in final spacecraft systems readiness test.

A final launch vehicle, launch complex, weather, range, spacecraft and operations mission readiness meeting was held at T−24 hr. All planned tests and checks were reported completed with no outstanding anomalies noted. Projected winds aloft were reported as 57 knots at 43 kft. with a maximum expected shear parameter of 7 knots/kft. of altitude. The launch window was established by the launch vehicle 3-σ propellant reserves as opening at 09:41:00 and closing at 10:27:00 eastern standard time.

c. Countdown operations organization. The organization in effect during the countdown is shown in Fig. 37.

3. Mission A (SC-1 / AC-10) Flight Results

The following information and data are based on early postflight data and are subject to change after further evaluation.

The spacecraft and launch vehicle entered the joint countdown at approximately T−140 min. The balance of the countdown progressed without anomalies through to launch at 14:41:00.099 GMT.

a. Sequence of events. Between liftoff and completion of the *Centaur* portion of the mission, there was a very close correlation between preflight estimates and actual

CONFIDENTIAL
UNCLASSIFIED

UNCLASSIFIED

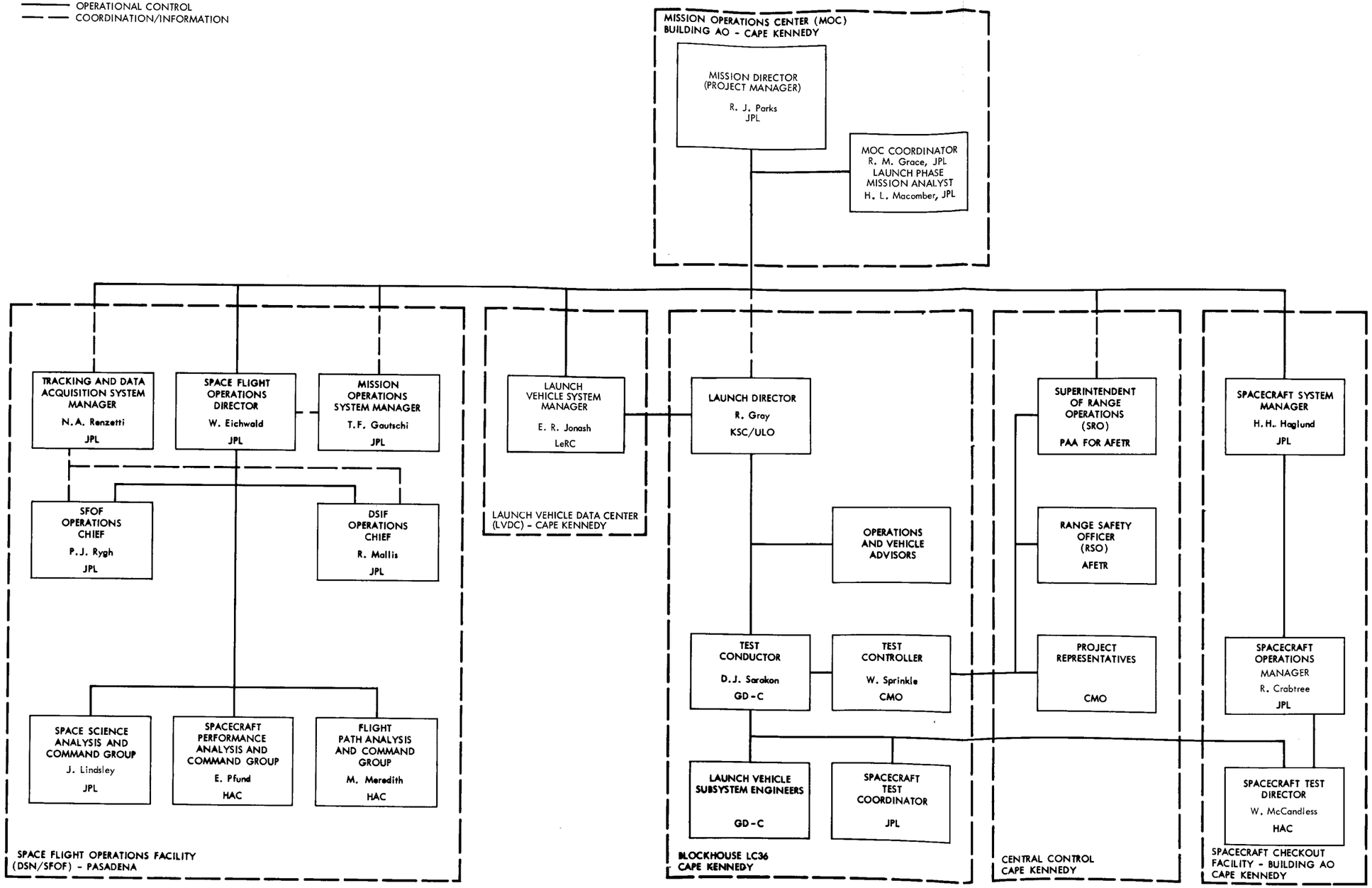

Fig. 37. Surveyor countdown operations organization

UNCLASSIFIED

UNCLASSIFIED

measured times of the occurrence of major flight events. Table 12 reflects this correlation. The only significant difference noted in the table is the longer than expected burn, approximately 5.0 sec, of the *Centaur* engines. The apparent reason for this is the slightly lower than expected thrust/weight ratio during the *Centaur* burn, probably due to the actual thrust being lower than the value used in the preflight simulation.

Table 12. AC-10 flight events

Event	Preflight time, sec	Actual time, sec
Booster engine cutoff (BECO)	T+142.5	T+142.2
Jettison booster package	T+145.6	T+145.6
Jettison insulation panels	T+176.5	T+176.2
Jettison nose-fairing	T+203.5	T+203.1
Sustainer engine cutoff (SECO); vernier engine cutoff; start *Centaur* programmer	T+239.7	T+239.3
Atlas/Centaur separation	T+241.6	T+241.8
Centaur main engine ignition	T+251.2	T+252.0
Centaur main engine cutoff (MECO)	T+683.9	T+689.3
Preseparation arming signal; extend landing gear signal	T+715.2	T+715.5
Unlock omniantennas signal	T+725.7	T+725.7
High power transmitter on signal	T+746.2	T+745.4
Electrical disconnect	T+751.7	T+752.3
Spacecraft separate	T+757.2	T+757.1
Begin *Centaur* orientation maneuver	T+762.2	T+759.5
Start *Centaur* tank blowdown	T+997.2	T+996.0
Centaur mission complete	T+1247.2	T+1247.7

b. AC-10/SC-1 injection data. Table 13 illustrates a close correlation between vehicle expected performance and actual trajectory data.

c. Spacecraft/launch vehicle separation. The *Surveyor* spacecraft is provided an initial separation velocity by three springs, one mounted at each of three attached points, and released by explosively actuated latch pins. Data from extensiometers indicate all three separation latches actuated within 2 msec of each other. The three springs operated normally and yielded approximately identical stroke vs time data. The uniform extension of the springs plus vehicle residual motion imparted an approximate 0.34 deg/sec vector sum turning rate to the spacecraft, well below the allowed 3 deg/sec.

Table 13. AC-10/SC-1 injection

Parameters[a]	Units	Predicted	Actual
Epoch	HMS, GMT	14:53:46	14:53:37
Radius	nm	3,535.7	3,537.2
Latitude	Deg	17.54	17.59
Longitude	Deg	312.45	312.14
Velocity	ft/sec	34,662	34,652
Path angle	Deg	−1.21	−1.26
Azimuth	Deg	115.77	115.79
C_3	km^2/sec^2	−1.255	−1.264

[a] Earth relative.

d. Centaur retromaneuver. The minimum required separation distance between *Centaur* and SC-1, five hours after separation, is 336 km. Actual measured distance was approximately 1,054 kilometers which exceeds the minimum requirements by a factor of 3. The *Centaur* stage continues in a highly elliptical Earth orbit with an apogee of approximately 237,000 nm and a period of approximately 12 days.

e. Guidance accuracy. The launch vehicle injected the spacecraft into a lunar transfer trajectory which would have resulted in lunar impact approximately 250 nm from the prelaunch aiming point. The "miss only" injection error was 4.04 m/sec. The "miss" plus "time-of-flight" error was 5.19 m/sec. (Both based upon a spacecraft midcourse maneuver being performed 20 hr after injection.) This error is equivalent to about 1-σ root-sum-square, guidance system dispersion.

f. Propulsion and propellant utilization. Performance of the propellant utilization system was satisfactory. This system is used to assure maximum available main engine burning time from the propellant loaded aboard the vehicle, thereby permitting maximum vehicle performance. This is achieved by varying the fuel-to-oxidizer mixture ratio during engine firing such that a near simultaneous depletion of both propellants is effected. The propellant unbalance at AC-10 MECO amounted to only 6 lb of LH_2. The useable propellants residuals at MECO would have provided an additional 1.6 sec of burning time beyond that required for satisfactory mission completion.

4. Interface Requirements

Since the last reporting period a number of changes to the Surveyor Project Document (PD-1) Revision 2 have

UNCLASSIFIED

UNCLASSIFIED CONFIDENTIAL

been resolved between LeRC/GD-C and JPL/HAC. These were:

(1) Electrical interface changes:
Shielding the helium dump command and return lines.
Deleting the nitrogen dump lines.
Revising the external battery charge and return line sizes.
Increasing the facility power requirements.
Revising the spacecraft main power switch control.
Determining main retrorocket igniters S&A switch power requirements.
Increasing the power supply to TV target lights.

(2) JPL to redraw the interface control drawings and replace GD/C 55-00050 Rev. Z with JPL 142800. The new interface control drawing will be under the same control as PD-1, i.e., no changes to be made without written concurrence from LeRC.

(3) New air conditioning requirements.

(4) Electromagnetic interference/radio frequency interference requirements addendum.

(5) Amendment to "injection accuracy" requirements.

(6) Separation sensing and arming devices new requirements.

These changes are being incorporated into the document and Revision 3 is planned for publication during the next reporting period. A general updating to reflect mission objective changes if available will also be included. NOTE: These changes except for mission objective changes have been described in *SPS 37-36, 37-37,* and *37-39,* Vols. I, pp. 40, 8, and 18, respectively. The mission objectives are currently being modified, but should not result in interface changes. The primary effects will be reflected in new but modest targeting requirements.

5. Interface Control Drawing

The present *Surveyor/Centaur* interface control drawing is GD/C drawing No. 55-00050. A decision has been made for a complete redraw by JPL, as discussed in *SPS 37-39,* Vol. 1, p. 18. The drawing number is JPL-142800, which will reflect true interface detail only, eliminating all "information only" type items. Interface details which will be shown are as follows:

(1) Interface plane.

(2) Dynamic envelope.

(3) Nose fairing structural outline.

(4) Solid or outline of spacecraft.

(5) Dimensions to describe locations of all spacecraft and launch vehicle mating components.

(6) Mating components in outline but not dimensioned, hardware installation drawing numbers and connector indexing, including appropriate tool clearances.

(7) Electrical schematics showing connector part numbers (including test connectors), pin assignments and functions, line sizes or appropriate characteristics.

(8) Location of toxic gas detector sampling ports, plus location of umbilical disconnects for transporting spacecraft to pad.

(9) Location and orientation of air conditioning ports.

Check prints of the new drawing, consisting of 4 sheets, have been completed and were mailed June 29, 1966 to all agencies concerned for review. Comments and recommended changes are due by July 18. It is expected that a second iteration of the drawing will be required before publication of an approved issue. JPL is now responsible for maintenance and control of the interface drawing.

6. Launch Complex Interconnections

The launch complex interconnection list, HAC document No. 274532 is a tabulation of pin-to-pin connections and functional assignments of electrical circuitry required by HAC between the blockhouse, transfer room, umbilical tower, launch vehicle and the spacecraft. GD/C is responsible for electrical cabling between these locations, hence an interface occurs at the entrance or exit to each of the HAC consoles. Launch complex 36-A was electrically connected in accordance with Revision F of the HAC interconnections list for the launch of AC-10/SC-1 on May 30, 1966.

Once interface connections are established they cannot be changed without the knowledge and consent of JPL, HAC, GD/C, and LeRC. Control has been established by including a schematic diagram of the interconnections as sheet No. 4 of the new interface control drawing, JPL No. 142800.

UNCLASSIFIED CONFIDENTIAL

UNCLASSIFIED

7. Launch Vehicle Payload Capability

A summary of current launch vehicle payload capability for the *Surveyor* missions, as of approximately June 1, 1966, is presented in Table 14. The data have been derived from the June 21, 1966 issue of the "*Centaur* Monthly Configuration, Performance & Weight Status Report," GD/C 63-0495-37.

The current status, shown in Table 14, includes the following more important changes in payload capability, which have been incorporated since the last reporting period:

(1) An approximate 50-lb loss for direct ascent missions (A, B and D) due to 50 lb of added H_2O_2 to provide for 10 lb of additional usage during retromaneuver and 40 lb of additional reserves.

(2) An approximate 23-lb gain on mission B due to the use of log book data on *Centaur* main engines in place of nominal values used prior to targeting.

(3) An approximate 20-lb loss on missions C, E, F and G due to revised estimates of *Centaur* engine weight.

(4) An approximate 10-lb gain on all missions except A and B based on preliminary estimate of hi-rel inverter weight.

(5) An approximate 16-lb gain on mission B based upon corrected thrust and flow rate data.

It is anticipated that an approximate 303-lb gain on missions E, F and G will be incorporated in the next reporting period based upon utilization of the *Atlas* SLV-3C, which will have a 51-in. tank extension and somewhat greater engine thrust.

E. Systems Testing

1. T-21 Type Approval Test Vehicle

The results of the lunar landing shock test are still being evaluated. A transient loss of lock and instantaneous recovery were observed in data from the shock absorber strain gauges during the first drop. This was the only drop where telemetry signals were received via air link. Studies of this anomaly are continuing to show antenna position versus time, with a zero displacement reference position established for orientation at the instant of first leg impact.

Test data are still being reduced to the form of plots of the shock spectra. More data are expected in the near future.

2. SC-2 Flight Acceptance Tests

a. Solar thermal vacuum test phase. All preparations (spacecraft, test equipment, and facilities) leading to the solar thermal vacuum (STV) test were completed April 22,

Table 14. Summary of current launch vehicle performance[a]

Mission	Flight	Payload	Ascent mode	Min burnout wt, lb[b]	*Centaur* jettison wt, lb	Payload capability, lb	Spacecraft wt, lb	Margin, lb
A	AC-10	SC-1 engineering	Direct	6393	3998	2395	2193	+202
B	AC-7	SC-2 engineering	Direct	6391	3971	2420	2202	+218
C	AC-12	SC-3 engineering	Parking orbit	6543	4100	2443	2177	+266
D	AC-11	SC-4 engineering	Direct	6372	3986	2386	2185	+201
E	AC-13	SC-5 engineering	Parking orbit	6543	4099	2444	2176	+268
F	AC-14	SC-6 engineering	Parking orbit	6543	4093	2450	2179	+271
G	AC-15	SC-7 engineering	Parking orbit	6543	4093	2450	2173	+277

[a] As reported in GD/C 63-0495-37, "*Centaur* Monthly Configuration, Performances and Weight Status Report," June 21, 1966, unclassified.

[b] "Minimum burnout weight (BOW)" equals "nominal BOW" less the "performance reserve" of 175 lb for direct ascent missions and 195 lb for parking orbit missions.

UNCLASSIFIED

UNCLASSIFIED
CONFIDENTIAL

and the pump-down for phase 1A was initiated at 15:00. At approximately 19:45 a liquid nitrogen leak was discovered in chamber C-4, causing a premature shutdown at 02:40 April 23. Although the spacecraft was operated during this period, the mission sequence was not initiated, and the operations are considered an abortive attempt at performing phase 1A.

These chamber problems were repaired, and phase 1A pump-down was initiated for the second time at 16:45 April 23. This attempt was entirely successful in attaining the desired environment, including a low solar intensity. Spacecraft launch operations were initiated at 05:30 April 24. Phase 1A was run as a 66-hr real time mission sequence under a simulated STV environment (including a low solar intensity for marginal thermal testing) on spacecraft power. The mission was a success, and system performance was satisfactory with the following two anomalies of principal concern:

(1) Main battery failure following first terminal descent.

(2) Compartment A and B high temperatures.

Following postlanding, television, and troubleshooting operations, the shutdown sequence was initiated, rather than proceeding to phase B, because of the battery failure.

During phase 1B preparation period, the battery and compartment problems were resolved and corrected as follows:

Problems:

(1) Main battery failure was attributed to a combination of a faulty battery and high compartment temperatures.

(2) Compartment A high temperatures were attributed to the following:

Heat generated in the faulty battery.
Improper operation of one or more thermal switches.
An oil deposit on compartment A radiator mirror surfaces.

Corrective action:

(1) Compartment A units and structure were replaced as required along with a new battery.

(2) Four thermal switches (2, 3, 6, and 9) were changed in compartment A and reset to close at 40 rather than 65°F.

STV phase 1B deviates from the test and operation plan in the following manner:

	TOP	*STV phase 1B*
Prime transmitter	Transmitter A	Transmitter B
Power to spacecraft	Christie	Spacecraft batteries

Phase 1B was started May 9 with pump-down initiated at 02:48. Following the completion of pump-down and a suitable environment including a high solar intensity, phase 1B was initiated with launch at 10:00. The phase was aborted at 23:32 (08:11 mission time) owing to high temperatures in compartment A and the main battery.

During the phase 2B preparation period, compartment A switches 3, 5, and 6 were reworked and replaced. The phase 1B overheating problems were attributed to foreign material found in switch 5 and to assembly errors in 3 and 6.

Phase 2B pump-down was initiated at 13:25 May 12. During this pump-down a liquid nitrogen leak was discovered which prevented the chamber from attaining the specified pressure. However, the stabilized pressure (2.4×10^{-5}) was sufficient to perform the mission; therefore, launch was initiated at 21:02. The spacecraft performed very well, thermally and functionally, during this phase. The batteries performed exceptionally well and supported a standard mission sequence in addition to one additional terminal descent. The anomalies of principal concern were as follows:

(1) Failure to perform a vernier descent owing to a short in the flight control sensor group on the positive side of vernier engine 3 thrust throttling amplifier.

(2) Vernier line 1 operated at 123°F, 23°F above maximum allowable.

(3) Loss of Canopus lockon owing to a buildup of coating on the inside of the Canopus sensor window.

(4) Abnormal operation of the null error amplifier in analog-to-digital converter 1 resulting in variations in telemetry data as a function of mode and bit rate.

Upon completion of all postlanding operations, both planned and special, shutdown was initiated at 11:18 May 16, and the spacecraft returned to ambient at 04:00 May 17. The flight control sensor group and central signal processor units were removed for repairs and retest.

CONFIDENTIAL
UNCLASSIFIED

UNCLASSIFIED
CONFIDENTIAL

Also, switch 9 on compartment A was replaced. Following return of the central signal processor and buttoning-up of compartments A and B, the spacecraft was placed in the chamber, minus the flight control sensor group, for chamber checkout related to the low vacuum in phase 2B.

The special STV runs (designated as phases XB-1 and XB-2) checked out chamber pressure problems and called for a brief period under 112% Sun to determine if compartment A switches and the fix on vernier lines 1 were functioning properly.

The pump-down for phase XB-1 was initiated May 26 at 07:00, and a serious liquid nitrogen leak was experienced at 10:47. As a result, the STV exposure for checking out several spacecraft thermal systems was postponed until 08:40 May 29, pending a chamber leak fix. The special STV test phase XB-2 was initiated at 12:10 and terminated at 15:10 May 29. The spacecraft was returned to ambient environment at 23:18 the same day.

The flight control sensor group was installed on the spacecraft, and preparations for phase 3B were initiated May 30. The phase 3B preparations were completed May 31, and pump-down started at 19:30. The mission sequence for phase 3B was initiated with launch at 06:30 and was successfully completed. The spacecraft was returned to ambient environment for phase C preparation scheduled for June 4.

The preparation of spacecraft, test equipment, and facilities for phase C (STV plugs-out) was completed June 11, with STV testing initiated the same day.

The phase C mission sequence started June 11 with the initiation of pump-down at 12:50. With completion of phase C pump-down, launch was started at 03:00 June 12. The mission sequence ran quite smoothly, from a spacecraft, test equipment, and facilities standpoint, until a boost regulator failure during terminal descent resulted in loss of communications with the spacecraft and a subsequent abort. The spacecraft was returned to ambient conditions at 14:00 hr June 14. The cause of this abort was investigated and repairs and preparations undertaken to rerun phase C. Phase C was rerun but was modified to include special tests to verify fix of the boost regulator.

b. Vibration test phase. Changes in test procedures and equipment are in work to reflect the experience gained on the SC-1 spacecraft. A second set of frequnecy indicator lights will be used to avoid loss of these data during high-speed motion picture tests coverage. The alignment checks have been revised to include a check of the retrorocket with respect to the spaceframe. In addition, the alignment checks have been revised to show the incremental level of distortion that might result from the vibration. The previous procedures verified absolute flight readiness and did not provide this incremental information.

The test plan has been changed to recognize that the spacecraft cannot be mounted on the test stand for precheckout and postcheckout when the retrorocket is installed. The pretest checkout will now be performed on the end-bell of the vacuum chamber following the STV test. The post-test checkout will be performed in the screen room prior to the start of the vernier engine vibration test after removal of the retrorocket.

The automatic accelerometer selection system for vibration test control has been modified to include a light display for instantaneous identification signaling of the controlling accelerometer. This information will enable the console operator to confirm that the test is progressing as expected from previous test data.

Precision test tapes of random vibration levels and frequency range have been prepared for checking out the oscilloscope monitoring provisions of the MB 80-type channel equalizer-analyzer. One objective for this checkout is to evaluate suitability of the oscilloscope presentation of test levels as verification of the 3-db down equalization runs. For each axis of test, a 2- to 4-hr saving in test time may be achieved if this is successful.

c. Vernier engine vibration test phase. The test plan for this phase has been rewritten and reissued to reflect experience gained on the previous tests. The test operation sequence control procedure has been revised. Chronological sequence of subphase C and special test 15 (transmissibility test and vernier engines to flight control sensor group accelerometers) have been reversed so that conversion of the vibration excitation equipment for special test 15 could follow completion of subphase C. New procedures for leak checking the vernier propulsion system, testing for jet valve leakage, checking pressure relief valve leakage, checking attitude control gas jets, and measuring spacecraft transmitter noise have been added.

The dummy vernier engines have been modified to provide for filling the fuel and the oxidizer systems. An alignment jig, to position the shakers for mating with the spacecraft, is in fabrication.

CONFIDENTIAL
UNCLASSIFIED

UNCLASSIFIED

3. S-3 Flight Acceptance Tests

The third flight spacecraft entered the initial system checkout test phase on April 18. The spacecraft was delivered with all major electronic units with the following exceptions:

(1) Flight control sensor group.

(2) Antenna and solar panel positioner.

(3) Radar altimeter and doppler velocity sensor (RADVS).

The initial system checkout phase was completed during this period with the exception of mechanisms and vehicle telecommunications which were delayed owing to the late delivery of the antenna/solar panel positioner (A/SPP). Telecommunications intergroup integration, TV, flight control, and flight control altitude marking radar (AMR) telecommunications, and a number of special tests were completed.

During this test phase, two problems were encountered. Phase jitter greater than tolerances permitted by specification was noted on both transmitters during the telecommunications (TCM) integration phase. This problem is presently under investigation. During the TV-TCM test phase, a failure was noted in the survey camera mirror assembly. The unit was reworked and retested.

4. Group Test Vehicle

Activity of the group test vehicle was halted owing to lack of a boost regulator and reconfiguration of STEA 5. The requirement for group tests on future spacecraft is being reevaluated.

5. T-2N Descent Dynamics Program

Two successful soft landings have been demonstrated at Holloman Air Force Base. One touchdown mission was performed by each of the two test vehicles, T-2N-1 and T-2N-2. Preliminary analyses of test data indicate all primary and secondary test objectives have been accomplished. Prior to these soft-landing missions, each vehicle completed an altitude recovery test with touchdown modifications incorporated to demonstrate system readiness for the touchdown mission. The T-2N-2 vehicle also completed system functional and environmental tests after touchdown modification.

The roll loop gain reduction was incorporated in both vehicles and tested during the last four descent tests, two altitude recoveries and two touchdowns. The roll control loop was very stable throughout each of these tests and exhibited no tendencies to limit cycle or rate saturate.

a. T-2N-1 descent tests. The T-2N-1 vehicle completed two descent tests. Descent test 4, an altitude recovery after touchdown modification, was conducted April 21; descent test 5, a soft landing mission, was conducted May 11.

Descent test 4 was first attempted April 14 but was aborted owing to a sudden severe wind condition occurring after balloon and vehicle release from the crane. Prior to release, two successive favorable wind reports were received. The balloon was properly positioned, and the tether line winches were locked. The windstorm caused violent vehicle and balloon buffeting, resulting in vehicle damage by a steel tether cable. Total emergency recovery procedures were initiated, and the vehicle was brought safely to the ground on its recovery parachutes. Soon after vehicle release, the balloon ruptured at an altitude too low for gondola parachute recovery. The gondola frame was damaged beyond repair.

The vehicle was retrieved and cycled through the complete Holloman preparation sequence including engine deservice and flow, alignment, weight and balance, radar altimeter and doppler velocity sensor (RADVS) acoustic test, and the T-48 and T-24 hour procedures. Descent test 4 was then completed April 21, and operation of the touchdown modification was confirmed by this altitude recovery test.

Following descent test 4, T-2N-1 was again cycled back through system functional test at Culver City in preparation for the first soft landing test without altitude bias. Upon completion of the test, the vehicle was shipped to Holloman for normal preparation sequences. Descent test 5 (touchdown) was accomplished May 11. Test data indicate the vehicle range versus V_z velocity is lower than predicted; however, the vehicle successfully accomplished a soft landing on the desert floor.

There were two reasons for the vehicle flying below the programmed trajectory:

(1) Noise on the V_z signal at the flight control input was caused by the combination of gain switching and by the telemetry on P_1 90-deg and P_3 90-deg presenting a capacitive load to the RADVS preamplifier outputs.

UNCLASSIFIED

UNCLASSIFIED
CONFIDENTIAL

(2) The radar range input to the flight control was on the order of 5% high, which caused the vehicle to actually fly low. Corrective action for the V_z noise consisted of removing the P_1 90-deg and P_3 90-deg telemetry circuits. These changes were incorporated in the T-2N-2 prior to its touchdown mission.

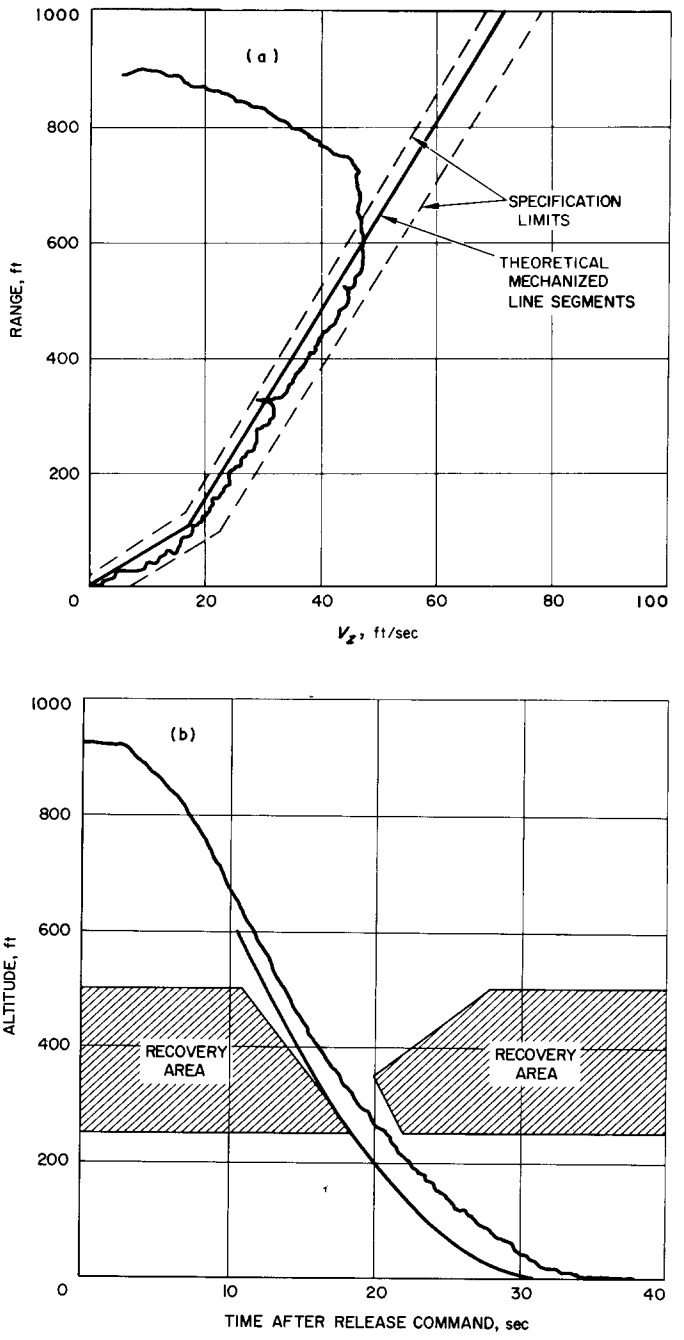

Fig. 38. T-2N-2 descent test: (a) range vs V_z; (b) recovery data

b. T-2N-2 descent tests. The T-2N-2 vehicle completed two descent tests. Descent test 3, an altitude recovery after touchdown modification incorporation, was conducted April 26. Descent 4, a touchdown mission, was successfully completed May 20.

Descent test 3, terminal countdown, was the smoothest of all test sequences at Holloman. All events took place on time. Even the planned holds were observed, and vehicle release was performed at the scheduled touchdown time of 06:15 MST. All subsystems exhibited excellent performance, and mission test objectives were satisfied. The vehicle descent trajectory and altitude-velocity profile were well within allowable tolerances, as confirmed by final optical data.

The vehicle was next cycled through the standard system functional test at Culver City and readied for its first touchdown test. After being shipped back to Holloman Air Force Base and having completed normal preparation sequences, descent test 4 (touchdown) was accomplished May 20. The vehicle subsystems again successfully demonstrated a capability to bring the craft to a soft landing. The altitude-velocity profile for this mission, as taken from telemetry data, is shown in Fig. 38. Although final optical data are unavailable at this time, all other data indicate that all test objectives were satisfactorily accomplished.

c. Final program plans. Both vehicles will be cycled through a final and complete system function test sequence at Culver City as a post-touchdown verification of subsystem status. When final optical data have been analyzed, and it can be shown that all test objectives have been met to the satisfaction of both HAC and JPL, the T-2N program will be terminated.

F. Launch Operations

1. Mass Model Operations

a. Atlas-Centaur AC-8/Surveyor mass model SD-6. The April 7 launch of the *Atlas/Centaur* AC-8/*Surveyor* mass model SD-6 was programmed for a transponder change to high-power operation after separation. There was some doubt at the time that the changeover actually occurred, but subsequent evidence indicated that changeover to high-power mode had been achieved.

UNCLASSIFIED
CONFIDENTIAL

UNCLASSIFIED CONFIDENTIAL

b. AC-9 mass model (Spare 1). The RF dynamic model system test equipment assembly (STEA) rack is scheduled for shipment to General Dynamics/Convair (GD/C) in San Diego. The schedule for AC-9 prelaunch operations requires that mass model operations at GD/C begin about June 20. A calibration and revalidation of test equipment and functional checkout of the transponder should be completed before June 29. The STEA will be shipped to GD/C, including all support equipment and transponder hardware items.

2. Combined Systems Test Facility

Upgrading and calibration of STEA 3, in preparation for SC-2 testing, has been suspended pending redirection of combined systems test facility (CSTF) activities. Mandatory modifications were incorporated to support SC-2 testing. Calibration was maintained in a current condition with a continuous recall system.

Some of the STEA equipment was used to support the spacecraft T-21 test at Goldstone while other units were returned to El Segundo for upgrade and to support SC-2 testing. STEA equipment required in support of SC-1 was sent to AFETR.

3. AFETR Activities

a. SC-1 spacecraft. Preparation for joint flight acceptance composite testing (J-FACT) and pressure decay testing was completed April 14. The spacecraft, while being monitored for environmental cleanliness, was encapsulated April 15. The mobile temperature control unit was connected to the fairing, and a systems readiness test (SRT) was performed. SC-1 was transported to the launch pad and mated to AC-10 April 17. Testing over the microwave link, SRT, and countdown were accomplished in preparation for J-FACT April 18. Spacecraft/Deep Space Instrumentation Facility (DSIF) compatibility testing commenced April 19 and progressed as scheduled.

The flight control and propellant tanking integrated test was completed April 20. Test objectives required rolling back the tower, then tanking and detanking with all systems except ordnance activated. Test of the radio frequency environment was included. No major problems were revealed by this test.

The spacecraft/DSIF compatibility test was completed after the tanking operation. Daily commutator assessment tests were then run prior to the countdown dry run April 25. No major problems were encountered. The J-FACT test was performed April 26 with the third countdown from a T-5 hold resulting in a simulated liftoff. The first two countdowns were a test exercise an *Atlas* problem situation, respectively.

SRT and several spacecraft special tests were performed during J-FACT. None of the stray energy monitors was blown, and all six squibs were fired as expected. Depressurization of the helium and nitrogen tanks was completed April 27.

The spacecraft was removed from the forward payload adapter and transported to the south bay of the explosive safe facility (ESF). Investigation of the safe and arming device indication anomaly revealed an open circuit that could not be located in the adapter or spacecraft harness after demating. The problem did not reappear when the spacecraft was remated to the adapter in an effort to locate the trouble. The spacecraft was demated and returned to the ESF south bay location where compartment A was opened and the auxiliary battery control, battery control regulator, and main battery were removed. The flight control programmer successfully passed a special test. The spacecraft was moved to the drill jig where new retrorocket adapters were drilled preparatory for spacecraft transfer to the optical dock.

Alignment procedures and a special test on vernier engine 1 were performed, after which the spacecraft was moved from the optical dock to the spacecraft checkout facility via ground transport vehicle 1 (GTV-1) May 4. Vehicle rework, performance verification test 5 (PVT-5) preparations, and launch vehicle flight preparations were conducted. A flight shock absorber fit check and several special tests were completed.

PVT-5 commenced May 8 with several steps, including TV, squib, and high-pressure securing being completed May 9. RADVS ranging problems caused a 24-hr delay for penalty testing and changing the RADVS signal data converter (SDC). Analysis and fault isolation tests failed to pinpoint the cause of tracker lock on the AM-2 SDC. Testing resumed May 11 and was completed May 13. Terminal descent testing revealed an anomaly in the spacecraft harness. The P_2 retrorocket separation squib simulators were prevented from firing. Defective splices in the harnesses were discovered and repaired. The mission sequence test was completed. PVT-5 was completed with the successful finish of the

UNCLASSIFIED

UNCLASSIFIED
CONFIDENTIAL

solar panel system test. The spacecraft was then moved from the system test stand and placed on the mobile work stand.

The spacecraft and stand were moved to the spacecraft checkout facility airlock, and the flight shock absorbers were fit checked. The flight and dummy shocks were then weighed, and the dummy shocks reinstalled. The spacecraft was returned to the high bay for separation sensing and arming device checks, spacecraft protective wrapping, and compartment A thermal switch installation, after which it was placed on GTV-1 and transferred to the propellant loading building (PLB) May 14.

Propellant loading to within 0.03 lb of predicted value was completed May 16. Final cleanup, after propellant loading, was completed May 13. The spacecraft was transferred to the flight assembly building south bay and installed on the weight and balance stand. The weight and balance check was conducted, and the spacecraft was removed to the auxiliary stand.

Table 15. SC-1 operations from April 14 to launch

Operation	April			May				
	14	19	25	2	11	16	25	1
Encapsulate								
System readiness								
Mate								
Volt-no volt test								
SRT and countdown								
Quad tank/countdown/RF								
J-FACT								
Demate								
Decapsulate								
High-pressure decay								
Remove J-FACT items								
Retrorocket weight and balance								
PVT-5 (post J-FACT)								
Load and weight propellants								
Install flight equipment								
Initial weight and balance								
Mate retrorocket weight and balance								
Install retrorocket fittings								
Weight and balance alignment								
Install AMR								
Pressurize tanks								
PVT-6								
Verify launch configuration								
Encapsulate and SRT								
Mate								
Volt-no volt								
SRT and countdown								
Commutator assessment and battery charge								
System readiness								
Countdown								

CONFIDENTIAL
UNCLASSIFIED

UNCLASSIFIED CONFIDENTIAL

Spacecraft testing on the auxiliary stand was suspended when a short circuit occurred in the battery monitoring cable causing overloading in three battery cells. The main battery and monitoring cable were replaced upon completing a review of the following operations:

The flight retrorocket was placed on the weight and balance stand and installed for final weight and balance checks. Checks were performed with and without the retrorocket demated; it was then cleaned. Weight, balance and alignment were completed May 23 except for alignment checks of altitude marking radar (AMR), thrust chamber assemblies (TCA), and flight control sensor group (FCSG). Antenna/solar panel positioner (A/SPP) pin pullers were installed and the micro switches adjusted. The omnidirectional antenna pin pullers were installed, and the omnidirectional antenna stowed. The helium release and dump squibs were installed. The spacecraft was moved to the auxiliary work stand where TV mirror and filter cleaning was performed and TV protective wrapping conducted. The A/SPP roll axis drive motor did not step properly and was replaced. An A/SPP roll axis anomaly electrical verification test was completed successfully May 23.

The AMR installation and alignment was accomplished at the optical dock May 24. Approximately 6 hr were picked up by an AMR alignment waiver when JPL permitted calculations to be used in setting the AMR tabs on the retrorocket. Alignment of the TCAs and FCSG was rechecked.

The PVT-6 pre-encapsulation test was completed May 25 and helium and nitrogen tank pressurization commenced. Flight shocks, pinlocks, squibs, and footpads were installed. The leg 3 shock absorber strain gauge amplifier could not be adjusted and was subsequently replaced. Pin retention tests were conducted on all squib connectors except retrorocket release and igniters. The flight squibs were connected and wrapped.

On May 26 the spacecraft was checked for flight readiness. Camera caps were removed, and the auxiliary battery was installed and connected. The main power switch was verified open. The strain gauge amplifier previously replaced was rerun for calibration. It was necessary to remove paint from the replacement shock absorber on leg 3. The GD/C pyrotechnics were installed, and final spacecraft verification was conducted. When the spacecraft was in the final stages of encapsulation at ESF, it was realized that the TV lights were not plugged in. A decision was made to go without these lights, and the encapsulation and SRT were completed May 26.

The mode 2 regulated current was 120 ma higher than the coast mode when the transmitter was in low power. The difference is usually 60 ma.

At pad 36A, the volt, no-volt check was made, and SC-1 was mated to AC-10. SRT and safe and arming check were performed. All systems, except the mode 2 high-regulated current anomaly, functioned normally.

System readiness and countdown ensued with no problems. A schedule of events for SC-1 operations from April 14 to launch is shown in Table 15.

G. Spaceflight Operations

1. *Surveyor* PCM Telemetry Down-Link System Performance Investigation

Special performance tests of the *Surveyor* down-link telemetry subsystem have been conducted, using command data handling console (CDC) No. 11, to determine the reason for bit error rate (BER) scatter which has been observed during the operation of various CDCs (Ref. 3). The tests were grouped into three parts: (1) electromagnetic susceptibility; (2) telemetry subsystem parameter optimization; and (3) decommutator assessment. Fig. 39 shows the test setup in the laboratory. The CDC

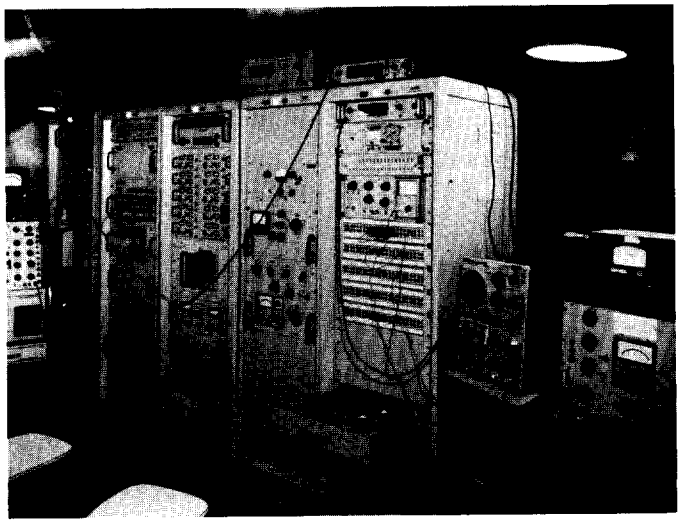

Fig. 39. Down-link telemetry subsystem test setup

CONFIDENTIAL UNCLASSIFIED

UNCLASSIFIED

equipment was located in a screen room that provided a 60-db attenuation in the stray electromagnetic environment. The input AC power to the equipment was suitably filtered during the tests at the screen room interface.

2. Electromagnetic Susceptibility Tests

The objectives of this test were: (1) to define the most susceptible point in the pulse-code modulation (PCM) telemetry link to conducted transient noise pulses, (2) to correlate susceptibility test data with bit error rate problems being experienced at CDC field installations, and (3) to design and demonstrate simple engineering solutions for discrepancies uncovered in these tests.

Summary of results. The CDC PCM decommutator is predominantly susceptible to negative transient pulses. These pulses act like timing pulses that cause transitions in the reconstructed PCM data which are randomly out-of-phase with the transitions of the input signal and associated normal timing pulses.

The electromagnetic interference susceptibility test has established that inadequate grounding exists in the PCM input drawer, inadequate grounding exists between the decommutator power supply DC return and its related terminal points, and wire routing throughout the CDC equipment is critical. Significant improvement in BER performance can be effected by using proper grounding techniques.

With the final ground modification intact, a complete series of BER measurements as a function of bit rate and signal-to-noise ratio (SNR) were made under the conditions of normal BER performance (no external pulses injected) and BER performance with external pulse injected. Test results are delineated in Ref. 4. At all bit rates, the increase in BER was negligible when injecting pulses into the system. Fig. 40 shows the resulting BER probability curves.

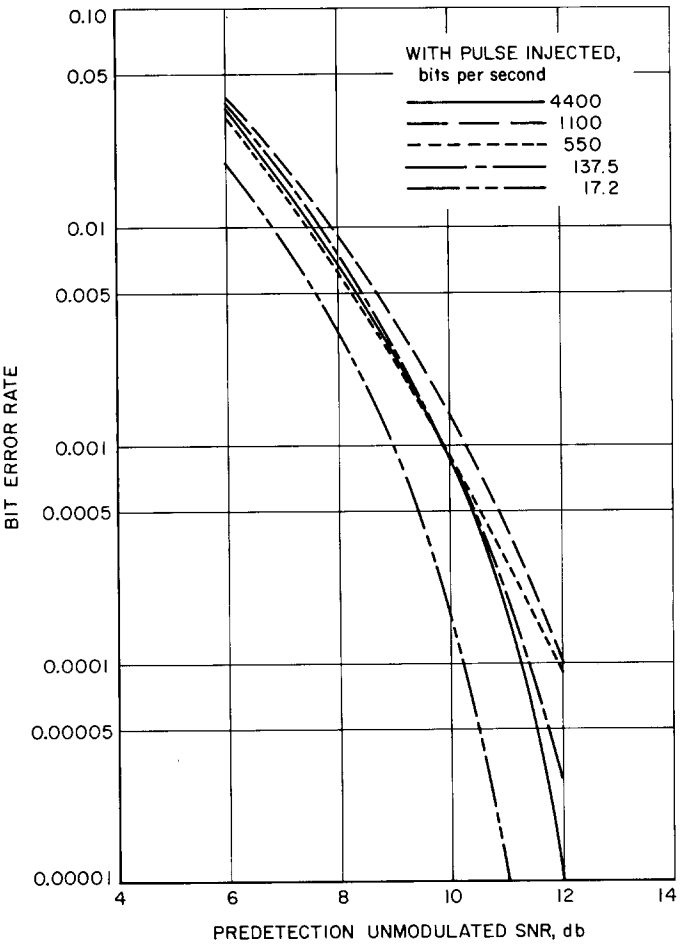

Fig. 40. BER probability curve after CDC-11 ground modification

3. Telemetry Subsystem Parameter Optimization

Objectives of test.

(1) Characterize the existing PCM down-link channel performance for all bit rates, for carefully controlled equipment setup conditions, and for a number of predetection SNR.

(2) Determine the variation of BER with changes in nominal system parameter values or characteristics. These changes would include variation of peak subcarrier deviation, subcarrier center frequency offset (drift simulation), and postdetection filter bandwidth.

(3) Determine the sensitivity of BER measurements to equipment setup and procedures. This includes the discriminator, decommutator gain and offset settings, and precision SNR mixer noise bandwidth.

(4) Determine sensitivity of BER to nominal link element characteristic spread, i.e., BER for several samples of channel selectors chosen from incoming acceptance lots so as, for instance, to display the maximum allowable divergence of bandwidth.

Summary of results. The plots of BER versus peak subcarrier deviation strikingly illustrate the strong dependence on data word bit pattern. The lower equivalent frequency patterns require lower modulation index values than do higher frequency patterns for optimum performance.

CONFIDENTIAL
UNCLASSIFIED

UNCLASSIFIED

Test results for BER vs subcarrier center frequency offset must be viewed in the proper context (Fig. 41). For each offset case, the corresponding discriminator output was offset so as to nullify the DC imbalance caused by the center frequency shift. The decommutator, whose zero-crossing threshold or slicing level was set at 0 v, therefore, always viewed a pulse train with 0 mean.

The data appeared quite repeatable as the data summary sheets show (Ref. 5), with some data points actually overlaying those taken hours or days apart. Testing sequences could be established to maximize repeatability. These sequences include complete runs with parameter variations that are difficult to readjust to an exact value, i.e., vary bit pattern while at a given SNR, as opposed to attempting to reset SNR for a given bit pattern.

The extreme sensitivity of the 17.2 bps channel to offset is due to at least two effects: (1) modulated subcarrier spectrum in the narrow (±2.04%) predetection bandwidth and (2) the voltage offset at the discriminator output. This characteristic indicates that the link may prove unusable operationally owing to setup and signal attenuation. A solution may be to use a wider bandwidth channel selector, sacrificing SNR over portions of the mission sequence where this is possible for reduction of these two effects.

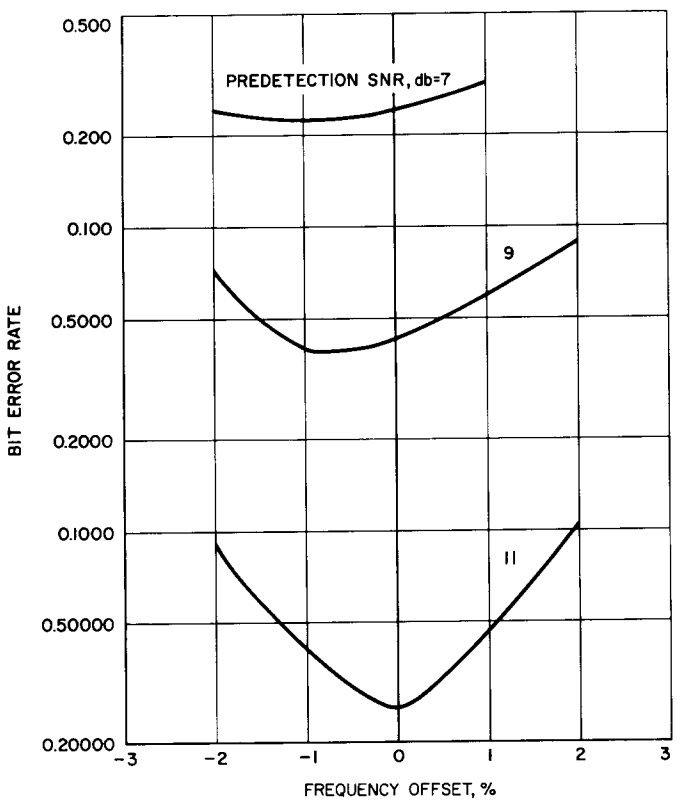

Fig. 41. BER vs subcarrier center frequency offset

The noticeable dependence of BER on word pattern may well prove to be due to the heavy premodulation filtering utilized in the existing PCM links. Rectangular PCM waveforms are implicit in the theoretical analysis.

The BER is essentially independent of postdetection filter characteristic and bandwidth except for certain word patterns and half bit rate bandwidth constant amplitude filter situation. This type of function is useful mainly in minimizing the shift of discriminator mean output level owing to the heavy attenuation of high-frequency bit patterns by the existing link filtering.

4. Decommutator Performance Test

The purpose of this test was to determine the effect on BER of the following CDC telemetry system adjustments:

(1) PCM discriminator balance

(2) Decommutator input attenuator setting

(3) Decommutator internal settings.

As a result of this portion of the tests conducted on CDC-11, the following changes are recommended:

(1) An adjustable bias circuit be incorporated in the PCM amplifier.

(2) A new procedure for setting up the decommutator for processing PCM telemetry signals during a mission be incorporated by the stations.

H. Aerospace Ground Equipment

1. Operational Ground Equipment

a. Aerospace Ground Equipment (AGE) power equipment. The rotating beacon on the power system test equipment assembly (STEA) indicates only when spacecraft main or auxiliary battery power, STEA battery simulators, or simulated boost regulator power (29 v) is being applied. The beacon circuitry has been redesigned to operate whenever any power, such as gyro preheat,

UNCLASSIFIED

UNCLASSIFIED
CONFIDENTIAL

the various group power supplies, etc., is applied to the spacecraft, and will be incorporated in all aerospace ground equipment (AGE) sets.

b. Battery power status recorder. A new direct writing recorder is required at AFETR to monitor spacecraft battery charge status. A recorder was borrowed for use with the launch complex equipment at AFETR for SC-1. Design has been completed for the new rack.

c. Squib test meter. Alinco meters and the necessary adapter cables are being supplied to AFETR for use in checking live squibs before installing them on the spacecraft.

d. Intercom for AGE solar thermal vacuum (STV) tests. An intercom channel selection box has been built for use in the data acquisition area at STEA 1 during STV tests. This box will permit the data chief to monitor and talk on any of the four intercom channels.

e. Data operator voice recorder. A stereo tape recorder was purchased for the data acquisition area. One channel records telephone time and the other records intercom conversations. Provision has also been made for the data chief to interrupt the telephone time channel to record by microphone.

f. Power line isolation protection. Isolation resistors are being installed as close to the spacecraft as practical in all hardline power monitoring leads, except in the cases where low impedance monitoring devices preclude this type of isolation.

g. AGE AFETR launch complex. As a result of experience with SC-1, several changes were made to the launch complex test equipment.

(1) New gyro preheat power supplies with over-voltage protection circuits were added to the launch control racks and safety console so that an adequate voltage would be available at the spacecraft.

(2) The TV target light circuit was modified to supply a higher voltage at the spacecraft by using a power supply rather than the 28 v from GD/C.

(3) The solar panel simulator was modified to provide remote control from the operations console.

(4) The operations console was modified to provide monitoring of gyro preheat voltage and current, spacecraft battery voltage, solar panel simulator voltage and current, and TV target light current.

h. AGE/SC-3 flight control compatibility. Engineering for cabling changes required to maintain interface compatibility with the SC-3 flight control was released.

i. AGE STEA upgrade. A budgetary cost estimate for the proposed STEA improvements was submitted.

j. AGE flight control closed loop equipment spares. Eighteen spare modules for the closed-loop test equipment were received from fabrication, checked out, and prepared for shipment to the various AGE sites.

k. Primary Sun simulator. Modification engineering to improve the reliability of the primary Sun simulator was released and some preliminary design work was done on a completely redesigned primary Sun simulator which would have the capability of simulating Sun error angles relative to the spacecraft coordinate system.

l. Command and data handling console (CDC)/AGE interface manual. Inputs are being prepared for a CDC/AGE interface manual which will cover signal, power, physical layout, and intercom interfaces.

m. TV line selector test unit. The line counter circuitry has been marginal in two units. To overcome this problem, larger capacitors have been installed in the counter flip-flop circuits. This change has been incorporated in all units.

2. Ground Support Equipment

a. Ground transport vehicle (GTV) 1. A recent requirement to move SC-2, with retrorocket motor installed, between buildings 350 and 365 has required the design and fabrication of an adapter for use on GTV-1. This adapter serves to raise the spacecraft attachment surfaces 15 in. to provide sufficient clearance between the retrorocket nozzle and the deck of GTV-1. Design and fabrication were accomplished in a 2-wk period. On May 26 a successful checkout of the adapter, supporting a *Surveyor* test vehicle on GTV-1, was made to demonstrate the feasibility of the transfer between buildings.

b. Spacecraft protective cover. In response to an urgent request from the *Surveyor* test area at AFETR, a cover was furnished to be placed on an assembled spacecraft just under the solar panel in order to protect the spacecraft and its many vital components from damage from any dropped tools, hardware, etc. Designed, fabricated, checked out, and sold to HAC and JPL quality control within a 12-day period, the first of this item was

CONFIDENTIAL
UNCLASSIFIED

UNCLASSIFIED
CONFIDENTIAL

placed in service with SC-1 during the final period of assembly and test prior to launch.

3. Support

a. STEA 5. STEA 5 is being upgraded to conform with the configuration of STEA 2 and to prepare for systems group test of SC-4. Although a few pieces of hardware remain to be delivered, the modification is under way. Rearrangement of STEA has required 62 new interconnecting cables, 47 new pieces of waveguide and waveguide protective covers, 2 new power modules, a new system test stand, and a number of new sections of false floor. In addition, 32 cables have required rework. Many equipment items have been loaned from STEA 5 to support SC-1, -2, and -3. The majority of these will be available with the conclusion of SC-1 operations or will be obtained from combined systems test facility or Goldstone for the support of upcoming SC-4 testing.

b. Standby spares for AGE support of SC-1. Additional launch assurance was incorporated by providing standby spares of certain critical AGE items at AFETR. Approximately 50 items were borrowed from AGE set 3 in San Diego and transported to AFETR. Most of this equipment was located on site at AFETR May 21. The remaining equipment arrived shortly thereafter and was available for immediate use in event of a failure of one of these critical components during the remaining time through launch.

c. Logistic spares catalogue. The AGE department has completed preparation of an AGE spare parts catalogue. This catalogue defines each AGE spare component or subassembly by name, part number, quantity, location, next assembly, etc. These lists are subdivided into the following categories:

Task 13—JPL approved spares for STEA

Task 13—STEA spares not yet approved by JPL

Task 14—JPL-aproved spares for programmed automatic telemetry evaluator, safety console, block house console launch rack control, mobile temperature control unit, and pneumatic console

Task 9 —JPL-approved spares for ground handling equipment

Task 9 —Ground handling equipment spares not yet approved by JPL

Task 7 —JPL-approved spares for propulsion.

Copies of these catalogues have been distributed to JPL and HAC organizations requesting them. Additional copies are available from the AGE department.

4. Product Design

a. TV camera alignment check techniques. Some research has been done in the use of photogrammetric methods for checking, before and after vibration, alignment of all cameras on SC-2. This was based on some data taken during the T-21 descent test program. Since these do not appear conclusive, the tried and proven, though less sophisticated, methods using theodolites, which were used on SC-1, are being adhered to.

b. Ultraviolet protection of landing leg thermo-paint. Discoloration of the thermo-paint on the landing legs during solar thermal vacuum tests of SC-1 indicated the necessity of some protection from the ultraviolet band of the solar simulator spectrum. Nylon sheets of various thicknesses were checked for percent transmission versus wavelength from 200 through 1000 mu. These results were extrapolated into the infrared region from the literature, which contains copious references in this particular region. The test results indicated essential exclusion of ultraviolet for the samples tested. Owing to pressing schedule commitments, an opaque material, aluminized mylar, which excluded all wavelengths, was used for SC-2. Therefore, the application of these studies must await future vehicles.

c. Primary Sun simulator lamps. The life test of the new 316 lamps for the primary Sun simulator has been completed. The average life of these lamps, when burned under the same conditions as in the spacecraft-mounted simulator, was 170 hr at 7.5 v AC. Modification engineering to incorporate these bulbs into the present design has been released.

5. A-24 Program Coordination Effort

A breakdown of the AGE interfaces was detailed and submitted to the task force. Interfaces between AGE and spacecraft were submitted to the spacecraft contract end item specification coordinating team.

Definitions for AGE contract end items (CEIs) and critical control items were established. A rough draft of the AGE set CEI has been started.

CONFIDENTIAL
UNCLASSIFIED

UNCLASSIFIED
CONFIDENTIAL

6. T-21 Goldstone Test Support

An extension on the T-21 Goldstone testing has delayed the return of AGE equipment to the assigned facilities.

7. Trouble Failure Report (TFR) Reliability and Engineering Evaluation

The new TFR criticality classification system for AGE has been adopted and is now in use. All AGE TFRs have been reviewed and assigned a classification in accordance with the new system. A proposed revision of the AGE TFR electronic data processor has been agreed upon by AGE Reliability, *Surveyor* Reliability, and Space Systems Division Product Effectiveness. The revision will permit more efficient utilization of the data, will permit simplification of the coding procedure, and will change the weekly mission-critical TFR (Open) status report to conform to the new AGE TFR classification system.

The rate of AGE TFR close-outs will increase from the present rate of approximately 230 per month with the reporting of new personnel to AGE reliability. The backlog of approximately 2080 TFRs, plus the 260 new TFRs per month, will be handled on a priority basis.

I. Flight Control

1. Introduction

The flight control subsystem is comprised of spacecraft units that provide velocity and attitude control during the transit and landing phase of the *Surveyor* mission. These units, which include optical sensors, inertial instruments, attitude controls, and flight control electronics, are discussed in this section.

2. SC-1 Flight Control System Mission Performance

a. Launch and Sun acquisition. Flight control coast phase power was turned on approximately 2 hr prior to launch (12:37:23 GMT). Gyro temperatures were normal (approximately 170°F), and telemetry indicated that the roll gyro heater was cycling at the time flight control power was turned on. Telemetry indication of pitch gyro heater cycling was obtained approximately ½-hr later. Rate mode was commanded on at 13:05:50 GMT. The nitrogen pressure indicated 4906 psi at 86°F, which is equivalent to approximately 4.7 lb of nitrogen. Liftoff occurred at 14:41:00 GMT. The inertia switch was open (3.5 g) between 14:42:56 GMT and 14:43:22 GMT, about the time of first stage cutoff. The acquisition Sun sensor that initiates the final Sun acquisition yaw maneuver was illuminated around 210 sec after separation indicating an initial (−) roll maneuver of approximately 80 deg. A Sun lockon signal was obtained 164 sec after the acquisition Sun sensor illuminated. The primary Sun sensor error signals were nulled approximately 8 sec later, indicating a final (+) yaw maneuver of approximately 87 deg.

b. Star verification and acquisition. Star verification (star map) was initiated with a Sun and (+) roll command at 18:53:42 GMT in the manual delay mode. A table of stars is identified in Table 16.

Since the Canopus lockon signal was not obtained during the initial passing of Canopus, it was decided to lock on the star manually. Cruise mode was commanded on at 19:12:58 GMT to stop the roll maneuver, and manual lockon was commanded at 19:13:22 GMT to null the star error signals. The Canopus lockon signal was not expected because of the addition of a Sun channel filter prior to launch, which provided greater assurance of a reliable error signal in the presence of any possible star window fogging. Nitrogen gas consumption up to this point on the mission was normal, with an estimated 4.6 lb still remaining after star acquisition.

Table 16. Table of stars

Star	SC-1 telemetry data		Star map data		
	Degrees from roll initiation	Intensity of telemetry, v DC	Degrees from Canopus	Degrees from Canopus	Brightness,[a] w/cm² (10^{-11})
Canopus	220	4.8	0	0	0.180
Markab	338	1.05	118	118.58	0.012
Alderamin	30	1.00	170	170.91	0.009
Merak	92	1.00	232	231.84	0.011
Regulus	138	1.75	278	278.10	0.031
Alpha Hydrae	162	1.00	302	301.38	0.005
Naos	199	1.30 (Average of two values)	339	338.47	0.022

[a] Brightness calculated from maps of May 30 and 31 using 19/24 of incremental brightness change between these 2 days.

CONFIDENTIAL
UNCLASSIFIED

UNCLASSIFIED

c. Midcourse maneuvers and velocity correction. The premidcourse maneuvers consisted of a (−) 86.5-deg roll and (−) 57.99-deg yaw. Both maneuvers were performed satisfactorily as verified with analog recorder data. The roll maneuver placed the Canopus sensor window a few degrees past the star Regulus, which was located approximately 82 deg from Canopus. The stars Naos and Alpha Hydrae were also seen during the roll maneuver.

The programmed vernier engine burn time was 20.8 sec. Thrust phase power was commanded on at 06:43:08 GMT, and the engines ignited at 06:45:04 GMT. The spacecraft was extremely stable during engine burning. A preliminary estimate of the peak gyro and roll actuator transients at ignition and shut off is as follows:

	Ignition, deg	*Shutdown, deg*
Pitch gyro	0	−0.8
Yaw gyro	−0.15	−2.07
Roll gyro	−0.20	0.7
Roll actuator	0.67	

The estimated thrust command levels are as follows:

Engine	*Initial, ma*	*Steady state, ma*
No. 1	32	16
No. 2	23	11
No. 3	19	15

The steady state acceleration during engine burn was approximately 3.2 fps^2, as indicated by telecommunications signals. The Sun and Canopus were reacquired by performing the reverse of the premidcourse maneuvers.

d. Gyro drift measurements. Gyro drift measurements made throughout the mission resulted in the following compensation during the preretrorocket terminal maneuvers in order to reduce the pointing error:

Roll 0.2 deg/hr

Pitch = 0

Yaw = 0.75 deg/hr

e. Terminal descent phase. The terminal maneuvers consisted of a (+) roll of 89.3 deg, a (+) yaw of 59.9 deg, and a (+) roll of 94.1 deg. All three were performed satisfactorily with the first roll initiated at 05:36:50 GMT. The nominal thrust bias (201 lb) was reset, and a vernier engine ignition delay following altitude marking radar mark of 7.825 sec was commanded. Thrust phase power was commanded on at approximately 06:11:02 GMT. The altitude marking radar mark (60 mi) was indicated at 06:14:42 GMT, followed by vernier engine ignition at 06:14:49 GMT. The spacecraft was stable throughout retrorocket engine burning, and successful descent segment acquisition was achieved with an estimated final touchdown velocity of 14 fps. Fig. 42 shows the actual SC-1 vernier descent profile for a midcourse propellant usage of 16 lb, a nominal descent profile for a midcourse propellant usage of 20 lb, and the descent segments.

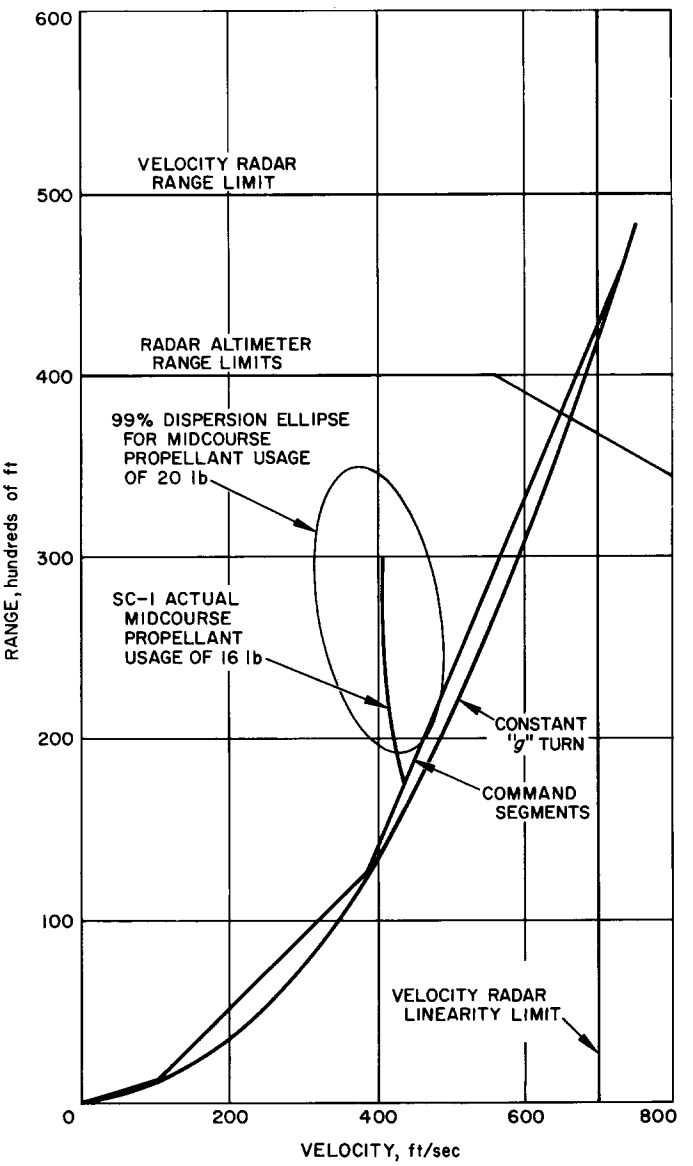

Fig. 42. SC-1 vernier descent phase

UNCLASSIFIED

3. T-2N Tests

a. Altitude descent tests. Telemetry and optical data analyses on T-2N-1 and T-2N-2 altitude descent tests to date indicate that all descent range-V_z trajectories were excellent.

Both the T-2N-1 and the T-2N-2 vehicles were modified to incorporate soft landing descent capability after which each vehicle was subjected to an altitude descent test prior to soft landing descent tests. A review of data from soft lander T-2N-1 altitude descent test 4 indicated that the descent range-V_z trajectory was lower than nominal. Optical data from this test were used in an analog simulation to obtain a descent range-V_z trajectory that was identical to the test trajectory (Fig. 43), thus yielding high confidence in the simulation model.

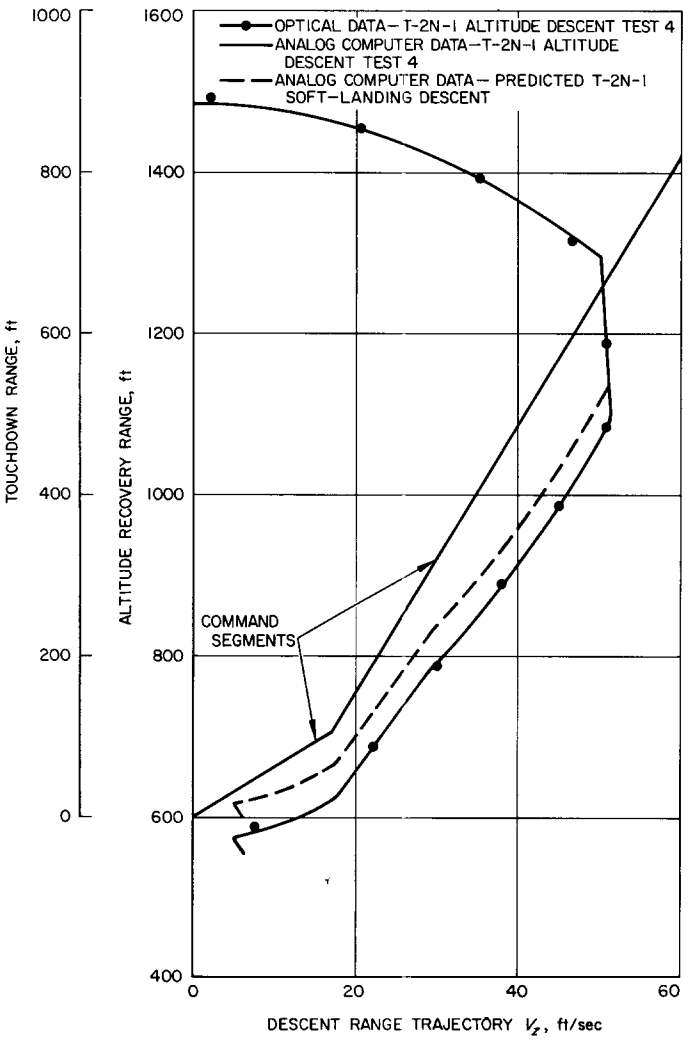

Fig. 43. T-2N-1 altitude and soft landing descent profiles

b. Soft landing descent tests. The 600-ft altitude range bias was removed from the analog simulation to obtain a predicted T-2N-1 soft landing descent profile as shown in Fig. 43. From this profile it was ascertained that the altitude of intercept at 5 ft/sec would be approximately 20 ft, with a very low probability that touchdown velocity would be any greater than 10 ft/sec.

The subsequent actual soft landing descent test of T-2N-1 resulted in an altitude of intercept at 5 ft/sec of approximately 7 ft. It was determined from telemetry analysis that this lower than predicted trajectory was due to short period decreases in V_z which in turn were attributed to unique T-2N telemetry instrumentation.

This telemetry instrumentation was disconnected for the T-2N-2 soft landing descent test that resulted in a trajectory much closer to the predicted profile. A final review of the T-2N-2 soft landing descent will be completed after optical data have been analyzed.

4. Flight Control Electronics Unit (FCEU)

During SC-2 phase B closed-loop testing, several failures were observed which were traced to incorrect vernier engine No. 3 throttle valve commands. A troubleshooting sequence indicated a short on one side of the FCEU differential throttle valve command lines to this engine.

Further troubleshooting of the particular chassis (1A5) involved revealed that the output, which is the collector-case of a stud-mounted transistor, of one side of the vernier engine valve amplifier would short to chassis ground when a slight mechanical displacement was introduced. Such a displacement can occur in mounting the chassis in the flight control electronics unit and/or changing temperature with its attendant thermal expansion. This particular failure was caused by too little clearance and incorrect centering between the transistor stud, which is the collector-case, and its mounting holes in the mounting bracket and chassis plate. Fig. 44 shows the failure configuration and the reworked configuration incorporating adequate stud-bracket-chassis clearance and centering.

Extensive checking of all other stud-mounted transistors in the SC-2 FCEU revealed no shorting, and a review of SC-1 FCEU test data indicated that no shorts existed.

SC-3 and subsequent FCEUs will be reworked to provide adequate stud-bracket-chassis clearance and centering, as shown in Fig. 44.

UNCLASSIFIED

UNCLASSIFIED

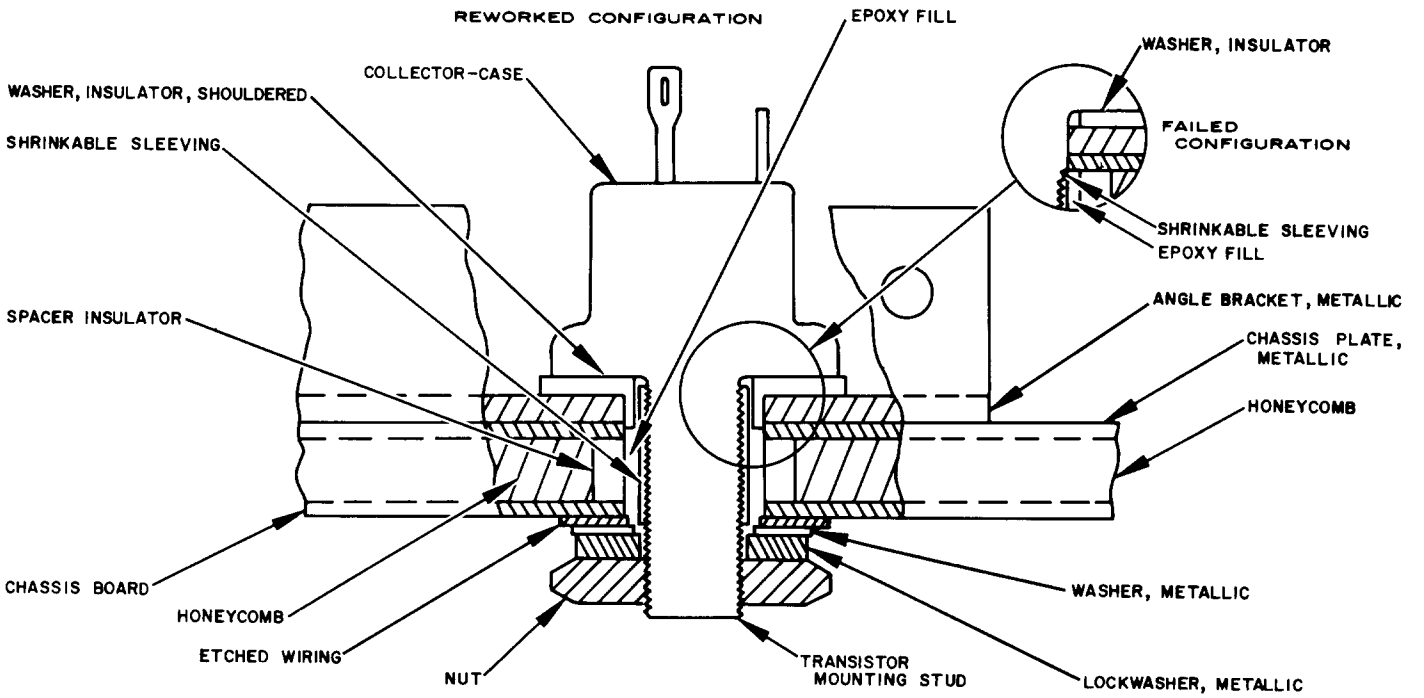

Fig. 44. Stud-mounted transistor installation

5. Inertial Sensors

Gyro signal generator secondary null values and non-*g* sensitive drift rate values have shifted noticeably between gyro acceptance testing and inertial reference unit (IRU) testing. Gyros installed in the pitch and roll positions in the IRU are electrically connected such that their signal generator primary leads are connected in the polarity opposite to that used in gyro testing at HAC and at the vendors. Gyros installed in the yaw position in the IRU are electrically connected the same as for gyro testing. Further, the signal generator primary windings of all three gyros in the IRU are connected in series and excited from one constant current signal generator excitation module. Thus the signal generator primary of each gyro has a different potential with respect to common, and each potential is across a different impedance resulting in three extraneous primary excitation currents that affect null values and generate torques on the gyro floats to affect non-*g* sensitive drift rates.

These two effects, primary lead reversal and primary potential above common, combine to yield different null values and non-*g* sensitive drift rates for gyros when installed in an IRU.

Gyro orientations in the IRU have been changed to correspond to that used during testing, thus providing valid data against which IRU performance can be checked.

6. Canopus Sensor

During SC-2 solar thermal vacuum testing, a gradual decrease was noted in the indicated star intensity coupled with a loss of the star lockon signal. Whenever this occurred, the simulated Sun source for the Canopus sensor was reduced in intensity to increase the sensor gain until lockon was reattained, only to be lost again after the apparent star brightness dropped below the threshold. When the spacecraft was removed from the chamber, a slight haze was visible on the star window of the Canopus sensor. Examination and unit testing revealed that the star output was about 30% less than obtained after cleaning the window. The material on the window, a very hard thin film, was very difficult to remove. Its light attenuation characteristics were barely detectable to the eye. This film could affect sensor performance by scattering, rather than attenuating, the starlight. Subsequently, spectrographic analyses have been attempted on several samples, but owing to the extremely small amount of material collected, positive identification has not yet been achieved. Results of earlier SC-1 and SC-2 solar thermal vacuum tests led to the conclusion that the degradation owing to this window fogging was rather slow and predictable as a function of temperature. Rates of 0 on SC-1 (100% Sun) with the sensor temperature at 70°F, ½%/hr on SC-1 (112% Sun) with sensor temperature of 111°F, and 1%/hr on SC-2 (112% Sun) with sensor temperature of 116°F were noted. For this reason,

CONFIDENTIAL
UNCLASSIFIED

UNCLASSIFIED

a modification to the SC-1 Sun channel filter, which effectively increased the sensor gain by 50%, was chosen to bias the sensor output upwards to where a degradation could be tolerated. Since the system operates just as well in manual mode (as compared to automatic mode where the star sensed is constrained to within ⅔ to ½ Canopus in intensity), it was considered far safer to provide this bias than to run the risk of not being able to acquire a star at all.

During subsequent solar thermal vacuum testing of SC-2, the Canopus roll error telemetry signal indicated a 2-deg roll angle when the star simulator was at 0-deg roll angle and the star intensity telemetry signal was at maximum. Further testing verified this phenomenon and isolated its cause to the pipper detector output in the Canopus sensor holding at 0 instead of switching as a 10-pps squarewave between 0 and 8 v. Upon opening Canopus sensor 6, the fault was traced to an intermittent capacitor that couples one of the pipper pulses to the flip-flop that generates the 10-pps squarewave, thus permitting the output to hold at 0 v. Subsequent examination of the capacitor revealed an inadequate amount of solder on an internal terminal. Other capacitors from the same batch are sound; thus, it appears that the intermittent capacitor represents a random failure.

7. Gas Jet System

a. Gas supply. The second engineering tank, No. 0013 (tank No. 0012 was previously reported), was tested for charging valve leakage. The valve was torqued three times to the previously determined optimum charging valve torque of 60 in.-lb, and the leakage increased from 2.2 to 73.0 $in.^3$/hr standard temperature and pressure (STP). Since this was too high, the valve was removed and dimensionally inspected. The stem was 0.0005 in. oversize, and the point total indicator reading was 0.002 in. instead of 0.001 in. maximum. The oversize stem and excessive point runout apparently prevented a normal closure. The valve was reworked to drawing tolerances, and the leakage was still excessive apparently because of a damaged seat in the tank. The valve point was then shortened by 1/32 in. to provide a new seating surface in the tank. The stem diameter was reduced 0.001/0.0015 in. to facilitate alignment of the valve point with the tank seat. The valve leakage at 60 in.-lb torque was then acceptable at 0.18 to 0.41 $in.^3$/hr STP.

The tank charging valve from tank 0012 was removed and dimensionally inspected. The stem diameter was 0.001/0.0015 in. undersize, and the point runout was 0.004 in. total indicator reading instead of 0.001 in. maximum. The fact that this valve operated satisfactorily was apparently due to excessive stem clearance that facilitated alignment of the valve point with the tank seat. This tank valve was also reworked, and the leakage was acceptable at 0.28 to 0.49 $in.^3$/hr STP.

This valve rework demonstrated that a valve can be modified to obtain satisfactory operation. Replacement valves will be provided for use if a vendor-supplied valve is not satisfactory.

The tank temperature sensor bonding process using an epoxy adhesive Type I PS 224807 appears to be marginal. In some cases, the bond is cracking at the boundary, apparently owing to excessive strain. A new process, Type II PS 724807 using reentry test vehicle adhesive, has been released for repair use and initial bonding.

b. Systems installations and testing. The SC-3 type landing leg flexible lines are available for flexure tests to determine if they are as adequate as the SC-1/SC-2 type lines.

AFETR difficulties with an excessively leaking tank-charging valve on SC-1 have been traced to improper operations. Special instructions will be incorporated in launch operations and systems test procedures to avoid this difficulty.

8. Radar Altimeter and Doppler Velocity Sensor (RADVS)

a. Microwave diodes. Two problems, breakage and moisture sealing, have arisen in obtaining satisfactory diodes for AM-6. As a result of tests conducted at Ryan Aeronautical Co., three diode lots, 6883, 6805, and 9097, were found to contain some unsatisfactory diodes which were unable to meet the rigid radar altimeter and doppler velocity sensor (RADVS) acceptance criteria. In response to Ryan's request, Mytronics Co., the case manufacturer, is investigating a new metalizing process that will, according to present test data, further enhance the diode bond reliability. As a further precaution, the procurement specification has been revised and, subject to further discussion and negotiation, will include an axial strain test. If accepted, all cull diodes will be so tested and if one breaks, a test will be performed on the flight diodes of that lot.

The second problem area concerns the hermetic seal. Tests at Ryan indicate that this seal is porous and that

CONFIDENTIAL
UNCLASSIFIED

UNCLASSIFIED

moisture can enter the diode. Ryan has developed a process to vacuum impregnate the diodes, and tests show that this process produces acceptable diodes. The materials have been formally submitted to HAC for approval. The remaining diodes on hand will be vacuum impregnated.

b. RADVS signal data converter parallel design. A parallel effort redesign of the signal data converter to incorporate double side band discrimination (DSBD) is presently under way. This will provide the capability to differentiate between the desired signals and interference arising from vibration effect, a discrimination that cannot be made by the present design.

This double sideband discrimination is achieved by a method of signal-to-noise sampling in the acquisition control circuit. The technique employed incorporated the use of an inverter and an additional summer following the balanced modulators to provide noise sampling at the frequency of the unwanted signal.

c. Circuit design DSBD. Doppler velocity sensor (DVS) tracker 1 is now completed, and design verification testing is well under way. Acquisition vs frequency curves for both wideband and narrowband in the signal-to-noise (S/N) mode (without noise) and power mode are completed. During the design verification testing, a problem with momentary lockon and then dropout at low signal levels was discovered. This situation results when the error frequency becomes zero as the tracking loop corrects the output frequency immediately after acquisition in pulling towards the positive offset. This problem is enhanced by the low jitter of the tracker. The solution now being studied is the addition of dither to the voltage control oscillator to prevent the tracker from dwelling in the zero frequency area.

Individual circuit studies are approximately 90% complete. Schematics and temperature transfer function curves are being submitted through regular reporting channels. They include the following:

IF amplifier and mixer (signal)

IF amplifier and mixer (noise)

Step low pass filter and amplifier (signal, DVS)

Step low pass filter and amplifier (noise, DVS)

Step low pass filter and amplifier (signal, alternate)

Step low pass filter and amplifier (noise, alternate)

The IF amplifier response data for gain, bandwidth, and center frequency versus temperature, as well as IF mixer conversion gain versus temperature and low pass filter response versus frequency, are also available separate from this report.

d. Analysis. A mathematical representation of noise, positive doppler, and negative doppler has been developed. Integrals of the output of the square law detector are being evaluated.

In preparation of an interim report on probability of detection, additional computer runs were required to determine the time delay involved in the detection process. Initial results show a delay of 30 msec at 4-Hz bandwidth and increasing with bandwidth. The 30 msec is only one-tenth the time allotted for this delay. The computer runs have indicated that the optimum time constant for the threshold detector is about 50 msec.

e. System sensitivity. The absolute threshold level has been added to the S/N mode plots previously reported. The absolute threshold level has been chosen on the DVS such that within the search frequency range the sensitivity is limited by the noise of the system and not the threshold value.

f. Tracker loop parameters. Computer runs were made to analyze the effects of bandwidth, doppler frequency, and SNR on the tracker loop gain. The DVS operating at 600-Hz bandwidth is affected the most with spectrum bandwidth and doppler frequency contributing 60% dropoff in gain; SNR contributes another 20%. The affects of these dropoffs are being taken into account in the signal data converter error budgets.

The expression for the SNR in the signal channel at acquisition with and without extraneous signal has been documented and is separately available.

g. Reliability. Preliminary work has been started on the reliability prediction analysis. Some of these data should be available for the next reporting period.

9. *Altitude Marking Radar*

Design and fabrication of the first 290270 low-noise wide-band IF amplifier are completed. A problem was encountered with the conductive epoxy coating, used to shield the open foam faces of the amplifier cells, shorting C63 to the case. It was necessary to relocate C63 in order to correct this. The amplifier was installed on

UNCLASSIFIED

the SC-5 altitude marking radar (AMR) after it had completed all its subsystem tests; it is performing as planned.

As required per ECA 112273-7, command line noise susceptibility tests and analysis were performed on the AMR electrical conversion unit (ECU), where AMR OFF and AMR ON commands are processed. The investigation revealed that both lines were sufficiently insensitive, and no additional filtering would be required. However, if a negative transient were to occur on the on line, possible damage to related circuit components could occur. To correct this condition, a diode was shunted across the line which would absorb any negative transients. This modification was incorporated beginning at SC-5 and will continue throughout the remainder of the program.

J. Electronics

1. Electronics Unit Status

SC-5 AMR is in test with delivery expected June 20, 3½-mo ahead of schedule. The problem of late delivery of transistors was solved by using qualification test units. Most critical problem on AMR is late delivery of RF assemblies; however, flight schedules are not in jeopardy.

Receivers are delivered through SC-5, and half of SP-2 is well ahead of the need schedule; there are no outstanding changes. The last receiver is expected August 31.

TV auxiliaries are delivered through SC-4, and the remaining units will be available on schedule and ahead of need dates. Owing to addition of the vidicon survival heater change, SC-5 is now expected by July 8.

Thermal control and heater assemblies have been delivered through SC-4. SC-5 has been delayed because engineering for a new transistor heat sink was not completed on schedule; however, spacecraft schedules are not in jeopardy.

Planar arrays are delivered through SC-4. The SC-5 unit has been range-tested, and solar thermal vacuum testing has been completed. Owing to availability far ahead of spacecraft need, considerable slippage of planar arrays has been encountered because of antenna range overload.

Omnidirectional antennas are delivered through SC-6, and half of SC-7 is ready for delivery. The second half of SC-7, the only remaining unit, is fabricated and is awaiting antenna range test.

Boost regulators are delivered through SC-3. The SC-4 unit that should have been delivered in mid-April has suffered the same failure twice in test. The problem has now been identified, and emphasis is being placed on delivering this unit during the first week of June. Battery charge regulators are delivered through SC-4.

All units are delivered through SC-4. SC-5 (first additional unit) has been delayed because of a test accident. The unit is in evaluation to determine necessary repairs. The spacecraft schedule is not in jeopardy.

All flight control electronic units have been delivered through SC-4. SC-5 is barely on schedule. The recently detected transistor insulation problem may affect the flight control electronic units severely.

Engineering mechanisms auxiliaries are delivered through SC-4. The SC-5 unit has been held for incorporation of a noise susceptibility change and is due June 30.

Transmitters would have been delivered through SC-4; however, a spacecraft accident to transmitter 17 involving KOH electrolyte from the battery leaves the last SC-4 transmitter to be delivered. The transmitter redesign on SC-5 and up is holding schedule with no further slip.

Discovery of a vidicon-yoke problem has set back SC-4 and SP-1 survey cameras. Discovery that asymmetries in the yoke connections strongly affect vidicon imaging performance should greatly improve performance; however, schedules have been delayed. SC-5 is held for a vidicon tube but can make the August 25 need date if a tube is selected soon. All approach cameras have been delivered.

Radar altimeters and doppler velocity sensors are delivered through SC-4. Mixer diode problems are being studied by HAC. If these are not solved expeditiously, a very costly schedule slip will occur.

2. Basic Bus Electronics

a. Antenna switch unit. An antenna switch is presently being designed to switch the secondary receiver between the upper hemispherical antenna and the existing omnidirectional antenna. This switch will provide circuitry to

UNCLASSIFIED

switch a latching coaxial RF switch from one antenna to the other. The coaxial switch and associated drive circuitry is identical to that in the transmitter.

The space envelope of the antenna switch is approximately 4.5 in. high, 6 in. long, and 1.5 in. wide. The basic structure is milled out of a single block of aluminum. A coaxial RF switch and two printed circuit boards make up the major subassemblies of the package. The unit will weigh about 1.5 lb.

Drafting for the antenna switch is complete and in final checking. Print release was completed in early June. The type approval antenna switch should be ready for testing in July.

b. Thermal control and heater. The heat sink used on the thermal control and heater assembly was made from a block of boron nitride utilizing a metal insert. Several of the heat sinks cracked in the boron nitride after flight acceptance test. This situation could result in overheating and subsequent failure of the transistor. Such a failure would result in loss of unit heating capabilities.

Engineering tests identified the problem as thermal rather than mechanical. The larger thermal expansion of the aluminum insert caused the boron nitride to crack. The heat sink was redesigned (ECA 112450) utilizing an aluminum mount, beryllium oxide washer, nylon insulator, flat washer, lock washer, and nut. The beryllium oxide washer was covered with HP16-99 type II epamide at installation.

Engineering tests have proven the design to be mechanically and thermally satisfactory.

c. Transmitter low power redesign (ECA 112229). One set of multiplier modules for the first SC-5 transmitter unit has been fabricated, tested, and foamed and is now being assembled to the rest of the transmitter. Transmitter 12 modules are now in test.

The prototype transmitter was assembled with foamed flight configuration modules. Approximately 75 thermocouples were attached, and then the transmitter was put through thermal vacuum tests. Data analysis indicates that the temperatures during this test agree quite closely with the calculated temperatures. During thermal vacuum test, the 19-MHz sidebands were higher than on the SC-1 transmitters. The output network in the A3 module has been modified to correct this problem. Temperature tests are in progress to prove out the fix. Output power of the prototype transmitter was greater than 100 mw at mounting temperatures as high as 145°F in the vacuum environment. Present maximum mounting temperature specification for the transmitter in a spacecraft compartment is 125°F. The minimum power specification is 100 mw.

d. Engineering mechanisms auxiliary. The RADVS external "on" command (pin 1 of J3) would turn on if a random signal 15 v by approximately 40 μsec wide was developed.

Since the actual coupling mechanism was in doubt, an active filter was designed to provide protection up to 20 v, 800 μsec, and reject this signal up to a repetition rate of 100 pps. Normal turn-on operation of this command will be a 9-v step function. The redesign will be incorporated in engineering mechanisms auxiliary 14 (SC-5).

e. Upper hemispherical antenna. Two upper hemispherical antenna configurations are being considered: (1) a separate control item, similar to the omnidirectional antenna, which would be boom-mounted on the spacecraft, and (2) an addition to the planar array antenna, permanently attached and tested with the planar array.

Configuration 1 is the more straightforward design but will result in greater spacecraft weight. The antenna will weigh about 0.28 lb, plus the coaxial cable. To this the weight of the boom and mechanisms required to attach it to the spacecraft must be added.

Configuration 2 has the disadvantage that unrepairable shortcomings of one antenna will require replacement of both. Also, structural loads on the planar array antenna will increase about 10%, resulting in the expenditure of a planar array antenna in providing type approval test assurance for this design. The question of retest of retrofitted planar array antennas will also have to be considered. This configuration will result in a net spacecraft weight increase of about 0.20 lb, plus the coaxial cable.

f. Antenna pattern and impedance measurement. Pattern and impedance measurements have been completed on an electrical prototype of the upper hemispherical antenna. The electrical design was released for fabrication May 11.

The prototype antenna differs from the breadboard antenna in that the groundplane of the prototype does not have a radial choke. Electrical performance of the antenna is very nearly the same with or without the

UNCLASSIFIED

UNCLASSIFIED
CONFIDENTIAL

choke. By omitting the choke, however, the weight of the antenna was reduced more than 50%. A typical radiation pattern for the prototype antenna is shown in Fig. 45.

g. Boost regulator. Drafting effort for the new 3024240 boost regulator was completed in May. Production drawings were released to the manufacturing facility, and fabricated parts are in process at the end of this report

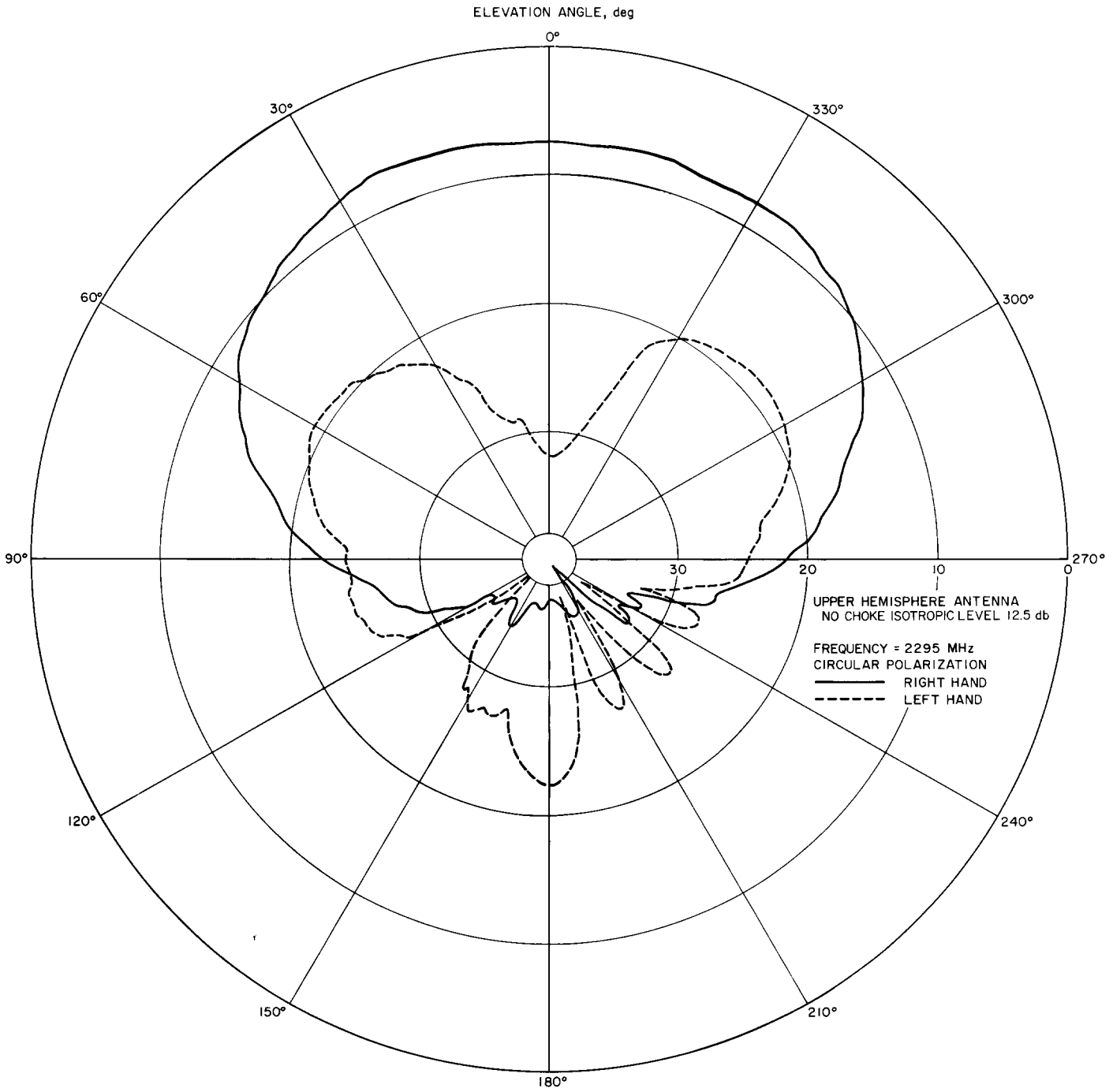

Fig. 45. Prototype antenna typical radiation pattern

UNCLASSIFIED
CONFIDENTIAL

UNCLASSIFIED CONFIDENTIAL

period. The regulator is scheduled for delivery in September and will be assigned for use in the new SC-5 power subsystem.

Two class III units of the new boost regulator will be assembled for use as engineering models. The first of these is nearing completion, and initial tests will be started about June 30.

JPL approval of expenditures for 3024240 boost regulator test consoles was received May 24. Orders for commercial test equipment are being processed, and modification of the existing test consoles was to be started about June 20.

h. Battery charge regulator. Screening of production orders for the 3024260 battery charge regulator and planning documents by quality control is in process at the close of this report period. The first of these regulators is scheduled for use in the new SC-5 power subsystem. Two class III units will be assembled for use as engineering models. Fabricated sheet metal parts and etched circuit elements for class III units are in process.

Construction of test consoles for the 4024260 battery charge regulator has been delayed pending JPL approval of expenditures for this portion of the test equipment allocation.

3. Digital Electronics

a. A-24 product design. The final product design drawing releases to the manufacturing activity were made for *Surveyor* A-24 flight hardware. These drawings included all the product improvements requested by the various *Surveyor* engineering activities according to formal ECA/ECRs. The product design engineers are presently supporting fabrication. Each recommended change to the released drawing is carefully reviewed for its effect on reliability, cost, and schedules. The major changes are:

(1) ECR 337185 provides better and more stringent control on the handling and filleting of modules on the etched boards. Such control lessens the weight fluctuation on the same control items and eliminates excessive use of epoxy. This ECR was made applicable to all units.

(2) ECR 337187 requires the callout of torque values on screws for all control items.

(3) ECR 337188 provides additional dielectric tests on the engineering signal processor (ESP) contour cables.

(4) ECA 112475 modifies the auxiliary engineering signal processor (AESP) and ESP A501 amplifier and yes/no input gating.

(5) ECA 112476 furnishes a signal processing nonessential bus filter for the ESP and AESP. This filter is comprised of an inductor and cable clamp.

(6) ECA 112477 calls out the redesign of the present commutator advance signal amplifier on ESP and AESP.

(7) ECA 112530 increased the value of the pull resistor in the commutator for the advanced flight control programmer (AFCP).

(8) ECA 112294 delays the turn-on time of the central command decoder (CCD) subsystem turn-off circuits.

The product design of *Surveyor* A-24 control items has been slowed by program redirection. However, some progress has been made in the following areas:

(1) Product design engineers are currently participating in A-24 program definitizing. Touchdown instrumentation subsystem specifications are being reviewed and formulated.

(2) Final circuit touchdown auxiliary, No. 29080, has been released, and some circuit refinements are currently being made. The design modifications were reflected in five modules and one etched card change. Affected modules contain the summing amplifier, one shot out of six, current overload, current limiting, and load power circuitry.

(3) A partial circuit release was received on the ESP analog-to-digital converter.

(4) Borg-Warner completed flight acceptance testing on tape recorder 253199.

(5) Work on strain gauge amplifier 253200 is being held up by Electro-Development Corporation until additional RF interference requirements are approved by HAC and JPL.

b. Central signal processor (A-21). Most of the circuit boards for a central signal processor breadboard have been built and tested. This breadboard will be used for evaluation and group test.

c. Central signal processor (A-24). The analog-to-digital converter has been redesigned to replace the null-error amplifier with a comparator and a zero binary voltage weighter (BVW) which nulls out the comparator

UNCLASSIFIED CONFIDENTIAL

UNCLASSIFIED

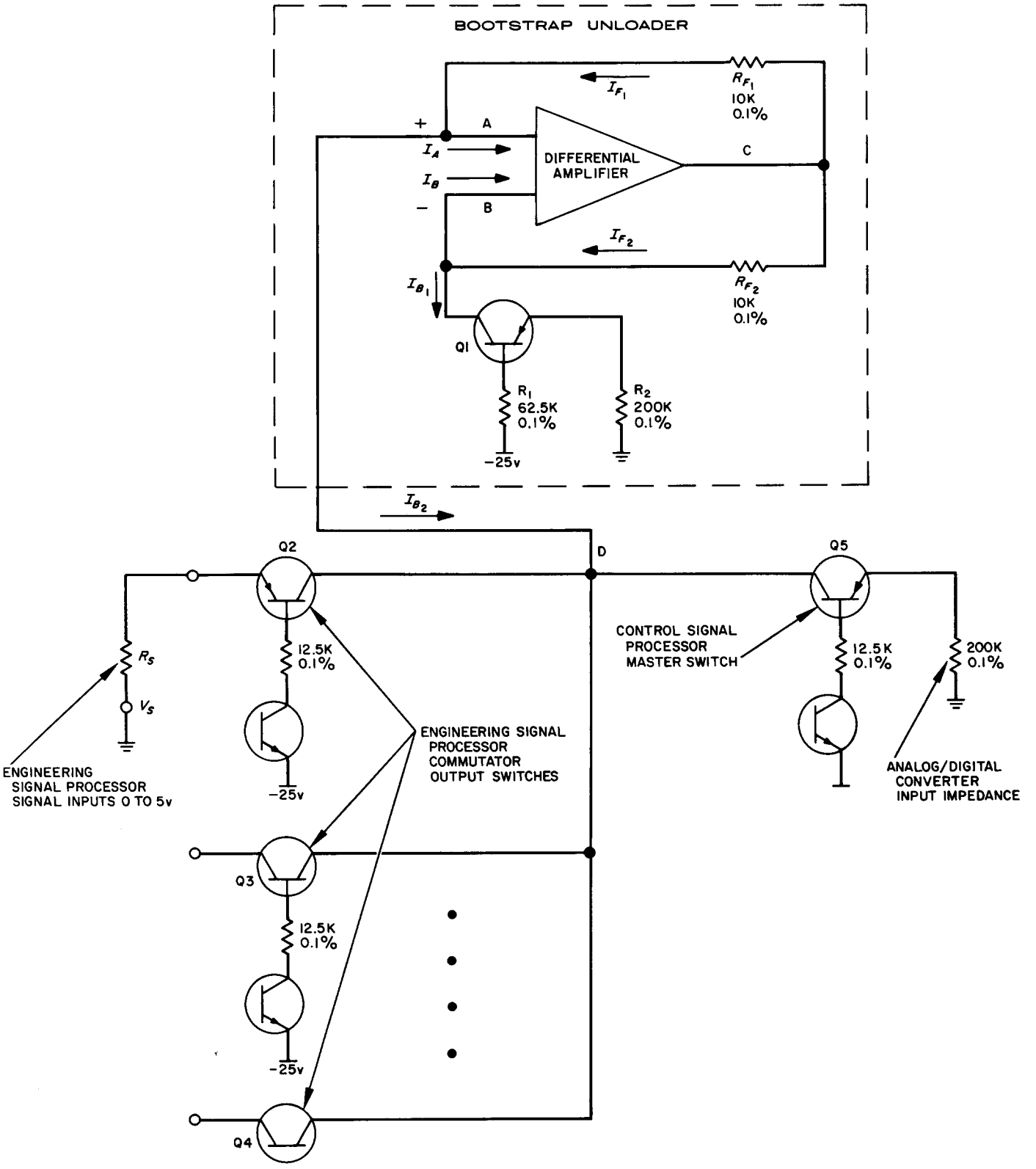

Fig. 46. Bootstrap unloader

CONFIDENTIAL
UNCLASSIFIED

UNCLASSIFIED CONFIDENTIAL

offset errors (ECA 112548). The −5-v reference supply was replaced with a 10-v reference supply. The worst case accuracy of the 10-v reference is 0.1%.

Zero BVW ladder and zero BVW switches were added to compensate for comparator offset, and additional logic circuits were included. Result was less than a 1% increase in the overall component count. A preliminary circuit release was made. Modification and test of the breadboard indicated an improvement in operational accuracy.

Concurrently with these changes, digit time amplifier circuitry was simplified and short circuit protection was included to protest unit operation. This reduced total power consumption.

d. A-21 ESP/AESP. The commutator advance amplifier (T301) was found to be inoperative in the worst case. Changes were incorporated on SC-5 and up to ensure worst-case operation.

Abnormally high commutator unbalance currents were observed in the ESP (reference trouble failure report 46590). The 988802-1 transistor parts used in the group select switches were subsequently replaced with a low $V_{EE\,Sat}$ epitaxial device.

A filter inductor was placed in series with the 29-v bus lines of the ESP and AESP on SC-2 and up to filter 29-v line transients, which were degrading operation of the constant current generators.

4. New Technology[3]

The bootstrap unloader is shown in Fig. 46 together with a diagram of the ESP commutator output switches and a partial diagram of the central signal processor (CSP) master switch.

At any one time during an ESP telemetry frame, one ESP commutator output switch will be turned on (Q2) and the CSP master switch will be on (Q5). Without a bootstrap unloader, Q2 and Q5 base current must be supplied by the ESP signal input voltage through the signal source impedance. This has the effect of introducing a considerable ESP measurement error owing to the voltage drop in R_s. The error will vary from channel input to channel input because current to the base resistors will depend on the value of input voltage to be measured, which is in the range of 0 to 5 v.

Main purpose of the bootstrap unloader is to supply the required base current for Q2 and Q5 (i.e., unload the signal input). The bootstrap unloader will thus appear as a negative resistance on the ESP commutator output line which always supplies the correct amount of current for Q2 and Q5 base resistors as the input voltage varies from 0 to 5 v.

The bootstrap unloader is to be used on *Surveyor* spacecraft beginning with SC-5. Its advantages are:

(1) It requires no elaborate module calibration procedure where several parts must be painstakingly handpicked.

(2) It requires considerably less power than the existing bootstrap unloader.

(3) It incorporates more reliable epitaxial transistors (rather than alloy types).

(4) It reduces the commutator unbalance current to approximately half the original value obtained with the existing bootstrap unloader.

(5) It is not subject to oscillation problems.

K. Electrical Power Source

1. Batteries

Poor voltage performance of batteries 43 through 47 has been attributed to a subquality lot of cellophane separator. This lot has been rejected by the vendor, and a closer control of this material has been implemented.

Battery simulator oscillations during combined systems test are under investigation in the power laboratory.

2. Spacecraft Power[4]

A preliminary design of *Surveyor* A-21 series spacecraft solar panels (for SC-5, -6, and -7) has been completed by JPL and work is in process at Electro-Optical Systems, Inc., Pasadena, California, to fabricate the first prototype hardware. This design incorporates the flat solar cell mounting technique, rather than the rigid shingle concept

[3] D. A. Hillis, innovator.

[4] Prepared by JPL Technical Section 342.

UNCLASSIFIED CONFIDENTIAL

UNCLASSIFIED
CONFIDENTIAL

incorporated in the solar panels on the first four engineering *Surveyor* spacecraft. Flat-mounted cells provide a more rugged mechanical and thermal design and should improve confidence in the capability of the panels to survive increased A-21 environmental requirements.

The baseline solar panel design incorporates a submodule very similar to that successfully used in the *Mariner* 1964 panels, seven 1 × 2 cm, P/N, 1-ohm/cm, silicon solar cells connected in series-parallel by kovar bus bars. Kovar is an iron, nickel and cobalt alloy with thermal expansion characteristics similar to those of silicon solar cells. Use of it will greatly reduce the effects of thermal shock and thermal cycling on cell interconnections.

P/N silicon solar cells planned for this panel are the residual cells remaining from *Mariner* 1964 and *Ranger* block III programs; hence, a significant amount of empirical data are available concerning their electrical and mechanical characteristics. Data from solar cell modules made for the first A-21 prototype panel indicate that the nominal postfabrication efficiency for this series of *Surveyor* panels will be the same as for *Mariner* 1964.

Fig. 47 is an I-V characteristic of the mean solar cell to be incorporated into the panel. The plot shows a maximum power output of 22.5 mw at 28°C under 100 mw/cm², 2800°K tungsten illumination. Fig. 48 is an

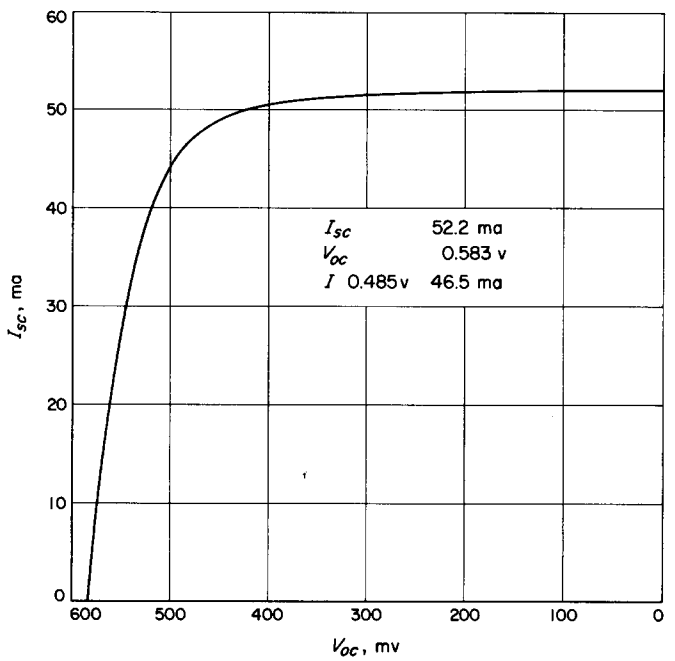

Fig. 47. Typical solar cell I-V characteristics

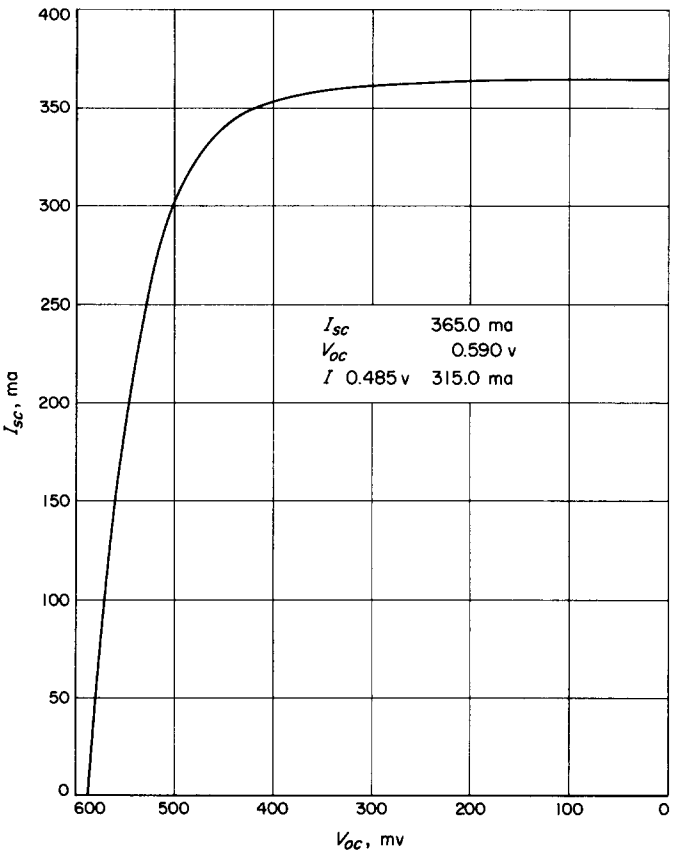

Fig. 48. Typical 7-cell submodule I-V characteristics

I-V characteristic of the expected mean solar cell submodule (7 cells in parallel) after it has been fabricated and filtered. This submodule curve is from empirical data generated for *Mariner* 1964 and was measured under the same conditions as that given for the solar cell above.

Present electrical design parameters for the redesigned solar panel include maximum power at 31.5 ±1 v during in-transit flight conditions of 140 mw/cm² and 62°C, and open circuit voltage > 28 v at lunar noon conditions of 140 mw/cm² and 121°C. To accomplish these requirements and obtain the highest packing factor (number of cells per square ft) for the particular configuration and size of the A-21 substrate, a cell matrix of 74 cells in series by 49 in parallel was developed.

To improve the reliability of the design, the panel is divided into three separate, electrically-isolated sections, 2 sections of 74 cells in series by 14 in parallel and one section of 74 cells in series by 21 in parallel. Electrical isolation is accomplished by two blocking diodes per section. Figs. 49 and 50 show expected in-transit and

CONFIDENTIAL
UNCLASSIFIED

UNCLASSIFIED
CONFIDENTIAL

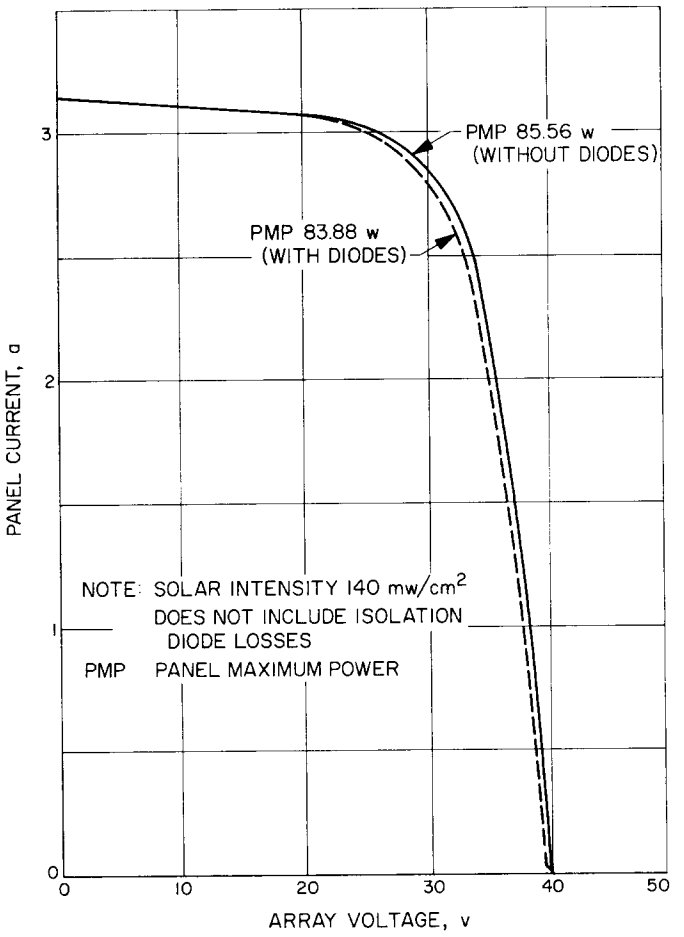

Fig. 49. *Surveyor* solar panel I-V characteristics (panel temperature 60°C)

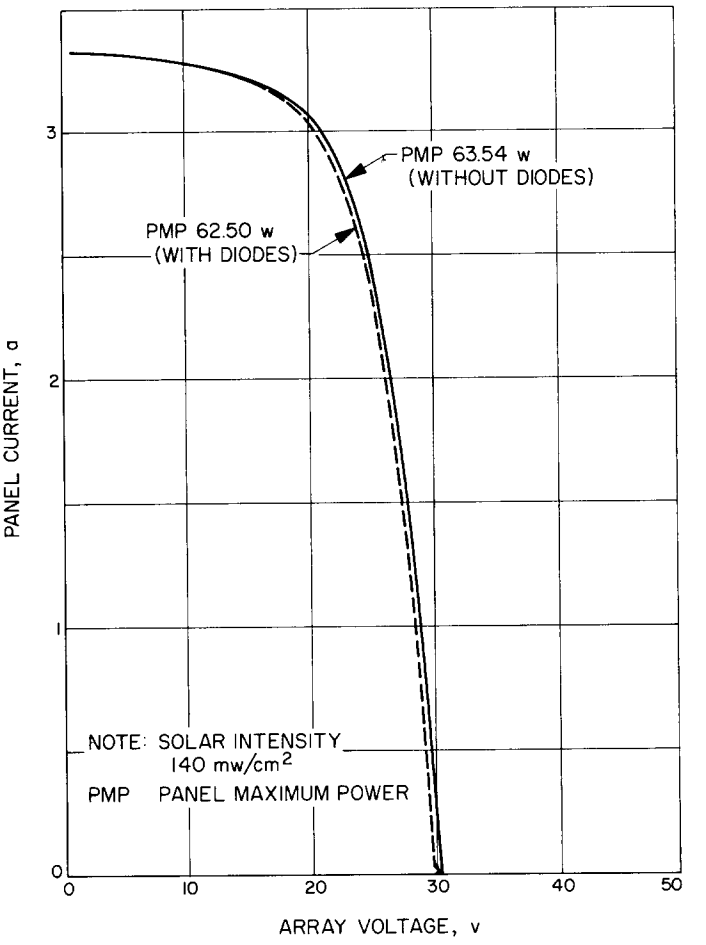

Fig. 50. *Surveyor* solar panel I-V characteristics (panel temperature 127°C)

lunar I-V characteristics of this panel. Fig. 51 is a block diagram of the A-21 panel's electrical layout.

The block diagram indicates an I_{sc}-V_{oc} transducer consisting of three specially standardized solar cells that are representative of the cells on the panel. These standardized cells are mounted on the panel and are provided with resistor loads. Their inflight performance is monitored and, through preflight calibration techniques, related to the performance of the panel.

Cell I of the transducer is loaded with a 1.5-ohm resistor to permit operation of the cell close to its short circuit current point. Cell II is similar to cell I in configuration and loading but has been degraded with 1 Mev electrons having a flux level of 10^{15} electrons/cm^2. This dose of radiation makes the cell relatively insensitive to further radiation damage. A comparison of the outputs of cells I and II should aid in evaluating the extent of radiation damage to the solar panel.

Cell III is similar in configuration to cell I except that its 1000-ohm resistance load places its operation close to its open circuit voltage point. Preflight calibration of this cell with the panel will aid in determining the open circuit voltage of the panel during space operation.

Other important features of the panel that are shown in this block diagram are the resistive current transducer that will monitor the output current of one electrical section and a temperature transducer that will be bonded to the center of the back of the panel.

The schedule for fabrication and testing of the solar panels is presented as Fig. 52. All panels are expected to be fabricated and flight acceptance tested by December 1966.

UNCLASSIFIED
CONFIDENTIAL

UNCLASSIFIED
CONFIDENTIAL

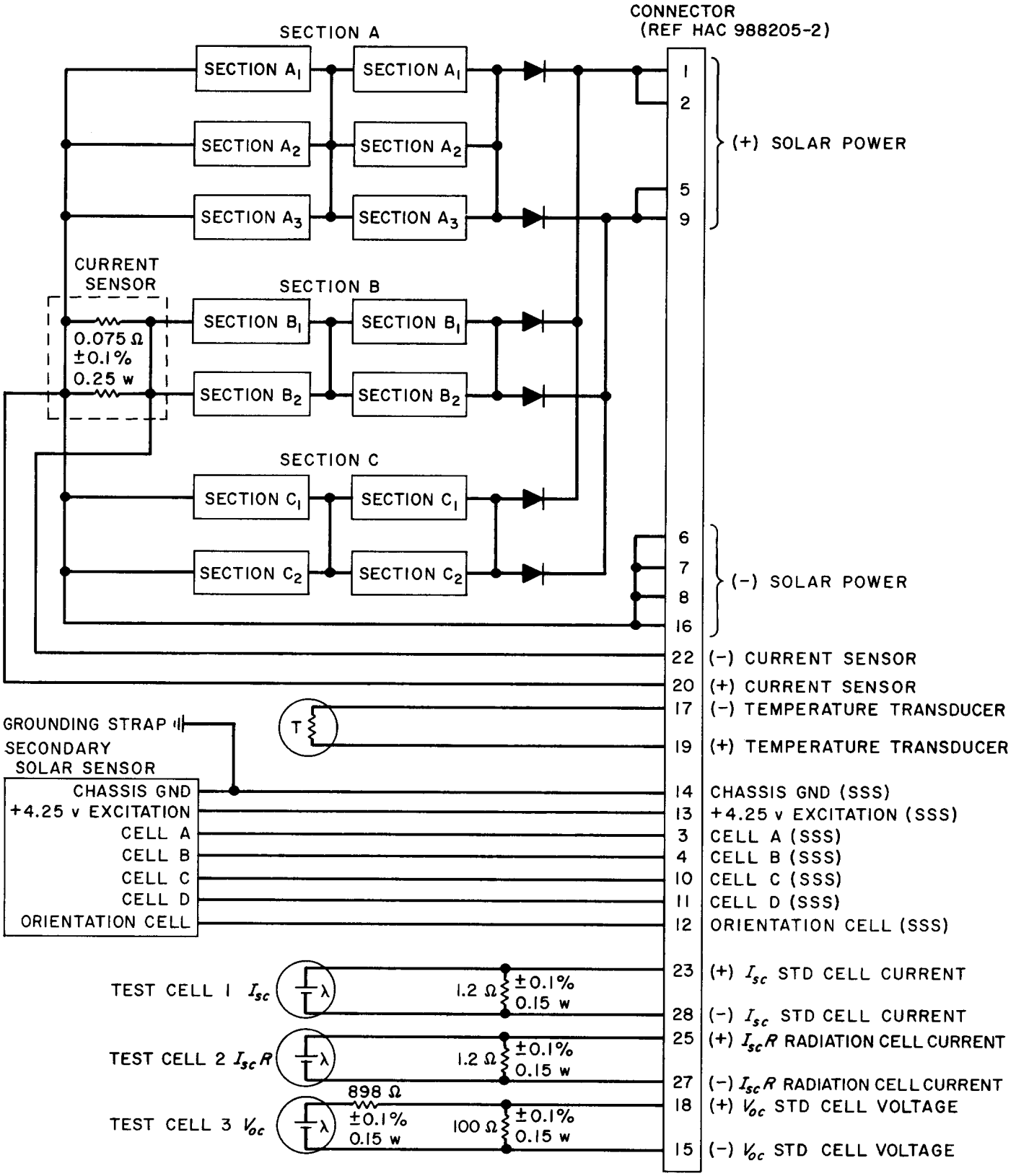

Fig. 51. A-21 panel connections

UNCLASSIFIED
CONFIDENTIAL

UNCLASSIFIED CONFIDENTIAL

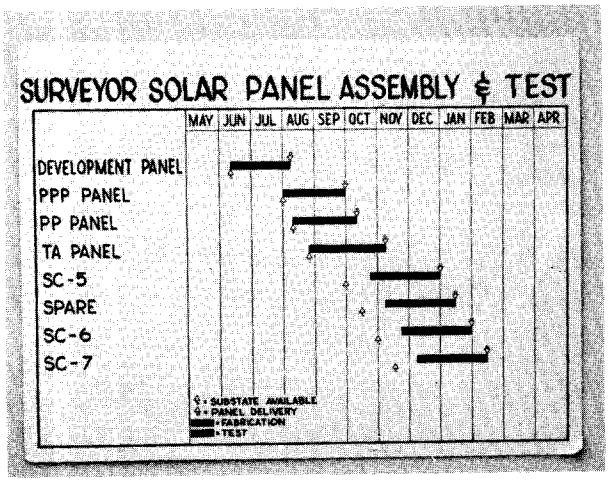

Fig. 52. Solar panel assembly and test schedule

L. Propulsion

1. Retrorocket Engine and Propulsion System Status

Both the SC-1 flight and flight-spare engines were fully prepared for flight by May 19. The SC-1 retrorocket engine performed satisfactorily in flight. The SC-1 flight spare became the SC-2 flight engine. The spare engine for SC-2 will soon be delivered to AFETR.

As the result of a spacecraft weight increase, a design study was undertaken to increase the propellant capacity of the retrorocket engine to 1470 lb. All work was stopped May 20 in accordance with the stop work order issued by JPL.

All remaining nonqualifying type approval tests (TAT) have been completed on the A-21 vernier propulsion system components. These components included the high pressure charging valves, fill and vent valves, and relief valves. The propellant tank pad pressure decay test has been completed. Test results showed that a 6.89-in. helium gas bubble remained within the bladder after the pad pressure had decayed to zero. The SC-1 vernier system was loaded with propellant within 0.03 lb of the target weight; allowable variation was ± 1.5 lb.

Component development work for the A-24 vernier feed system is nearing completion. Some components have completed TAT and others are nearing completion of this phase.

In-house engineering of the A-24 vernier propulsion system has been stopped per direction of change order 3, amendment 1. Recommendations have been made to JPL regarding termination of component subcontracts. HAC is awaiting firm direction before taking any action to terminate.

The propulsion system for the T-2N vehicles successfully completed altitude recovery and soft landing tests. The T-2N test program has been completed.

2. Main Retrorocket Engine

Engines A21-26 (SC-1) and A21-27 (SC-1 spare) completed X-ray, safe-arm unit checkout, and installation of the thermal insulation blanket by May 19. According to preliminary data from the SC-1 mission test, the main retrorocket engine performed satisfactorily. Of particular significance was the low roll moment recorded during burning. Further data reduction will be conducted.

Final reduced data for engine A21-15 indicate that all test objectives were met. Engine performance was unaffected by 23 months of storage, and engine integrity was unaffected by temperature cycling down to 10°F. The T-3500 time for A21-15 was 39.35 sec.

Based on the anticipated growth in the A-24 spacecraft weight, it was deemed necessary to make provisions in the main retrorocket engine design to permit specification performance at propellant weights up to 1470 lb. Upon review of the alternative design changes, it was decided that the most straightforward change would be the addition of 1.36 in. to the cylindrical section in the case and a 7.3% increase in the nozzle throat area. Further work was stopped in accordance with the stop work order issued by JPL May 20.

3. Vernier Propulsion System

a. System analysis. As reported previously, helium that has permeated the propellant tank bladder and gone into solution with the propellants at the pad pressure prior to launch may come out of solution and form a gas bubble inside the bladder as the pad pressure decays owing to unavoidable leaks in the system. A test plan was prepared to investigate whether or not this phenomenon will occur. The test was performed and completed at the Placerita propulsion test facility. The results indicated that as the pressure decayed, the dissolved gas came out of solution and formed a 6.89-in.^{3} bubble inside the bladder. At an operating pressure of 720 psig, this

UNCLASSIFIED CONFIDENTIAL

UNCLASSIFIED
CONFIDENTIAL

volume, in terms of MON-10 absorptivity, would be 0.313 in.^{3}, which is negligible. The duration of the test spanned a month for the pressure to decay to zero. A test report has been prepared and published.

Because of the emphasis placed on the foregoing test, the propellant flow decay test preparation has been temporarily postponed. However, the test will be in progress by the next report period.

Propulsion preparations for spacecraft performance analysis and command (SPAC) participation during the upcoming SC-1 mission are proceeding on schedule. A SPAC propulsion handbook, which is being produced, will contain information concerning expected pressure and temperature sensor history during the mission and minimum required helium pressures and propellant weights for midcourse and terminal descent operations. Additionally, the thrust chamber assembly log books and flight acceptance test (FAT) results of major vernier propulsion system control items, together with a copy of all SC-1 applicable trouble and failure reports (TFRs), will be available. Practice training for the mission averaged 10 to 20 hr per week and was increased prior to SC-1 launch. During the SC-1 mission, no anomalies relative to the propulsion system were noted, and system operation agreed well with the premission predictions. Postmission analysis operations are now under way.

b. Thrust chamber assemblies (TCAs). Thrust chamber assemblies were received from JPL at AFETR following preflight checkout for the SC-1 vehicle. Owing to failure of several units during preflight checkout, TCAs originally planned for SC-3 were shipped to support the SC-1 launch at AFETR. The TCAs used on *Surveyor I* performed satisfactorily during the mission.

JPL delivered three TCAs for each of the SC-3, SC-4, and SC-5 vehicles. The SC-3 units were installed on the vehicle for the leak check and solar thermal vacuum phases of FAT.

c. Valves. During this report period, all remaining nonqualifying TATs were completed on the vernier propulsion system A-21 high pressure charging valves, fill and vent valves, and relief valves. These tests, which include lunar survival (high and low temperature) proof pressure and endurance are performed for engineering information only and generally supplement the qualifying series of tests which were completed during the last report period. Engineering records covering the TAT programs have been released.

A modified helium tank and valves assembly configuration has been approved for use on SC-5 through SC-7 and SP-2. This configuration decreases the complexity of the tank valve assembly by making a separate control item of the check valve assembly and relief valves assembly.

This assembly will be mounted individually and will no longer be part of the helium tank and valves assembly control item. Drawings have been prepared and released, and parts have been subsequently assembled. The FAT on this assembly is under way.

d. T-2N. The T-2N-1 successfully completed the altitude recovery testing phase and then concluded its activity with a successful soft landing test. Propulsion operation during these tests was normal. No anomalies were noted.

The T-2N-2 vehicle, like the T-2N-1 vehicle, completed altitude recovery testing and followed with a successful soft landing test.

These tests conclude the T-2N test program at AFMDC. Final reports on all testing are scheduled for release by June 30.

e. A-24. All helium tank shells required for the A-24 program have been received, and TAT of the shell design has been successfuly concluded.

Preliminary thermal predictions for the lunar-environment temperature of the A-24 propellant tanks indicate that an oxidizer dump system may be necessary to ensure survival of a 3-σ low tank shell. There are two factors causing this: (1) the heavier thermal standoff required by A-24 causes the tanks to stabilize at a higher temperature than on A-21, and (2) actual burst results on the A-24 tanks produced to date are slightly below those for A-21 (while still meeting specification requirements). Work is continuing on subcontracted components of the manifold dump system pending directions to terminate from JPL.

TAT of the manifold antimigration check valve has been successfully completed by the vendor, and 90% of the production parts have been delivered.

All bodies have been assembled for the squib-actuated dump valve. The manufacturer is letting out subcontracts for the required TAT, and the manufacturer's

CONFIDENTIAL
UNCLASSIFIED

UNCLASSIFIED
CONFIDENTIAL

subcontractor is approximately 20% complete with assembly of squibs for this valve.

Completion of the TAT of the helium release and dump valve has extended into this report period. This was caused by late delivery of O-rings of the proper material for use in rebuilding the test valves after pressure-hold tests. Rebuild has now been accomplished, and propellant-exposure testing is complete. Final analysis of valve performance will be made early in the next report period.

Buildup of one A-24 propellant tank for engineering tests was stopped at the time of engineering effort cessation. A parts kit to complete this tank is being held for future use.

The feasibility of an alternate thermally actuated pump device employing a fusible alloy has been investigated. Preliminary drafts of a specification and statement of work for procurement of such a device were prepared, but are being held because of cessation of the A-24 engineering effort.

f. Metal foil bladder program. HAC is working on change order 119 to procure and test metal foil bladders to provide for an improved helium gas barrier between the pressurizing gas and the propellants used in the propellant tanks for the vernier propulsion system. The program will last for 5 mo and will include such test items as propellant storage and expulsion, helium and nitrogen gas and propellant permeability tests, physical characteristics determination, TAT level vibration, fold and crease formation, and improved bladder assembly techniques. Flight control analysis will be performed to determine how much improvement in spacecraft stability margins may be expected from the reduction of helium permeability into the vernier engine propellants.

g. Investigation of SC-2 bladder failure. All engineering analysis of the SC-2 bladder failure is complete. Two phases of investigation were undertaken: (1) bladder manufacture and tests, and (2) system effects during and after assembly to the spacecraft. HAC was able to duplicate the split in the bladder (Figs. 53 and 54) by heating the bladder to 200°F for 20 min, then letting it cool, and finally making the assembly into a propellant tank. During a normal filling operation with referee propellant, the bladder failed in a manner similar to the SC-2 failures. The conclusion was that if a bladder is

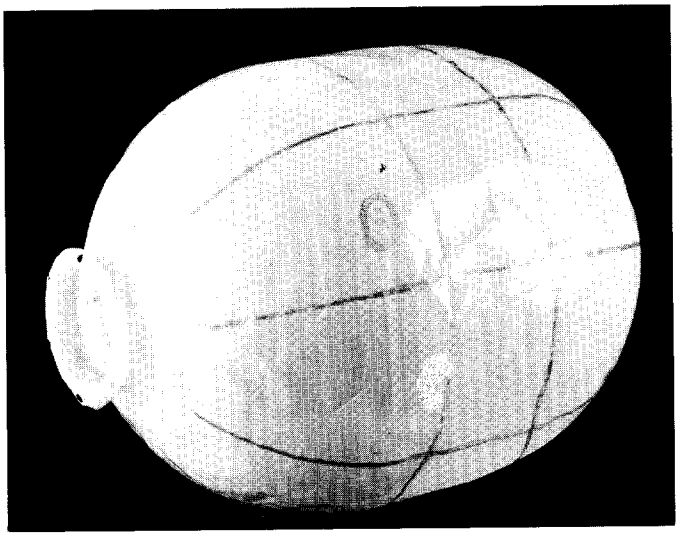

Fig. 53. Propellant tank bladder

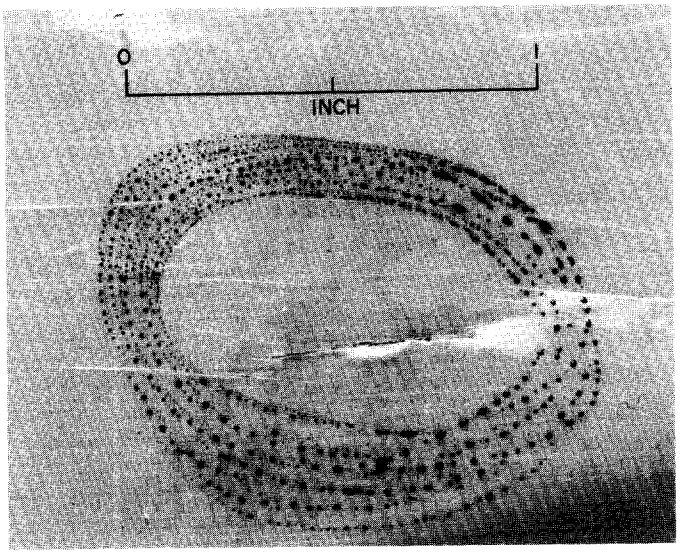

Fig. 54. Propellant tank bladder split

heated to a temperature of approximately 200°F, shrinkage, and subsequent tearing, will occur during a filling operation. A complete engineering report of the investigation and analysis has been generated.

4. Thrust Chamber Assembly[5]

The program for *Surveyor* vernier engine [Reaction Motors Division of Thiokol Chemical Corporation (RMD) model No. TD-339] evaluation continued with six firing tests, all at Edwards Test Station (ETS) in May and June, and completion of the Pyrochrome paint confidence

[5]Prepared by JPL Section 384.

CONFIDENTIAL
UNCLASSIFIED

UNCLASSIFIED

tests during April and May. A summary of these activities follows:

Group	Test No.	Test date	Purpose
28	DY 101 (previously reported)	April–May	Pyrochrome paint confidence tests
29	DY 102, DY 103	May 4	Hardware temperature conditioning
30	DD 123 to DD 126	June 6-9	Simulated lunar TCA firings

a. Pyrochrome paint confidence test—Group 28. This is a complete summary of the test briefly reported in *SPS 37-39*, Vol. I, p. 59.

The exterior surface of the molybdenum exhaust-nozzle extension cone on each of the flight-type vernier engines (Fig. 55) is coated with several layers of green-colored "Pyrochrome" ceramic paint.[6] The emissivity of this coating keeps the maximum operating temperature of the nozzle extension in the neighborhood of 1800°F, well below the 2500° recrystallization temperature of the molybdenum.

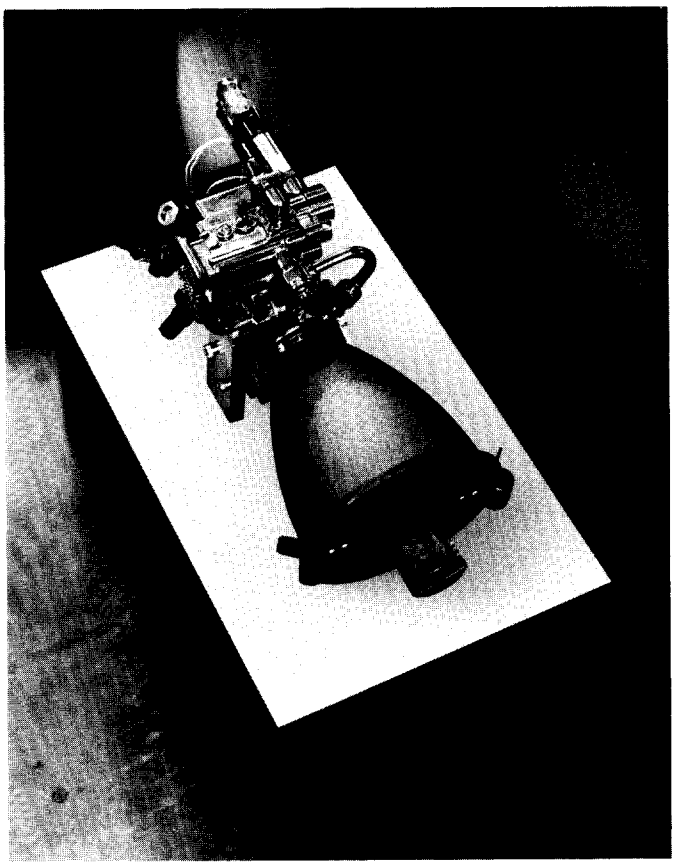

Fig. 55. *Surveyor* vernier engine thrust chamber assembly with nozzle-closure plate and desiccant container attached

Visual examination of engines delivered to JPL for flight use revealed that the outer layer of Pyrochrome contained tiny blisters (less than 1/16 in. diameter) constituting 3 to 5% of the total area. Some 25 to 50% of the blisters were broken. Also, on the lip at the exit of the nozzle extension, there were small uncoated areas. In this highly stressed area, repeated installation and removal of the nozzle closure plate and desiccant holder (Fig. 55) may have contributed to Pyrochrome flaking.

An analysis of possible reduction in heat transfer due to the observed degradation of the Pyrochrome showed that the expected increase of operating temperature is less than 15°F.

It was also recognized, however, that the condition of the nozzle coating might result in the release of small particles of Pyrochrome during flight. A particle drifting into the field of view of the Canopus tracking sensor would, of course, pose a hazard to proper operation of the flight-control subsystem. Therefore, a special test was undertaken at JPL to evaluate the integrity of the Pyrochrome on the nozzle extension of a typical flight engine under simulated launch vibration, shock, and depressurization environments followed by a simulated midcourse firing of the engine.

For this test, a complete vernier engine thrust chamber assembly (TCA), part No. 315800, serial No. (S/N) 559, was used. The as-received condition of the Pyrochrome on this engine was considered slightly worse than that of the engines installed on SC-1. *Surveyor* quality assurance surveillance was maintained during all test operations. The sequence of test operations is outlined below.

(1) The engine was subjected to an oven temperature of 135 ± 5°F for 2½ hr to simulate the cure cycle which a flight engine usually receives after the final thermal-paint pattern has been applied.

(2) The engine was flow checked on the *Surveyor* flow bench at the JPL-ETS, using the appropriate flow check procedure.

[6]Preferred Utilities Mfg. Corp., New York, N. Y.

UNCLASSIFIED

UNCLASSIFIED
CONFIDENTIAL

(3) High-resolution color photographs of the nozzle extension were taken to record the pretest condition of the Pyrochrome paint.

(4) Vacuum cleaning of the nozzle extension was performed using a special vacuum brush (Fig. 56), proposed for use on spacecraft-mounted engines. Particles collected on a 200-mesh screen filter in the vacuum line were examined, identified and counted under a microscope.

(5) The TCA alignment fixture was mounted on the nozzle extension and then removed, simulating the stress application usually experienced during prelaunch alignment.

(6) The nozzle extension was again vacuum cleaned with the special brush, and the number and size distribution of additional particles removed was recorded.

(7) A second set of color photographs of the Pyrochromed nozzle extension was taken.

Table 17. TCA Pyrochrome confidence test vibration and shock specifications

Environment	Axis	Frequency, cps	Level
VFSW[a] at 2 octaves/min	Longitudinal Z	5-28 28-50 50-150 150-50 50-28 28-5	0.5 in. D.A.[b] 20g (0-peak) 12g 12g 20g 0.5 in. D.A.[b]
VFSW[a] at 2 octaves/min	Lateral X and Y	5-21 21-150 150-21 21-5	0.5 in. D.A.[b] 12g (0-peak) 12g 0.5 in. D.A.[b]
Random vibration 3 min each axis	Z, X, Y	100-1500	4.5g rms (band limited)
Shock: Each axis (Z, X, Y) 2 pulses at 11 sec intervals.		Pulse description $\ddot{X}(g) = 30e^{-70t}\cos 2\pi(550)t + 2e^{-3.5t}\cos 2\pi(27)t$, $0 \leq t \leq 0.2$ sec	

[a] Variable-frequency sine wave.
[b] Double amplitude (displacement limit).

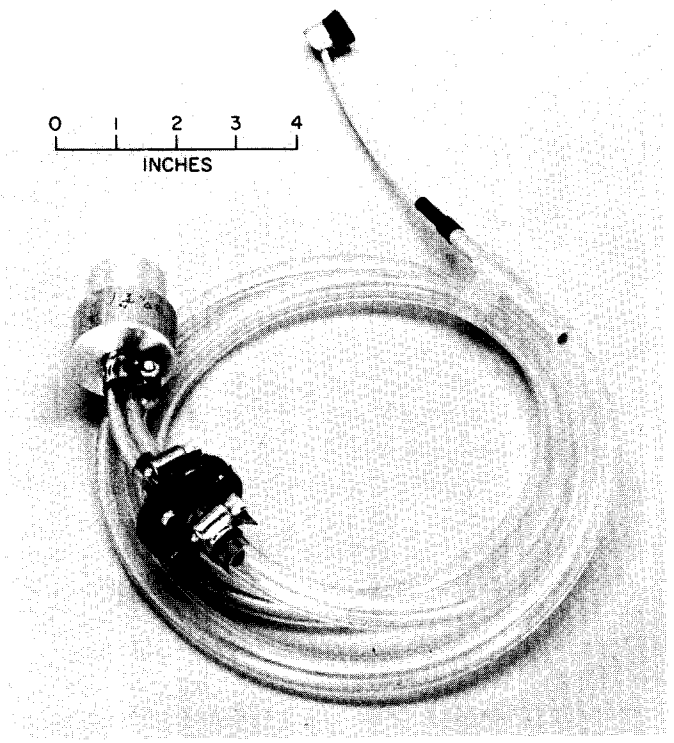

Fig. 56. Special brush and filter assembly for vacuum cleaning of nozzle extensions on spacecraft-mounted TCAs

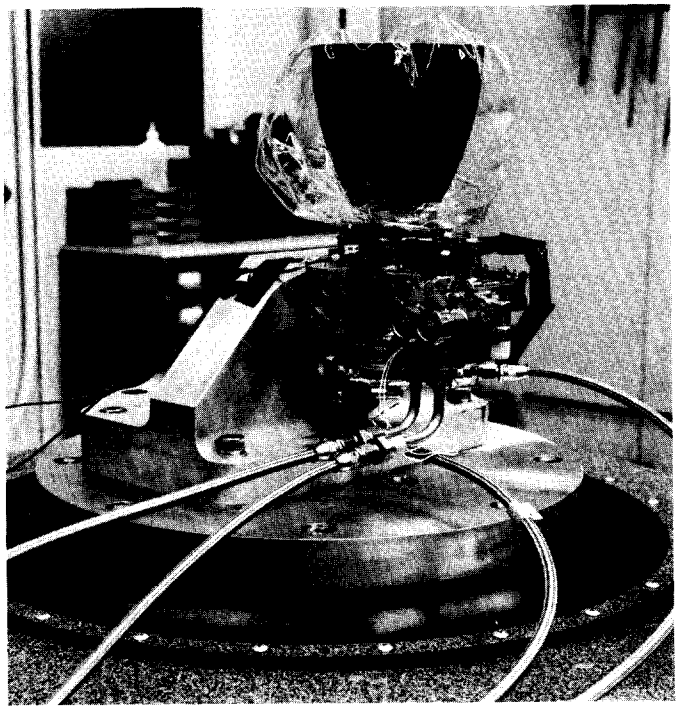

Fig. 57. Vibration and shock test installation of TCA with vinyl bag covering Pyrochrome-coated nozzle extension

CONFIDENTIAL
UNCLASSIFIED

UNCLASSIFIED

(8) With the engine filled with solvents pressurized at 250 psi (pad pressure), a simulated launch vibration and shock test on each of 3 orthogonal axes was conducted, as described in Table 17. The test set-up is shown in Fig. 57. During this test the nozzle extension was enclosed in a vinyl bag. On completion of vibration and shock testing, a count was made of the Pyrochrome particles collected in the bag.

(9) A third set of color photographs of the Pyrochromed nozzle extension was taken.

(10) The engine was placed in the JPL 7 x 14-ft vacuum chamber for simulated launch depressurization. The chamber pressure was reduced from atmospheric to 1 psi in 81 sec, as shown in Fig. 58. The engine was kept in the vacuum environment for an additional 40 min, by which time the pressure had reached 10^{-5} mm Hg. While in the vacuum chamber the nozzle extension was contained in a wire basket having an inner liner of 200-mesh screen (Fig. 59). Microscopic examination of debris obtained from cleaning of the basket on completion of vacuum testing revealed no Pyrochrome particles.

(11) A fourth set of color photographs of the Pyrochromed nozzle extension was taken.

(12) The nozzle extension was again vacuum cleaned with the special brush, and the number and size distribution of collected particles was recorded.

(13) A prefiring flow check was performed on the flow bench at ETS.

(14) Simulated midcourse firing of 40 sec at approximately 75 lb thrust, followed by 10 sec at maximum thrust (above 104 lb), was accomplished in the vacuum-firing test chamber at ETS. The firing is identified as ETS No. DY-101. Motion-picture coverage of the nozzle extension during this firing was obtained from both sides of the chamber. Color film was used at 48 frames/sec.

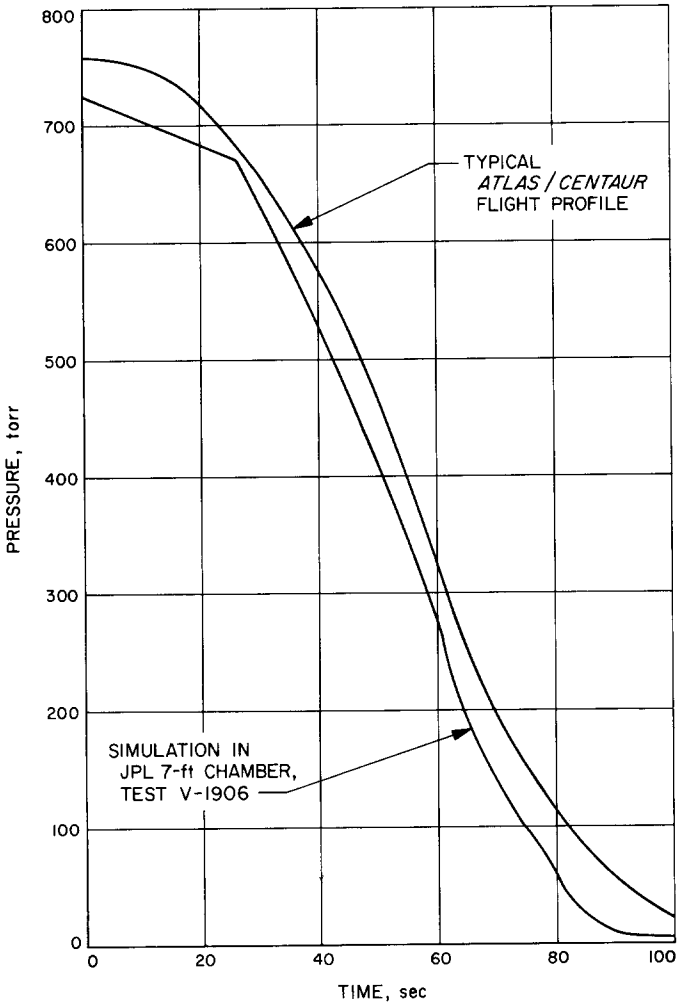

Fig. 58. Simulated launch pressure profile for test of Pyrochrome coating on nozzle extension of *Surveyor* vernier engine TCA (S/N 559)

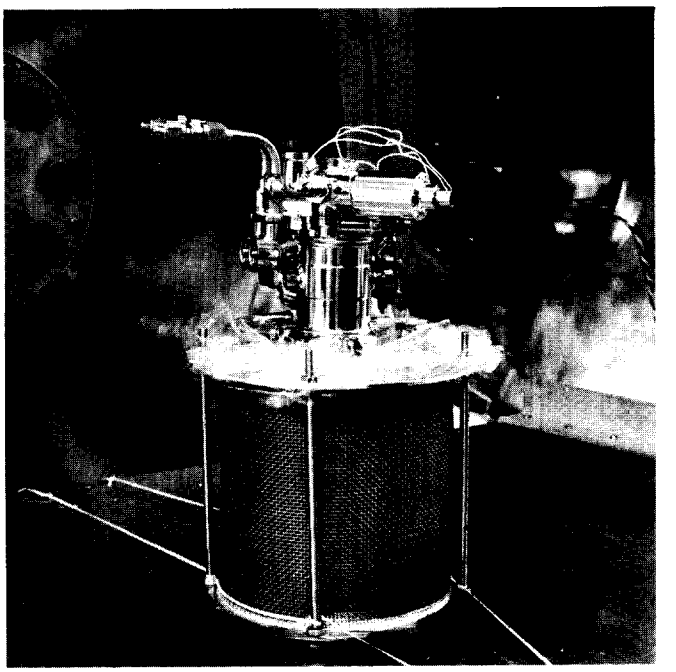

Fig. 59. Depressurization test installation with TCA nozzle extension contained in mesh-lined basket

UNCLASSIFIED

UNCLASSIFIED
CONFIDENTIAL

(15) A postfiring flow check was performed.

(16) When the engine was returned to JPL, a final (fifth) set of color photographs of the Pyrochromed nozzle extension was taken. Comparison of these photos with the initial photos can provide auxiliary evaluation of any degradation resulting from the test.

(17) A postfiring vacuum cleaning of the nozzle extension was performed in two steps, so that particles collected from within ½-in. of the exit-end lip could be counted separately from the particles obtained from the remainder of the nozzle extension surface.

A record of the particle count and size distribution obtained at each of the various stages in this test is presented in Table 18.

The vacuum cleaning operations performed before and after alignment procedure (Table 18, item 1) resulted in a total count of 64 particles of Pyrochrome in the size range of 1 to 5 mils.[7] There were no particles larger than 5 mils. (Particles < 1 mil were obtained but are not considered significant, since the Canopus tracker is insensitive to Pyrochrome particles that small).

Examination of particles collected in the vinyl bag which covered the nozzle during the vibration and shock exposure indicated that 40 Pyrochrome particles (1 to 5 mils) had shaken loose (Table 18, item 2A).

Examination of the 200-mesh wire basket used in the simulated launch depressurization operation revealed no Pyrochrome particles (Table 18, item 2B).

[7] Particle shapes were irregular; size is quoted in terms of largest dimension. One mil equals 0.001 in. or 25.4 μ.

Table 18. Pyrochrome paint particles collected during special test of thrust chamber assembly Serial No. 559, April 13–19, 1966

Item	Test phase	Particle size,[a] mils[b]	Number of particles (10 20 30 40 50)
1	A. Initial vacuum cleaning	> 1	
		1 to 2	
		2 to 4	
		4 to 5	
	B. Vacuum cleaning after alignment	> 1	
		1 to 2	
		2 to 4	
		4 to 5	
2	A. Collection in vinyl bag during vibration and shock	> 1	
		1 to 2	
		2 to 4	
		4 to 5	
	B. Collection in wire-mesh basket during depressurization	Any size	None
3	Vacuum cleaning after simulated launch environments	> 1	
		1 to 2	
		2 to 4	
		4 to 5	
4	Vacuum cleaning after simulated midcourse firing	> 1	
		1 to 2	
		2 to 4	
		4 to 5	
		5 to 7	

[a] Particle shapes irregular; size refers to largest dimension.
[b] 1 mil = 0.001 in. = 25.4 μ.

CONFIDENTIAL
UNCLASSIFIED

UNCLASSIFIED
CONFIDENTIAL

After the vibration, shock, and depressurization exposure only 11 particles larger than 1 mil were obtained, using the same vacuum cleaning procedure previously used (Table 18, item 3). This suggests that the vibration and shock environment had provided very effective removal of practically all loose Pyrochrome particles.

The 50-sec engine firing and subsequent cooling apparently caused the development of a moderate number of new, loose particles. After the firing, 93 Pyrochrome particles ranging from 1 to 7 mils were removed from the nozzle extension by vacuum cleaning (Table 18, item 4). Thirteen flakes of gold plate were also collected in the vacuum cleaner filter during this cleaning.

Prior to the postfiring vacuum cleaning it was evident that the edge of the Pyrochrome coating at the exit-end lip was slightly chipped in several places. It is suspected that this condition results partly from mounting and removing the nozzle closure many times during prefiring and postfiring operations. The postfiring vacuum cleaning was, therefore, performed in two steps so that the particle count from near the lip could be distinguished from the count obtained from the main portion of the nozzle extension. The results are shown in Table 19, where it is clear that the majority of the loose particles were obtained in the neighborhood of the lip.

Relating of the results of this Pyrochrome confidence test to the spacecraft flight leads to the following conclusions:

(1) The nozzle-extension vacuum-cleaning procedure developed for this test affords a means for removing existing loose particles of Pyrochrome paint prior to spacecraft launch. To be most useful the cleaning should be performed after all alignment procedures have been completed and after the final removal of the nozzle closure–desiccant container. This procedure (JPL 66-310) was incorporated into the SC-1 prelaunch cleaning procedures.

(2) The launch environment can create additional loose particles of Pyrochrome, but essentially all of these will be shaken free during this boost phase and will be deposited on the head end of the *Centaur* stage along with debris from other sources.

(3) It can be predicted that, during the coast period prior to midcourse maneuver, only about 30 loose Pyrochrome particles will exist on the nozzle extensions of all three engines. This number is too small to constitute any hazard to flight control, a conclusion based on the statistical probability that only one in a thousand particles will drift into the Canopus tracker field from any place on the spacecraft.[8] In addition, solar pressure should move most of the loose particles away from the sensor.

(4) The midcourse firing of the vernier engines will probably cause an increase in the number of loose Pyrochrome particles available for liberation. The maximum expected number from all 3 engines is about 300, from 1 to 7 mils in size. It is predicted that none, or at most one, of these will pass into the field of view of the Canopus tracker.

[8] From an analysis by K. C. Beall reported in HAC interdepartmental correspondence.

Table 19. Details of particle count from two-step vacuum cleaning after simulated midcourse firing (TCA S/N 559, April 26, 1966)

Location[a]	Particle size, mils	Number of particles[b] (10 20 30 40 50)
Half-inch band at exit end of nozzle extension	< 1 1 to 2 2 to 4 4 to 5 5 to 7	
Remaining area of nozzle extension	< 1 1 to 2 2 to 4 4 to 5 5 to 7	GOLD FLAKES PYROCHROME PARTICLES

[a] Orientation of TCA for all cleaning operations simulated spacecraft-mounted condition: longitudinal axis vertical with exit end downward.
[b] Overall count of particles corresponds to Item 4 of Table 18.

UNCLASSIFIED
CONFIDENTIAL

UNCLASSIFIED
CONFIDENTIAL

b. Hardware temperature conditioning–Group 29. This test was performed to demonstrate operation of the TCA after the hardware had been conditioned to a head-end temperature of 165°F and an aft-end temperature (on the molybdenum nozzle extension) of 130°F. It is necessary that the TCA be capable of operating under these conditions since they are the best estimate of conditions encountered in space. The head-end temperature is particularly critical, since the TCA components with moving parts (shutoff valve, throttle valve and back-pressure regulator) are located at that end.

This test was a repeat of a test made at RMD (as part of the TAT program) except that during the RMD test the temperatures were inadvertently reversed, the high temperature being the nozzle end.

Two tests, DY 102 and DY 103, were run at ETS with TCA 535. The first was a 55-sec dynamic-profile test that represented midcourse thrust levels (Fig. 60); the second, made after a 1-hr hold, consisted of the first 22 sec of a dynamic profile representing lunar descent thrust levels (Fig. 61).

To condition the hardware, heated gaseous nitrogen, thermostatically controlled, was ducted into a plastic bag that enclosed the TCA from the nozzle joint to the inlet lines. A second bag enclosed the nozzle extension, with unheated gaseous nitrogen discharging over the nozzle (Fig. 62). The propellants were unsaturated with helium gas and were at ambient temperatures.

There was some difference in the two starts, the first being fast and smooth while the second start occurred at a slower rate. However, both tests were satisfactory, and the thrust-time characteristics met specification requirements.

c. Simulated lunar TCA firings—Group 30. Following touchdown, it was proposed that the vernier engines be ignited in an attempt to disturb the lunar surface. If successful, such an attempt would provide additional data on the mechanical properties of the lunar surface.

When this experiment was proposed, the helium used for pressurizing the propellant tanks had been vented, and the oxidizer-side relief valve in the helium tank and valve assembly had repeatedly actuated as the temperature rose during the lunar day. It is believed that the relief valve on the fuel side probably withstood this environment, although no direct measurement is available. The relief valve on the oxidizer side, however, in

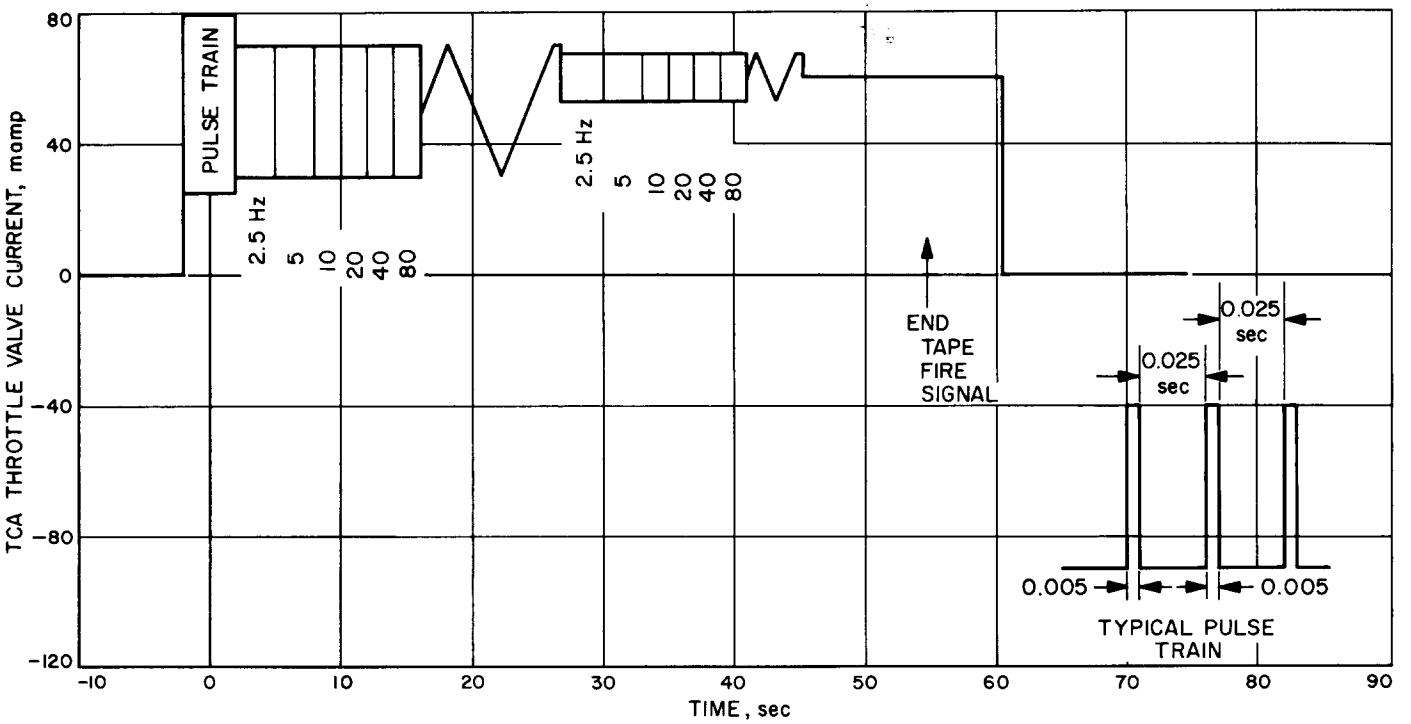

Fig. 60. Midcourse-thrust dynamic profile, test DY 102, TCA 535

CONFIDENTIAL
UNCLASSIFIED

UNCLASSIFIED
CONFIDENTIAL

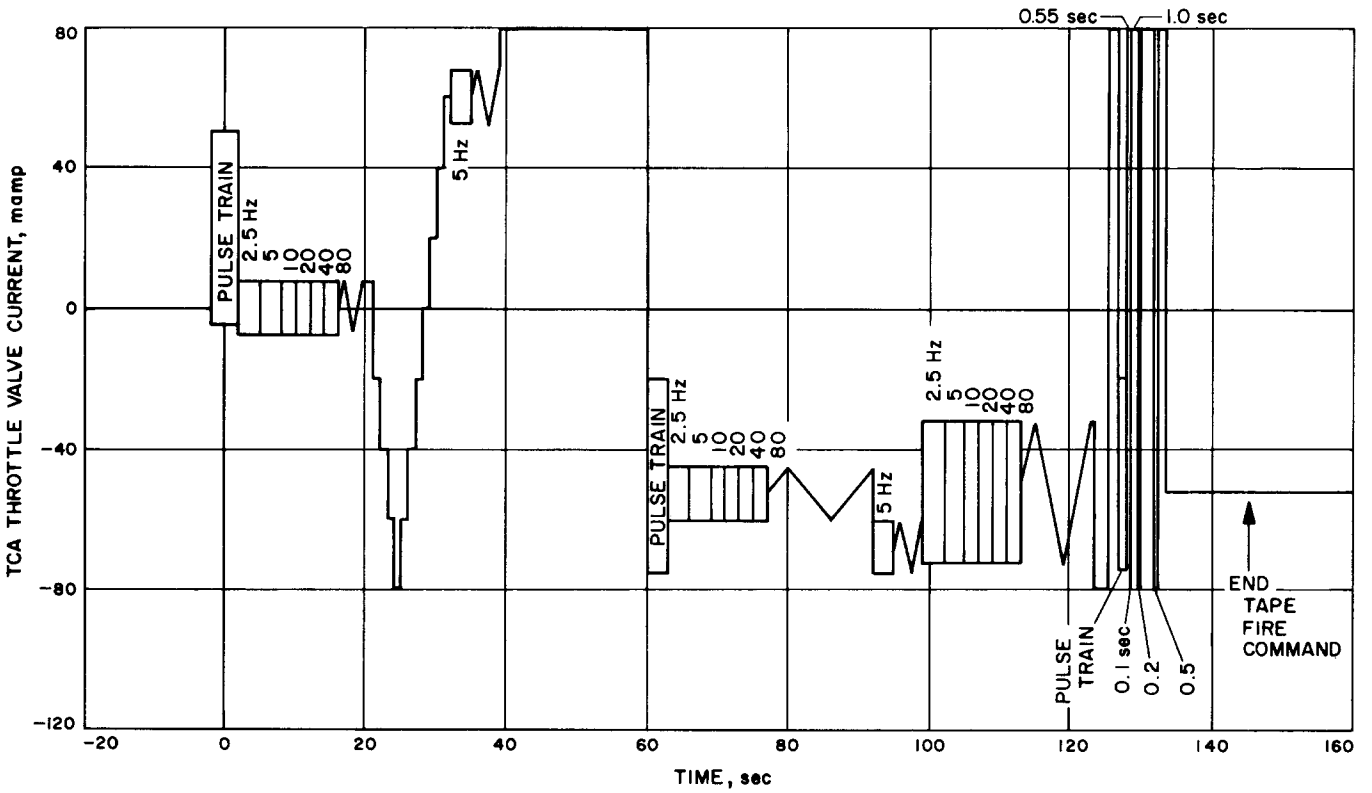

Fig. 61. Dynamic profile representing initial portion of lunar descent, test DY 103, TCA 535

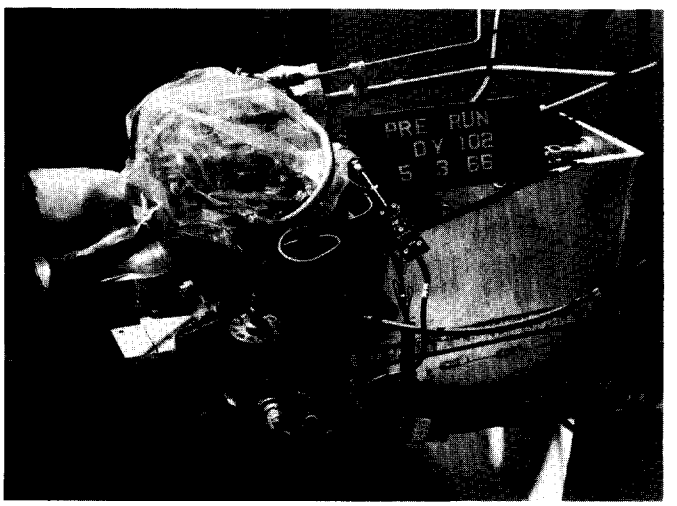

Fig. 62. Temperature conditioning set up, TCA 535

the presence of the oxidizer vapor, failed after approximately 10 cycles. Consequently, the pressure on the oxidizer side of the system dropped to the oxidizer vapor pressure, while that on the fuel side probably remained at approximately 800 psia. These pressures depend on the volume available to gas after the helium was vented, the propellant tank temperatures, and leakage rates.

Before the vernier engines can be ignited on the lunar surface, one must ascertain whether the engines will ignite at all under these operating conditions, and, if they do ignite, what sort of operation they will provide.

On June 6, 1966, two tests were performed at ETS to simulate the spacecraft conditions prevailing that evening. These tests were made to determine if engine ignition would occur and to determine the thrust that would result under these conditions. Both tests were performed with TCA S/N 522, a sea-level engine. The tests were performed in an environmental chamber capable of preconditioning the engine and propellants to desired temperature and pressure levels. The ambient pressure in the chamber was first lowered to approximately 0.2 to 0.1 psia with a mechanical pump; a steam ejector was then used to lower the pressure to approximately 0.05 psia and maintain it at that level while the engine was operating.

Test DD-123 was run simulating conditions at leg three of the lunar spacecraft. The oxidizer side was conditioned to 132 psia and 159°F, the fuel side to 802 psia and 181°F, and the engine itself was conditioned to 240°F. With an ambient pressure of approximately

UNCLASSIFIED
CONFIDENTIAL

UNCLASSIFIED CONFIDENTIAL

0.05 psia, engine ignition was observed with a chamber pressure of 10.8 psia, corresponding to a thrust of 4.5 lb.

Test DD-124 simulated conditions at leg one of the lunar spacecraft. The oxidizer side was conditioned to 50.5 psia and 119°F, the fuel side to 801 psia and 166°F, and the engine itself was conditioned to 210°F. Due to the extremely low oxidizer pressure, no ignition was observed, and a chamber pressure of 2.5 psia corresponding to a thrust of 1 lb was recorded. The chamber pressure and thrust are ascribed to evaporation of the propellants from the hot engine. The ambient pressure in the test cell was approximately 0.06 psia.

Following these experiments, two more tests were performed (June 9, 1966) simulating the more favorable environmental conditions which would prevail on the spacecraft later in the week. Because previous experiments indicated that the engine could be presumed to operate, these tests were intended to demonstrate the effect a vernier engine may have on the lunar surface. Should soil deposit on critical areas such as thermal control surfaces or the television camera mirror, spacecraft operation would be seriously impaired.

These experiments were conducted in the same chamber with the steam ejector described above. The engine used was TCA S/N 535, an altitude engine, oriented to fire vertically down into an 18-in. diameter container of soil. The engine exit plane was located 12 in. above the center of the soil surface. The monitored parameters of interest here were soil pressure and engine chamber pressure. The soil pressure was measured with an electrical pressure transducer located on the engine center line flush with the soil surface. In addition, high speed motion pictures were taken of the experiment with two cameras each operating at 250 frames/sec. The initial test setup is shown in Fig. 63.

The soil used in these experiments was chosen to simulate the particle size distribution evidenced in previously transmitted *Surveyor* pictures. It also simulated the current "best guess" of the lunar surface bearing strength. The soil, however, was intentionally cohesionless to illustrate the effects of the engine thrust.

For the first test, DD-125, the engine was conditioned to a temperature of 105°F; the oxidizer line was conditioned to 111 psia and 115°F, and the fuel line to 803 psia and 126°F. The ambient pressure was reduced to 0.23 psia with the mechanical pumping system; the steam ejector was turned on and the ambient pressure

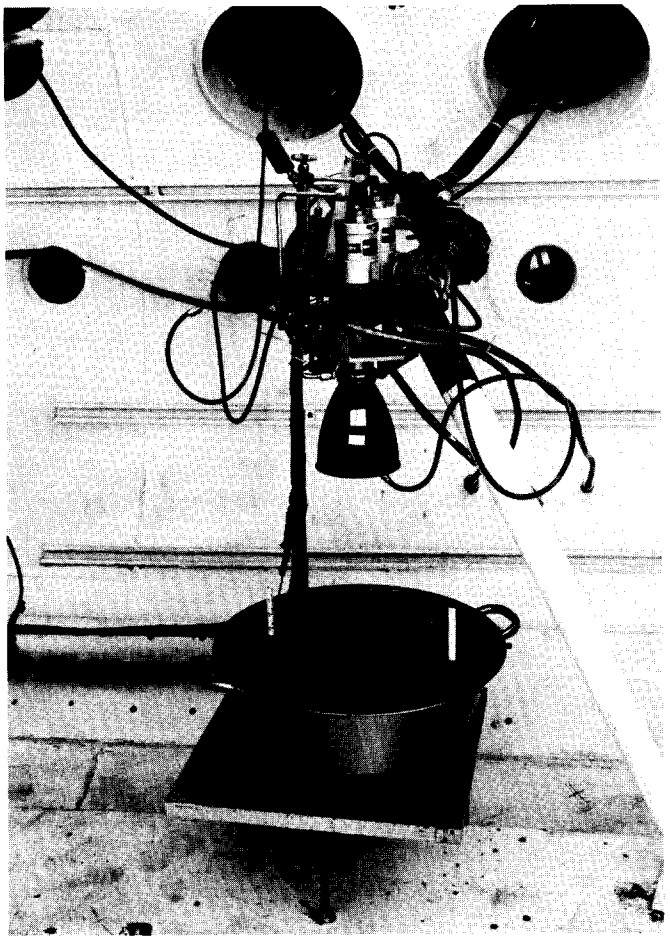

Fig. 63. Photograph of the initial test setup for runs DD-125 and DD-126 and of the initial conditions for DD-126

Fig. 64. Soil exploding from container during run DD-125 before engine ignition due to a steep ambient pressure drop

UNCLASSIFIED CONFIDENTIAL

UNCLASSIFIED

rapidly reduced to 0.05 psia. The resulting pressure difference across the porous soil caused the soil to erupt from its container (see Fig. 64). The vernier engine was then ignited, fired for 0.1 sec, and was shut down.

In the course of this experiment the soil pressure transducer was damaged by the hot TCA exhaust gas; it was replaced for the next experiment and relocated approximately 0.5 in. beneath the soil surface.

For the next experiment, DD-126, the engine was conditioned to a temperature of 88°F; the oxidizer line was conditioned to 112 psia and 108°F, and the fuel line to 800 psia and 113°F. The steam ejector was not used. The test chamber pressure was reduced to 0.11 psia mechanically; at the end of the vernier engine firing this pressure rose to 0.156 psia. Fig. 65 shows vernier engine chamber pressure, thrust, and the pressure in the soil as a function of time. These data were reduced from the oscillograph recordings of the variables recorded during the experiment and are intentionally smoothed. Figs. 63 and 66 show the condition of the soil before and after (respectively) the engine firing and show that some soil has been transported out of the container. Fig. 67, made from frames of the high-speed motion picture films, shows the manner in which soil was transported from the container. The radial spray directed almost tangent to the surface conformed to what was expected, but the central column, which seemed to be stable, is presently inexplicable. This column at times rose to within 1 or 2 in. of the nozzle exit plane. A method of characteristics solution of the flow in the vernier engine nozzle is now underway to determine if a local minimum in the soil pressure at the nozzle centerline could be caused by this engine's nozzle contour.

Although highly qualitative, experiments in this group have shown that the vernier TCA will operate at some of the off-design conditions existing on the lunar surface.

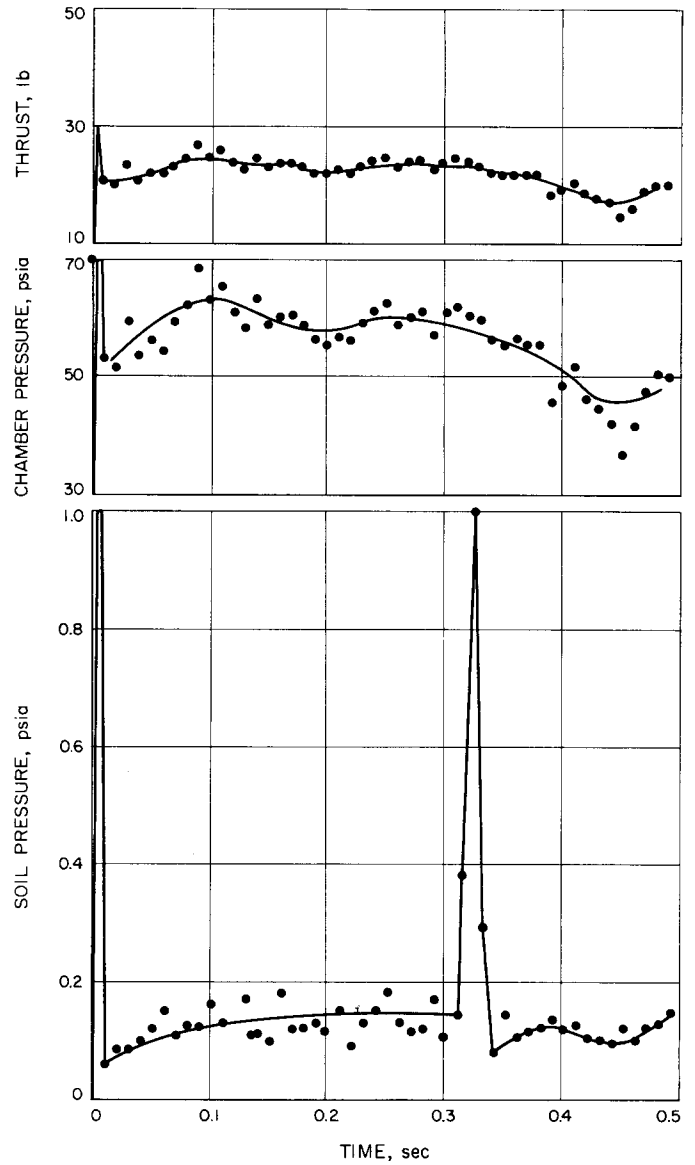

Fig. 65. Engine thrust, engine chamber pressure, and soil pressure as functions of time

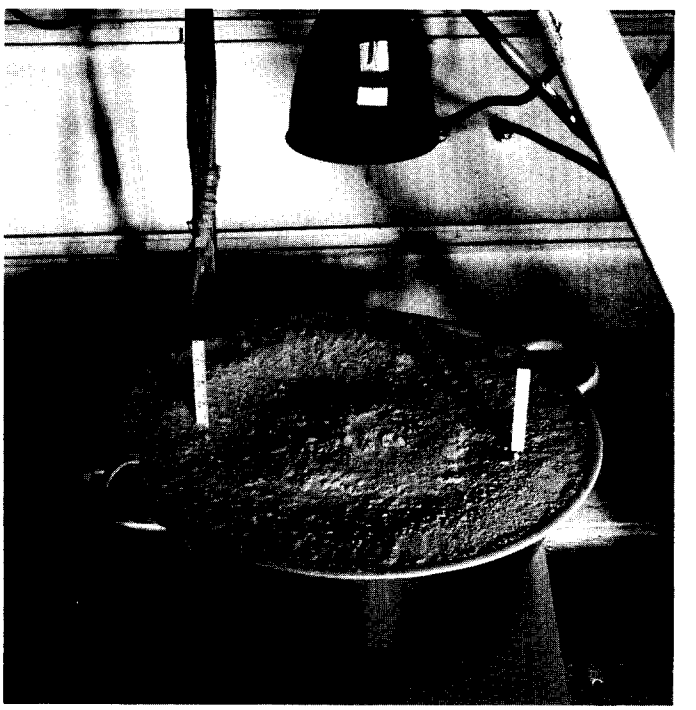

Fig. 66. Soil condition at the end of DD-126

UNCLASSIFIED

UNCLASSIFIED
CONFIDENTIAL

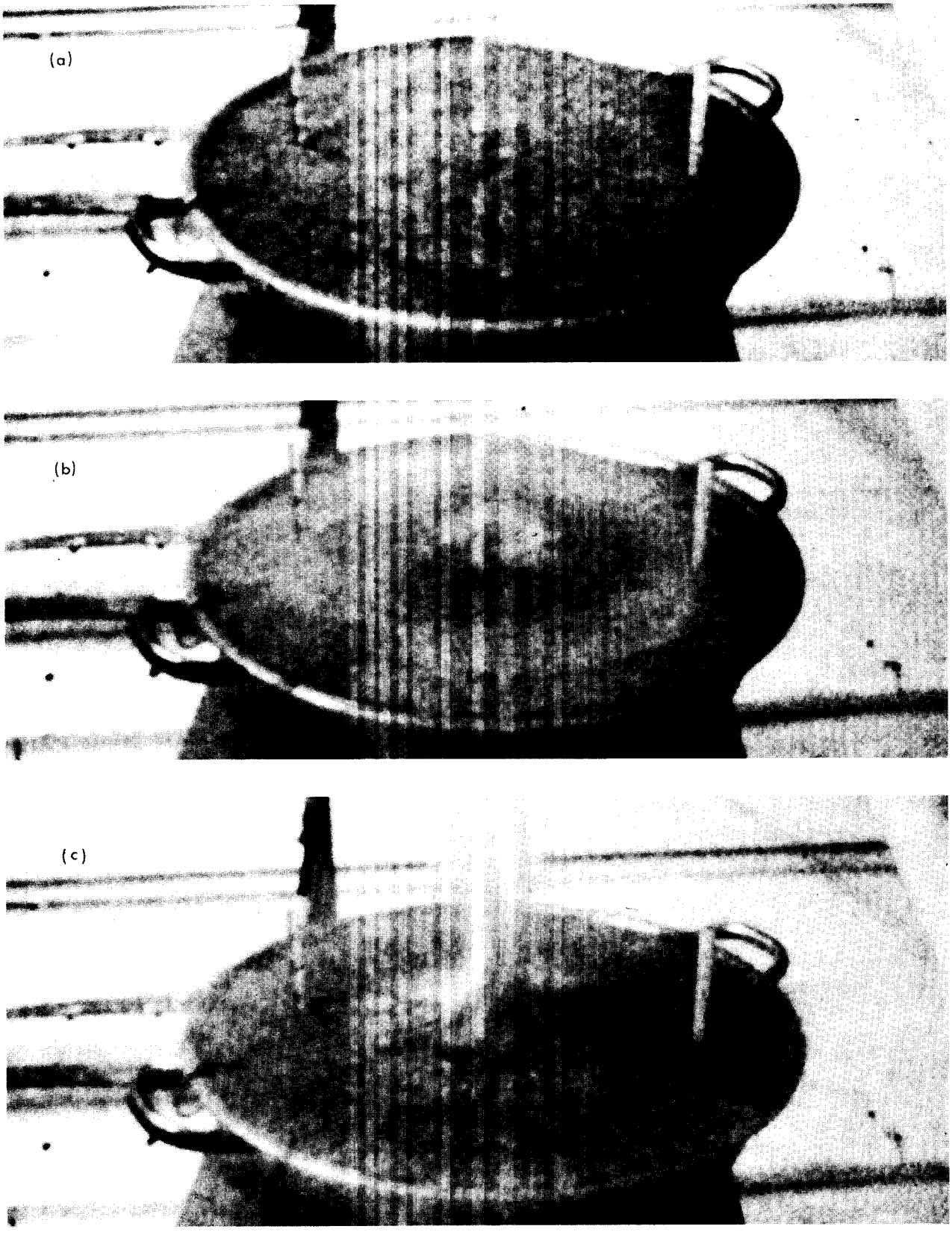

Fig. 67. Frames from high speed motion pictures taken during engine operation of DD-126 showing soil behavior

CONFIDENTIAL
UNCLASSIFIED

UNCLASSIFIED

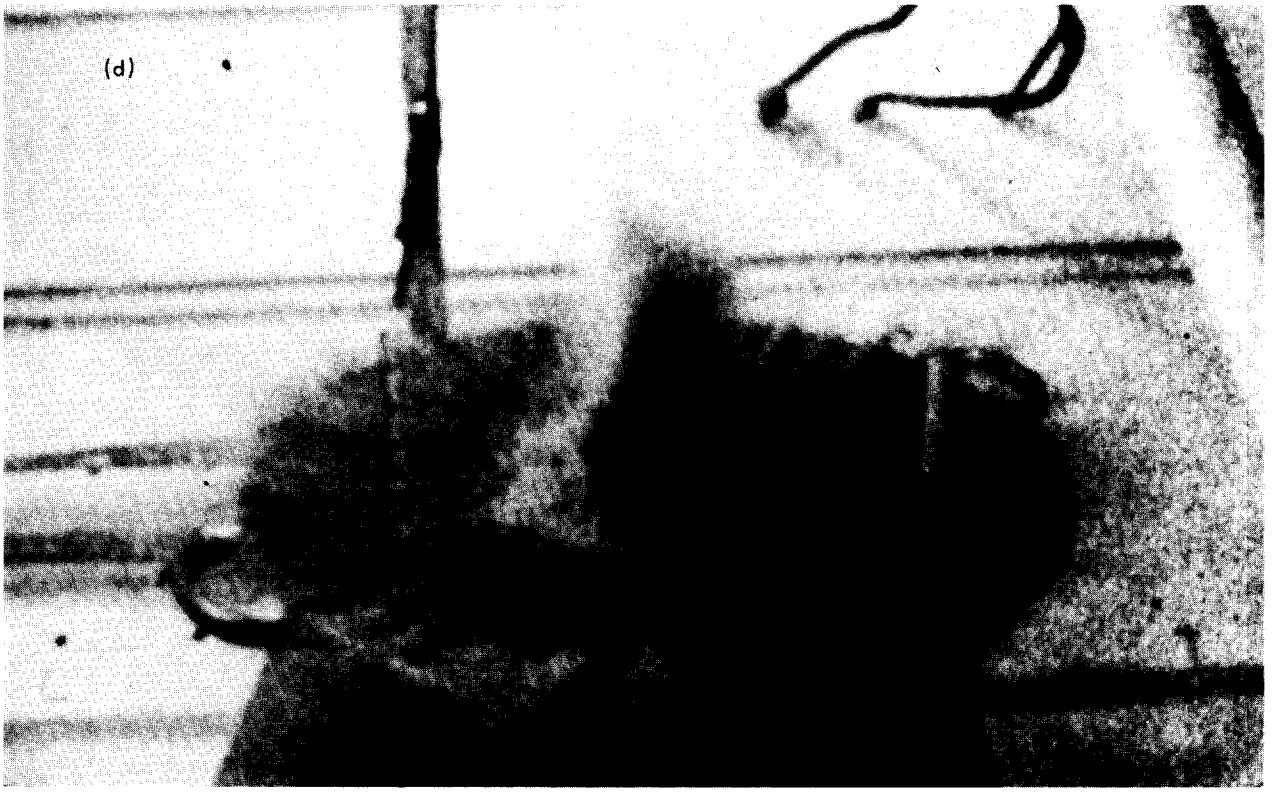

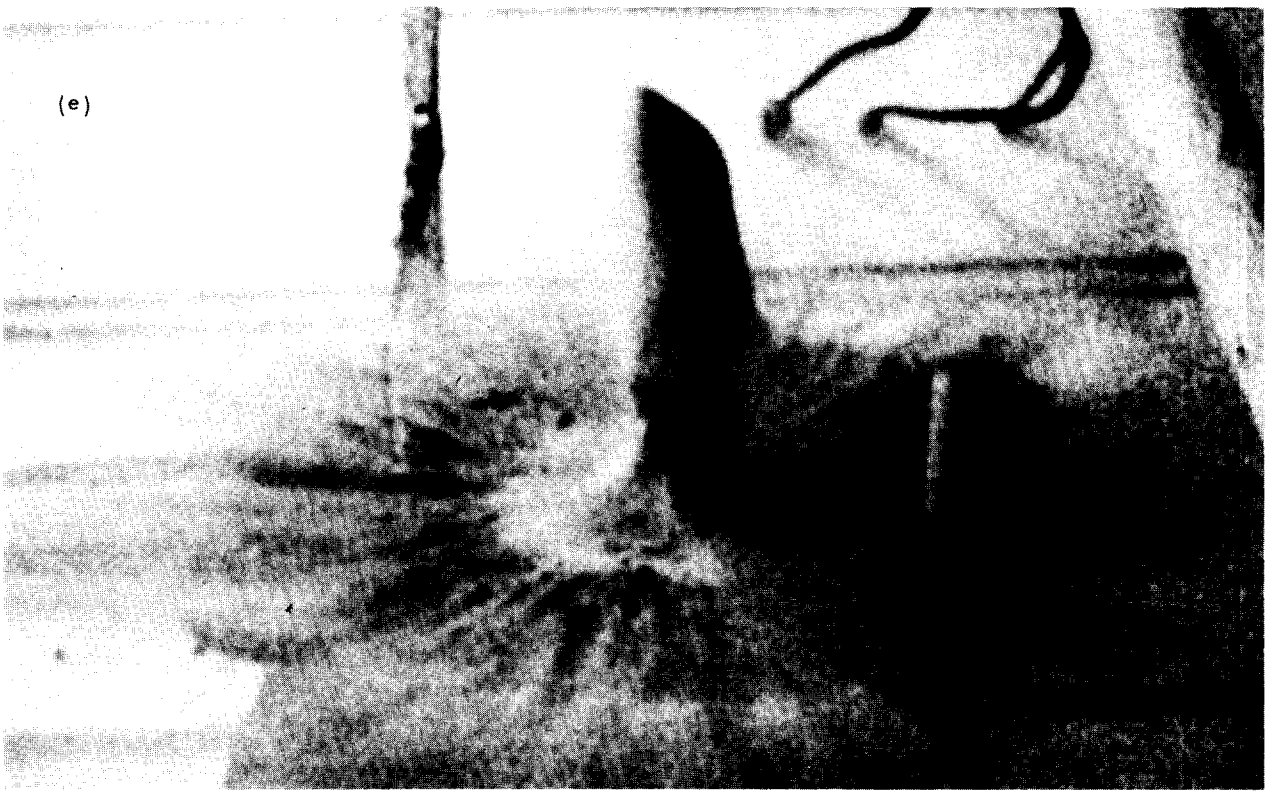

Fig. 67 (Cont'd)

UNCLASSIFIED

UNCLASSIFIED
CONFIDENTIAL

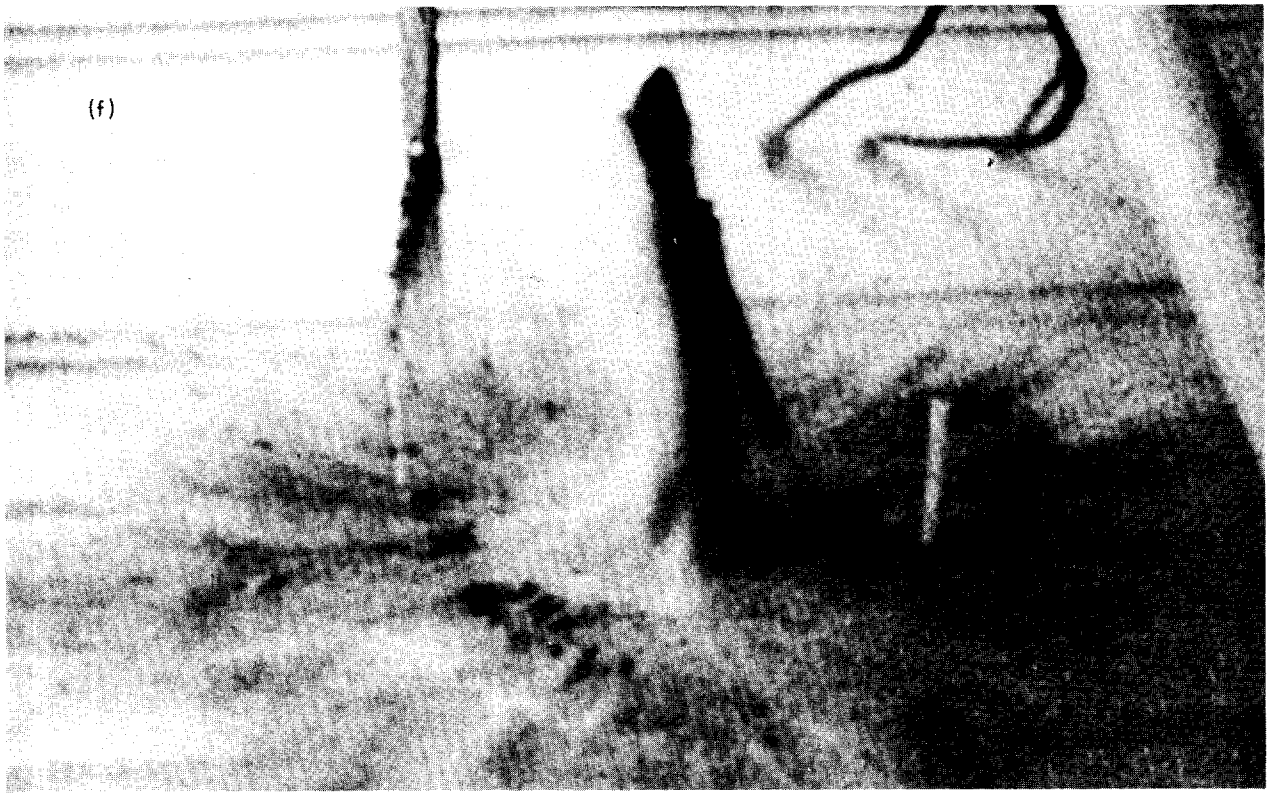

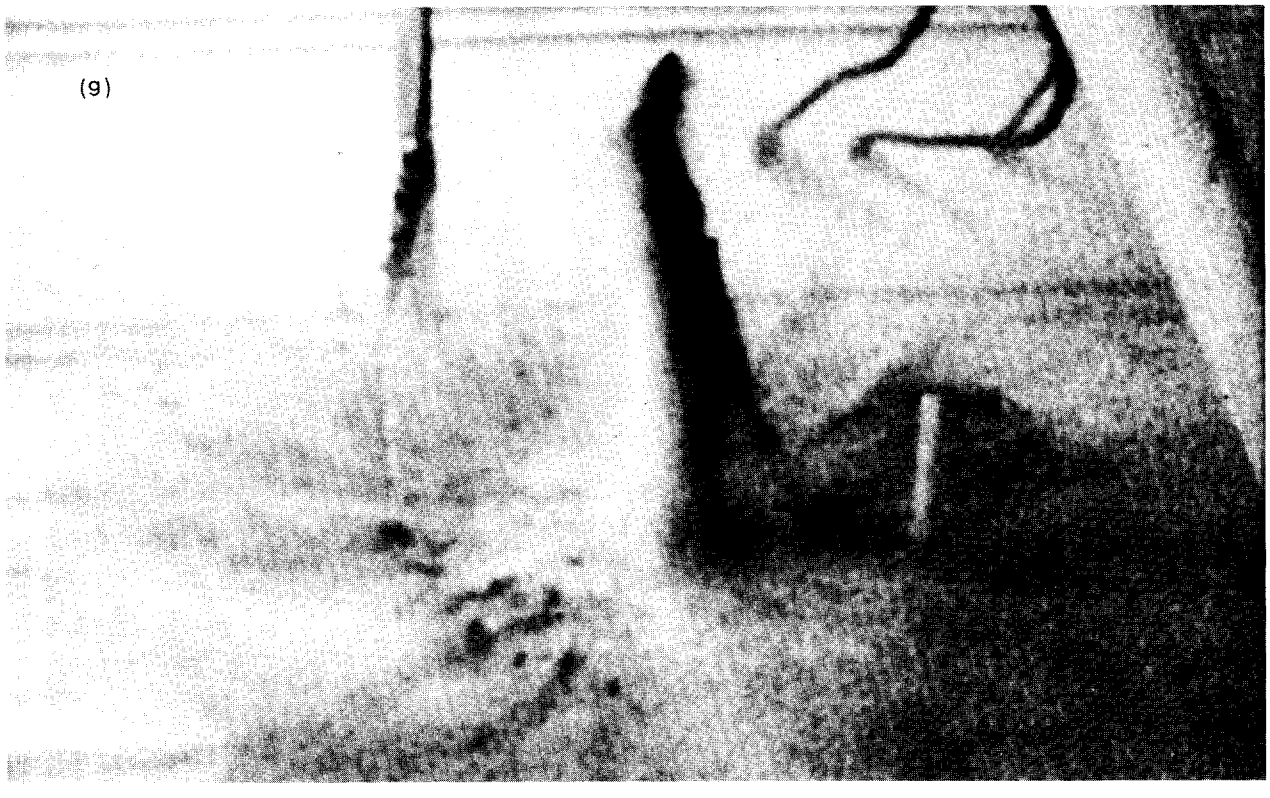

Fig. 67 (Cont'd)

UNCLASSIFIED
CONFIDENTIAL

UNCLASSIFIED

There is sufficient energy in the exhaust to transport and raise to significant heights an appreciable quantity of the soil tested. However, should the lunar soil possess a significant amount of cohesion, the force required to break these bonds will reduce, or could eliminate entirely, surface erosion. These tests indicate that an experiment of this nature performed on the lunar surface could be evaluated on Earth, less the gravity effects, by simulating the lunar conditions at the time of firing in an environmental chamber using models of lunar surface as the variable parameter.

M. Spacecraft Vehicle and Basic Bus Mechanisms

1. Basic Bus Mechanisms

a. Antenna/solar panel positioner (A/SPP). The A/SPP provides mounting, positioning, position indicators, and launch and landing locks for the planar array antenna and solar panel. The antenna support structure includes controllable axes for roll, elevation, and solar and polar rotations. The drive for each axis uses a solenoid stepper motor for power and a wirewound potentiometer for position indication.

During flight acceptance test (FAT) of the A/SPP 287580, serial number 2 (S/N-2), two drives exhibited erratic operation in thermal vacuum at −225°F. This condition was reproduced in the laboratory and determined to be an occasional failure of the armature return spring. This did not occur while running at low temperature but did occur shortly after the start of a gradual return to ambient temperature. Increased clearances between moving parts and improved dry film lubrication of mating parts corrected the problem.

The new lockpin puller/switch module (self-aligning and bench adjustable) class III hardware has been installed on the developmental X-1 A/SPP, as shown in Fig. 68, and functional tests were performed satisfactorily. These tests consisted of type approval test (TAT) qualification-level vibration followed by a repositioning to the transit position, automatic relock, and pin puller firing in thermal vacuum at −225°F.

Class IV flight hardware fabrication is complete, and module parts are being match drilled and assembled using the new tools and assembly fixtures.

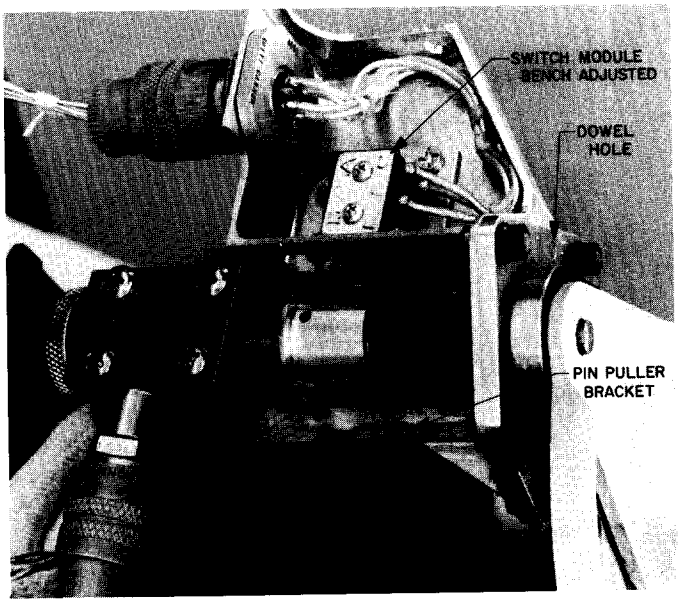

Fig. 68. Manual pin puller assembly module, solar

Thermal vacuum tests of the cone worm and sector gear were performed in the hi-vacuum chamber. The worm-sector center to center distance was decreased an order of magnitude greater than the drawing tolerances to represent the highest torque condition, and the test was conducted at 235, 75, −115, and −240°F. Pressure varied from 6×10^{-7} torr at high temperature to 5×10^{-9} torr at low temperature. Torque measurements were consistent in value in all tests. A maximum input torque to the worm of 12 in.-lb was required to carry a load of 64 in.-lb applied to the sector gear shaft. Results positively indicate that the torque required to drive the worm gear will not be affected adversely by existing drawing tolerances.

The A/SPP polar axis position potentiometer attachment was revised to prevent potentiometer shift during vibration. The modifications included installing a pin at the pot support bracket to structure attachment, adding a third potentiometer housing clamp, machining a flat on the potentiometer shaft, and increasing shaft end play. One unit with these modifications passed flight acceptance vibration testing with no indication of potentiometer shift.

Interference between the A/SPP, planar array antenna, solar panel, TV camera, and spaceframe have been defined by a simplified formula that indicates there are no interferences when the sum of the solar angle and the polar angle is less than 340 deg and the elevation axis is within ±70 deg (±97.5 deg if the polar angle <45 deg). A detailed layout is being prepared which will include

UNCLASSIFIED

UNCLASSIFIED CONFIDENTIAL

two three-dimensional graphs to express gimbal system combinations which produce interference. A plastic one-fifth scale model (Fig. 69) has been reworked to include the new roll pin pullers and TV mirror envelope. This model will be used as a backup at spacecraft performance analyses and command to follow A/SPP gimbal motion during *Surveyor* missions.

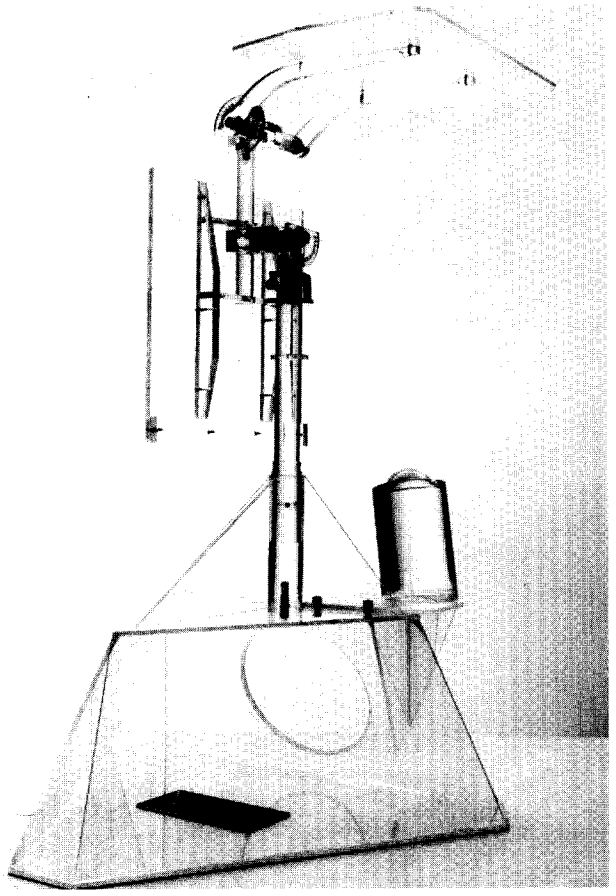

Fig. 69. A/SPP model for use at spacecraft performance analysis and command

b. Revised A/SPP. The revised A/SPP, P/N 293275, has been partially released to production. The May 16 complete release date was delayed by 1 wk in order to incorporate a high-strength roll axis landing lock pin (Fig. 70) and other necessary structural revisions. The need for a steel bushing at the roll lock pin location was verified by test May 7 when it was demonstrated that the roll retention pin/socket failed at the maximum predicted landing load of 23,200 in.-lb (Fig. 71). This corresponding moment is 20,800 in.-lb in the 287586 A/SPP design.

A test to confirm the structural integrity of the bushing concept will be conducted as soon as the stub mast, roll axis adapter, roll axis landing lock pin, and high-strength steel bushing can be fabricated and assembled.

The detail specification is in the final review cycle. The flight acceptance test specification will be distributed for review June 30. The design verification test plan is in the formulation stage. The inventory for a final design review in early June was distributed May 23.

All detail parts, subassemblies, and assemblies for the design verification test models are on order, with some parts having been received.

The A/SPP jackscrew design (293300) development program was initiated in January as the advanced design unit for SC-5 effectivity. The development program has progressed through the design analysis, layout, and detail drawing preparation stage and is now in the detail stress analysis and drawing check phase. Development test hardware and test fixtures have been fabricated, and design verification test plans have been prepared to conduct developmental testing of the polar axis jackscrew drive.

Schedule problems have made it necessary to incorporate the 293275 A/SPP into SC-5 and subsequent spacecraft. The 293300 A/SPP currently has the status of a backup effort, portions of which will be carried through testing. A complete backup development is not planned.

The major features of the A/SPP jackscrew design include the following:

(1) A jackscrew mechanism for operation of the polar axis in place of the existing A/SPP worm and sector gear.

(2) A torque-tube design solar axis that provides for torque transfer between the stationary housing of the axis and a torsion tube that enables coupling of the two solar panel support arms at the axis of rotation.

(3) A torque-tube design elevation axis that provides a torque transfer between the stationary housing and the central torsion tube to permit coupled rotation of both ends of the axis.

(4) Incorporation of the high-torque stepper motors and improved transmission to provide greater performance margins of torque (available vs required) that of the current Ledex motor.

(5) Increased structural capability of the A/SPP.

UNCLASSIFIED CONFIDENTIAL

UNCLASSIFIED

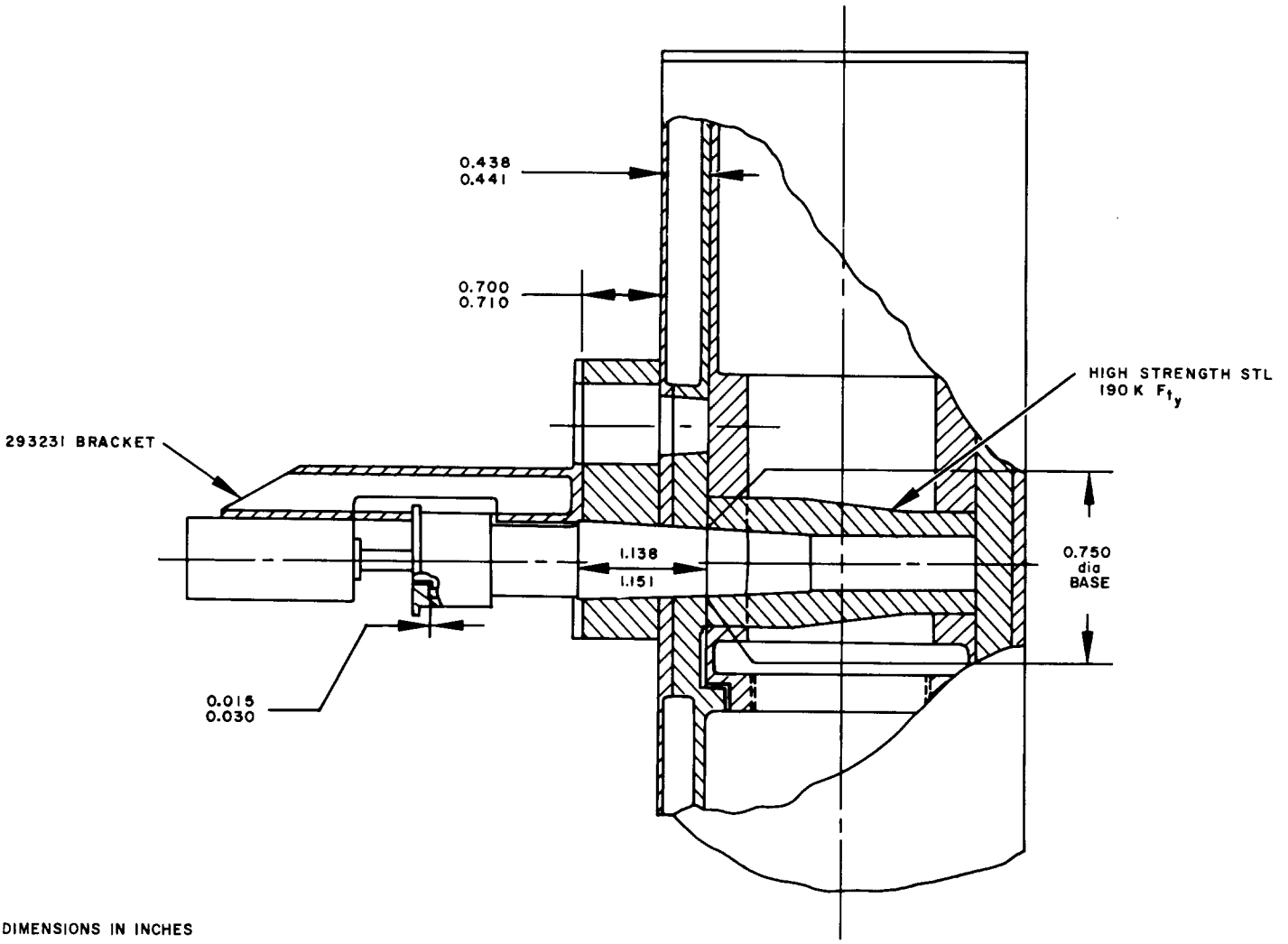

Fig. 70. Roll axis landing lock with steel bushing for A/SPP 293275

(6) Design of pin puller subassembly to enable bench-alignment of taper pins to taper holes and limit switch adjustment without the need for adjustment on the A/SPP.

The initial design of the A/SPP wiring harness has been completed utilizing a mockup jackscrew unit for layup of the harness to evaluate harness routing and service loop requirements. Low-temperature ($-250°$F) tests of the service loops are being conducted to verify acceptability of the torsional constraints on axis motion.

Fabrication and assembly of developmental pin puller subassemblies have been completed, and design verification tests are in progress. The test plan for the pin puller has been prepared to verify suitable performance over the complete environmental range and to ascertain that performance of the existing (qualified) gas generator squib has not been compromised by the pin puller design revisions.

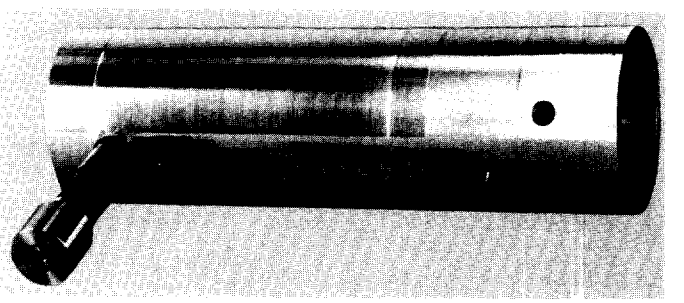

Fig. 71. Test hardware for roll axis landing lock pin on A/SPP 293275

Test fixtures and test equipment design for pin puller, and solar axis, subassemblies have been completed, and

UNCLASSIFIED

UNCLASSIFIED
CONFIDENTIAL

fabrication is partially complete. Additional fixtures for the roll and elevation axes are presently in design.

Potentiometers for all axes have been ordered to a newly prepared source control drawing and procurement specification that provide for increased performance and reliability at extreme low-temperature, high-vacuum environments. Tests performed on equivalent potentiometers at less than 10^{-10} torr vacuum indicate satisfactory electrical performance after 10,000 cycles of operation. This performance provides a large margin over expected life requirements.

c. Hi-torque motor and transmissions. Design and detailing of the hi-torque drive motor and all transmission combinations were completed and released May 16 for fabrication of production units. A design analysis and optimization study report on the drive motor kinematics, stresses, and performance characteristics was completed. Additional analytical data are being assembled for incorporation into a design analysis report that will encompass the entire development program.

A parts layout of the hi-torque flight-type motor is shown in Fig. 72 and cam followers with one roller removed are shown in Fig. 73. Room temperature life cycling testing was initiated on one motor to evaluate the capability of the cyclically loaded parts to withstand the design life of 120,000 cycles. The power cam of the drive motor tested did not have the theoretically optimum profile owing to misinterpretation of the drawing by the machinist; consequently, the torque produced by this developmental model is short of the design goal of 48 oz-in. Fig. 74 illustrates the torque versus angular position performance of this motor after 120,000 cycles of operation.

The life cycling was conducted in two phases of 120,000 cycles with a teardown and examination of parts after each phase. During the first phase, the cam follower bearings and cams showed no signs of damage, and the only difficulty encountered was a loosening of the ring nut joining the two motor housings. This is being corrected by redesign of the key and slot used to hold the relative position of the two halves.

After 206,100 total cycles, the motor stalled owing to a chipping of the driven edge of the polycarbonate sprocket that couples the solenoid armature to the output shaft. Failure analysis showed that much of the problem was due to discrepant parts. Nevertheless, stress analysis has been initiated on the sprocket to determine

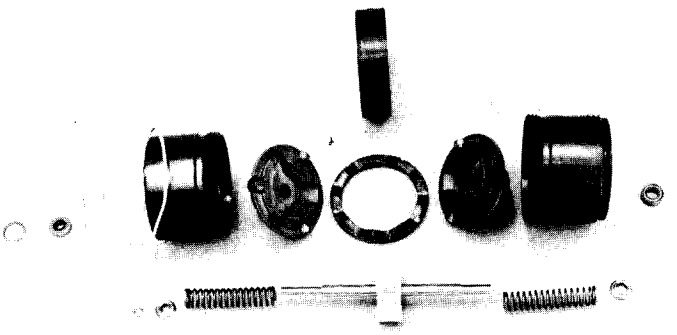

Fig. 72. Hi-torque stepper motor

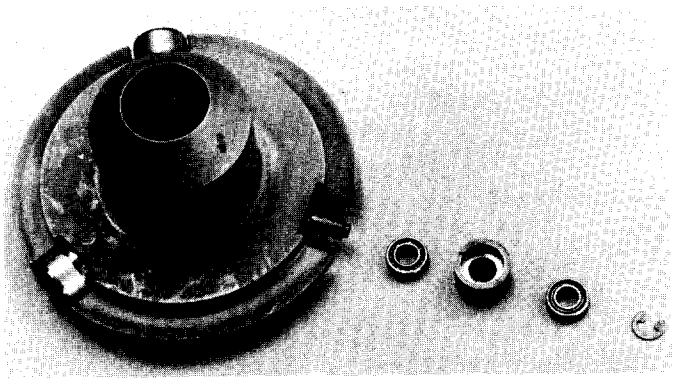

Fig. 73. Armature for hi-torque stepper motor with one cam follower disassembled

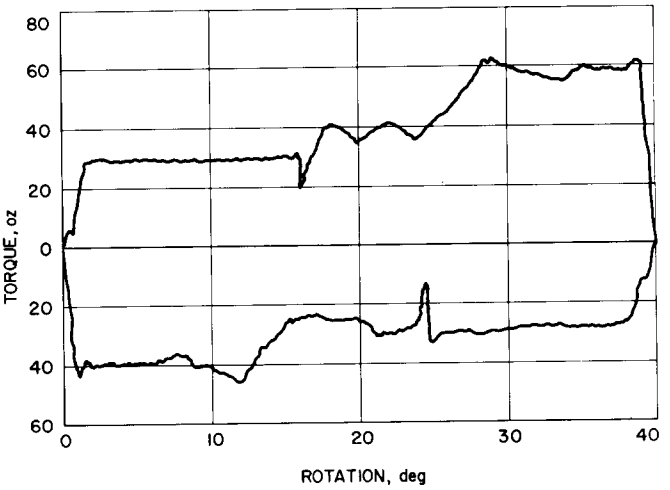

Fig. 74. Hi-torque motor DVT-02 test after 12,000 cycles

if a minor design change or material of higher strength would provide greater margin. A backup metal sprocket will be tested. Ultimate strength tests were conducted on the 289:1 prototype planetary transmission to determine the strength of the various assembly parts. Visual

CONFIDENTIAL
UNCLASSIFIED

UNCLASSIFIED
CONFIDENTIAL

inspection of the transmission tested to 975 lb-in. output showed no distress of the parts. The splined output shaft indicated a maximum capacity of 350 lb-in. for the 293275 A/SPP and 600 lb-in. for the 293300 A/SPP.

Fabrication of all developmental hardware is expected to be entirely completed and assembled during the report period. Production hardware has been ordered and is in process.

d. Thermal switches. Important elements of the *Surveyor* thermal control system are the bimetallically operated thermal switches. These switches, nine on compartment A and six on compartment B, are designed to provide a thermal path for heat exhaustion from the compartments, as required, or to open the path and retain heat within the compartment, as required.

A program has been continued during this report period to improve the heat dissipation characteristics of the switch radiators. This involves a silver-deposited mirror in place of the present aluminum-deposited mirror. Potential advantages of this modification, if it proves feasible, will be not only to reduce the solar heat input to the compartments during the critical descent sequence, but also to allow a greater flexibility of compartment operations closer to the lunar noon.

Retest of switches held in bonded stores for several months showed that the contacts of most switches have a tendency to adhere to each other, thereby lowering the temperature at which the switch will open the conductive path. Alternate materials to be used in the interstice for coating the contact face and changes in process are being evaluated to correct this condition.

Behavior of items within compartment A during SC-2 solar thermal vacuum testing generated the requirement for reducing the opening temperature of compartment A switches from 65 to 40°F effective on SC-3 and up. SC-1 and SC-2 have been retrofitted with four switches with a 40-deg opening on a critical area of compartment A.

e. Omnidirectional antenna mechanisms. The A and B omnidirectional antenna mechanisms use tapered fiberglass cloth tubes bonded to aluminum hinge bracket assemblies. They deploy and lock the two omnidirectional antennas into operating position before separation from *Centaur*. A geometrical study based on the present released drawings was completed. Detailed drawings from which hard tooling will be fabricated are scheduled for release. This tooling will be used for the bonding and drilling of the assembly and for the fabrication of the tubes. These new assemblies are scheduled for SC-3. A redesigned locking clip was retrofitted on the mechanisms for deploying omnidirectional A antennas on SC-1 and SC-2 to simplify the unlocking of the mechanism once it has been deployed during test.

f. Separation sensing and arming devices. Three separation sensing and arming devices for each spacecraft provide redundant actuation of the postseparation squib firing circuits and vernier engine solenoid circuit after the spacecraft separates from *Centaur*. Units of a modified design with increased plunger travel have been assembled onto SC-1 and SC-2. The qualification test conducted on two units of this design (293400) is complete, and the TAT review committee has reviewed and approved the results.

g. Pyrotechnic devices. Liaison and technical assistance were supplied to the launch operations department both at the El Segundo plant and at AFETR for the drafting and finalization of report number 227431, Pyrotechnic Handling, Testing and Installation Procedure.

Squib operated pin pullers arriving at AFETR were observed to have poorly adhering thermal paint, even though they had been inspected and accepted prior to shipment. Consultation with the materials technology department failed to determine a positive cause for this condition, although the use of a silicone mold release agent on the parts prior to painting was suspected. In order to positively eliminate the necessity for paint adhesion, it was decided to change the thermal finish of the pin puller bodies from white painted to polished, as shown in Fig. 75. Data from the S-10 vehicle thermal tests indicates that a polished pin puller reached 150°F

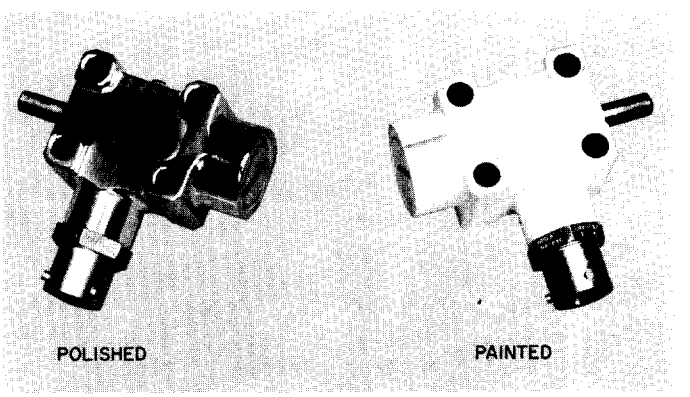

Fig. 75. Pin pullers

CONFIDENTIAL
UNCLASSIFIED

UNCLASSIFIED
CONFIDENTIAL

maximum temperature, whereas the qualification temperature was 250°F. This safe operating margin was further confirmed by conducting a solar thermal vacuum test on SC-2 with polished pin pullers. Normal functioning was obtained.

2. New Technology

Harness-to-connector strain relief. Most electrical-interface connectors called for by government-equipment contracts include backshells for the strain relief of crimped or soldered connector terminal contacts and conductors. Harness flexing and stressing (in fabrication, test, and installation) react at these strain-relief points, rather than at vulnerable connector contacts, to ensure circuit reliability.

Standard MS-type connectors are unsuitable for the *Surveyor* program because they incur excessive weight penalties and have envelopes that are too large. Therefore, a typical connector thus far used in the spacecraft is a subminiature, molded, rectangular unit which is mated with jackscrews. This high-density, compact, lightweight connector employs a shrink sleeving over a solder contact and conductor insulation for strain relief. Past experience in SC-1 service handling, however, indicates such strain relief is marginal—since frequent unit replacements and system testing have resulted in a few harness failures at solder-pot connections.

Consequent design efforts and models have resulted in the strain-relief unit shown in Fig. 76.[9] Here, the rod is insulated by shrink tubing; harness tiedowns are limited to sets of three to ensure minimal preloading of surface contacts; end plates are eliminated, and the mounting bracket surface substituted, when the connector is employed as a receptacle; lock nuts do not extend beyond the connector recess, and both halves of a connector may be strain relieved without interference. Harness entry to the connector may be from the side, back, or end; and access to the mating jackscrew is facilitated with the harness dress split on its end entry. Yet this strain relief unit adds only 0.0176 lb to the weight of a 50-pin connector.

A swinging-flexure fixture (Fig. 77) was used to establish confidence in the new strain-relief design. Side and end entry harness dress connectors were tested, since harness flexure at solder pots is most severe on these configurations. Further, models with and without strain relief were tested, side by side, to assure uniform test conditions. Results:

(1) All specimens without strain relief failed in fewer cycles than those with strain relief.

(2) Specimens without strain relief failed at contact solder pot connections (Fig. 76).

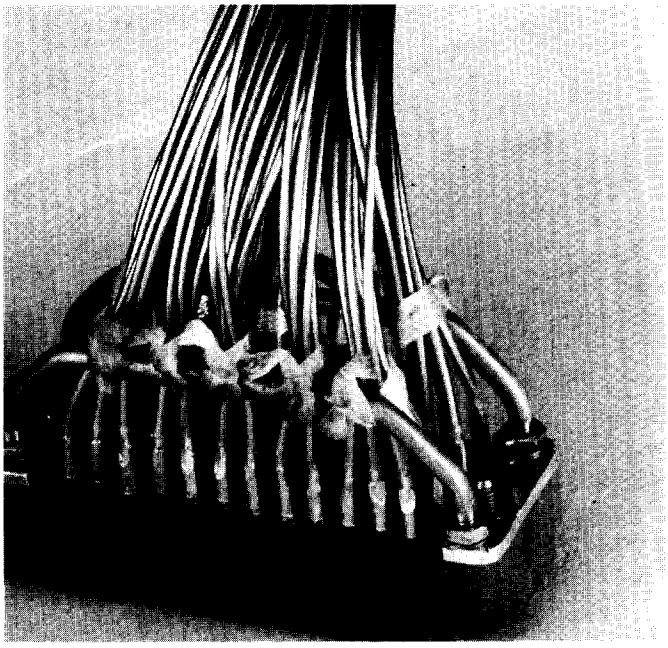

Fig. 76. Strain relief design

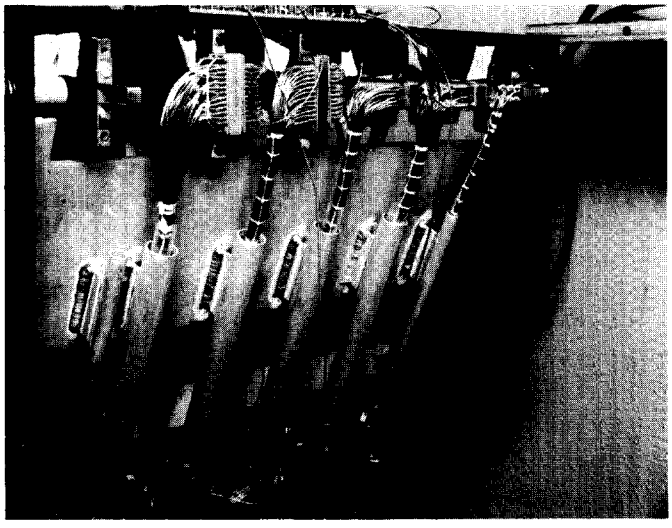

Fig. 77. Strain relief flexure test fixture

[9] R. A. Masek, innovator.

UNCLASSIFIED
CONFIDENTIAL

UNCLASSIFIED
CONFIDENTIAL

(3) No failures occurred at contact solder pot connections in strain-relieved specimens, although some failed at harness ties to their rods due to wire fatigue.

Results of additional tests (to check the effects of socket misalignment on mating and unmating life) will be presented in a future issue of the Space Programs Summary.

N. Payload and Scientific Mechanisms

1. Scientific Mechanisms

a. Soil mechanics/surface sampler (SM/SS). Redesign of the SM/SS continues and engineering drawings are scheduled for release by mid-September. Partial releases are to be made earlier to allow fabrication of an engineering unit to begin the first of August. Mechanical redesign incorporates:

(1) Improvement of scissor mechanism joints for increased vertical and lateral stiffness.

(2) Replacement of large tension springs for extension with small torsional springs at each scissor joint.

(3) Use of gears, rather than a tape drive, in the elevation drive mechanism.

(4) An over-running, one-way clutch to prevent overdriving tape in the retraction tape mechanism.

(5) Improvement of azimuth drive to minimize backlash and increase lateral stiffness.

(6) Addition of a load cell to measure applied scoop loads only.

Most of these changes will increase the accuracy with which position and load information can be obtained. A preliminary analysis of the proposed scoop redesign indicates the following instrument accuracies can be obtained (errors do not include spacecraft signal processing or telemetry errors):

Scoop position

Azimuth—±0.201 in. root-sum-square (RSS)

Elevation—±0.098 in. (RSS)

Extension—±0.013 in. (RSS)

Vertical load—±0.07 lb (±2.3% RSS)

Horizontal load—±0.44 lb (±2.2% RSS)

Shock:
50 g scale—±3.5 g (±7% RSS)
2000 g scale—±147 g (±7.4% RSS)

New procurement specifications have been or are being written for: strain system amplifier; load cell (for strain system); shock system; all four drive motor assemblies (azimuth, elevation, retraction, and scoop door).

All these specifications reflect changes to improve unit operation and reliability.

A joint test fixture has been fabricated and calibrated for high-vacuum (10^{-11} to 10^{-14} torr) testing at Arthur D. Little, Cambridge, Mass. The joint to be tested simulates redesigned scissor joints. A load spring will apply a maximum working load to this joint. Test information will include the coefficient of friction and wear rate for the lubricant (Lubeco 905) as a function of temperature, vacuum, and life.

2. Television

Failure of the *Surveyor* TV mirror drive to respond, when commanded to move 118 azimuth steps, prompted an investigation of the mirror drive cable to determine its thermal flexibility.

Three various-size cable wires were evaluated by defining the net torque of each cable when the mirror drive was rotated in the specified manner and by observing how the amount of this torque varied with changes in temperature, length and flexure of the cable, and location of the cable mount. The production cable (19 AWG No. 22 wires), two redesigned cables (19 AWG No. 24 wires and 5 AWG No. 22 wires), and the cable mount were tested to determine which would offer the least resistance to the operation of the mirror assembly at room temperature and −100°F ambient.

Test results indicate that, by using the proposed cable and method of installation, maximum flex torque will be approximately 55% less and minimum voltage to the stepper motor will be approximately 45% less.

The proposed cable and method of attachment were used on SC-2 (before this vehicle was subjected to solar

UNCLASSIFIED
CONFIDENTIAL

UNCLASSIFIED
CONFIDENTIAL

thermal vacuum tests) on the basis of the following test results:

(1) The recommended cable offered the least resistance to rotational torque.

(2) The recommended camera strut least affected the motion of the cable when the mirror was rotated in azimuth.

(3) A cable 23.50 ± 0.25 in. long was least likely to flip over when the mirror was rotated.

(4) When its clamp was 5.75 in. from the strut bolt, the cable did not snag on the attitude jet.

The mirror drive cable or cable attachment configuration needed enough flexibility for rotational freedom in azimuth during solar, thermal, vacuum simulation, as well as during a mission.

Thermal flexibility tests show the maximum torque to flex the mirror drive cable can be reduced by approximately 55%, and average torque can be reduced approximately 50%. Minimum voltage to the stepper motor for completing 118 steps can be reduced by 45%. The new (recommended) cable offers 17.3% less twisting torque (referenced to the cable connector) than the production cable.

3. Surveyor *Single-Axis Seismometer Development*[10]

Single-axis seismometer development has been in progress since 1965. The primary objectives have been to design, develop, and fabricate flight quality hardware that (1) would satisfy the experiment operational requirements after having been subjected to the prescribed *Surveyor* TA level environmental tests, and (2) would meet the *Surveyor* spacecraft interface requirements.

The experiment and scope of the specific activities that have been accomplished or are in progress are summarized below.

a. Instrument description. The *Surveyor* seismograph is composed of a single axis, short period (1 sec nominal period) vertical seismometer sensor, with a calibration circuit and amplifier to provide a properly conditioned signal for transmission. The seismometer sensor consists of a spring-supported inertial mass, which is the magnet of a magnet-coil velocity transducer. The coil is stationary and fixed with respect to the frame of the transducer. The seismometer is electromagnetically damped, near critical, through the input impedance of the amplifier. The analog signal produced provides standard short and intermediate period seismic data.

(1) *Sensitivity.* The seismograph system has the capability of detecting 1 mμ (10^{-9}) vertical motion at 1 Hz.

(2) *Response.* The system response covers the range from 1/20 to 20 Hz. Within this range, the instrument response is nominally that of a one second, critically damped pendulum.

(3) *Calibration.* The system is provided with a means of self-calibration through the incorporation of a known force to displace the seismic mass. This force is produced by passing a current through the calibration coil.

(4) *Gain level.* Provisions are made for three separate gain levels, differing by a factor of ten, and obtainable on command. Gain level changes and calibration force changes occur simultaneously.

(5) *Caging.* A method for caging the seismic mass during transit is provided to prevent transducer damage. Uncaging occurs on command after the spacecraft has completed touchdown.

(6) *Mounting.* The seismometer sensor is supported within thermal shells by preloaded fiber glass support rings. The thermal support structure is then hard mounted to the spacecraft.

(7) *Leveling.* The instrument sensor is capable of operation with the vertical spacecraft axis aligned vertically or rotated as much as 15 deg from the vertical at any azimuth angle.

(8) *Temperature.* The seismometer electronics are functionally operational over the temperature range of −25 to +150°F. The sensor is operational over the temperature range of −150 to +300°F. The seismometer sensor temperature is monitored with an accuracy of ±10°F and a 1-w internal heater, switched by ground command, can provide temperature control when the sensor temperature falls below operating limits.

b. Engineering activities summary.

Instrument design. A breadboard model of the instrument intended to be incorporated in the *Surveyor* program was built by the principal investigator, Dr. G. H. Sutton, at Lamont Geological Observatory (LGO). The

[10]Prepared by JPL Section 322.

CONFIDENTIAL
UNCLASSIFIED

UNCLASSIFIED

feasibility of the design was verified through extensive testing at LGO.

JPL, while working closely with LGO, assumed responsibility for delivering the project-required hardware. A brief description of several of the ancillary pieces of hardware used in the seismograph system is given below.

As stated above, the seismic mass has to be caged during the transit phases of the spacecraft to prevent transducer damage. This was accomplished by attaching a retractable ball to the mass assembly, which is then pulled downward and forced against the lower housing of the sensor assembly with approximately 600 lb of force. Two pistons in the cable release assembly collar the ball and prevent it from retracting.

During uncaging, two squibs are fired which force the pistons away from the ball and, thus, allow it to retract while freeing the mass assembly. The system reliability is increased by using redundancy. Uncaging would be accomplished if only one squib fired.

The reasons for designing and using an insulation assembly were to:

(1) Provide a structure which supports the seismometer in the vertical and then facilitates mounting to the spacecraft.

(2) Use the structure (thermal shells) for passive thermal control of the sensor.

In carrying out the design, it was necessary to consider the structure's weight, ability to survive the type approval environment, and make certain that it readily allowed access to the sensor. These objectives and constraints resulted in an insulation assembly consisting of three components:

(1) Fiber glass support ring.

(2) Thermal shells (upper dome and lower shell).

(3) Support structure.

The sensor assembly is supported and separated from the near-spherical thermal shells by the conical fiber glass rings. The rings provide low thermal conductivity between the sensor and the shells but are very strong. The thermal shells are then attached to the cylindrical support structure, which mounts to the spacecraft. Fig. 78 is a sketch of the seismometer insulation assembly.

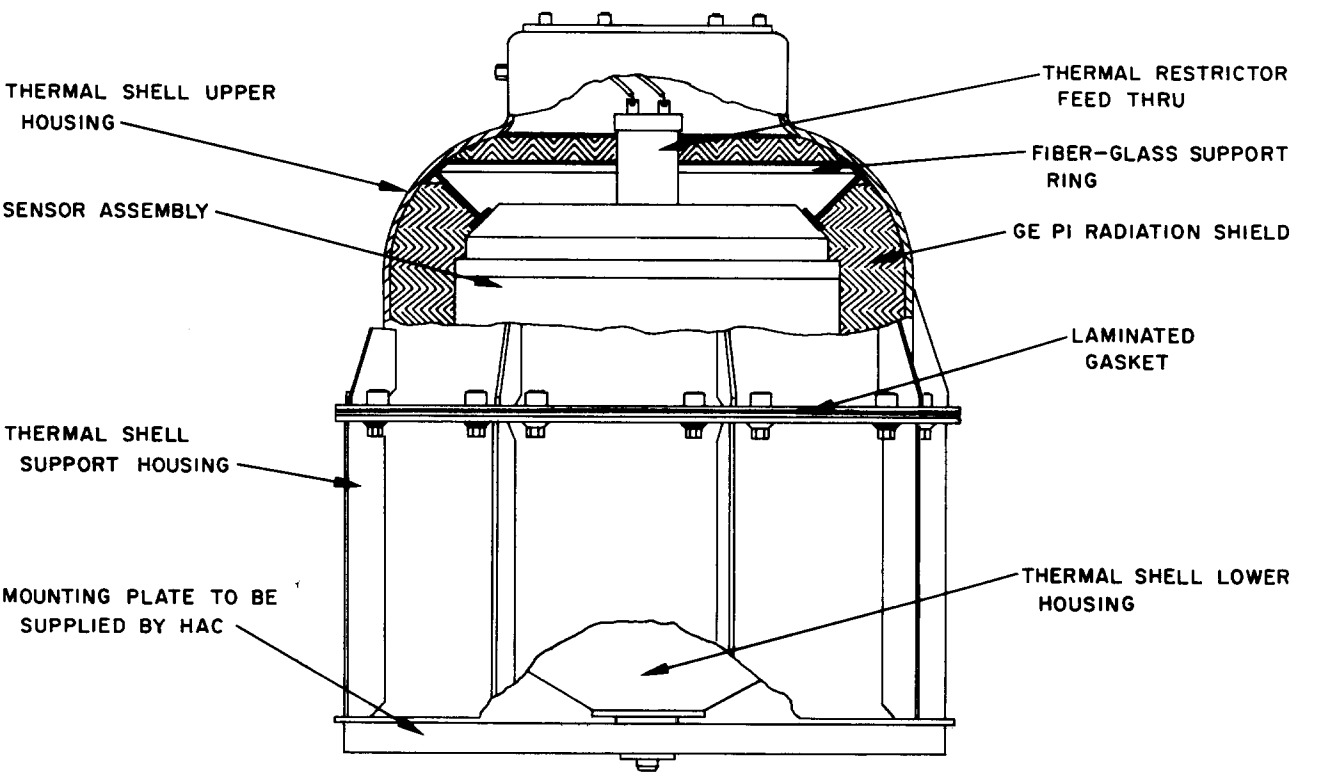

Fig. 78. Seismometer insulation assembly

UNCLASSIFIED

UNCLASSIFIED CONFIDENTIAL

In conjunction with trying to passively control the temperature of the seismometer, a development contract was given to General Electric Company (GE) for the design and development of radiation shields which would fit between the sensor assembly and the thermal shells (i.e., fill the gap created by the support rings). The purpose of the shields was to reduce as much as possible the heat loss from the sensor due to radiation without significantly increasing the conduction heat loss.

GE fabricated the shields in three assemblies to facilitate access to the sensor as well as allow easy installation. Basically, the shields consist of an optimum layer of Hastings aluminized mylar, which is aluminized on both sides.

The P1 assembly is cylindrical and fits around the cylindrical portion of the sensor and thermal shells. The P2 assembly fits between the upper dome and the sensor's upper housing. The P3 shield fits around the cable release assembly in the lower shell.

Instrument fabrication. After competitive bidding, a fixed-price contract was awarded in early fiscal 1966 to Marshall Laboratory for the fabrication of two prototype and four flight instruments. The basic requirements of the contract were:

(1) Fabricate all hardware to JPL-furnished drawings.

(2) Use JPL preferred or Hi-Rel electronic parts.

(3) Satisfy the quality assurance requirements outlined in JPL specification 30284.

The vendor received "go-ahead" from JPL on September 3, 1965, and on April 27, 1966, Marshall Laboratory delivered the last flight instrument to JPL.

Fig. 79 is a photograph of the sensor and electronics assembly. Fig. 80 is a photograph of the sensor during the assembly phase. The magnet mass assembly is shown being supported by the lower spring while the inductor coil legs are seen protruding from the mass assembly. The high quality of workmanship used in fabrication of the electronics is seen in Fig. 81.

The Missile and Space Division of GE was awarded a contract for the fabrication of six sets of flight quality radiation shields. GE had previously designed and developed a prototype set of radiation shields per the requirements discussed above. Prior to the follow-on contract, JPL performed extensive qualification tests on the prototype set.

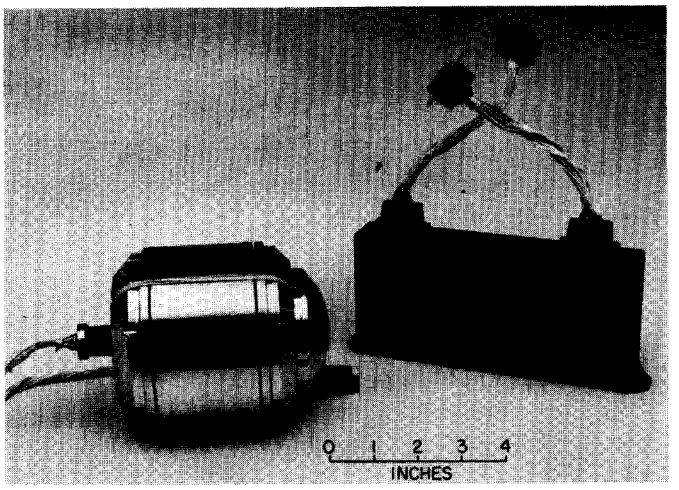

Fig. 79. Sensor and electronics assembly

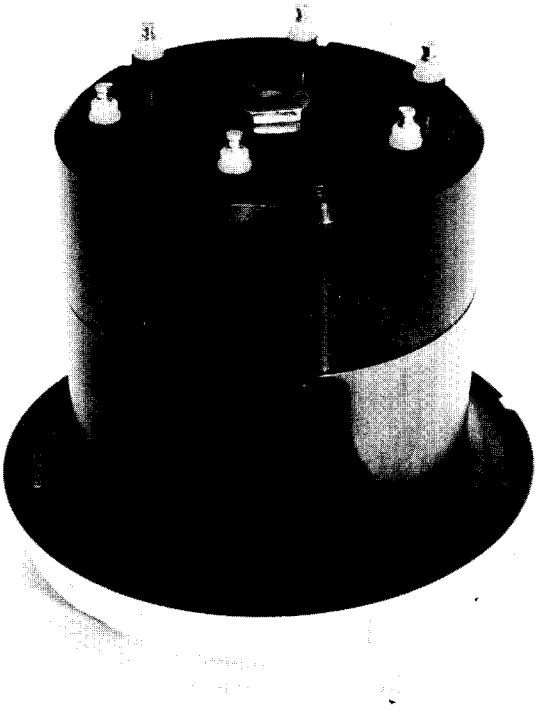

Fig. 80. Sensor mass and spring assembly

Fig. 82 is a photograph of a typical flight quality P1 radiation shield.

LaRae Industries, Hawthorne, California, which has extensive experience in machining and forming magnesium, was given a contract for fabrication of the insulation

UNCLASSIFIED CONFIDENTIAL

CONFIDENTIAL UNCLASSIFIED

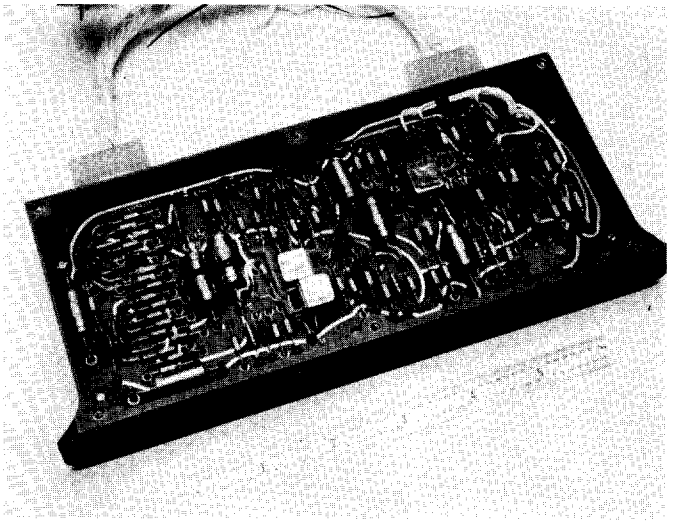

Fig. 81. Seismometer flight electronics circuit board and housing

Fig. 83. Seismometer thermal shell upper dome

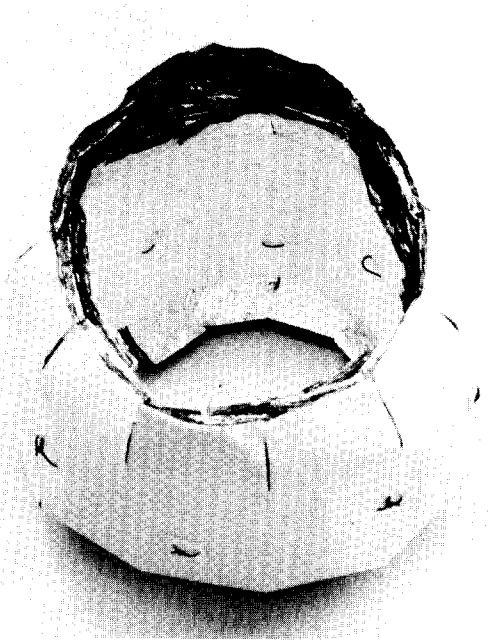

Fig. 82. Seismometer radiation shield P1 assembly

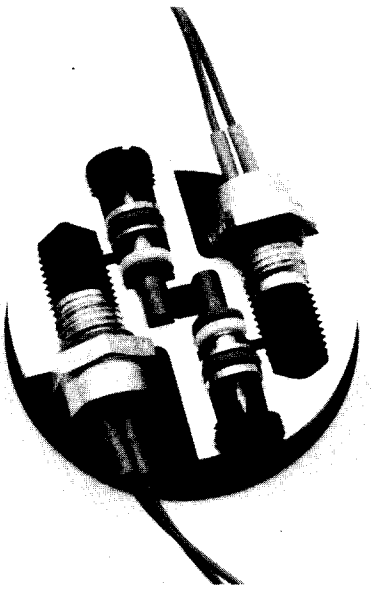

Fig. 84. Seismometer cable release assembly cut-away view

and support structure. All pieces of hardware were gold-plated, because gold provides a good substrate for possible future thermal coatings. A photograph of the upper dome is shown in Fig. 83.

Responsibility for fabrication of the cable release assemblies remained with Division 38 of JPL. Fig. 84 is a photographed cross-section of a typical assembly.

The fiber glass support beams (Fig. 85) were made by World Plastics Corporation. They fabricated the beams in three pieces—top flange, continuous web, and bottom flange. The three pieces were then placed in a fixture and bonded together with Epon 828 resin.

UNCLASSIFIED CONFIDENTIAL

UNCLASSIFIED
CONFIDENTIAL

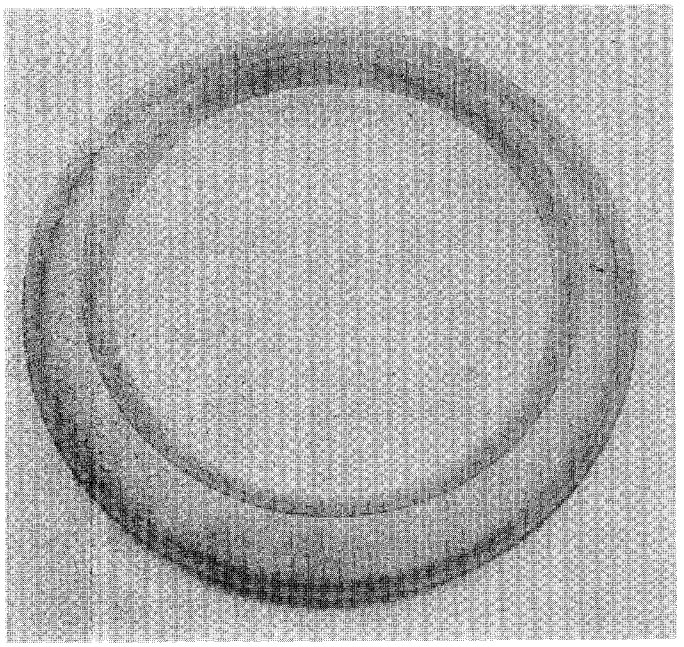

Fig. 85. Seismometer fiber glass support ring

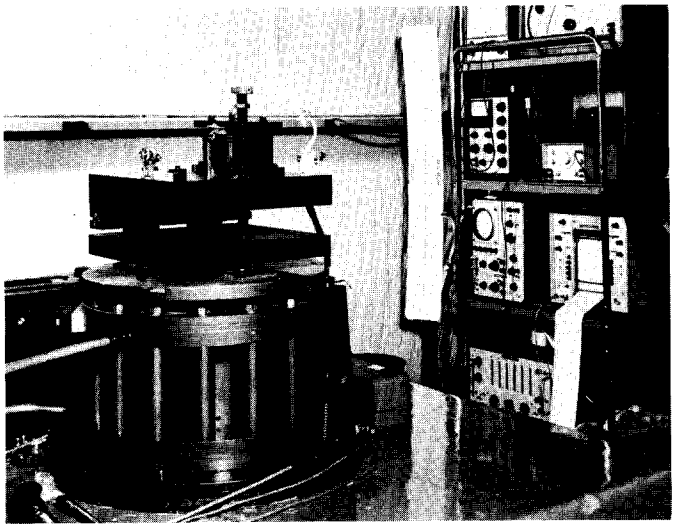

Fig. 86. Geotech calibration/acceptance testing

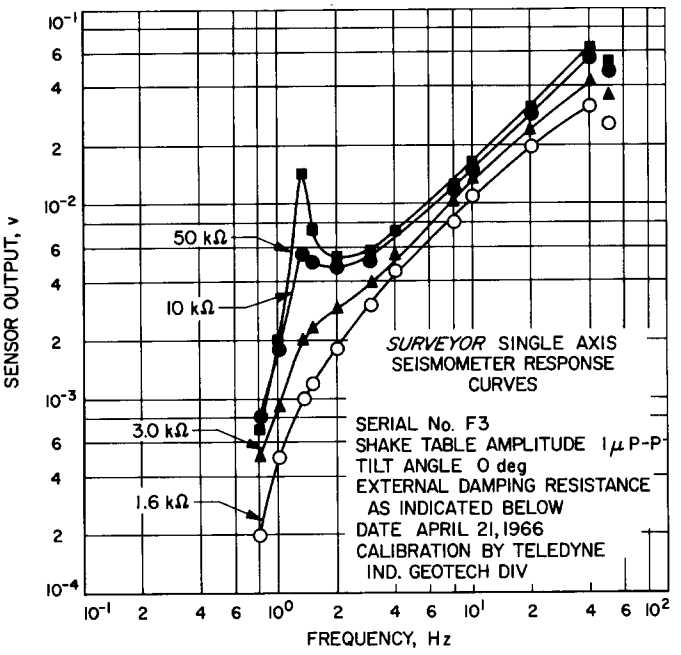

Fig. 87. Seismometer sensor frequency response curve

Acceptance testing. Although final acceptance of sensor and electronic assemblies will depend upon future type approval test results, preliminary acceptance of the sensor assemblies from the vendor was based on the results of calibration/acceptance tests performed at Geotech Corporation. These tests were performed using a shaker table mounted on a seismic pier (Fig. 86). Instrument parameters such as (1) intrinsic voltage sensitivity; (2) damping; and (3) frequency response were recorded.[11] Fig. 87 contains typical frequency response curves of an instrument output coil which is shunted with varying damping resistors. The electronics acceptance tests were performed at Marshall Laboratory and included frequency response tests over the temperature range of −20 to +150°F. JPL quality assurance and engineering personnel monitored and approved all tests.

Fig. 88 is a photograph of a flight *Surveyor* seismograph being tested with its associated bench checkout equipment, which has the capability of simulating all spacecraft commands.

Upon receiving the prototype radiation shields which had been designed and developed by GE, JPL installed them in the sensor thermal control model (TCM) insulation assembly and subjected the TCM to the following *Surveyor*-type approval level tests:

(1) Thermal vacuum.

(2) Three-axis vibration.

(3) Thermal vacuum.

(4) Thermal vacuum without radiation shields.

[11] All instruments were assembled with Earth-type springs which made testing the sensor in this manner possible.

UNCLASSIFIED
CONFIDENTIAL

UNCLASSIFIED

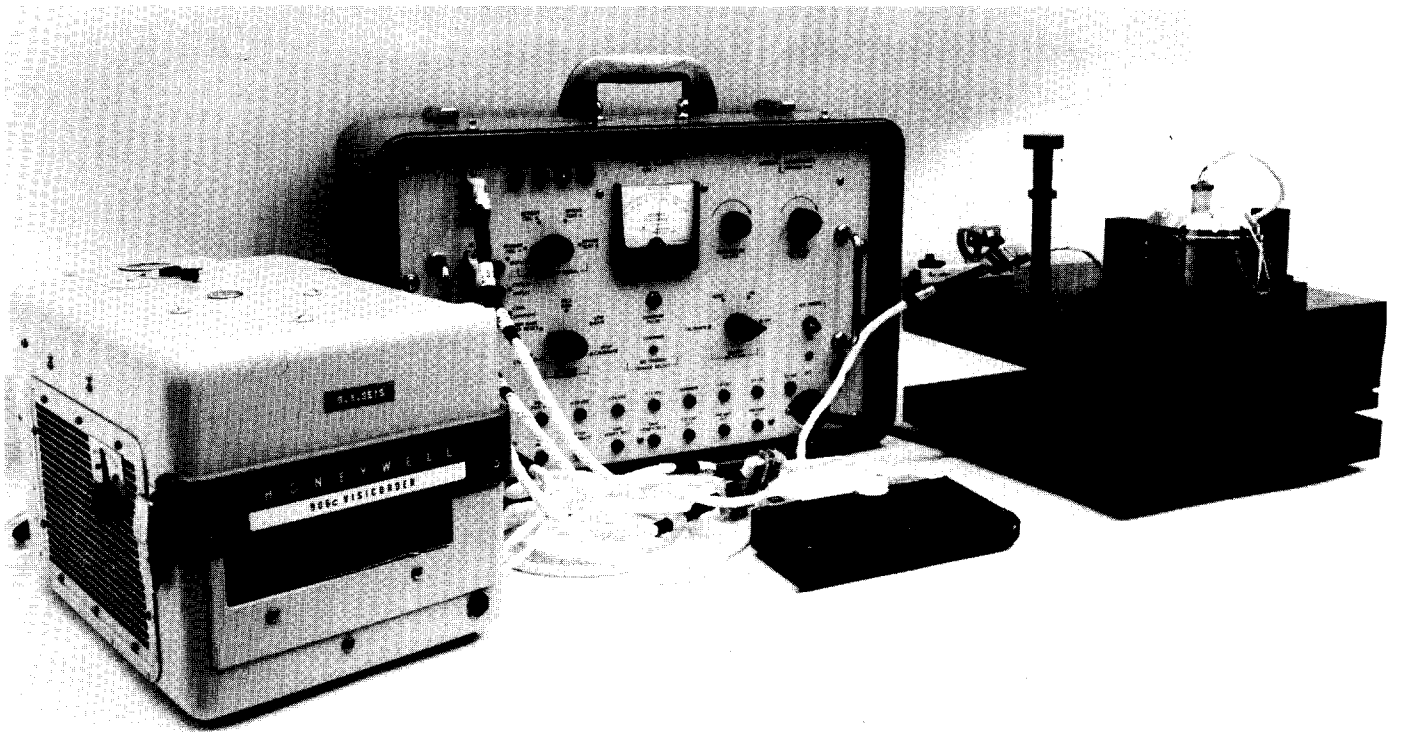

Fig. 88. Seismometer bench tests

Fig. 89 contains temperature versus time graphs for the sensor's internal temperature recorded during each of the thermal vacuum tests. As the graphs indicate, the radiation shields improve the thermal performance of the insulation and support package by approximately 100%. Degradation of the radiation performance after having been subjected to the vibration environment was less than 5%. The efficiency of the radiation shields approximated the value predicted by GE.

Elinvar Extra lunar spring development program. In parallel with the development of a satisfactory thermal control package for the sensor, a small research and development program has been carried on for the purpose of developing seismic lunar springs (i.e., springs whose mass support equals ⅔ that of Earth springs) whose parameters are insensitive to temperature.

Elinvar Extra (EE), a Hamilton Watch Company product, contains approximately 43% nickel with traces of cobalt, titanium and other metals. EE was selected as one of the more promising spring materials, since its thermal elastic coefficient of expansion is near zero, depending upon the heat treatments used. A contract was awarded to Hamilton Watch Co. in May 1965 to provide JPL with EE material, heat-treat facilities and technical support, as required.

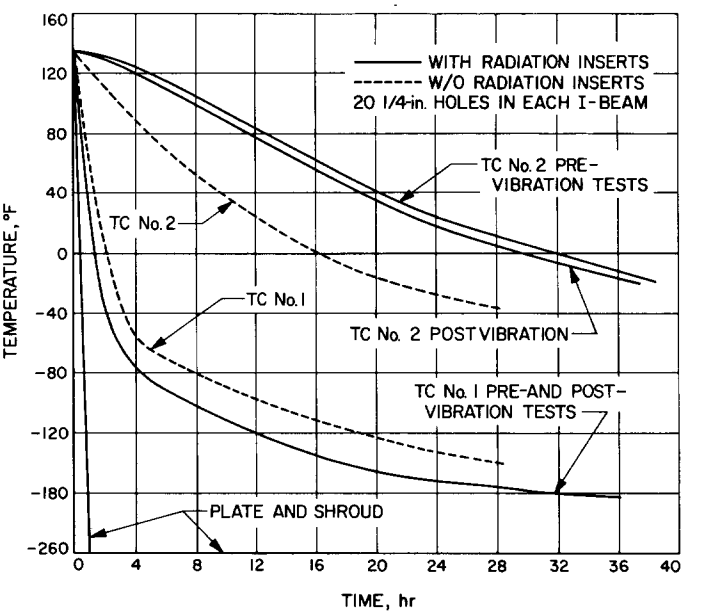

Fig. 89. Thermal vacuum test results—GE radiation shields

After the springs are heat treated at Hamilton Watch Co., they are shipped to JPL and tested both singly and in pairs. Load versus deflection curves at ambient conditions are obtained for spring pairs from which decisions

UNCLASSIFIED

UNCLASSIFIED
CONFIDENTIAL

are made as to required changes in spring thicknesses, preform, or heat treatment.

The following combination of lunar springs has resulted in acceptable pairs:

(1) 0.012 in.-thick spring with preform -0.37 ± 0.020 in.

(2) 0.014 in.-thick spring with preform -0.62 ± 0.020 in.

Temperature tests on the EE and BeCu springs indicate that although BeCu lunar springs are usable with their characteristically large changes in natural period and mass support with temperature, calibration of the sensor is made much easier by using the EE springs, which have constant spring characteristics. EE lunar springs will be installed in all flight sensors.

O. Thermal Control

1. STV Test Support

This discussion summarizes the SC-2 STV mission sequence tests, thermal anomalies, and verification of changes to the thermal control system for test phases 1A, 1B, and 2B, conducted from April 23 through May 16.

a. Test sequence. The first real time mission sequence test (phase 1A) performed at low intensity (87% of a solar constant at the test plane) was initiated April 24. The test included a simulation of a 66-hr real time transit sequence and special functional tests conducted during coast phase II.

The second test (phase 1B), which was to have been another 66-hr real time transit mission simulation at 112% of a solar constant, was aborted 13 hr into the mission.

Abnormal temperature readings on two compartment A thermal switches indicated that the switches were malfunctioning. This malfunction would have caused a probable overtemperature condition in compartment A had the test continued.

Following a shutdown period, a third test (phase 2B) was conducted at 112% of a solar constant, encompassing the full 66-hr transit sequence of events.

b. Anomalies observed and corrected. Compartment A tray temperatures ran slightly higher (5 to 10°F) in the SC-2 low Sun sequence compared to the past SC-1 sequence. All units, except the main battery, remained well within specification and were predicted to do so at high Sun. The battery temperature limit of 125°F was exceeded at midcourse (130°F) and again late in the mission where a 152°F peak temperature was reached. The latter temperature rise was attributed to increased dissipation within the battery. Corrective action was taken to reduce compartment tray temperatures by lowering the temperature at which thermal switch closure occurs on four switches beneath the solar panel simulation shrouds. These switches carry the majority of the internal dissipation load. Reducing switch closure from 65 to 40°F increases the conductance developed by the switch, thereby permitting more efficient disposal of heat. Accordingly, switches 2, 3, 6, and 9 were replaced.

Compartment B tray temperatures in SC-2 were approximately 18°F higher compared to the SC-1 sequence; however, all temperatures were within specification limits. The temperatures observed on SC-2 compared well with S-10 data, and, while the cause for the compartment B temperatures is still under study, no functional or operational deficiency or mechanical defect has been uncovered. Corrective action was not indicated.

Late in the mission, the heater on oxidizer tank 2 failed to function, resulting in an out-of-specification condition of −4°F instead of the 0°F minimum. The failure, traced to pinched wires in the harness, has been repaired. The No. 1 propellant lines were warmer than expected for the low Sun condition, and extrapolation indicates an expected hotspot of 120°F at high Sun (112% solar constant) compared to a 100°F upper limit.

Early in the mission, abnormal temperature trends developed in compartment A. Thermal tray temperatures were 5 to 8°F higher than those observed in SC-1 phases 4 and 6 high level tests at common points in the mission. Also, two thermal switch radiator temperatures were low, pointing to an open switch condition. Switch 6 radiator was −174°F instead of 30°F, and switch 5 radiator was −40°F instead of 40°F. Extrapolation of the temperatures associated with operating in this mode revealed that battery temperatures in excess of 125°F would occur after midcourse and jeopardize the main battery; hence, the mission was aborted. Post-test examination indicated that both switches were operating improperly.

Temperatures on vernier propellant lines No. 1 near the thrust chamber assembly reached approximately 130°F (Fig. 90). Post-test examination of the lines revealed the

CONFIDENTIAL
UNCLASSIFIED

UNCLASSIFIED
CONFIDENTIAL

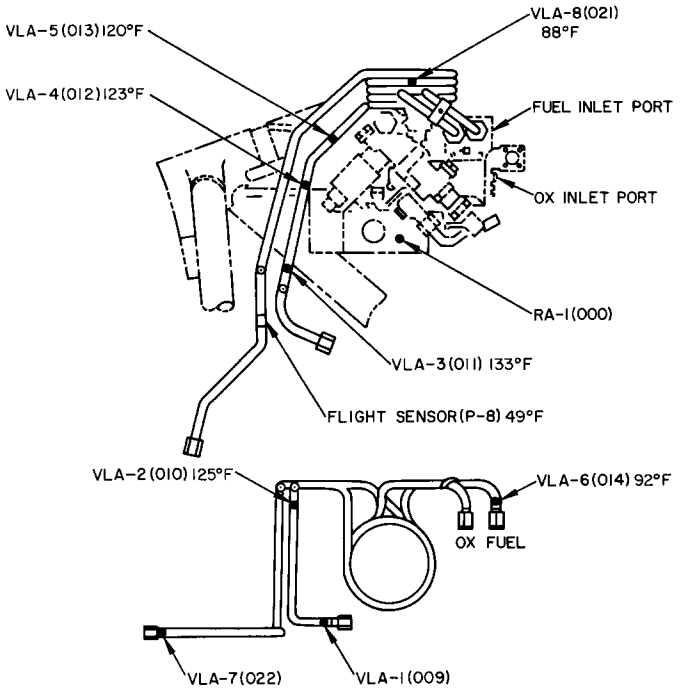

Fig. 90. Vernier engine No. 1 fuel and oxygen lines—phase 1B

Sun shade to be short; corrective action was taken to lengthen the Sun shade prior to the next STV phase.

A 66-hr mission sequence was completed in which compartment A temperatures, as measured by the battery and thermal tray, were less than 125°F throughout the entire transit sequence and, also, were less than those observed during the phase 1A low level sequence. The cumulative corrective action taken regarding thermal switches proved adequate. Comparative temperature histories within compartments A and B for the three STV testing phases conducted to date on SC-2 are shown in Figs. 91, 92, and 93.

The anomaly previously observed on propellant lines No. 1 recurred in that temperatures of 120°F were recorded on the line. An in-depth examination to determine the cause is in progress in anticipation of further corrective action to be taken prior to resumption of SC-2 STV testing.

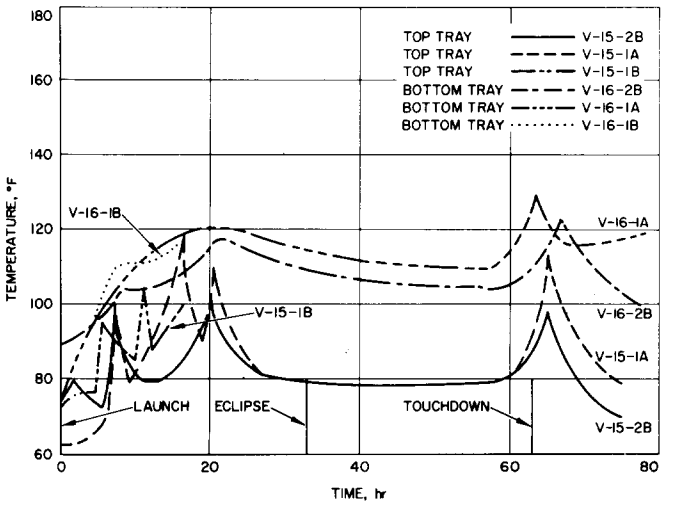

Fig. 91. Compartment A upper and lower tray temperatures

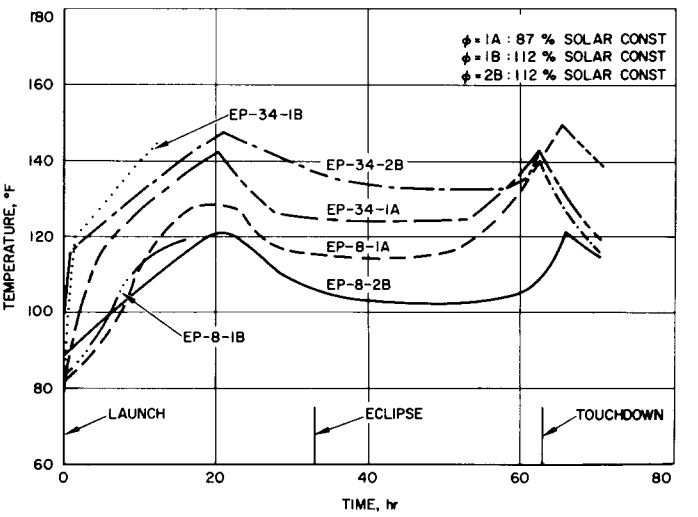

Fig. 92. Compartment A main battery and battery charge regulator temperatures

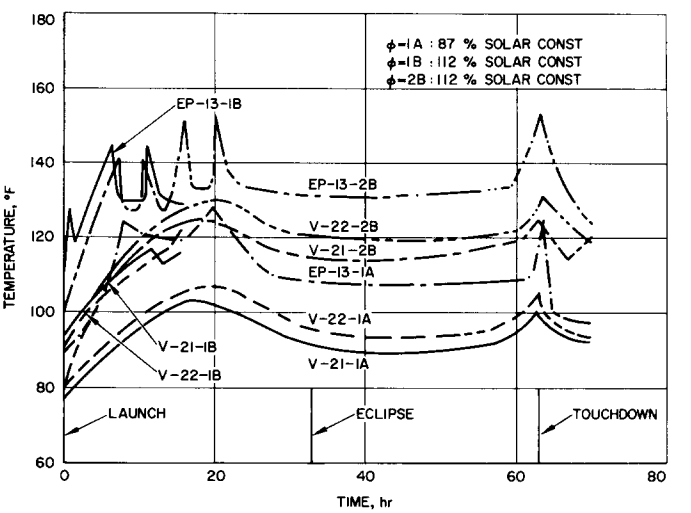

Fig. 93. Compartment B temperatures

CONFIDENTIAL
UNCLASSIFIED

UNCLASSIFIED
CONFIDENTIAL

P. Engineering Mechanics

1. Introduction

Activities reported in this section include touchdown dynamics, static and dynamic structural analyses, and structural tests. Touchdown dynamics include the specification, analysis, and testing of the soft-landing system. A significant portion of this work pertains to procurement of landing gear shock absorbers. A similar activity is the specification of design and test parameters for spacecraft retrorocket engine separation.

2. Summary

Evaluation tests of the shock absorber shipping container, including deliberate failure of a shock absorber inside a closed container, have been successfully completed. Receipt of shock absorbers for mission A and for spare parts completed preflight verification-of-readiness checks. Fabrication of the new design for qualification and flight is on schedule.

Investigations of load, stroke, and stability parameters of the new hydraulic shock absorber (238927) used on the A-21 and A-24 vehicles, as well as the crushable shock absorber, are continuing. Performance of the hydraulic shock absorber as analytically predicted is acceptable. A dual crushing force level in the crushable shock absorber will be necessary to limit response loads.

Abutment stability has been examined with respect to shock absorber rebound. Although abutment stability is improved by the higher center of gravity resulting from leg extension, additional kinetic energy imparted to the vehicle by the present hydraulic shock absorbers results in a net decrease in stability for this situation.

The two-dimensional phase of the S-15 drop test program has been completed. A calibration of the vehicle instrumentation system, resulting in some improvements, has established greater confidence in data. Two-in. cube protuberances were added to the surface to achieve sufficient surface resistance to obtain instability. Analysis of drop test leg force data substantiated the existence of apparent friction coefficients approximating unity.

Structural test vehicle S-9 has been upgraded, weighed, and moments of inertia measured prior to shipment to JPL for model testing. The vehicle will be at JPL until October.

A static test program has been completed to obtain buckling data for thin-walled aluminum tubing in bending, torsion, and combined loading. Test results show that the interaction curves presented in MIL-HDBK-5 are conservative when used in the design of tubular members machined to very close tolerances with respect to straightness, roundness, and wall thickness. Test data will result in weight reduction in some areas of the antenna/solar panel positioner, and will allow use of completed parts as flight hardware which would otherwise be scrapped.

3. Shock Absorber Procurement

Shock absorber shipping container evaluation tests have been successfully completed at the National Water Lift Company. The evaluation program included vibration and drop tests as well as a deliberate fracture of a shock absorber inside the container. The container completely contained the fragments and high pressure generated by the ruptured shock absorber which, prior to the induced failure, was pressurized to 1930 psi to simulate internal pressure caused by maximum temperature during shipping or storage.

SC-1 flight shock absorbers (4, 6, and 7) and the spare set (8, 9, and 10) were put through preflight verification-of-readiness checks at AFETR May 11 and 12. Shock absorber 6 was rejected owing to loss of preload pressure, and was subsequently replaced for the first flight by shock absorber 8. Fit and function checks of shock absorbers 4, 7, and 8 were successfully performed on SC-1 May 13.

National Water Lift Company predicts that the scheduled fabrication, assembly, and test dates for the type approval tests (TAT) for SC-3, SC-4, and S-15A redesigned shock absorber will be met. However, their schedule for completion and shipment of the shock absorbers can be maintained only if no significant problems occur. In the event scheduled problems occur on the new units, existing model 1859 units have been designated for use on SC-3, as alternates for the redesigned units. The development model is complete and presently in the preliminary test cycle.

4. Touchdown Dynamics

a. Stability of A-21 and A-24 vehicles equipped with shock absorber 238927. A preliminary investigation has been made into the loads, stroke, and landing stability for shock absorber 238927 on A-21 and A-24. On A-21 the maximum shock absorber stroke found was 4.59 in., and the maximum load was 7780 lb. On A-24 the maximum stroke was 5.05 in., and the maximum load was 9470 lb.

UNCLASSIFIED
CONFIDENTIAL

UNCLASSIFIED
CONFIDENTIAL

Figs. 94 and 95 show the preliminary stability boundaries for A-21 and A-24.

b. Crushable shock absorber. Preliminary response load levels have been obtained for the A-24 equipped with crushable shock absorbers.

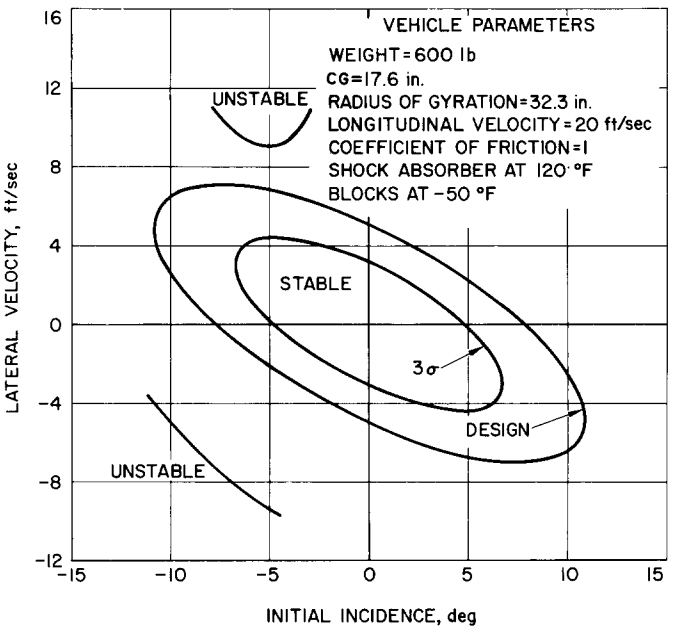

Fig. 94. A-21 preliminary stability boundary for shock absorber 238927

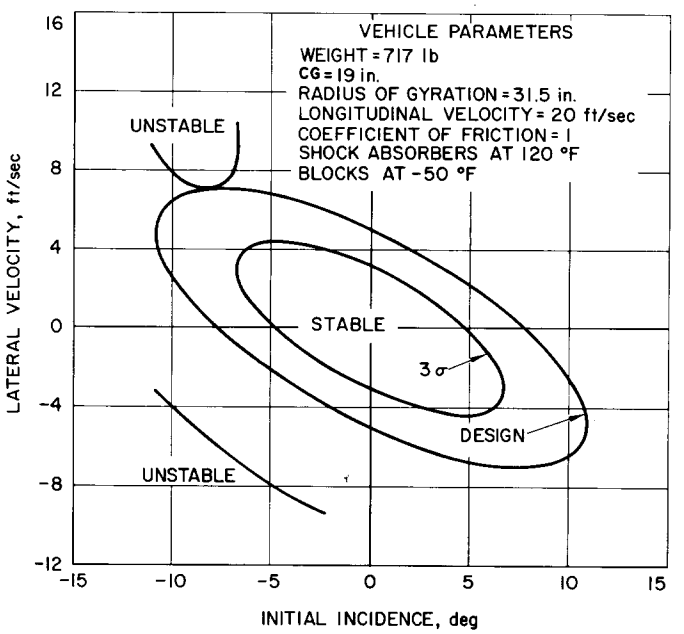

Fig. 95. A-24 preliminary stability boundary for shock absorber 238927

Preliminary schedule and cost estimates relating to the design, fabrication, test, and flight unit procurement of a crushable shock absorber have also been made. A presentation of these estimates, together with performance

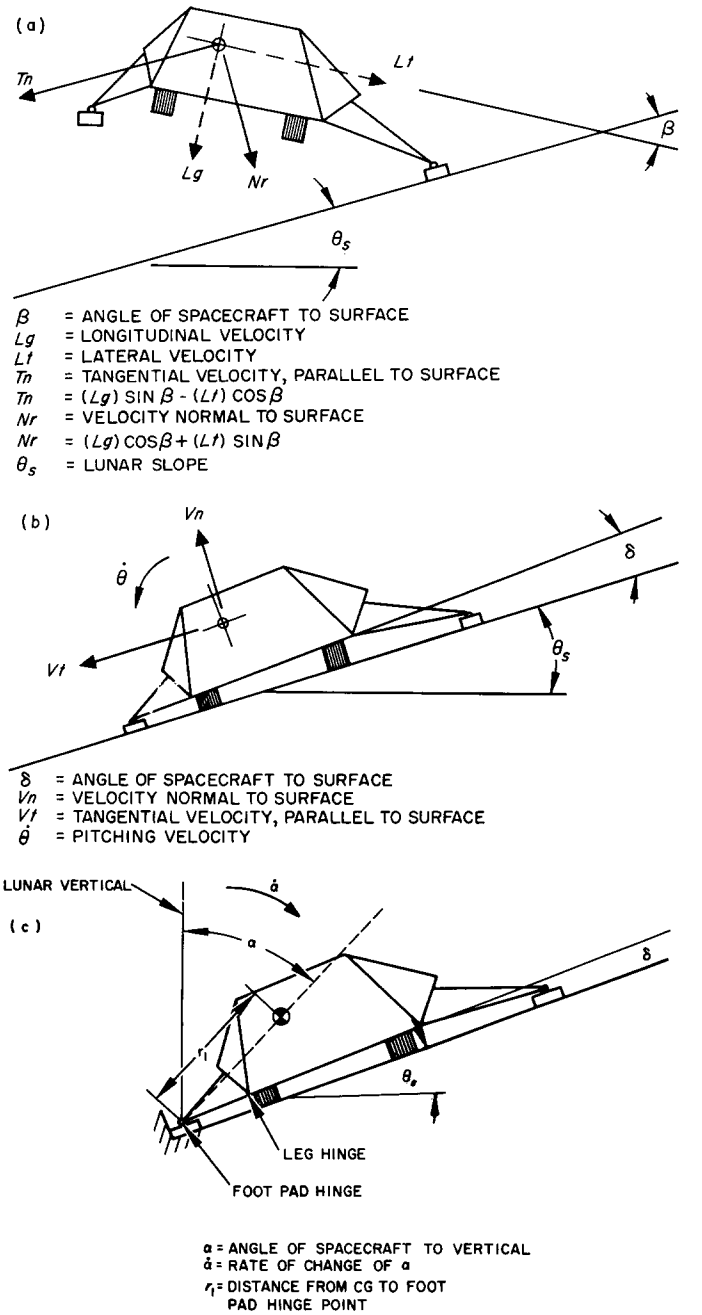

Fig. 96. Landing conditions: (a) Touchdown conditions defining velocities parallel and normal to lunar surface; (b) Final conditions immediately after large forces of landing have subsided; (c) Conditions at the instant after impact with an abutment

CONFIDENTIAL
UNCLASSIFIED

UNCLASSIFIED
CONFIDENTIAL

results and operating characteristics of the crushable shock absorber concept, was made to representatives of JPL at HAC May 17.

c. **Surveyor *abutment stability capability with shock strut rebound.*** The case of abutment stability, including the effects of shock absorber rebound, has been studied, and current shock absorbers have been found to reduce abutment stability capability.

Fig. 96 defines touchdown landing conditions where the coefficient of friction is assumed to be zero, and shows the vehicle immediately after the large forces of landing have subsided and at the instant after impact with an abutment. The footpad is assumed to be held stationary with the vehicle pivoting about the footpad hinge. Translational and angular velocities before impact are converted to an angular velocity, α, about the footpad hinge. The angle α measured from the lunar vertical is also shown in Fig. 96.

Stability boundaries shown in *SPS 37-39*, Vol. I, p. 76, were in the form of touchdown tangential velocity versus lunar slope for the SC-1 and SC-5 vehicles with no shock strut rebound. Stability boundaries (Fig. 97) differ from those in the above *SPS* because of the separation into

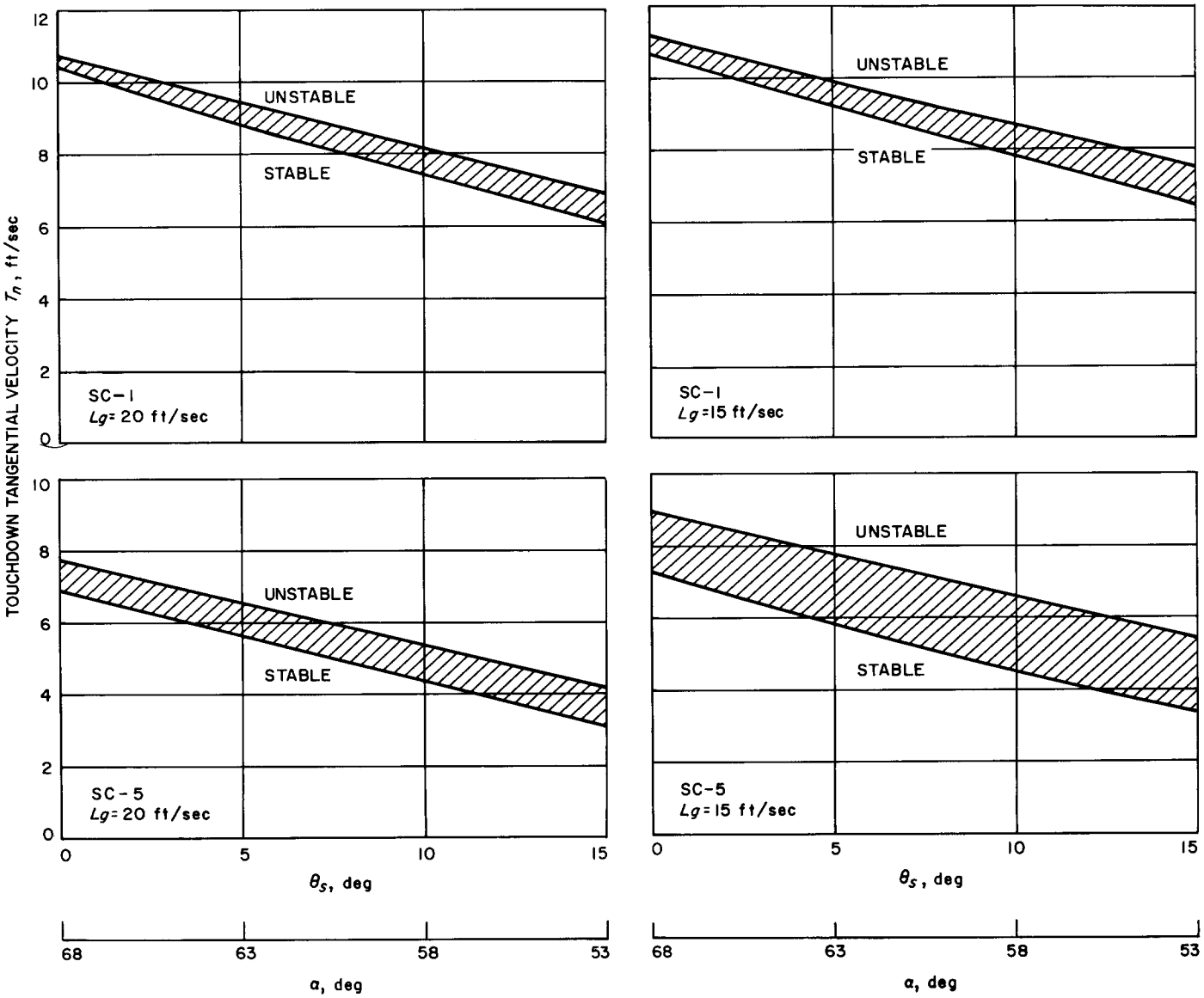

Fig. 97. Stability boundaries without rebound, touchdown tangential velocity T_n vs lunar slope θ_s

CONFIDENTIAL
UNCLASSIFIED

UNCLASSIFIED

cases of 20 and 15 ft/sec longitudinal velocities and because of a refinement in the criteria for the best and worst cases of instability.

Without rebound, the spacecraft pivoting about the footpad hinge is assumed to represent a conservative system. Thus, the total energy after impact is constant without rebound. If this total energy is above a critical value, the vehicle will topple. The energy margin is defined as the difference between the total energy possessed by the spacecraft after impact and the critical value of energy necessary to topple the spacecraft with no rebound. After impact with an abutment, rebounding of the shock strut affects the energy margin as follows:

(1) Rebounding causes the *Surveyor* center of gravity to move with respect to the footpad hinge (Fig. 96) so that the distance r_1 from the footpad hinge to the center of gravity is increased by some distance Δr_1. This effect is noted by an increase in the potential energy portion of the critical energy necessary for toppling, and thus represents an increase in the energy margin and an aid to stability.

(2) During rebound, a portion of the spring energy stored in the shock strut during compression is returned to the spacecraft. This causes an increase in kinetic energy of the spacecraft and thus a decrease in the energy margin and a reduction in stability.

For *Surveyor*, item 1 represents an increase in the energy margin of 45 ft-lb. *SPS 37-39*, Vol. I, p. 76, showed that one SC-1 double shock strut returns an average of 41.3 ft-lb of energy while an SC-5 double shock strut returns an average of 61.3 ft-lb of energy. Thus, item 2 represents a decrease in the energy margin of 83 ft-lb for SC-1 and 123 ft-lb for SC-5. Table 20 shows energy effects of rebound action where

E_{crit} = critical value of energy necessary to topple spacecraft with no shock strut rebound

Δ = increase in potential energy portion of the critical energy owing to moving the center of gravity (item 1 above)

E_s = energy returned by double legs during rebound (item 2 above)

E_{all} = maximum energy spacecraft can possess after impact without toppling

Table 20. Energy effects of rebound action

Action	E_{crit}, ft-lb	Δ, ft-lb	E_s, ft-lb	E_{all},[a] ft-lb
No rebound	361	0	0	361
SC-1 rebound	361	45	83	323
SC-5 rebound	361	45	123	283

[a] $E_{all} = E_{crit} + \Delta - E_s$

Fig. 98 shows stability boundaries in the velocity-displacement plane for the *Surveyor* with no rebound, the SC-1 *Surveyor*, and the SC-5 *Surveyor*. These boundaries can be converted to initial spacecraft velocities on a surface with zero coefficient of friction, as shown in Fig. 99. Fig. 100 shows results of Figs. 97 and 99 for $\theta_s = 15$ deg cross-plotted to the more familiar design ellipses.

Shock strut rebound following an impact with an abutment can both aid and hinder stability, as shown in items 1 and 2 above. Energy Δ is the advantage gained by changing the vehicle configuration (i.e., moving the center of gravity) during rebound of the strut. Energy E_s is the disadvantage owing to strut rebound energy imparted to

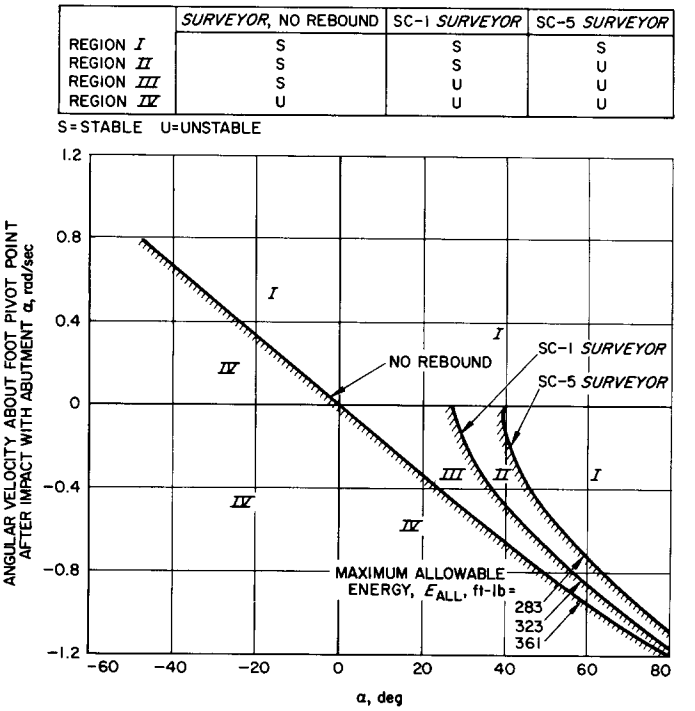

Fig. 98. Stability regions, vehicle striking an abutment

UNCLASSIFIED

UNCLASSIFIED
CONFIDENTIAL

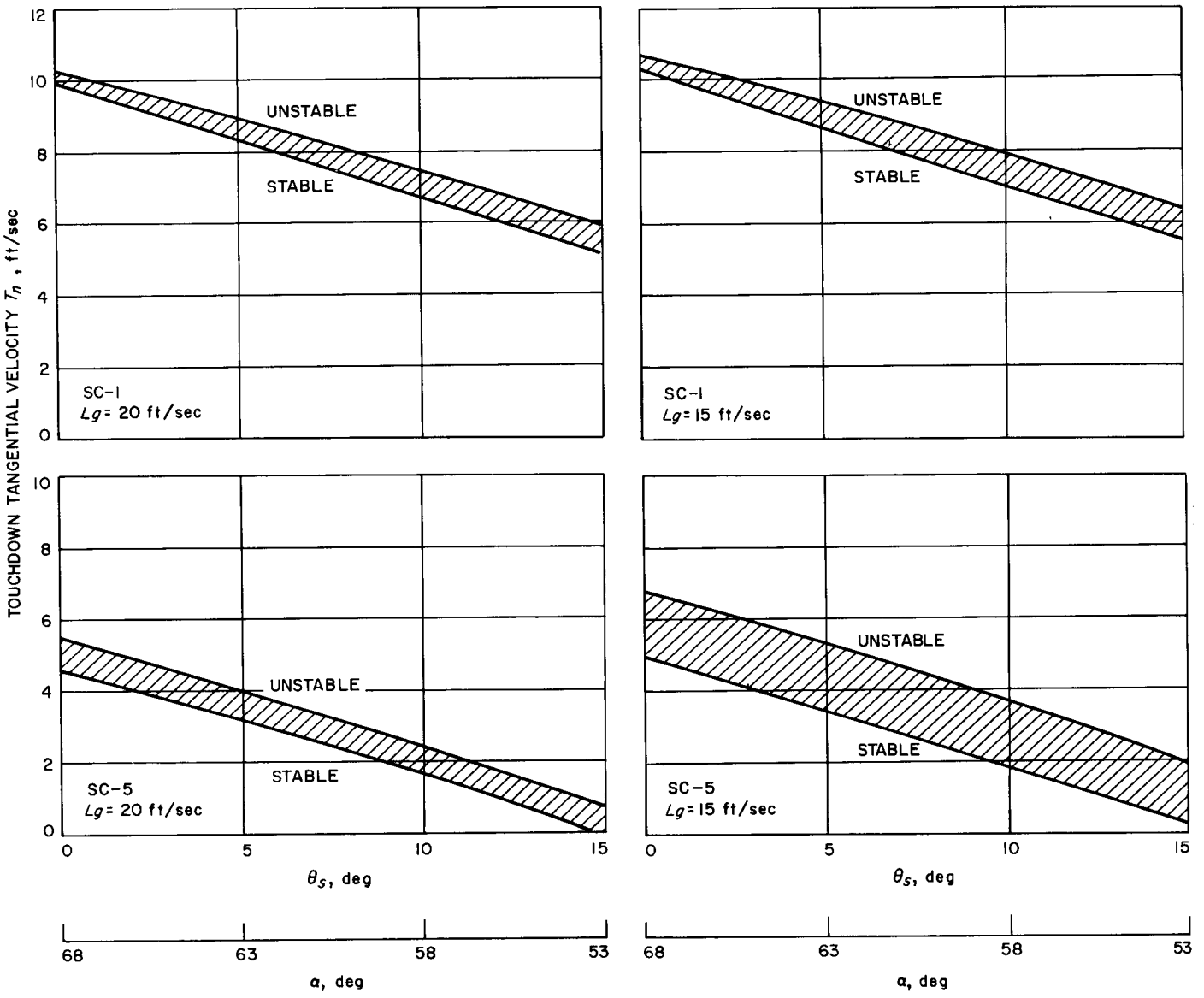

Fig. 99. Stability boundaries with rebound

the spacecraft. For SC-1 and SC-5, the energy disadvantage outweighs the energy advantage (compare Δ and E_s in Table 20) so that shock strut rebound following impact with an abutment is a disadvantage. For a strut with a long rebound time constant, E_s would approach zero, and the full advantage of Δ could be obtained. These results only establish trends, since the spacecraft parameters used were typical rather than extreme.

5. Dynamic Tests

a. S-15 drop tests. The two-dimensional phase of the S-15 drop program was completed May 12. Table 21 and Fig. 101 indicate various conditions under which the 2D drops were made, and friction coefficients used in predicting vehicle stability.

A mechanical and electrical calibration of the complete S-15 instrumentation system was performed, and, as a result, an upgrade of the system was made to assure acquisition of all data channels and to establish greater confidence in the system's accuracy.

Neoprene rubber sheet was bonded to the vehicle footpads to obtain a higher friction coefficient than had been previously achieved. Drops 3, 4, 5, and 7 were then made and showed a higher degree of stability than that being predicted theoretically using a friction coefficient

CONFIDENTIAL
UNCLASSIFIED

UNCLASSIFIED

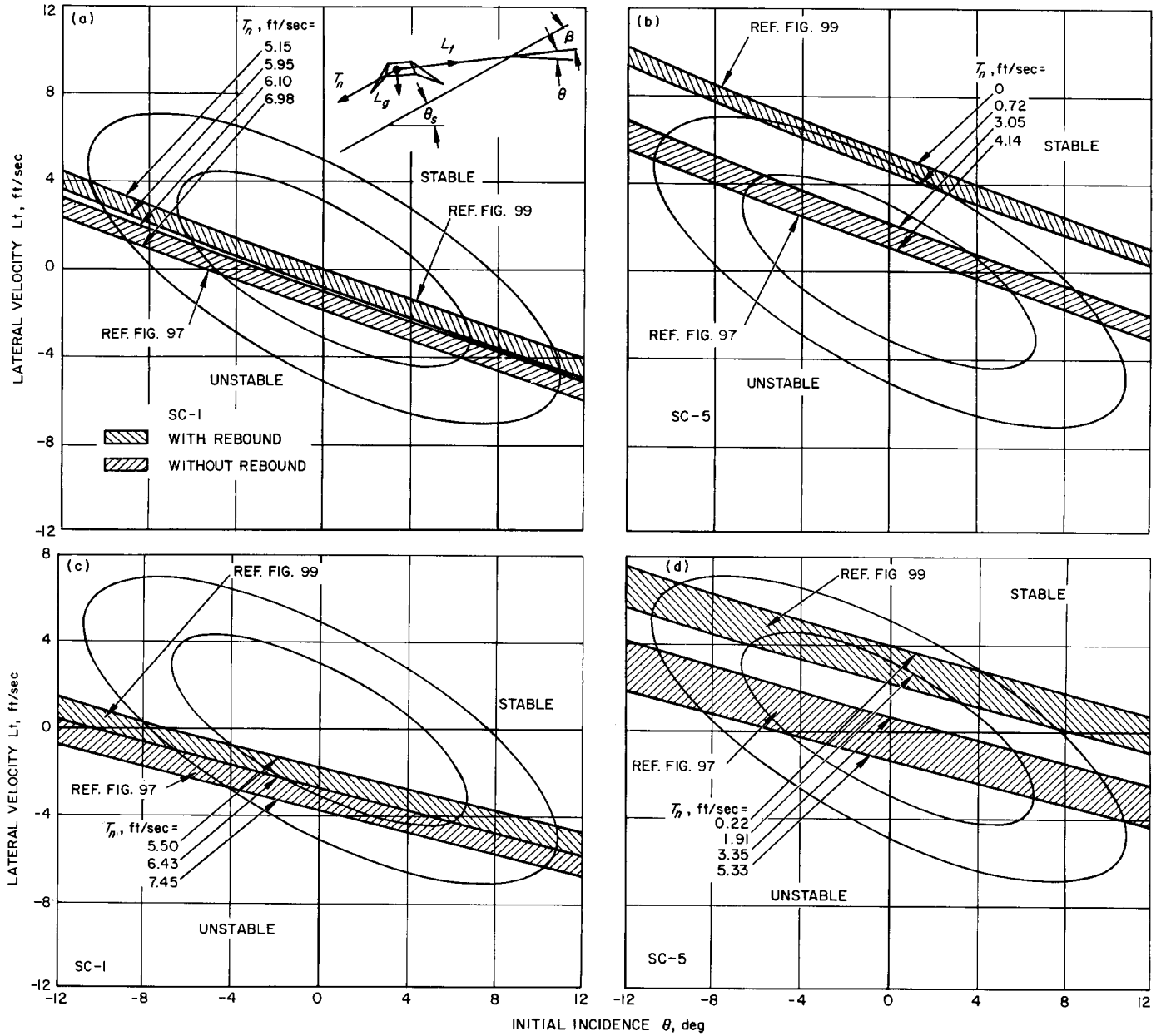

Fig. 100. Stability boundaries: (a) SC-1 Lg = 20 ft/sec; (b) SC-5 Lg = 20 ft/sec; (c) SC-1 Lg = 15 ft/sec; (d) SC-5 Lg = 15 ft/sec

of 0.84 on the footpads. However, comparable stability was achieved analytically by reducing the friction coefficient by 5%. In order to define a stability boundary by drop tests, a further increase in apparent friction on the footpads was effected by placing 2-in. aluminum cubes on the landing surface. (The cubes are placed 8 in. apart on staggered lines 4 in. apart.) Drops 8 through 18 were made on this surface, and the corresponding analytical predictions were considered a friction coefficient of 1.0 on the footpads. Analytical results were again conservative, but a stability boundary was achieved by the drop tests.

Efforts are being made to establish the degree of correlation that exists between analytical predictions and test results. To facilitate this, a computer program has been written which uses test measurements of shock absorber and rigid leg forces to calculate the friction coefficient acting on the footpads. Results obtained with this program for drop 7, in which landing surface and

UNCLASSIFIED

UNCLASSIFIED
CONFIDENTIAL

Table 21. 2D vehicle stability test data

Drop number	Longitudinal velocity, ft/sec	Lateral velocity, ft/sec	Initial incidence, deg	Predicted stability	Measured stability[a]	Friction coefficient used in prediction		Surface condition
						Footpads	Blocks	
1	−14	− 7	− 5	S	S	0.7	0.7	Aluminum/rubber
2	−14	− 9	− 5	U	S	0.7	0.7	Aluminum/rubber
3	−14	− 9	5	U	M	0.84	0.2	Rubber footpads
4	−17	− 9	5	S	S	0.84	0.2	Rubber footpads
5	−17	−12	5	U	S	0.84	0.2	Rubber footpads
6	Delayed release, no data							
7	−17	−11	−10	U	S	0.84	0.2	Rubber footpads
8	−17	−11	− 5	U	M	1.0	0.2	2-in. cubes
9	−17	− 9	− 5	U	S	1.0	0.2	2-in. cubes
10	−14	−11	− 5	U	M	1.0	0.2	2-in. cubes
11	−20	−11	− 5	U	S	1.0	0.2	2-in. cubes
12	−11	−11	− 5	U	M	1.0	0.2	2-in. cubes
13	−20	1.7	− 5	S	S	1.0	0.2	2-in. cubes
14	−20	11	− 5	U	M	1.0	0.2	2-in. cubes
15	−16	11	− 5	S	S	1.0	0.2	2-in. cubes
16	−12	11	− 5	S	S	1.0	0.2	2-in. cubes
17	−20	7	− 5	M	S	1.0	0.2	2-in. cubes
18	−17	7	− 5	S	S	1.0	0.2	2-in. cubes

[a] M indicates marginal stability.

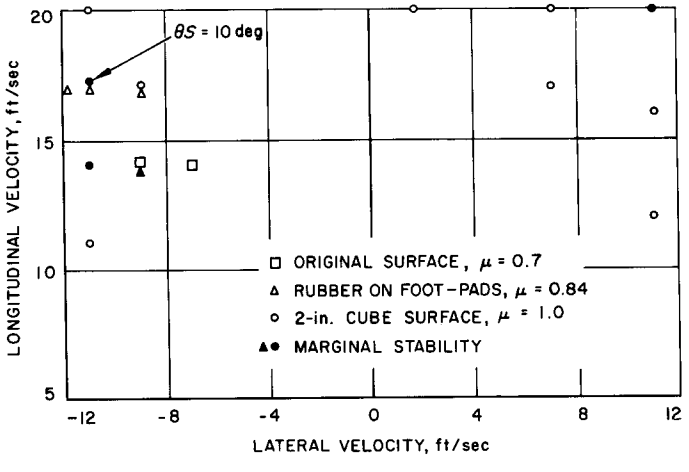

Fig. 101. S-15 2D phase drop tests

footpads were covered with rubber, are shown in Fig. 102. For the same drop condition, Figs. 103 and 104 show analytical and test comparisons for pitch attitude and shock absorber force, respectively.

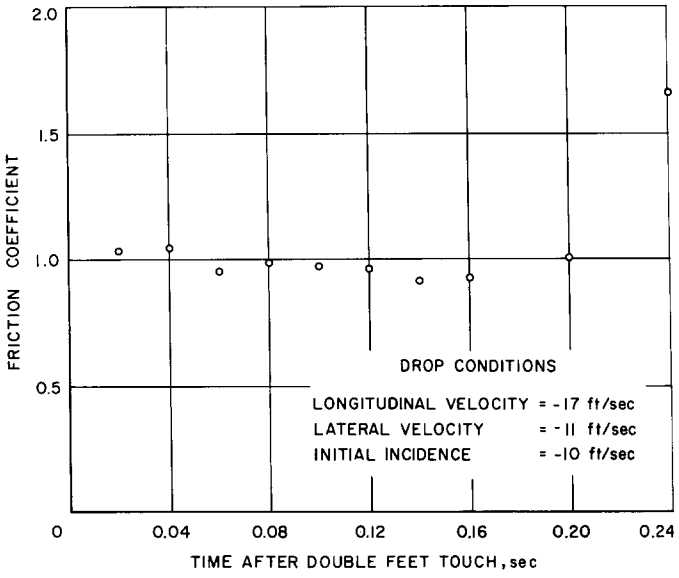

Fig. 102. S-15 friction coefficients calculated from leg 3 strain gauge readings

UNCLASSIFIED
CONFIDENTIAL

UNCLASSIFIED
CONFIDENTIAL

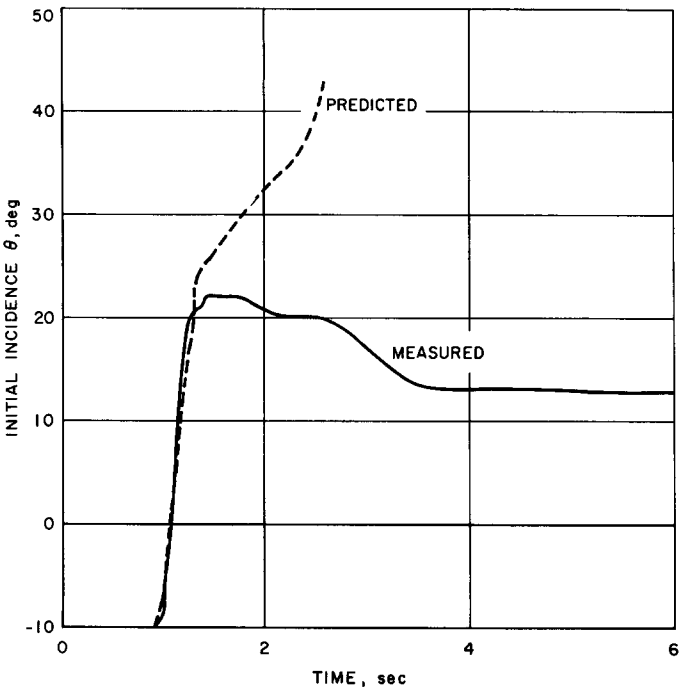

Fig. 103. Predicted and measured pitch angle for S-15, drop 7 conditions

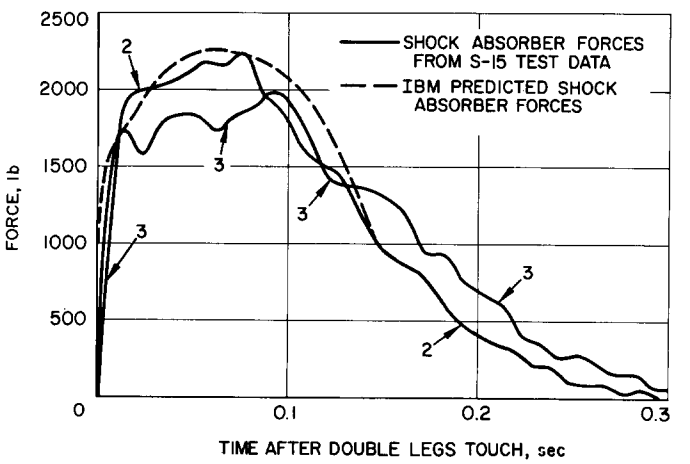

Fig. 104. Predicted and measured shock absorber forces for S-15, drop 7 conditions

b. S-9 structural test vehicle. Following the completion of the vernier bracket thermal loads test April 8, the S-9 structural test model was moved from the structures laboratory in building 309 to the *Surveyor* assembly area in building 350. A post-test inspection of the vehicle confirmed that no structural damage occurred during the static load program.

Work began April 15 to upgrade S-9 to the dynamic test configuration in preparation for modal surveys and controls vibration tests at JPL. Prior to shipment to JPL May 19, weight, center of gravity, and three axes moments of inertia measurements were obtained for the assembled upgraded test vehicle.

c. Static test. Further evaluation of the static test results performed on the *Surveyor* S-9 structural test vehicle showed that all pertinent requirements of document 224510E, "Detail Specification Surveyor System Functional Requirements," were met with the exception of that specified in paragraph 4.1.3.7.3, which establishes the allowable angular alignment error of the flight control sensor group. A method of compensating for the observed alignment error has been formulated.

A separate test was performed to determine the effect of temperature gradients caused by the action of vernier engine operation on the deflection of the thrust chamber assembly brackets. While a simulated thrust load of 100 lb was acting on vernier engine 2, temperatures closely approximating those determined during a test conducted by JPL at Edwards Air Force Base June 15, 1965, were generated by means of radiant heat lamps and monitored by means of strategically placed thermocouples.

The test results indicate that the application of heat causes a peak increase in rotation of 0.05 deg at one point during the heating cycle, which subsequently drops to 0.03 deg rotation.

The rotational deflection of the vernier engine at mid-thrust during main retrorocket burning at the bracket temperatures indicated above was determined by adding the maximum value of incremental rotation about the radial axis to the appropriate deflection obtained from the S-9 (12 g) test, i.e., $\theta_{max} = 0.46 + 0.05 = 0.51$ deg.

A summarization of the test results along with a comparison with the applicable requirements of Document 224510E is presented in Table 22. All test values listed herein are based on an lg starting point, except for item 3. Item 5 contains a correction of the basic test value to account for the effects of elevated temperature. Heat distortion effects on all other components are considered negligible.

d. Static tests of antenna support tube. Static strength tests were recently conducted to define the allowable

CONFIDENTIAL
UNCLASSIFIED

UNCLASSIFIED
CONFIDENTIAL

Table 22. Summary of S-9 static test results

Item	Paragraph number of document 224510E and function	Requirement, maximum	Test value
1	4.1.3.16.6: "The vernier engine bracket bending constant shall be less than 0.50 degree per 100 pounds of load applied along the vernier engine centerline."	0.50	0.46
2	4.1.3.11: "The antenna axis (at the altitude marking radar) shall be within 0.50 degree of the vehicle roll axis provided the radar attach points shall be within 0.25 degree of proper orientation, following exposure to all pre-retro SC environments."	0.25	0.05
3	4.1.3.16.1: "For all expected environmental conditions, the displacement between the retro nozzle centerline and the combined SC-retro engine c. g. shall change no more than ±0.07 inch from the static no-thrust position during retro thrusting."	0.070	0.038[a]
4	4.1.3.16.2: "For all expected environmental conditions, the angle between the retro nozzle centerline and the SC roll axis shall change no more than 0.15 degree from the static no-thrust condition due to main retro thrusting."	0.15	0.05
5	4.1.3.5.1.2: "Throughout main retro burning with the vernier engines at mid-thrust, the angle between the actual thrust vector[b] of any one engine and the SC roll axis shall not exceed 0.55 degree."	0.55	0.51[b]
6	4.1.3.7.3: "Angular alignment error of the (flight control) sensor group to the vehicle roll axis due to acceleration and vibration loads and heat loads shall not exceed 0.20 degree."	0.20	0.56
7	4.1.3.12: "During vernier descent, the radar altimeter axis shall be aligned within 0.40 degree of the vehicle roll axis; and the doppler velocity sensor axes shall be aligned within 0.20 degree of the desired directions. During main retro burn, the doppler velocity sensor axes shall be aligned within 2.0 degrees of the desired directions."		
	Thus:		
	a. Altimeter during vernier descent (0.5 g SC deceleration)[c]	0.40	0.03
	b. Altimeter during retrorocket burn	(Not specified)	0.26
	c. Velocity sensor during vernier descent	0.20	0.01
	d. Velocity sensor during retrorocket burn	2.00	0.19

[a] Extrapolation of displacement to a zero-g field is not included to conform to 1-g reference.

[b] Test value given is rotation of engine centerline.

[c] Maximum deceleration of SC $= \frac{\text{maximum vernier thrust}}{\text{minimum SC weight}} = \frac{312}{712} = 0.44$ g.

buckling strength of the 287580 antenna/solar panel positioner antenna support tube for bending, torsion, and combined bending and torsion loading. Fourteen tubular specimens were fabricated from 7075-T6 aluminum alloy to simulate the thin-walled upper section of the highly stressed antenna support tube.

The region simulated by the test specimens is that portion of the tube between the solar and polar axes, as shown in Fig. 105. The tests were performed in order to obtain empirical data from which an accurate interaction relationship for tubes subjected to combined bending and torsion could be obtained. The use of MIL-HDBK-5 interaction equations was felt to be conservative when applied to close tolerance, machined, straight tubes similar to those used in the spacecraft.

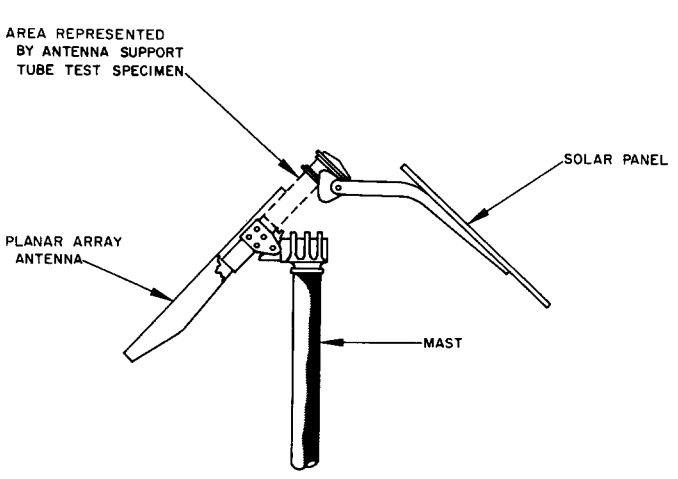

Fig. 105. Antenna/solar panel positioner test specimen

UNCLASSIFIED
CONFIDENTIAL

UNCLASSIFIED

The data have yielded three significant results: (1) an increase of 20% over the bending modulus values given in MIL-HDBK-5; (2) the derivation of a torsional modulus of rupture curve, which will exceed the values outlined in MIL-HDBK-5, provided the material strength properties are above the minimum values used in the handbook; and (3) the generation of a new interaction equation when the torsional load is predominant (Fig. 106). The maximum scatter of data throughout the tests was less than 3% at each test point. Use of the above test data has resulted in a greater optimization of the design together with some weight reduction.

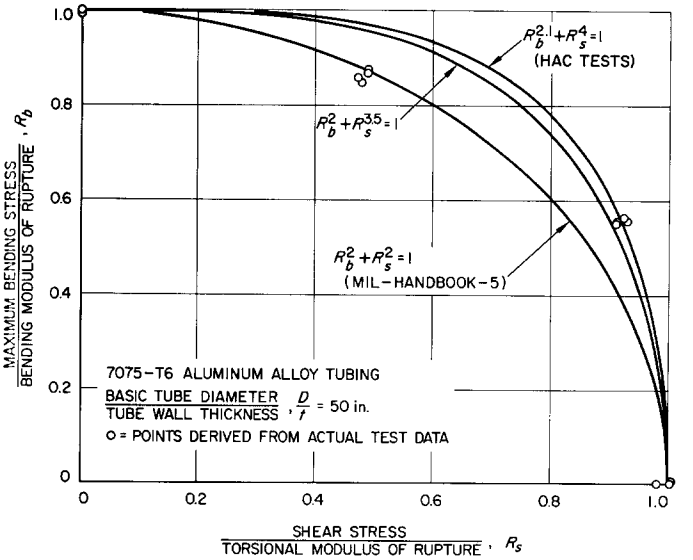

Fig. 106. Interaction curve for combined bending and torsion

References

1. "*Surveyor* Mission A Postinjection Standard Trajectories," Hughes Aircraft Company, Space Systems Division, SSD 64085R, April 1964.
2. "Optical Performance Test Report of Variable Focal-Length Television Lens Assembly Serial Number X-8," Bell and Howell Company Test Report No. 6024B, February 25, 1963.
3. *Surveyor Spacecraft Bimonthly Progress Summary*, SSD 56021R, Hughes Aircraft Company, Culver City, California, December 23, 1965.
4. Burkhardt, G. N., and Kramer, P. W., *CDC No. 11 Electromagnetic Susceptibility Test*, IDC 2255.2/530, Hughes Aircraft Company, Culver City, California, April 26, 1966.
5. Rechter, R. J., and Fashano, M., *PCM Link Performance Characterization and Optimization Tests Performed on CDC 11*, IDC 2253.1/621, Hughes Aircraft Company, Culver City, California, April 13, 1966.

CONFIDENTIAL
UNCLASSIFIED